

THE UNIVERSITY
of EDINBURGH

This thesis has been submitted in fulfilment of the requirements for a postgraduate degree (e.g. PhD, MPhil, DClinPsychol) at the University of Edinburgh. Please note the following terms and conditions of use:

This work is protected by copyright and other intellectual property rights, which are retained by the thesis author, unless otherwise stated.
A copy can be downloaded for personal non-commercial research or study, without prior permission or charge.
This thesis cannot be reproduced or quoted extensively from without first obtaining permission in writing from the author.
The content must not be changed in any way or sold commercially in any format or medium without the formal permission of the author.
When referring to this work, full bibliographic details including the author, title, awarding institution and date of the thesis must be given.

Resting State Functional Magnetic Resonance Imaging in Fragile X Syndrome

Joanna Smith B.Sc. M.H.S M.Sc.



THE UNIVERSITY
of EDINBURGH

Doctor of Philosophy

Biomedical Sciences

School of Medicine and Veterinary Medicine

University of Edinburgh

July 2020

Abstract

Autism Spectrum Disorders (ASD) and Intellectual Disabilities (ID) are two co-occurring neurodevelopmental disorders that affect approximately 100 million individuals worldwide, making them leading causes of disability in children. Current therapeutic interventions are restricted to managing symptoms and behavioural therapy. There is therefore an urgent unmet need for rational treatments targeting underlying causes.

The study of animal models of monogenic disorders associated with a high prevalence of ASD/ID, such as Fragile X Syndrome (FXS) can help us gain a better understanding of the pathophysiology of ASD/ID and hence develop new disease-modifying therapies. However, a key requirement for effective therapeutic development is the ability to directly compare findings from basic neuroscience in rodent models with human studies. Methodological approaches that can be applied to both human and rodents would greatly facilitate this endeavour.

In this thesis, I used resting state functional magnetic resonance imaging (rsfMRI) to study functional brain connectivity in rat models of FXS and affected humans. RsfMRI is a non-invasive imaging technique that is directly translatable across species, therefore providing a powerful tool to investigate how brain activity is modulated across development and in disease.

First, I established and validated a methodology to acquire and analyse rsfMRI data from anaesthetised rodents. I verified my methods by successfully identifying resting state networks (RSNs) in both humans and rats. I additionally demonstrated that anaesthesia concentration, but not duration, affect RSNs connectivity in wild type (WT) rats.

Second, a parallel imaging approach was used in individuals with FXS and in the *Fmr1*$^{-/y}$ rat model of the disorder to investigate the functional connectivity of FXS. I observed a global decrease in connectivity in *Fmr1*$^{-/y}$ Long-Evans Hooded (LEH) rats, as well as a specific decrease in their Default Mode Network (DMN) connectivity. To determine how this change in functional brain connectivity in the rat model related to the human condition, I next examined whether similar alterations in functional connectivity occurred in individuals with FXS. I observed that cortico-cortical connectivity was reduced at a whole-brain scale and that the DMN was underconnected in FX individuals, indicating that the *Fmr1*$^{-/y}$ rat is a good model for global changes in brain connectivity

found in FXS.

Several other interesting findings observed in the rat data may be relevant to the human condition. First, I found that *Fmr1*$^{-/y}$ LEH rats were less sensitive to isoflurane anaesthesia than WT rats. I also observed strain-specific functional connectivity impairments. In comparison with Sprague-Dawley (SD) rats, LEH rats showed a relative decrease in hypothalamic connectivity. Additionally, genetic deletion of *Fmr1* in SD rats resulted in a selective hypoconnectivity of the cerebellum and caudate putamen.

Finally, I examined the developmental trajectory of DMN connectivity and tested the hypothesis that reducing ERK activity with lovastatin would restore DMN connectivity in *Fmr1*$^{-/y}$ rats, as lovastatin was previously found to restore behavioural, electrophysiological and molecular impairments in rodent models of FXS. I found that DMN connectivity between *Fmr1*$^{-/y}$ rats and WT littermates is comparable at 4 weeks of age, but diverges by 8 weeks, leading to an underconnected DMN in *Fmr1*$^{-/y}$ rats. In addition, I demonstrated that lovastatin treatment during this developmental period does not prevent the emergence of DMN underconnectivity in *Fmr1*$^{-/y}$ rats.

In summary, this thesis provides the first account of altered functional brain connectivity in a rat model of FXS, adding to the existing body of literature reporting altered connectivity in ASD. In addition, it provides evidence that functional connectivity abnormalities observed in a rat model of FXS directly translate to individuals with FXS. It further shows that while effective in preventing some of the pathophysiology resulting from the loss of FMRP, early lovastatin treatment was unsuccessful at restoring DMN connectivity in *Fmr1*$^{-/y}$ rats. Taken together, these findings highlight the potential of using rsfMRI as a diagnostic tool and in assessing therapeutic efficacy in rodent models of neurodevelopmental disorders.

Lay Summary

Autism Spectrum Disorders (ASD) and Intellectual Disabilities (ID) affect approximately 100 million individuals worldwide, making them leading causes of disability in children. However, there is no effective treatment for them. The study of rodents with deliberate modifications ('mutations') to genes known to cause ASD and ID can help better understand these disorders, and come up with possible treatment options.

The brain is composed of different regions that communicate with one another. Some groups of brain regions have coordinated periods of activity, being active and inactive at the same time, which requires a high degree of communication. We call them 'functionally connected' brain regions. It is possible to measure how well groups of functionally connected brain regions are communicating with one another using a technique called 'resting state functional magnetic resonance imaging (rsfMRI)'. In this thesis, I investigated the coordination of functionally connected brain regions in Fragile X syndrome (FXS), a disorder caused by a known mutation that is associated with a high incidence of ASD and ID.

First, I established a method to investigate the communication of functionally coordinated brain regions in rodents.

Then, I applied it to rats with the FXS mutation ('FXS rats'), and found that the communication between functionally connected brain regions was decreased in FXS rats compared to normal rats. I used a similar protocol to study functionally connected brain regions in humans with FXS, and found that they also had a decreased communication between the same brain regions.

Finally, I examined whether lovastatin, a drug that has been shown to be effective in helping with some symptoms of FXS in FXS rats and mice, could increase the abnormal communication identified in FXS rats. However, a 5-week lovastatin treatment was unable to restore a normal communication between functionally connected brain regions in FXS rats.

In summary, this thesis provides the first account of impaired communication between functionally connected brain regions in FXS rats, and provides evidence that similar impairments are observed in FXS individuals. It further shows that while effective in preventing some of FXS symptoms, lovastatin treatment was unsuccessful at

improving brain communication in FXS rats. Taken together, these findings highlight the potential of using rsfMRI to study ASD and ID in rodents, and as a way to assess new treatments.

Acknowledgements

I have many people to thank for their support during the past 4 years. Firstly, I would like to thank my supervisors Prof. Peter Kind, Dr Andrew Stanfield and Dr Sally Till. Peter, thank you for your academic support and guidance throughout the past years, and especially for helping me deal with allergy-related obstacles. I wouldn't have been able to complete my experiments without your help. Andy, thank you for your advices and support with the clinical side of my project. A massive thank you to Sally. When I started this project you told me it was going to be the blind leading the blind. I like to think that we uncovered some MRI mysteries together. Thank you for all your advices, support, guidance and help in dealing with all the MRI mishaps.

Secondly, I would like to thank those who have helped me with resting state experiments. Dr Andrew McKechanie, thank you for trusting me with the analysis of the human data, and for your input and advice on the project. To Mr Ross Lennen and Dr Maurits Jansen, a massive thanks for all the hours spent imaging rats, dealing with coils breaking and other help in acquiring all these images. Thank you for stepping up with Mr Mike Walls and Dr Sally Till, when I couldn't go into the facility anymore. Finally, I'd like to thank Dr. Rick Dijkhuizen and his lab, and especially Milou Straatford, for welcoming me to Utrecht and teaching me the basis of resting state analysis.

I would also like to thank everyone from the Kind/Wyllie lab, for their friendship throughout the years. A very special thanks to Laura Oliveira and Natasha Anstey, my PhD buddies. I couldn't have done this without all your support, messages and laughter/tears! Thank you to Melania Muscas, for all of the sushis, pizza and other support, and to Tiago Marcos, for making demonstrating fun and for all the sharks. I'd also like to thank Kirsten Wilson, my rodent allergy buddy.

A special thank you for Camille, Jade, Estelle and Laura. To my wonderful family, thank you for your constant love, support and laughter. I'm very lucky to have all of you in my life.

Finally, to my wonderful fiancé, Luke Surl, thank you for everything. I can't wait to marry you.

Declaration

I declare that this thesis was composed by myself and that the work contained herein is my own, unless otherwise states and with exception of the following:

- The clinical data was collected by Dr Andrew McKechanie and Dr Andrew Stanfield; the author performed all the data analysis.
- Mr Michael Walls, Dr Sally Till, Mr Ross Lennen and Dr Maurits Jansen contributed to the data collection for some preclinical MRI experiments.

No part of the work contained in this thesis has been submitted for any other degree or professional qualification.

Signed: ---------- Date: ----------

Contents

1 **Introduction** **1**

1.1 Neurodevelopmental disorders 1

1.2 Fragile X Syndrome 2

1.2.1 The fragile X gene 3

1.2.2 Preclinical models of FXS 3

1.2.3 The fragile X mental retardation protein 8

1.2.4 The mGluR theory of FXS 8

1.3 Magnetic Resonance Imaging 13

1.3.1 MRI scanner 13

1.3.2 Obtaining MR signals 14

1.3.3 Pulse sequences 16

1.4 Functional MRI 18

1.4.1 The hemodynamic brain response 18

1.4.2 The BOLD contrast 19

1.5 Resting state fMRI 20

1.5.1 Why study the brain at rest? 20

1.5.2 Resting State Networks 23

1.5.3 Considerations for resting state studies in preclinical animal models 27

1.6 Functional connectivity in ASD/ID 28

1.6.1 Resting state studies in individuals with idiopathic ASD 29

1.6.2 Resting state studies in rodent models of ASD 33

1.7 Aims of this thesis 35

2 **Materials and Methods** **39**

2.1 Animals . . . 39
2.1.1 Housing and breeding . . . 39
2.1.2 *Fmr1*$^{-/y}$ Sprague Dawley rats . . . 39
2.1.3 *Fmr1*$^{-/y}$ Long-Evans hooded rats . . . 40
2.2 Genotyping . . . 40
2.2.1 DNA extraction and isolation . . . 40
2.2.2 *Fmr1*$^{-/y}$ Sprague Dawley Primers . . . 40
2.2.3 *Fmr1*$^{-/y}$ Long-Evans hooded Primers . . . 41
2.2.4 Polymerase Chain Reaction (PCR) . . . 41
2.3 Preclinical MRI . . . 41
2.3.1 Habituation . . . 41
2.3.2 Pharmacological intervention . . . 42
2.3.3 Acquisition of MRI scans . . . 42
2.3.4 Analysis of MRI scans . . . 45
2.4 Clinical MRI . . . 50
2.4.1 Participants . . . 50
2.4.2 Participant acclimatisation to the scanning procedure . . . 51
2.4.3 Acquisition of MRI scans . . . 51
2.4.4 Analysis of MRI scans . . . 52

3 Establishing a methodology to study Functional Connectivity in rodents 57

3.1 Introduction . . . 57
3.2 Results . . . 58
3.2.1 Methodology troubleshooting . . . 58
3.2.2 Resting state networks are shared across species . . . 73
3.2.3 Effect of anaesthesia on resting state networks . . . 73
3.3 Discussion . . . 78
3.3.1 Methodological flexibility . . . 78
3.3.2 Other methodological considerations . . . 78
3.3.3 Resting state networks or noise? . . . 81
3.4 Summary . . . 82

4 Impaired Functional Connectivity in Fragile X Syndrome 85
4.1 Introduction . . . 85
4.2 Results . . . 87
4.2.1 Functional connectivity in a rat model of FXS . . . 87
4.2.2 Functional connectivity in individuals with FXS . . . 101
4.3 Discussion . . . 108
4.3.1 FXS connectivity across species . . . 108
4.3.2 Inter-strain differences in brain connectivity in rat models of FXS 112
4.3.3 Impact of anaesthesia on functional connectivity . . . 114
4.3.4 Methodological limitations . . . 117
4.4 Summary . . . 119

5 Impact of early lovastatin treatment on Default Mode Network connectivity of *Fmr1*$^{-/y}$ rats across development 121
5.1 Introduction . . . 121
5.2 Results . . . 123
5.2.1 Developmental trajectory of DMN connectivity . . . 123
5.2.2 Can Lovastatin enhance DMN connectivity in *Fmr1*$^{-/y}$ rats? . . 126
5.3 Discussion . . . 129
5.3.1 The Default Mode Network development . . . 129
5.3.2 Lovastatin and FXS . . . 133
5.3.3 Timing of the intervention . . . 137
5.4 Summary . . . 138

6 Discussion 141
6.1 Concluding remarks . . . 141
6.1.1 Can preclinical rsfMRI be used to predict therapeutic success? . 141
6.2 Future Directions . . . 144

Appendix A Resting state protocol 147

A.1 FMRI file conversion . . . 147

A.1.1 Create .hdr/.img files in **MRIcro** . . . 147

A.1.2 Reorientation in **SPM8** . . . 148

A.2 FMRI file preparation for FSL . . . 149

A.2.1 Conversion to nifti . . . 149

A.2.2 Brain extraction with **skullstriper** . . . 150

A.3 Resting state analysis using MELODIC . . . 152

A.3.1 Data . . . 153

A.3.2 Pre-Stats . . . 153

A.3.3 Registration . . . 153

A.3.4 Stats . . . 154

A.3.5 Post-Stats . . . 154

A.4 Dual regression . . . 154

A.5 Seed-based analysis . . . 156

Appendix B Classification of signal and noise components 159

B.1 Spatial maps . . . 159

B.1.1 Signal components . . . 159

B.1.2 Cardiac components . . . 159

B.1.3 Motion components . . . 160

B.1.4 White matter component . . . 160

B.2 Timecourses . . . 161

B.3 Powerspectra . . . 162

Bibliography 165

List of Abbreviations

B_0	Static magnetic field
CHD8	Chromodomain Helicase DNA binding factor 8
CNTNAP2	Contactin associated protein-like 2
Fmr1	fragile X mental retardation gene
ACC	Anterior cingulate cortex
AMPA	α-amino-3-hydroxy-5-methyl-4-isoxazolepropionic acid
ASD	Autism spectrum disorders
ASL	Arterial spin labelling
ATP	Adenosine triphosphate
CNR	Contrast-to-noise ratio
DMN	Default Mode Network
DOF	Degrees of freedom
DTI	Diffusion Tensor Imaging
EEG	Electroencephalography
EPI	Echo-Planar Imaging
EPSC	Excitatory postsynaptic current
ERK	Extracellular signal–regulated kinases
fMRI	Functional Magnetic Resonance Imaging
FMRP	fragile X mental retardation protein
FWHM	Full width half maximum
FXS	Fragile X Syndrome
GABA	γ-aminobutyric acid
GLM	General Linear Model
GM	Grey matter
GRE	Gradient echo
HDL	High density lipoprotein
i.v.	Intravenous
ICA	Independent component analysis
ID	Intellectual disabilities
IPSC	Inhibitory postsynaptic current
IQ	Intelligence quotient
LDL	Low density lipoprotein

LEH	Long Evans Hooded
MEG	Magnetoencephalography
$mGluR_5$	Metabotropic glutamate receptor 5
mGluR1/5	Group 1 metabotropic glutamate receptors
mPFC	Medial prefrontal cortex
MRI	Magnetic Resonance Imaging
mTOR	Mammalian target of rapamycin
NF1	Neurofibromatosis 1
NMDA	N-methyl-D-aspartate
PCC	Posterior cingulate cortex
PCR	Polymerase chain reaction
PFC	Prefrontal cortex
RARE	Rapid Imaging with Refocused Echoes
RF	Radiofrequency
ROI	Region of interest
rsfMRI	resting state functional Magnetic Resonance Imaging
RSN	Resting state network
SD	Sprague Dawley
SE	Spin echo
SNP	single nucleotide polymorphism
SNR	Signal to noise ratio
TBE	Tris/Borate/EDTA
TD	Typically developing
TE	Echo time
TR	Repetition time
VBM	Voxel-based morphometry

List of Figures

1.1 *FMR1* Protein and Gene 4
1.2 A comparison between individuals with FXS and the mouse model of FXS 6
1.3 The mGluR theory of FXS 9
1.4 Drug targets of the mGluR5 signalling pathway in FXS 10
1.5 Position of the different coils within a MRI scanner 13
1.6 Gradient coils magnetic field 15
1.7 Spin Echo pulse sequence 17
1.8 Gradient Echo pulse sequence 18
1.9 The hemodynamic brain response 19
1.10 Task based *vs* resting state fMRI 22
1.11 Aims of the thesis 36

2.1 Flowchart of the steps required to get the images ready for analysis . . . 47
2.2 Multi-session temporal concatenation ICA 49
2.3 Single-session ICA 53

3.1 K-space sampling during EPI 60
3.2 Impact of the number of shots on functional images acquired on an Agilent scanner 61
3.3 Impact of the number of shots on functional images acquired on a Bruker scanner 62
3.4 GRE sequence parameters TR and TE 62
3.5 Impact of the Echo Time on functional images 63
3.6 Comparison of the effect of head coils on functional image quality 65
3.7 Flowchart of preprocessing steps 66
3.8 Impact of bounding box size on images registration during preprocessing. 68

3.9 Resting State Functional Connectivity Methods 70
3.10 Resting state networks are comprised of equivalent brain structures in rats and humans 74
3.11 Impact of anaesthesia duration on the Default Mode Network connectivity in adult WT Sprague Dawley rats 76
3.12 Impact of anaesthesia strength on Default Mode Network connectivity in adult WT Sprague Dawley rats 77

4.1 Resting State Networks identified in adult WT and *Fmr1*$^{-/y}$ Sprague Dawley rats using Independent Component Analysis 89
4.2 Between genotype comparison of the Resting State Networks identified by ICA in *Fmr1*$^{-/y}$ Sprague Dawley rats and WT littermates 90
4.3 Between genotype comparison of the Default Mode Network identified by seed-based analysis in *Fmr1*$^{-/y}$ Sprague Dawley rats and WT littermates 91
4.4 Global decrease in functional connectivity in *Fmr1*$^{-/y}$-LEH rats 92
4.5 Resting State Networks identified in adult WT and *Fmr1*$^{-/y}$ Long Evans hooded rats using Independent Component Analysis 93
4.6 Resting State Networks identified in adult WT and *Fmr1*$^{-/y}$ Long Evans hooded rats using Independent Component Analysis 94
4.7 Between-group Default Mode Network functional connectivity obtained by Independent Component Analysis 95
4.8 Between-group Default Mode Network functional connectivity 96
4.9 Resting State Networks identified in WT and *Fmr1*$^{-/y}$ rats on a Sprague Dawley or Long Evans Hooded background, using Independent Component Analysis 97
4.10 The hypothalamus is hyperconnected in LEH compared to SD rats . . . 98
4.11 Functional connectivity correlation in adult LEH rats under three different levels of anaesthesia (1%, 1.5%, 2.5% isoflurane). 100
4.12 Resting state fMRI scanning in individuals with Fragile X Syndrome . . 103
4.13 Decreased cortico-cortical connectivity and increased thalamo-cortical connectivity in individuals with FXS 104
4.14 Increased frontal connectivity and decreased DMN connectivity in individuals with FXS 105

4.15 Increased frontal connectivity and decreased DMN connectivity in males with FXS . . . 106
4.16 Seed-based functional connectivity of the anterior cingulate cortex . . . 106
4.17 Between genotype voxel-wise differences in local grey matter . . . 107

5.1 Experimental timeline . . . 123
5.2 Developmental trajectory of DMN connectivity in *Fmr1*$^{-/y}$-LEH and WT rats on a control diet . . . 124
5.3 No between-group difference in DMN connectivity in 4-week old *Fmr1*$^{-/y}$-LEH rats and WT littermates . . . 125
5.4 DMN connectivity in 8 week old *Fmr1*$^{-/y}$-LEH rats and WT littermates on lovastatin or control diet . . . 127
5.5 DMN connectivity in 12 week old *Fmr1*$^{-/y}$-LEH rats and WT littermates treated with a lovastatin or control diet . . . 128
5.6 DMN connectivity in 15 week old *Fmr1*$^{-/y}$-LEH rats and WT littermates fed with lovastatin or control diet . . . 130

A.1 High resolution image set at the template's origin . . . 149

B.1 Signal component . . . 160
B.2 Cardiac component . . . 160
B.3 Motion component . . . 161
B.4 White matter component . . . 161
B.5 Independent component timecourses . . . 162
B.6 Independent component powerspectra . . . 163

List of Tables

1.1 A comparison between the *Fmr1* KO mouse and rat 7

2.1 Tail buffer mix 40
2.2 PCR reaction mix 41
2.3 PCR thermocycling conditions 42
2.4 Agilent structural scan sequence characteristics 43
2.5 Agilent EPI scan sequence characteristics 43
2.6 Bruker structural scan sequence characteristics 44
2.7 Bruker EPI scan sequence characteristics 45
2.8 Bruker DTI scan sequence characteristics 45
2.9 Participant demographics 50
2.10 Siemens structural scan sequence characteristics 51
2.11 Siemens EPI scan sequence characteristics 52

3.1 Pros and cons of MRI software tested for resting state analysis. 72

Chapter 1

Introduction

1.1 Neurodevelopmental disorders

Neurodevelopmental disorders are a broad group of highly heritable disorders, such as autism spectrum disorders (ASD), intellectual disabilities (ID), attention deficit hyperactivity disorder (ADHD) and childhood epilepsy, that typically onset during childhood, prior to puberty (Thapar et al., 2017). The co-occurrence of two or more neurodevelopmental disorders is frequently observed and tends to be associated with severe conditions (Hansen et al., 2018).

ID is a prevalent neurodevelopmental disorder, affecting 2-3% of the population worldwide (Leonard and Wen, 2002). It is defined as having an intelligence quotient (IQ) below 70 and significant limitations in adaptive functioning, with an onset before the age of 18 years (Kaufman et al., 2010; Ropers and Hamel, 2005). It can be further classified according to its severity, with mild ID corresponding to an IQ of 50-70, moderate ID to an IQ of 35-50 and severe ID to an IQ below 35 (Leonard and Wen, 2002; Ropers and Hamel, 2005). It is thought that approximately 50% of ID cases are caused by *de novo* mutations (Rauch et al., 2012).

ASD are a group of neurodevelopmental disorders that affect approximately 1% of the population worldwide (Baxter et al., 2015). It has been reported that men are three times more commonly affected than women (Baxter et al., 2015), although women might express ASD differently to men and might therefore be underdiagnosed (Hull et al., 2020). It is a heterogeneous group of disorders with a strong genetic basis, its heritability estimated to be around 90% (El-Fishawy and State, 2011). ASD is characterized by impairments in communications, in social interactions and repetitive

patterns of behaviour and interest (Lai et al., 2014). It is among the leading causes of disability in children (Baxter et al., 2015) and is associated with many comorbidities including other neurodevelopmental disorders, as well as phobia and anxiety (Lai et al., 2014; Leyfer et al., 2006).

The severity of ASD and ID, and the presence and severity of comorbidities can greatly vary between individuals. This clinical heterogeneity of ASD/ID is to an extent a reflection of its genetic heterogeneity, with cases being largely sporadic and often caused by variants in several genes (Lai et al., 2014; Kaufman et al., 2010; Rauch et al., 2012). This clinical and neurobiological heterogeneity therefore complicates the study of ASD/ID.

Focusing on monogenic forms of neurodevelopmental disorders associated with a high incidence of ASD and ID enables the study a more biologically homogeneous population and this, combined with the ability to model the condition using animal models, can help us gain a better understanding of the underlying neurobiology. In addition, studies have shown that different single-gene disorders associated with a high prevalence of ASD/ID may share common pathophysiological mechanisms and might be amenable to common therapeutic interventions (Barnes et al., 2015; Auerbach et al., 2011). Study of monogenic forms of ASD/ID may therefore have importance for understanding the underpinnings of other forms of autism more generally.

1.2 Fragile X Syndrome

Fragile X Syndrome (FXS) is a leading single-gene cause of both ASD and ID. It is an X-linked disorder caused by the absence or deficiency of the fragile X mental retardation protein.

Children with FXS often present with cognitive delay and delays in language development (Cornish et al., 2008; Baranek et al., 2005; Roberts et al., 2009). FX individuals further present emotional and learning difficulties, and ID affects most males with FXS and about one-third of females (de Vries et al., 1996; Loesch et al., 2004). In addition, 50-60% of males and 20% of females also have ASD (Kaufmann et al., 2017). Hyperactivity, impulsivity, anxiety, sensory hypersensitivity and sleep disturbances are also common in individuals with FXS (Hagerman, 1997).

Physical characteristics of FX individuals include a long face, prominent ears, flat feat and features related to connective tissue abnormalities (Hagerman, 1997). Macroorchidism also develops at puberty (Hagerman, 1997).

1.2.1 The fragile X gene

The fragile X gene (*FMR1*), was identified in 1991 (Verkerk et al., 1991). It lies on the X chromosome at position q27.3 (Verkerk et al., 1991). This site is constricted and prone to breakage in FX individuals, and therefore termed "fragile X site" (Verkerk et al., 1991). In the 5' untranslated region of *FMR1* is a trinucleotide CGG repeat. It is common to have around 30 trinucleotide repeats. However, individuals with FXS have an expansion of the length of CGG repeats over 200, which is referred to as the full mutation (**Fig.1.1**). This leads to a heavy methylation of *FMR1*, its transcriptional silencing and to the loss or deficiency of its protein product, the fragile X protein (FMRP) (Coffee et al., 1999; Sutcliffe et al., 1992; Pieretti et al., 1991). The prevalence of the full *FMR1* mutation is estimated to be 1 in 5000 in males, and between 1 in 4000 and 1 in 8000 in females (Hagerman et al., 2017).

It is also possible to have an intermediate length of trinucleotide expansion, between 55 and 200 CGG repeats (Hagerman et al., 2017; Bassell and Warren, 2008). Those individuals are premutation carriers. Premutation alleles are unstable during meiosis, and tend to expend in length with each generation, increasing the chance of having a full mutation in later generations. Premutation carriers do not have FXS but can present different phenotypes. They can develop fragile X associated tremor ataxia syndrome (FXTAS), a neurodegenerative condition (Hagerman and Hagerman, 2007), or fragile X associated premature ovarian insufficiency (FXPOI), which causes ovarian dysfunction and early menopause (Hagerman and Hagerman, 2007).

1.2.2 Preclinical models of FXS

The *FMR1* gene is highly conserved across species (Verkerk et al., 1991; Ashley et al., 1993), rendering it possible to investigate the pathophysiology of FXS using animal models.

A mouse model of FXS was the first preclinical model of FXS to be developed (Bakker et al., 1994). Since then, other models have been developed including rat

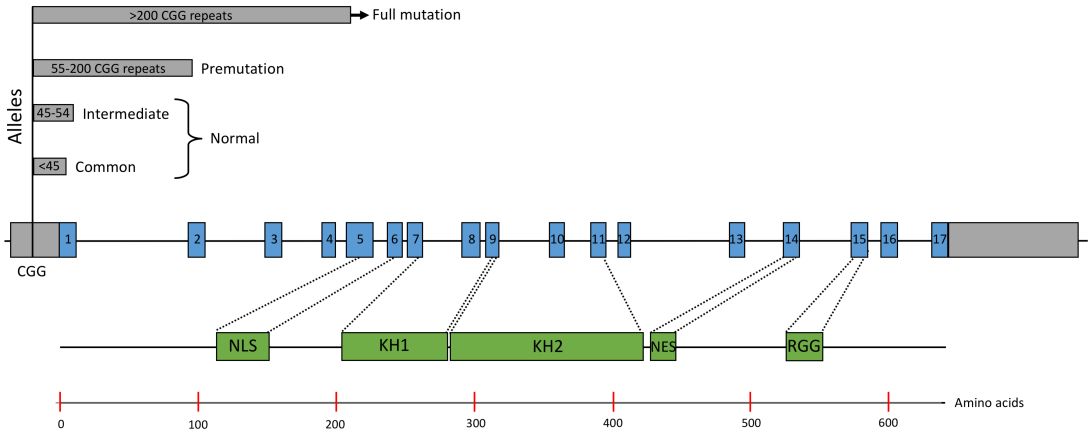


Figure 1.1: *FMR1* Protein and Gene. (Top) *FMR1* gene, with exons shown in blue and untranslated regions shown in grey. The CGG repeats lie in the 5' untranslated region, and can vary in length. A length of <45-54 repeats is normal, a length of 55-200 repeats is a premutation allele, and a length over 200 repeats is a full mutation, as indicated. (Bottom) *FMR1* protein domains: nuclear localisation signal (NLS) domain, hnRNP-K-homology (KH) 1 and 2 domains, nuclear export signal (NES) domain arginine-glycine-glycine (RGG box) domain. Figure based on information from Bassell and Warren (2008)

models (Engineer et al., 2014; Till et al., 2015; Tian et al., 2017; Asiminas et al., 2019), a *Drosophila* model (Drozd et al., 2018) and a zebrafish model (den Broeder et al., 2009).

1.2.2.1 Mouse models of FXS

Mice and humans share 99% of their genes (Waterston et al., 2002). The *FMR1* gene is highly conserved between mice and humans, with 97% of the amino acid sequence being conserved (Ashley et al., 1993). FMRP expression in the brain is also comparable in mice and in humans (Bakker et al., 2000).

Since FXS results from the absence of FMRP, the first strategy to create a mouse model of FXS was to knockout the *Fmr1* gene (Bakker et al., 1994). This contrasts with humans where the loss or deficiency of FMRP results from the expansion of the CGG repeat in the 5' region of the *FMR1* gene. The significance of this difference is that while *Fmr1* knockout mice never have any FMRP, FX individuals do during the first weeks of prenatal development, before *FMR1* is epigenetically silenced (Sutcliffe et al., 1992; Iida et al., 1994). Moreover, some individuals may present with a mosaic pattern of *FMR1* inactivation and might still have some residual full-length mRNA and proteins (Kaufmann et al., 1999; Loesch et al., 2004; Tassone et al., 2001).

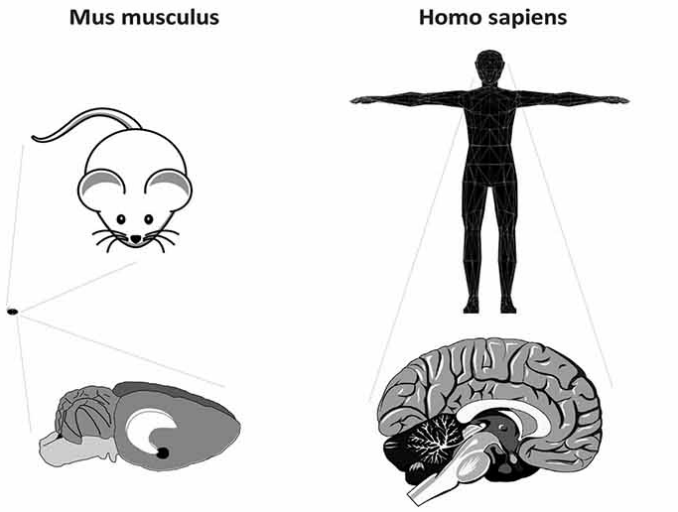
To overcome this discrepancy, a knock-in mouse model of FXS with the human CGG expansion was developed (Bontekoe et al., 1997; Lavedan et al., 1997; Fleming et al., 2003; Entezam et al., 2007; Ludwig et al., 2014). However, this did not render the *Fmr1* gene unstable or lead to its hypermethylation and transcriptional silencing (Bontekoe et al., 1997; Lavedan et al., 1997; Fleming et al., 2003), and did not produce any behavioural impairments (Ludwig et al., 2014; Entezam et al., 2007), which would suggest that expansion of CGG repeat to a length of 200-350 repeats does not represent a full mutation situation in mice contrary to humans. Thus, a different mechanism seems to govern *FMR1* inactivation in human and mice.

Despite the fact that the epigenetic silencing of *Fmr1* cannot be modelled in mice, *Fmr1*-knockout mice recapitulate many of the biochemical phenotypes of FXS and partly recapitulate behavioural phenotypes (**Fig. 1.2 and Table 1.1**) (Dahlhaus, 2018).

1.2.2.2 Rat models of FXS

The evolutionary distance between mice and humans might be the cause of the poor recapitulation of the genetics and of some FXS behaviours in the mouse model. The development of genetic engineering has made it possible to precisely edit the genome of animals. Thus several groups have developed rat models of FXS to investigate the pathophysiology of the disorder in another mammalian model (Engineer et al., 2014; Till et al., 2015; Tian et al., 2017). Specifically, an *Fmr1* knockout rat (Engineer et al., 2014; Till et al., 2015; Asiminas et al., 2019) and an *Fmr1* exon 4 knockout rat were developed (Tian et al., 2017).

Till et al. (2015) found that key synaptic and cellular phenotypes that had been identified in *Fmr1* knockout mice were also seen in *Fmr1* knockout rats (**Table 1.1**), demonstrating the cross-species validity of those phenotypes associated with loss of FMRP, and the potential relevance for the human disorder. However, species specific differences were apparent when looking at behavioural phenotypes (**Table 1.1**) (Till et al., 2015), suggesting that similar cellular phenotypes of FXS express themselves differently in different species.



	Mouse: Fmr1$^{-/y}$		Man: FXS
Genetics	gene disrupted		transcriptional silencing
	premature stop		expansion of repeats
Silencing	no hypermethylation up to 300 repeats		hypermethylation causes heterochromatin formation starting at app. 200 repeats
Background	inbred		not inbred
Transcript	aberrant		present prior to silencing
FMRP	no protein present		lost, reduced and/or mosaic rare: mutations in the protein
FMRP Identity	97%		100%
Network Activity	enhanced excitability, mainly in the cortex		not well studied yet, evidence for increased and decreased activity
Behaviour	a broad spectrum with high variability		a broad spectrum with high variability
Cognition	variable results		selective impairments
Sociality	mixed results		decreased active social contact
Communication	impaired		cluttered speech
Aggression	no aggression despite similar mechanisms		increased
Epilepsy	seizures are consistently observed in the audiogenic seizure paradigm		seizure activity is highest during adolescence and decreases after the age of 20

Figure 1.2: A comparison between individuals with FXS and the mouse model of FXS. This figure highlights the main differences between the mouse model of FXS and affected individuals. The epigenetic silencing of the CGG repeat expansion cannot be modelled in mice. The biochemical phenotypes of FXS are well conserved, although the resulting behaviours are expressed differently across the two species. Figure taken from Dahlhaus (2018), distributed under the terms of the Creative Commons Attribution License (CC BY).

	Fmr1 KO mouse	*Fmr1* KO rat	
Genetics	Gene disrupted Premature stop	Gene disrupted Premature stop	[1]
Background	Inbred	Outbred	[2]
FMRP	No protein	No protein	[1,3]
Molecular	Increased hippocampal basal protein synthesis	Increased hippocampal basal protein synthesis	[3,4]
Intrinsic properties	Hyperexcitability in CA1 pyramidal neurons. Hyperexcitability in BA. No changes in excitability in the mPFC	No changes in CA1 pyramidal neurons. Hyperexcitability in BA. Hypoexcitability in mPFC prelimbic-BLA projecting neurons	[5-8]
Morphology	Altered spine structure	Altered spine structure	[3,9]
Plasticity	Enhanced mGlur-LTD in the hippocampus	Enhanced mGlur-LTD in the hippocampus	[3,10]
Anxiety	Mixed results	Normal	[11-13]
Locomotor activity	Increased	Normal	[13,14]
Cognition	Normal or decreased	Impaired learning of complex associative memory tasks	[3,6, 11,15]
Sociability	Impaired in social novelty task (reduce time spent with novel mouse compared to familiar mouse), not in sociability task	Impaired in social novelty task (reduce time spent with novel mouse compared to familiar mouse), not in sociability task	[13,16]
Communication	Increased number of pup calls, but decreased specific features of vocalisation	Unknown	[17,18]
Aggressiveness	Normal	Normal	[2,20]
Seizure susceptibility	Increased for audiogenic seizures	Normal	[4]
Sensory sensitivity	Mixed results	Unknown	[11,21, 22]
Cognitive rigidity	Impaired reversal learning in the Morris water maze task	No impairment in reversal learning in the Morris water maze task	[3,23]
Macroorchidism	Present	Present	[1,13]

Table 1.1: A comparison between the *Fmr1* KO mouse and rat. This table highlights the main differences between the *Fmr1* KO mouse and rat models of FXS. The biochemical phenotypes of FXS are well conserved, although the resulting behaviours are expressed differently across the two species.
CA1: Hippocampal cornu ammonis, BA: Basal amygdala, BLA: Basolateral amygdala. [1] Bakker et al. (1994), [2] Dahlhaus (2018), [3] Till et al. (2015), [4] Osterweil et al. (2010), [5] Booker et al. (2020), [6] Olmos-Serrano et al. (2010), [7] Martin et al. (2016), [8] Jackson (2017), [9] Wijetunge et al. (2014), [10] Huber et al. (2002), [11] Peier et al. (2000), [12] Restivo et al. (2005), [13] Tian et al. (2017), [14] Michalon et al. (2012), [15] Yan et al. (2004), [16] Mines et al. (2010), [17] Lai et al. (2014), [18] Rotschafer et al. (2012), [19] Tian et al. (2017), [20] Saxena et al. (2018), [21] Renoux et al. (2014), [22] de Vrij et al. (2008), [23] Baker et al. (2010).

1.2.3 The fragile X mental retardation protein

FMR1 encodes for FMRP. It is an mRNA-binding protein, that has been found to bind approximately 4% of all mRNA in the mammalian brain (Darnell et al., 2011). It is expressed ubiquitously and is particularly abundant in the brain and in testicles. FMRP is mainly found in the nucleus and cytosol of neurons (Feng et al., 1997), but can also be located in dendrites, axons and synapses (Weiler et al., 1997; Akins et al., 2017; Greenough et al., 2002).

FMRP is composed of highly conserved domains (**Fig.1.1**): the nuclear localisation signal, the nuclear export signal and the two hnRNP-K-homology (KH) and arginine-glycine-glycine (RGG box) RNA-binding domains (Bassell and Warren, 2008).

FMRP is mainly involved in regulating mRNA metabolism. It has been found to interact with a variety of mRNAs, including several that encode proteins which have been implicated in ASD (TSC2, PTEN, Neuroligin3, Neurexin1, SHANK3 and NF1) (Darnell et al., 2011). FMRP regulates mRNA transport (Estes et al., 2008), stability (Bagni and Greenough, 2005) and translation (Zalfa et al., 2003), FMRP having been shown to be associated with actively translating polyribosomes (Khandjian et al., 2004), presumably via the KH domain. It has also been found to be involved in the stabilisation of newly transcribed mRNA (Eberhart et al., 1996), in alternative splicing (Didiot et al., 2008), in DNA damage response (Alpatov et al., 2014) and in heterochromatine organization (Tan et al., 2016), thereby controlling many steps leading to protein production.

1.2.4 The mGluR theory of FXS

FMRP synthesis is controlled by group 1 metabotropic glutamate receptors (mGluR1/5) signalling (Narayanan et al., 2008). The mGluR theory posits that many phenotypes observed in FXS are due to a hypersensitivity to mGluR1/5 signalling (Bear et al., 2004; Osterweil et al., 2010). mGluR1/5 activation elicits the synthesis of proteins at synapses. FMRP acts as a negative regulator of mRNA translation downstream of mGluR1/5. In the absence of FMRP, there is an exaggerated protein synthesis downstream of mGluR1/5 activation, which is postulated to be responsible for the synaptic pathophysiology that underlies many aspects of FXS, including increased internalization of AMPAR and enhanced mGluR-LTD (**Fig. 1.3**).

The theory therefore predicts that FXS phenotypes should be rescued by decreasing

mGluR1/5 signalling (**Fig. 1.4**) (Bear et al., 2004).

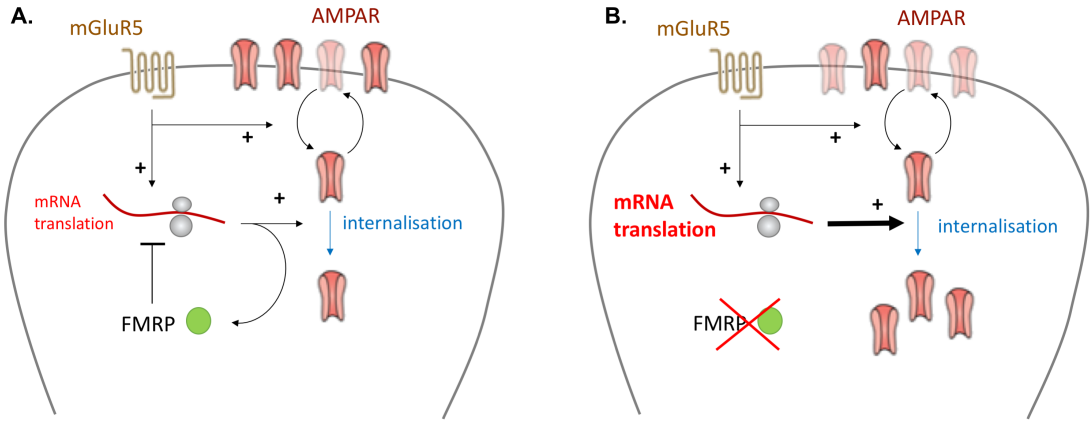


Figure 1.3: The mGluR theory of FXS. Hypersensitivity to group 1 mGluR signalling is thought to contribute to many symptoms of FXS. (A) FMRP acts as a negative regulator of mRNA translation, downstream of mGluR5 activation. mGluR5 activation also initiates the internalisation and trafficking of AMPA receptors. (B) In the absence of FMRP in FXS, loss of the translational repressor leads to increased protein synthesis and increased internalisation of AMPA receptors, leading to enhanced protein-synthesis-dependent LTD. This figure is based on information from Bear et al. (2004).

1.2.4.1 Inhibition of group 1 mGluR

Dölen et al. (2007) used a genetic strategy to assess whether down-regulation of mGluR5 signalling would improve FXS phenotypes. To test that, they crossed *Fmr1* knockout mice with *Grm5* knockout mice to generate *Fmr1* knockout mice with a 50% reduction in mGluR5 expression. Reduction of mGluR5 expression rescued dendritic spine density, increased basal protein synthesis, inhibitory avoidance extinction, increased sensitivity to audiogenic seizures and accelerated growth in *Fmr1* knockout mice (Dölen et al., 2007). However, macroorchidism was not rescued by the *Fmr1* knockout/*Grm5* heterozygote cross (Dölen et al., 2007). Similarly, a genetic approach to reduce mGluR5 expression was taken in a *Drosophila* model of FXS (Pan and Broadie, 2007; Pan et al., 2008; Repicky and Broadie, 2009), which was found to partially rescue several altered phenotypes in the *Drosophila* model of FXS, including decreased GluRIIB expression (Pan and Broadie, 2007), increased synaptic branching (Pan et al., 2008) and synaptic hyperexcitability (Repicky and Broadie, 2009).

It has also been reported that acute administration of mGluR5 antagonists successfully rescues a variety of phenotypes in mouse models of FXS, including increased

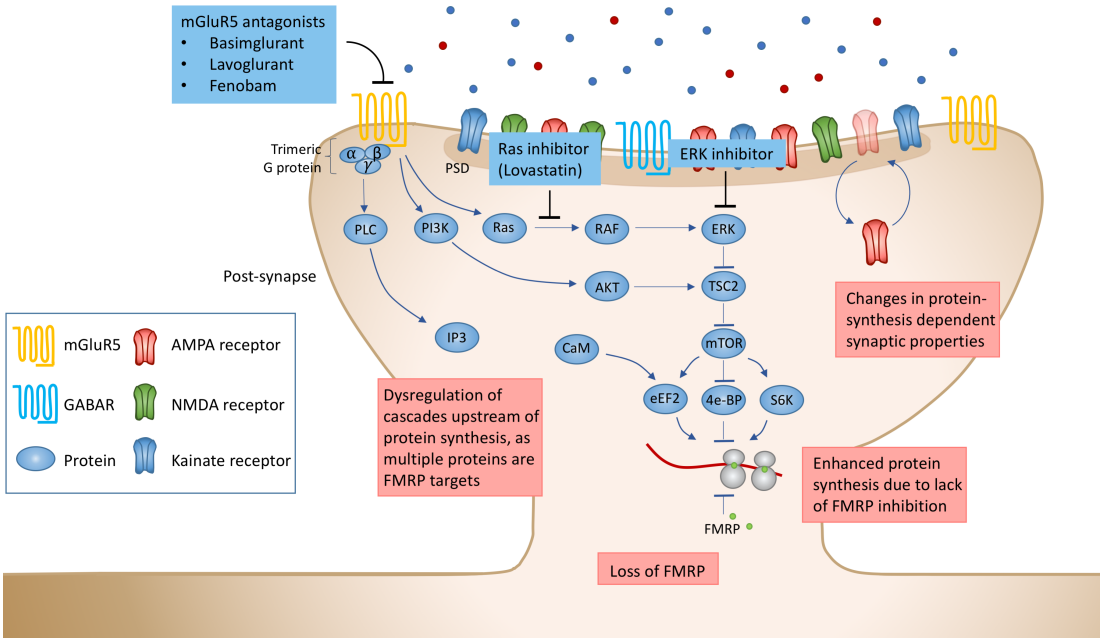


Figure 1.4: Drug targets of the mGluR5 signalling pathway in FXS. Glutamate activates multiple metabotropic and ionotropic receptors, including mGluR5. Activation of mGluR5, activates different pathways, including the Ras-ERK pathway, ultimately leading to protein synthesis. mGluR5 also acts on NMDA and AMPA receptors. FMRP acts as a mRNA translation inhibitor downstream of mGluR5. Effects of loss of FMRP are indicated in red boxes. Blue boxes show different drug targets on this pathway that have been investigated in FXS: mGluR5 antagonists, Ras signalling antagonist and ERK inhibitor. Figure based on information from Berry-kravis et al. (2018).

incidence of audiogenic seizures (Yan et al., 2005), thigmotaxis (Yan et al., 2005), hippocampal epileptiform discharge (Chuang et al., 2005), prepulse inhibition startle defects (de Vrij et al., 2008), levels of mRNA granules (Aschrafi et al., 2005), protein synthesis (Osterweil et al., 2010), dendritic filapodia density (de Vrij et al., 2008) and glycogen synthase kinase-3 activity (Min et al., 2009). Acute administration of mGluR5 inhibition was similarly shown to rescue several phenotypes in a *Drosophila* model of FXS (Mcbride et al., 2005; Bolduc et al., 2008; Chang et al., 2008; Pan et al., 2008) and in a zebrafish model of FXS (Tucker et al., 2005).

In addition, chronic treatment with AFQ056/Mavoglurant, a mGluR5 antagonist, rescued sociability behaviour (Gantois et al., 2013), and the connectivity of the somatosensory resting state network in *Fmr1* knockout mice (Zerbi et al., 2019), but not of the default mode resting state network (Zerbi et al., 2019). Michalon et al. (2012) further showed that chronic pharmacological inhibition of mGluR5 with the selective inhibitor CTEP in *Fmr1* knockout mice corrects multiple phenotypes including increased protein synthesis, enhanced mGluR-LTD, impairments in inhibitory avoidance, auditory startle response, locomotor hyperactivity, enhanced sensitivity to audiogenic seizures, dendritic spine density, as well as activity of the extracellular signal–regulated kinases (ERKs) and mammalian target of rapamycin (mTOR). They also reported a partial rescue of macroorchidism (Michalon et al., 2012).

1.2.4.2 Inhibition downstream of mGluR5

Since mGluR1/5 activation leads to increased ERK1/2 activation, Osterweil et al. (2010) hypothesised that inhibition of ERK1/2 could also rescue FXS phenotypes (**Fig. 1.4**). They showed that inhibition of ERK1/2 rescued excessive protein synthesis and audiogenic seizures in *Fmr1* knockout mice (Osterweil et al., 2010).

In a subsequent study, Osterweil et al. (2013) demonstrated that lovastatin, a Ras signalling inhibitor upstream of ERK1/2 activation (**Fig. 1.4**), could also rescue *Fmr1* knockout mouse phenotypes. Lovastatin restored excessive protein synthesis, epileptiform activity, visual cortex hyperexcitibility and the incidence of audiogenic seizures (Osterweil et al., 2013).

Lovastatin was also shown to be effective in improving cognitive phenotypes in *Fmr1* knockout rats (Asiminas et al., 2019). Asiminas et al. (2019) showed that chronic

treatment with lovastatin restored the normal development of associative memory tasks, as well as basal protein synthesis and long-term potentiation deficit. Interestingly, these changes were sustained over time, and persisted 15 weeks after the end of treatment (Asiminas et al., 2019).

In contrast, lovastatin was found to be unable to restore increased gamma power present in *Fmr1* knockout mice (Goswami et al., 2019) or the exaggerated instrumental extinction of *Fmr1* knockout mice (Sidorov et al., 2014).

1.2.4.3 Clinical trials

A number of clinical trials have been carried out to assess the therapeutic efficacy of compounds targeting the mGluR5 signalling pathway (Reviewed in Erickson et al. (2017), Berry-kravis et al. (2018)). Three mGluR5 inhibitors were tested in adults and adolescents with FXS: fenobam, basimglurant (RO4917523) and mavoglurant (AFQ056).

An initial pilot study on fenobam reported improvement in prepulse inhibition in 50% of FX individuals (Berry-Kravis et al., 2009), however the manufacturing company failed financially and further studies were discontinued. Three placebo controlled trials evaluating mavoglurant were completed in FXS. All three studies failed to show any drug improvement in their primary outcome measures (Jacquemont et al., 2011; Berry-Kravis et al., 2016). Similarly, basimglurant did not show any sign of therapeutic efficacy.

In addition, an open-label study and a randomized, double-blind trial were undertaken to assess the safety and efficacy of lovastatin in FXS (Caku et al., 2014; Thurman et al., 2020). The open-label study showed significant improvement in aberrant behaviour, their primary outcome measure, and in 12 secondary outcome measures (Caku et al., 2014). However, the follow-up randomized controlled trial failed to replicate these findings and did not show any clear benefit of lovastatin over placebo (Thurman et al., 2020). Ongoing clinical trials on lovastatin (NCT02680379 and NCT02998151) might help shed light on this discrepancy.

The failure of clinical trials despite promising preclinical findings, might be due to species differences. However, differences in the age of participants might also be underlying it; the preclinical studies largely used juvenile animals that had not yet

reached sexual maturity, while clinical trials were done in adults and adolescents. The discrepancy could also be explained by a difference in the duration of treatment and of the outcome measures selected. In addition, behavioural outcomes were dependent on parental report, which resulted in a strong placebo response. The use of quantifiable outcome measures would help limit the placebo effect. The translation of therapeutic compounds identified in preclinical studies to the clinics might also be generally improved through methods that can be applied in a similar way to animal models and affected individuals, such as magnetic resonance imaging.

1.3 Magnetic Resonance Imaging

Magnetic resonance imaging (MRI) is a non-invasive imaging technique that is widely used in a clinical and research setting. MRI can be used to look at the structure of different body parts, as well as to investigate brain function and connectivity.

1.3.1 MRI scanner

An MRI scanner is composed of several parts. It is necessary to understand the function of each component in order to understand the mechanism through which an MR image is acquired. I have summarized the main points below; for an in-depth account, see Currie et al. (2013); Dale et al. (2015).

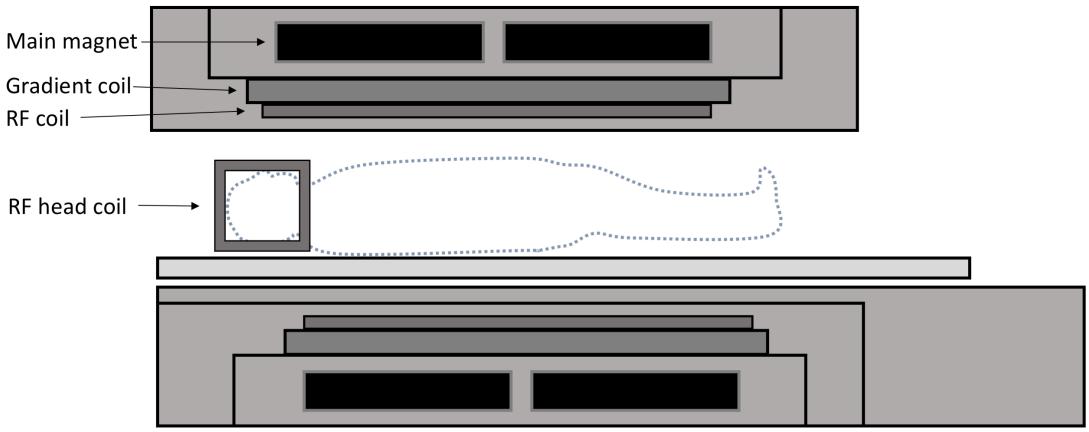


Figure 1.5: Position of the different coils within a MRI scanner. The different coils lie in concentric order from one another. The main magnet is situated the furthest away from the subject, then lie the gradient coils and the RF coils. Finally, a RF head coil is used in neuroimaging. Figure is based on information from Currie et al. (2013).

1. **Main magnet.** The subject of an MRI experiment is exposed to strong constant magnetic field (B_0) that is generated by a main magnet (**Fig. 1.5**). The strength of the magnet is measured in Tesla (T). One Tesla is equivalent to approximately 20 000 times the earth's magnetic field. Preclinical scanners usually use a stronger magnet than clinical scanners.

2. **Gradient coils.** The direction of the magnetic field is defined by a set of coordinates (x,y,z). Gradient coils of three orthogonal directions lie in concentric order to each other within the main magnet (**Fig. 1.5**). Each gradient coil generates a magnetic field in the same direction as B_0, the strength of which decreases with position along the x, y or z direction, depending on the gradient coil used. This results in the main magnetic field varying in strength along one of the orthogonal directions selected (**Fig. 1.6**).

3. **Radiofrequency coils.** Radiofrequency (RF) coils also lie concentric to the gradient coils and to the main magnet (**Fig. 1.5**). They are responsible for exciting the tissue of interest, by transmitting RF energy to it, and for receiving the induced RF signal back. For neuroimaging, a RF head coil is usually used to maximize the brain RF signals detected. RF gradients also allows the MR signal to be spatially localised. The signal received by a RF coil is digitised and encoded under the form of a graphic matrix called k-space, which will be converted to a MR image following a Fourier transform.

4. **Shim coils.** A homogeneous B_0 field is required for the effective localisation of the MR signal. Placing a subject within the scanner disrupts the homogeneity of B_0. Improvement of the homogeneity of the magnetic field can be achieved through shimming.

1.3.2 Obtaining MR signals

The MRI signal originates from hydrogen protons. Protons generate their own magnetic field, behaving like small magnets. Under B_0, protons will align themselves either with the magnetic field (parallel), which requires the least energy, or against it (antiparallel). In addition, B_0 will cause the proton to precess, that is to spin around an axis. Protons precessing parallel and antiparallel to B_0 will cancel each other out.

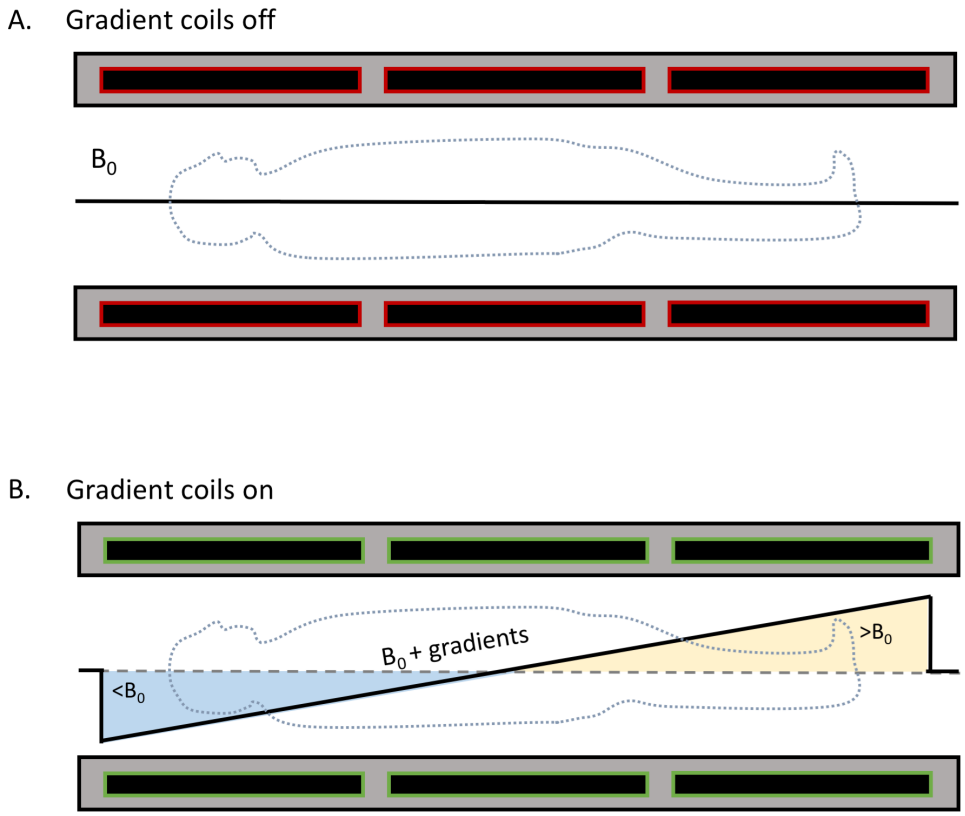


Figure 1.6: Gradient coils magnetic field. (A). When gradient coils are turned off (shown in red on the figure), the magnetic field is produced only by the main magnet (B_0). (B) When the gradient coils are turned on (shown in green on the figure), they generate a magnetic field of varying intensity along the x,y or z axis, depending on the coils direction. The resulting magnetic field (B_0 + gradients) therefore vary along the x, y or z axis. In the situation depicted in this figure, the resulting magnetic field strength is lower than B_0 towards the head of the person being scanned (blue), and reaches a strength higher than B_0 towards his feet (yellow).

Since more protons will align with the state of least energy, parallel to B_0, it results in a magnetic field parallel to B_0, called longitudinal magnetisation.

RF pulses, emitted by the RF gradients, can then be activated, which will transfer energy to the protons and enable them to move antiparallel to B_0, in a state of higher energy. Here again, protons will cancel each other out, resulting in a decreased longitudinal magnetisation. RF pulses also cause protons to move in phase, the result of which is a new magnetisation in the x-y plane, the transverse magnetisation. This is the source of an MR signal. A receiving coil picks up the electric current generated by the transverse magnetisation vector, forming the MR signal.

When RF pulses are switched off, the protons return to a state of lower energy. This process is called relaxation. There are two simultaneous and independent relaxations: the relaxation of the transverse magnetisation (T2 relaxation) and of the longitudinal magnetisation (T1 relaxation) (Currie et al., 2013).

The MR signal is greatest just after deactivating the RF pulse, and then decreases as the relaxations occur. It is common practice to measure an MRI signal in the form of an echo, either a spin echo (SE) or a gradient echo (GRE).

1.3.3 Pulse sequences

A pulse sequence is the set of instructions given to the MRI scanner hardware to obtain an MRI image.

1.3.3.1 Spin Echo

SE sequences typically have two RF pulses, an excitation pulse, that excites the protons, and a refocusing pulse, which rephases the protons (**Fig. 1.7**). The rephasing of the protons results in a temporary increase in the MRI signal at time echo time (TE), termed spin echo (Currie et al., 2013).

In a SE pulse sequence, one line of imaging data, that is one line of k-space, is acquired per RF excitation. The SE sequence needs to be repeated multiple time to collect the whole imaging data and fill the k-space (Poustchi-Amin et al., 2001).

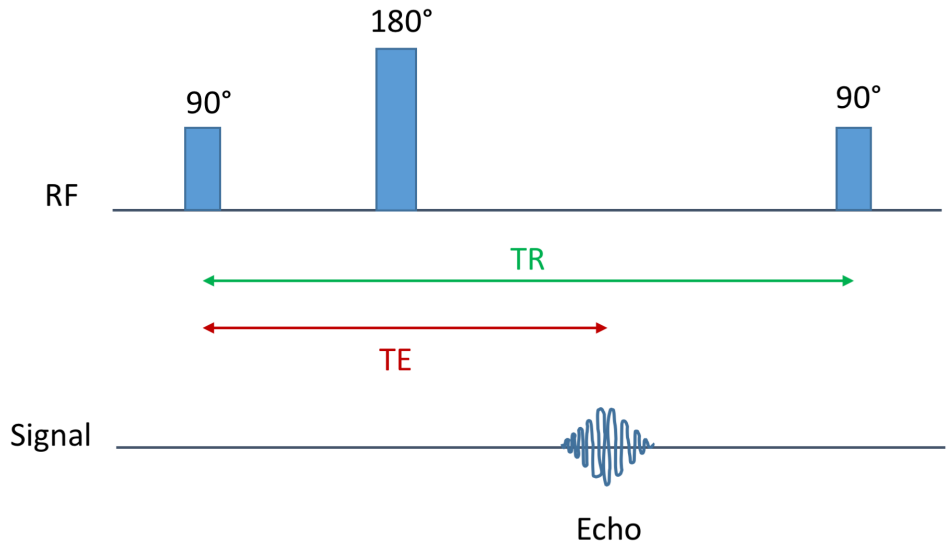


Figure 1.7: Spin Echo pulse sequence. SE sequences commonly have a 90° excitation RF pulse and a 180 ° refocusing RF pulse. Signal maximum (echo) is found at time equals TE. The time between two excitation RF pulses is the TR.

1.3.3.2 Gradient Echo

GRE sequences do not use a 180° refocusing pulse. Instead, the echo is generated through a gradient reversal (**Fig. 1.8**) (Currie et al., 2013). The first gradient application de-phases the signal. The application of a second gradient with a slope of equal amplitude but opposite direction causes the proton to rephase, and the signal to increase to a maximum called gradient echo at TE (Currie et al., 2013).

Similarly to a SE sequence, a GRE sequence only acquires one line of the k-space at a time and needs to be repeated to acquire the whole imaging data (Poustchi-Amin et al., 2001).

1.3.3.3 Fast techniques

In contrast to the conventional GRE and SE pulse sequences, fast imaging techniques such as Echo-planar Imaging (EPI) encode multiple lines of k-space per RF pulses (Poustchi-Amin et al., 2001). In EPI, multiple GREs are generated during a TR, the amount of time between two RF pulses, through the rapid oscillation of gradients (Currie et al., 2013).

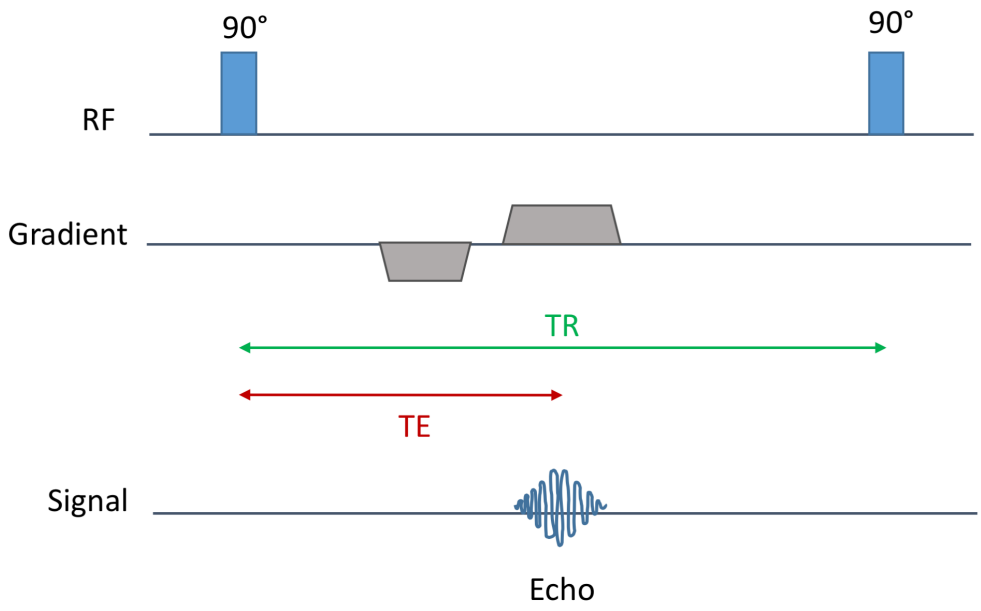


Figure 1.8: Gradient Echo pulse sequence. GRE sequences commonly have a 90° excitation RF pulse (shown in blue), followed by a gradient reversal (shown in grey). Signal maximum (echo) is found at time equals TE. The time between two excitation RF pulses is the TR.

1.4 Functional MRI

Functional MRI (fMRI) is a non-invasive imaging method based on MRI that has been widely used to study brain function. Brain activation can be elicited by a specific event (task-based fMRI) or by intrinsic brain processes (resting-state fMRI).

1.4.1 The hemodynamic brain response

Increased neuronal activity, such as when a brain region is recruited to perform a cognitive task, results in a local increase in energy requirement (Glover, 2011). Energy, in the form of adenosine triphosate (ATP), is produced by the glycolytic oxygenation of glucose. During high neuronal activity, local oxygen stores are depleted and waste products of glycolysis build up (Kim et al., 2008). In response, blood vessels dilate and blood flow increases to restore oxygen levels (Kim et al., 2008). However, more oxygen is delivered than is required to offset the deficit, resulting in a net surplus of oxygenated haemoglobin and a reduction of deoxygenated haemoglobin (**Fig. 1.9**) (Kim et al., 2008).

Increase in neuronal activity therefore results in two parallel responses: an increase

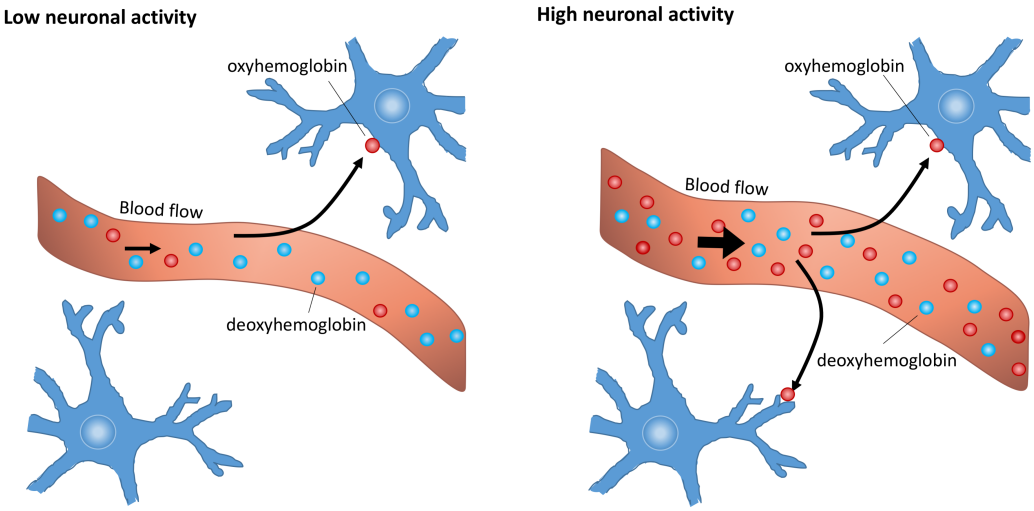


Figure 1.9: The hemodynamic brain response. High neuronal activity locally increases the requirement in energy and oxygen. The blood vessels dilate in response, and blood flow increases to restore oxygen and glucose levels. However, more oxygenated haemoglobin is delivered than needed to offset the deficit, resulting in an increase in the ratio of oxygenated haemoglobin (red) to deoxygenated haemoglobin (blue). Neurones are shown in dark blue.

in cerebral blood flow (CBF) and an increase in oxygenated haemoglobin. Both can be detected by MRI; changes in CBF can be detected by the arterial spin labelling (ASL) technique (Detre et al., 1992) or using a contrast agent (Belliveau et al., 1991), and blood oxygenation by the blood oxygen level dependent (BOLD) contrast (Ogawa et al., 1990). ASL is less sensitive and requires a longer acquisition time than the BOLD contrast (Glover, 2011). In addition, it is more sensitive to motion (Glover, 2011). As a consequence, the BOLD contrast is predominantly used in fMRI.

1.4.2 The BOLD contrast

Ogawa et al. (1990) first reported that it was possible to map brain function using BOLD contrast. Oxygenated haemoglobin is diamagnetic and cannot be magnetically distinguished from brain tissue that is also diamagnetic, while deoxygenated haemoglobin is paramagnetic (Ogawa et al., 1990). The local change in the ratio of oxygenated haemoglobin to deoxygenated haemoglobin in an activated brain region is therefore accompanied by a change in paramagnetic content (Ogawa et al., 1990), the strength of which is proportional to the change in haemoglobin concentration. In turn, changes in paramagnetic susceptibility influences T2 and T2* (Kim et al., 2008), to which pulse

sequences are sensitive. The evaluation of differences in fMRI image intensity over time can therefore reveal neuroanatomical markers of brain activity (Ogawa et al., 1990).

1.5 Resting state fMRI

fMRI has been the first and most widely used imaging technique to study brain activity at rest. This method, known as resting state fMRI (rsfMRI), is based on the temporal correlation of low-frequency BOLD signal fluctuation between different voxels of the brain at rest, which creates a pattern of functionally connected brain regions.

The presence of low frequency fluctuation in the BOLD signal had been noted since the inception of fMRI, but it was not until 1995 that its possible link to neuronal activity was noted (Biswal et al., 1995). Biswal et al. (1995) were interested in the background noise in the BOLD signal. They noticed temporally correlated fluctuation in large-amplitude spontaneous low-frequency BOLD signal between voxels in the brain that are part of the somatosensory cortex, both within and across hemispheres. The voxels identified were found to be highly similar to those activated during a finger tapping fMRI task. The functionally connected brain regions identified formed a network, that was later defined as the somatomotor network, a resting state network involved in sensory and motor functions.

1.5.1 Why study the brain at rest?

The motivation for looking at the brain's activity in the absence of a task comes from its energy consumption. The brain consumes 20% of the body's total energy, despite accounting for only 2% of the total body mass (Rolfe and Brown, 1997). However, its consumption increases by less than 5% during task performance, indicating that the majority of the brain's energy is being used by intrinsic neuronal activity (Petersen et al., 1988; Sokoloff et al., 1955). It has also been shown that neurotransmitter recycling accounts for the majority of the brain's energy expenditure (Attwell and Laughlin, 2001). These findings suggest that most of the brain's activity is intrinsic, highlighting the importance in term of overall brain function to look at its activity at rest.

In addition, individuals are scanned while at rest in resting state experiments. This means that participants do not need to learn and execute a task while in the scanner, which can be challenging for some clinical or paediatric populations, allowing for a wider

range of individuals to be studied using a resting state protocol than a task-based one (Smitha et al., 2017).

1.5.1.1 Task based *vs* resting state fMRI

Task-based fMRI is used to investigate modulations in the BOLD signal underlying a specific cognitive process elicited by a visual, auditory or other task (Glover, 2011). Typically, there are 2 conditions in an experiment; an experimental condition during which the task is performed and a control condition (Glover, 2011). The trial alternates between the control and experimental conditions, with the aim of identifying differences between the two states (**Fig. 1.10A**) (Glover, 2011). Participants' cooperation is therefore essential in task-based fMRI, as they need to understand the task they need to perform, learn it and perform it in the scanner (Smitha et al., 2017). Poor performance of the task will affect the results obtained. In addition, longitudinal task-based fMRI experiments will induce a familiarisation with the task, which can impact results (Smitha et al., 2017). As brain activation is specific to the task in task-based fMRI, the imaging dataset obtained in a session cannot be reused to investigate another brain function in the same population (Smitha et al., 2017). In task-based fMRI most of the BOLD signal is discarded as noise, focusing on very specific signal. However, because that event is time-locked, one can predict when to look for brain activation, facilitating its detection.

In contrast, resting-state fMRI is used to investigate spontaneous fluctuation in the BOLD signal in the absence of any explicit tasks (**Fig. 1.10B**) (Fox and Raichle, 2007; Raichle, 2010). The BOLD signal that is discarded in a task-based fMRI experiment is the basis of resting-state analysis (Smitha et al., 2017; Fox and Raichle, 2007). As no tasks need to be performed, paediatric individuals, individuals with an ID and even individuals in vegetative and coma state can take part in a resting-state experiment (Smitha et al., 2017), the only requirement is for them to be able to lay sufficiently still in the scanner for the duration of the scan. Longitudinal experiments can be carried out as there is no risk of familiarisation with the task (Smitha et al., 2017). Additionally, the dataset can be analysed multiple times to look at different brain functions (Smitha et al., 2017).

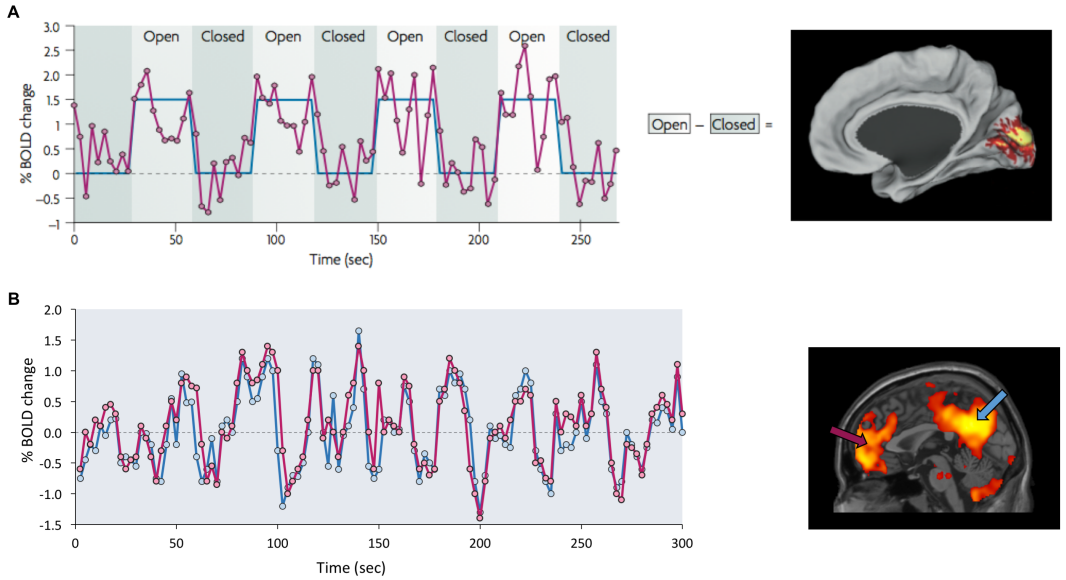


Figure 1.10: Task based *vs* resting state fMRI. (A) BOLD signal timecourse (fushia) during a visual task, during which the participant is asked to open (white) and close (light blue) his eyes at defined intervals. The BOLD signal during each condition (eyes opened or closed) can be averaged. The subtraction of the control condition (eyes closed) from the experimental condition (eyes opened) reveals the brain regions whose activity change between the two conditions (shown on the right), in this case, the visual cortex. (B) BOLD signal fluctuation over time can also be measured at rest. In fushia is shown the BOLD signal timecourse of the anterior cingulate cortex (shown by the fushia arrow on the image to the right), and in blue the posterior cingulate cortex timecourse (shown by the blue arrow on the image to the right). Correlation of the two timecourses indicates the functional connectivity of the two regions. Functionally connected brain regions will have similar timecourses and a high level of correlation, as shown here. Brain regions that are not functionally connected will have dissimilar BOLD signal timecourses and a low correlation value. Figure adapted from (Fox and Raichle, 2007).

1.5.2 Resting State Networks

Since the identification of the somatomotor network by Biswal et al. (1995), other large scale resting-state networks have been reported: the default mode network (DMN), salience network, visual network, language network, auditory network, basal ganglia network, dorsal attention network, ventral attention network and executive control network (Beckmann et al., 2005; Damoiseaux et al., 2006; Raichle et al., 2001; Zhang and Raichle, 2010). Brain regions that comprise resting state networks (RSNs) can be anatomically connected or separated, but in any case they are functionally connected, as indicated by their synchronized activity at rest (Fox and Raichle, 2007). In addition, most RSNs were found to be comprised of brain regions known to be involved in a common function, such as vision, language, attention or executive control, as suggested by their name (van den Heuvel and Hulshoff Pol, 2010; Fox and Raichle, 2007). It has therefore been hypothesized that the spontaneous synchronous neuronal activity of a resting state network may be involved in maintaining the functional systems in an active state in preparation to executing a task (van den Heuvel and Hulshoff Pol, 2010).

RSNs have been identified in multiple species, including humans, rats, mice, dogs and monkeys (Jonckers et al., 2011; Lu et al., 2012; Vincent et al., 2007; Biswal et al., 1995; Kyathanahally et al., 2015). They were found to vary with age, sex, mental state and diseases (Biswal et al., 2010; Soares et al., 2016; Song et al., 2015). Multiple clinical populations have been investigated, notably individuals with Alzheimer's disease, where the DMN activity was found to be associated with disease progression (Buckner et al., 2005). Functional connectivity of ASD has also been extensively investigated (Hull et al., 2017). Functional connectivity impairments have also been reported in dementia, major depression, schizophrenia, attention deficit/ hyperactivity disorder and multiple sclerosis (Seeley et al., 2006; Greicius et al., 2007; Liang et al., 2006; Castellanos et al., 2008; Lowe et al., 2002).

RSNs have been found to correspond to networks identified using task-based fMRI (Biswal et al., 1995). Crossley et al. (2013) performed a meta-analysis of task-related fMRI studies and created a brain co-activation matrix from it. The characteristics of the co-activation networks were analysed using graph network theory and compared to RSNs. They found that although not identical, the co-activation networks and RSNs

had a similar community structure, with brain regions found to be strongly connected in RSNs also found to be strongly connected in co-activation networks. They also had a similar modularity and rich-club organization (networks composed of a majority of nodes with few connections and of a few highly connected hub nodes) (Crossley et al., 2013).

1.5.2.1 Default Mode Network

The DMN has been by far the most widely studied RSN in both health and disease. The DMN has also been found to be highly conserved between humans, monkeys and rats (Lu et al., 2012; Vincent et al., 2007), therefore providing a good translational tool to investigate the brain's activity at rest. It is comprised of the anterior cingulate cortex (ACC), posterior cingulate cortex (PCC), precuneus, medial prefrontal cortex, and lateral parietal cortex. The entorhinal cortex is also frequently associated with the DMN.

The DMN is thought to be involved in interoception and in the continuous acquisition and evaluation of external and internal information, reflecting the brain's basal activity – or its default mode of function (Raichle et al., 2001). This has engendered a lot of interest in the DMN and its role in cognitive function and psychiatric disorders. In contrast to other networks, its activity decreases during a task, and it is consequently also called task-negative network in opposition to the other networks which are deemed task-positive (Raichle et al., 2001).

However, recent studies have challenged the idea that the DMN is not engaged during tasks. Task-based fMRI studies have reported the DMN to be involved in different cognitive functions, such as thinking about oneself (Kelley et al., 2002) and one's future (Daniel L. Schacter and Donna Rose Addis, 2007), the retrieval of episodic (Huijbers et al., 2013) and bibliographic memories (Philippi et al., 2015) and adopting another person's perspective (Mitchell et al., 2005), and while the interpretation of the DMN as processing internal information and reflecting the brain's default mode of function explain some of the DMN function reported, it fails to provide a complete account for it.

Konishi et al. (2015) have shown that the DMN is activated during tasks requiring the participant to remember the location of symbols and have therefore suggested that

the DMN might be involved in cognitive processing in situations relying on information not currently available to the senses, i.e. reliance on episodic and semantic memory, and not on perception. This alternative view of the DMN function is consistent with two prior studies (Smallwood et al., 2013; Nathan Spreng, 2012) and would explain the activation of the DMN during daydreaming, rumination and mentalizing (Konishi et al., 2015; Poerio et al., 2017). Smallwood et al. (2013) found that the activity of the mPFC and PCC increased when participant needed to recall details not currently available to perception to make a decision and decreased when the details needed were directly available to them. Similarly, Nathan Spreng (2012) observed that the DMN activation was increased during a face recognition trial involving famous faces, which relied on both working memory and episodic memory, in comparison with the anonymous face-matching condition.

1.5.2.2 Origin of Resting State Networks

The similarity between resting state and task-induced networks suggests that low frequency fluctuations in the BOLD signal might have a neuronal origin (Biswal et al., 1995; Crossley et al., 2013). However, temporal fluctuations can arise from a variety sources and not only as a direct result of neuronal activity. Several physiological processes have been shown to elicit low-frequency fluctuation in the BOLD signal, including cardiac and respiratory function (Frank et al., 2001; Lund, 2001) and autonomous hemodynamic regulation (Obrig et al., 2000). Magnetic field drift is also a known source of temporal fluctuation in the BOLD signal (Durand et al., 2001).

Support for its direct link to neuronal activity comes from the application of other techniques to investigate brain activity at rest, notably electroencephalography (EEG), magnetoencephalography (MEG) and electrophysiology. These electrophysiological techniques measure voltage changes (EEG and electrophysiology) and magnetic changes (MEG) resulting from ionic current produced by discharging neurons and can therefore give us insight on the neuronal origin of the spontaneous brain activity observed.

A number of studies have looked at the electrophysiological signature of BOLD signal fluctuations. They seem to agree that the BOLD signal is driven by slow fluctuations in neuronal activity, however there is a debate concerning the carrier band contributing to it. Electrophysiological studies point to a direct correlation between BOLD signal

and gamma activity (Leopold et al., 2003; Nir et al., 2008; Shmuel and Leopold, 2008), while EEG and MEG studies suggest a correlation with fluctuations in the alpha and beta frequency range (Greicius et al., 2003; Laufs et al., 2003; Mantini et al., 2007). However, these findings are not necessarily contradictory. Since high and low frequencies are negatively correlated, BOLD signal might be driven by both gamma-band during an increase in metabolic rate, and alpha/beta-band oscillations during a decrease in metabolic rate (Scheeringa et al., 2011).

If the fMRI BOLD signal is an accurate representation of neuronal activity, similar RSNs than seen using fMRI should also be observed using these other imaging techniques. Brookes and colleagues (2011) performed an independent component analysis on frequency-filtered MEG data and obtained similar RSNs to those obtained in fMRI studies, supporting the idea that the BOLD signal is driven by neuronal activity. The RSNs identified in this study were mainly linked to fluctuations in the beta frequency range (Brookes et al., 2011).

DTI studies also support the neuronal origin of RSNs. Several groups have investigated the link between structural and functional connectivity with the idea that if RSNs truly reflect functional connection between brain regions, those brain areas should also be structurally connected to support communication. DTI studies found that functional connectivity reflects the underlying structural connectivity (Greicius et al., 2009; Honey et al., 2009; van den Heuvel et al., 2009; Koch et al., 2002). It is however worth pointing out that while the strength of structural connectivity can predict the functional strength, the reverse is not necessarily true (Honey et al., 2009; Koch et al., 2002).

1.5.2.3 Reliability of Resting State Networks

One advantage of rsfMRI is that the absence of a task enables the use of the same protocol in participants regardless of the presence of chronic conditions or disabilities, which is interesting for the study of clinical populations. However, it is crucial to assess the test-retest reproducibility of RSNs and the variation between individuals before using rsfMRI as a biomarker for disease progression or therapeutic efficacy.

Several studies have looked at test-retest reproducibility, with sessions being separated by short (<45min) (Zuo et al., 2010; Shehzad et al., 2009), moderate (1 week to 1 month) (Chen et al., 2015; Damoiseaux et al., 2006) and long intervals (5 months to

1.5 years) (Zuo et al., 2010; Choe et al., 2015; Laumann et al., 2015; Chou et al., 2012; Shehzad et al., 2009). RSNs were reported to have a moderate-to-high test-retest reproducibility when looking at a single subject (Zuo et al., 2010; Choe et al., 2015; Chen et al., 2015; Chou et al., 2012; Laumann et al., 2015; Shehzad et al., 2009; Damoiseaux et al., 2006) and at group-level RSNs (Choe et al., 2015; Laumann et al., 2015; Damoiseaux et al., 2006). The DMN was also found to be highly reproducible (Chou et al., 2012). Inter-subject variability was observed to be greater than the between-session variability (Zuo et al., 2010; Chen and Glover, 2015; Chou et al., 2012; Laumann et al., 2015). Choe et al. (2015) also reported a high reproducibility of between-network connectivity at the subject level across sessions.

In addition to between-sessions variability, several studies have looked at reliability of rsfMRI data across groups, scanners and sites. Two studies found the topographical organisation of cortical hubs to be consistent across datasets, and therefore reliable across groups of individuals (Buckner et al., 2009; He et al., 2009). Biswal et al. (2010) reported consistent pattern of functional connectivity across 20 centres. Sites-induced variability was also found to be low in a study by Marchitelli et al. (2016).

Together these studies point to a high level of reliability over time within an individual, but to a lower between-individual reliability. They further show that although the same RSNs can be identified across individuals, voxels forming the networks are not systematically recruited in every individual and at every session, demonstrating the personalised and highly dynamic nature of the RSNs (Damoiseaux et al., 2006; Choe et al., 2015).

1.5.3 Considerations for resting state studies in preclinical animal models

1.5.3.1 Anaesthesia

Anaesthesia is typically used in preclinical rsfMRI studies to minimize movement and distress to the animals. However, anaesthesia has been shown to influence neural processing and the brain vasculature, which in turn impact the BOLD signal and therefore the RSNs obtained (Bukhari et al., 2017; Grandjean et al., 2014; Masamoto and Kanno, 2012). To remove this confounding factor, some groups are developing protocols to perform awake rsfMRI studies (Becerra et al., 2011; Liang et al., 2011,

2012; Upadhyay et al., 2011). Nevertheless, it is possible to identify RSNs under anaesthesia in human, monkey, mice and rats (Palanca et al., 2015; Jonckers et al., 2011; Lu et al., 2012; Vincent et al., 2007) and under light sleep in human (Horovitz et al., 2008; Larson-prior et al., 2009), although the strength of the RSNs varies with the level of consciousness (You et al., 2013).

1.5.3.2 Maintaining stable physiology

In contrast to task-based studies with predictable neuronal responses, rsfMRI experiments are based on spontaneous neuronal activity. It is therefore not possible to remove noise by averaging stimulation-evoked periods of activity. As physiological processes can also induce fluctuations in the BOLD signal (Frank et al., 2001; Lund, 2001; Obrig et al., 2000), it is crucial to maintain stable physiological conditions in order to improve the reproducibility of the study.

Experimental groups of animals should be consistent in strain, sex, age, weight, diet and housing conditions (Hildebrandt et al., 2008). In addition, physiological conditions should be monitored and maintained within a defined range to the extent possible. This includes controlling body temperature, respiratory cycle, cardiac rates, blood oxygenation and anaesthetic dose, which have all been shown to contribute to rsfMRI signal (Frank et al., 2001; Lund, 2001; Wu et al., 2016; Grandjean et al., 2014; Vanhoutte et al., 2006). It is good practice to record and time-lock these physiological parameters during scanning so that they can be removed during the preprocessing of functional images.

When comparing groups of animals, it is important to show that differences in functional connectivity are not driven by physiological processes, by demonstrating that there are no between-group difference in physiological parameters.

1.6 Functional connectivity in ASD/ID

Imaging techniques have been widely used to study ASD, both during tasks and at rest. Resting state analyses are particularly interesting for the study of ASD, as patients might find it challenging to learn a task and to remain still in the scanner for a long period of time.

1.6.1 Resting state studies in individuals with idiopathic ASD

Resting state studies have reported a decrease in functional connectivity in ASD individuals of average intellectual ability at the whole-brain scale (Anderson et al., 2011; Balsters et al., 2016; Barttfeld et al., 2012; Dinstein et al., 2011; Ebisch et al., 2011; Gotts et al., 2012; Guo et al., 2017; Hahamy et al., 2015; Iidaka, 2014; Itahashi et al., 2014; Jones et al., 2010; Lai et al., 2010; Lee et al., 2016; Long et al., 2016; Rudie and Dapretto, 2013; Spisak et al., 2014; Washington et al., 2014), supporting the underconnectivity theory of ASD (Just et al., 2004). This theory, originating from functional connectivity analysis of task-based fMRI, proposes that ASD results from a deficit in the integration of information, due to impaired integrative circuitry. It predicts that cognitive deficits in ASD are likely to be apparent during tasks requiring integration of information and coordination between brain regions (Just et al., 2004).

Reports of underconnectivity also arise from network-specific analyses of functional connectivity. The DMN has been by far the most studied network in ASD, and the majorities of studies have reported a decrease in functional connectivity in this network (Barttfeld et al., 2012; Jung et al., 2014; Kennedy and Courchesne, 2008a; Nebel et al., 2014; Starck et al., 2013; Weng et al., 2009; Ypma et al., 2016) and in the brain regions that compose it (Assaf et al., 2010; Eilam-stock et al., 2014; Jung et al., 2014; Kennedy and Courchesne, 2008b; Lynch et al., 2012; Murdaugh et al., 2012). Although some have reported an increase in connectivity when using the PCC as a seed region (Eilam-stock et al., 2014; Lynch et al., 2012; Monk et al., 2009).

Underconnectivity has also been reported in other brain networks, notably in the language network (Dinstein et al., 2011; Verly et al., 2014), in regions involved in emotional awareness (Ebisch et al., 2011), in the social brain (Gotts et al., 2012) and in the amygdala circuitry (Guo et al., 2016; Shen et al., 2016).

Conversely, some studies have found evidence of whole-brain overconnectivity in ASD individuals of average intellectual ability (Cerliani et al., 2017; Delmonte et al., 2013; Supekar et al., 2013; Uddin et al., 2013). However, most were specifically studying the functional connectivity of children with ASD (Supekar et al., 2013; Uddin et al., 2013). The authors have suggested that overconnectivity might be specific to children with ASD and might not disagree with the underconnectivity results found in other resting state studies that predominantly used adults.

More recently, groups have found evidence of a mix of over- and underconnectivity in individuals with ASD of average intellectual ability (Cerliani et al., 2017; Chen and Glover, 2015; Cheng et al., 2015; Cherkassky et al., 2006; Dajani and Uddin, 2015; Doyle-thomas et al., 2015; von dem Hagen et al., 2013; Itahashi et al., 2015; Keown et al., 2013; Di Martino et al., 2014, 2010, 2013; Murdaugh et al., 2015; Nair et al., 2014, 2013). Underconnectivity appears to be widespread across long-range cortico-cortical connections, while overconnectivity is confined to short-range subcortical connections (Bos et al., 2014; Damarla et al., 2010; Di Martino et al., 2014; Ray et al., 2014; Redcay et al., 2013; Venkataraman et al., 2015). Such a pattern of mix connectivity reconciles the seemingly opposite findings of over- and underconnectivity that has been reported in ASD by revealing both trends in single studies. It further suggests that the studies reporting underconnectivity in ASD might not have been sufficiently powered to detect the limited increased in connectivity present in ASD brains.

A mix of over- and underconnectivity has also been observed at a local scale in ASD (Alaerts et al., 2015; Bos et al., 2014; Di Martino et al., 2014; Maximo et al., 2013; Nair et al., 2018; Shukla et al., 2010), as well as in specific brain regions including the posterior superior temporal sulcus (Abrams et al., 2013; Alaerts et al., 2014, 2015), the cerebellum (Khan et al., 2015), in brain regions involved in mentalizing (Fishman et al., 2014), in the reading network (Murdaugh et al., 2015) and in thalamo-cortical (Nair et al., 2015, 2013; Olivito et al., 2016) and striatal-cortical connections (Di Martino et al., 2010; Paakki et al., 2009).

1.6.1.1 Single-gene disorders associated with ASD/ID

In addition to rsfMRI studies on idiopathic ASD, a number of complementary functional connectivity studies have been carried out in single-gene disorders associated with a high prevalence of ASD/ID and on single nucleotide polymorphisms (SNPs) associated with an increased risk of developing ASD.

Fragile X Syndrome Hall et al. (2013) reported that 5 major RSNs were underconnected in male and female individuals with FXS (mean IQ 66.8) compared to controls matched for age, IQ and the severity of autistic symptoms (mean IQ 63.8) : the salience network, precuneus network, left executive control network, language network and visuospatial network. In contrast, the visual network was overconnected in FXS (Hall

et al., 2013). They also reported that at a local scale, both over and underconnectivity was detected in FX individuals (Hall et al., 2013). Matching for both ASD symptoms and IQ means that the FC impairments identified in this study are specific to FXS and not common to these developmental disorders. However, as controls were not matched for gender, and as there were more female FX individuals and more male controls, this difference in FC could also be driven by gender, which has been shown to affect FC (Biswal et al., 2010; Alaerts et al., 2016; Ypma et al., 2016).

Neurofibromatosis 1 Underconnectivity has been reported in individuals with Neurofibromatosis 1 (NF1) of average intellectual ability across both hemispheres and along antero-posterior connections. Decreased connectivity in the DMN and visual network was also observed in NF1 individuals of average intellectual ability compared to age and gender matched controls (Chabernaud et al., 2013; Tomson et al., 2015), as well as diffuse local connectivity (Chabernaud et al., 2013) and overconnectivity in short range unilateral connections (Tomson et al., 2015).

Interestingly, Chabernaud et al. (2013) demonstrated that lovastatin, an inhibitor of the mGluR5 signalling pathway that has been shown to rescue synaptic and behavioural deficits in rodent models of FXS, can rescue the local diffusiveness and the decrease in long range connectivity observed in the DMN of individuals with NF1.

***MET* risk genotype** Met Receptor Tyrosine Kinase (*MET*) is an ASD candidate gene with common variants (Campbell et al., 2008, 2010) and individuals with ASD carrying one or two copies of the rs1858830 C alleles ('high risk') have been found to have higher levels of social impairments than ASD individuals with no copies of this allele ('low risk') (Rudie et al., 2012; Campbell et al., 2010). Rudie et al. (2012) demonstrated that DMN connectivity is decreased in individuals with the high risk *MET* variant compared to those with a low risk variant.

Serotonin transporter genotype The serotonin transporter-linked polymorphic region (5-HTTLPR) variant leading to a lower serotonin transporter expression is associated with a higher level of social impairments in ASD (Tordjman et al., 2001). DMN antero-posterior connectivity was increased in ASD individuals with a low-expressing serotonin transporter genotype compared to individuals with a high expressing genotype

and to controls with a low-expressing serotonin transporter genotype (Lee Wiggins et al., 2013).

1.6.1.2 Classification of autism based on functional connectivity

Resting state studies have consistently reported impaired brain functional connectivity in ASD. As a result, several groups have examined whether altered connectivity patterns identified in individuals with idiopathic ASD could be used to distinguish between individuals with ASD and typically developing (TD) individuals.

Differences in DMN connectivity (Murdaugh et al., 2012) and in the interhemispheric connectivity of the inferior frontal gyrus and of the superior temporal gyrus (Dinstein et al., 2011) have been found to be sufficient to successfully differentiate individuals with ASD and TD individuals. Full connectivity patterns have also been used to successfully classify individuals into an ASD or TD group (Murdaugh et al., 2012; Anderson et al., 2011; Chen and Glover, 2015; Iidaka, 2014; Nielsen et al., 2013).

Several groups compared ASD classification methods based on the functional connectivity of one *versus* multiples networks (Price et al., 2014; Wee et al., 2016; Uddin et al., 2013; Plitt et al., 2015) and found that accuracy increased when using multiple networks. Uddin et al. (2013) further compared classification algorithms based on 8 different RSNs and found that differences in salience network connectivity achieved the highest accuracy, specificity and sensitivity in classifying ASD and TD children. Plitt et al. (2015) demonstrated that rsfMRI data can be used to predict with a high sensitivity improvement in adaptive behaviours in the years following the scan. However, Pruett et al. (2015) showed that rsfMRI data could not predict whether a 6 or 12-month old infants would go on to develop ASD. Additionally, it is worth noting that Plitt et al. (2015) reported that classification based on behavioural features outperformed a functional connectivity based classification.

1.6.1.3 Functional connectivity relationship to symptoms severity

Several groups also explored the relationship between altered functional connectivity and symptom severity. FC connectivity impairments have been found to be significantly correlated with Autism Diagnostic Observation Schedule (ADOS) scores (Abrams et al., 2013; Assaf et al., 2010; Cheng et al., 2015; Guo et al., 2017; Hahamy et al., 2015;

Keown et al., 2013; Lee et al., 2016; Lynch et al., 2012; Nebel et al., 2014; Nielsen et al., 2014; Redcay et al., 2013; Shen et al., 2016; Supekar et al., 2013; Washington et al., 2014), Autism Diagnostic Interview (ADI) scores (Abrams et al., 2013; Cardinale et al., 2014; Delmonte et al., 2013; Di Martino et al., 2010; Eilam-stock et al., 2014; Fishman et al., 2014; Kennedy et al., 2006; Lee et al., 2016; Maximo et al., 2013; Monk et al., 2009; Supekar et al., 2013; Washington et al., 2014), Social Responsiveness Scale (SRS) scores (Alaerts et al., 2015; Assaf et al., 2010; Cerliani et al., 2017; Gotts et al., 2012; Khan et al., 2015; Nebel et al., 2014; Verly et al., 2014; Washington et al., 2014), Social Communication Questionnaire scores (Dajani and Uddin, 2015; Verly et al., 2014), Autism Spectrum Quotient test (AQ) scores (Itahashi et al., 2015; Jung et al., 2014; von dem Hagen et al., 2013) and the Short Sensory Profile (Shen et al., 2016).

In contrast, other groups reported that FC alterations identified in individuals with ASD were not significantly correlated with ADOS scores (Alaerts et al., 2015; Barttfeld et al., 2012; Khan et al., 2015; Maximo et al., 2013), SRS scores (Alaerts et al., 2015) or AQ scores (Itahashi et al., 2014).

This discrepancy could be due to the fact that not every group that found a positive association between disease severity and functional connectivity impairment performed or reported multiple comparison corrections (Maximo et al., 2013; Khan et al., 2015; Itahashi et al., 2014). Some of these findings might not hold if a multiple comparison correction was performed. Di Martino et al. (2010) has for example reported that a positive association between ADI scores and the functional connectivity between the right dorsal-caudal putamen and the right pons did not survive correction for multiple comparisons.

1.6.2 Resting state studies in rodent models of ASD

RSNs have been identified in rodents (Jonckers et al., 2011). Jonckers et al. (2011) acquired resting state functional data from mice and rats and compared the RSNs obtained. They identified similar RSNs in both species, although they observed more unilateral components in mice than in rats. Furthermore, they identified a sensorimotor, visual, auditory and default mode networks in both species, which were comparable to what has been described in humans. Lu et al. (2012) also showed that rats have a

DMN that is comparable to the monkey (Vincent et al., 2007) and human one. Resting state fMRI can therefore provide a platform to study ASD in a comparable way across species. A few resting state studies have been carried out in mouse models of ASD.

***Chd8* heterozygous mouse model** Mutations in the Chromodomain Helicase DNA binding factor 8 (*CHD8*) gene is associated with a high incidence of ASD (Bernier et al., 2014). Suetterlin et al. (2018) investigated the functional connectivity of *Chd8* heterozygous mice and observed an overconnectivity in the ventral hippocampus and auditory cortical regions of *Chd8* heterozygous mice.

***Cntnap2* knockout mouse model** Mutations in the contactin associated protein-like 2 (*CNTNAP2*) gene is also a risk factor for ASD (Alarcon et al., 2008). Liska et al. (2018) reported that *Cntnap2*-null mice had a decreased long-range DMN connectivity compared to WT littermates. In a developmental study, Zerbi et al. (2018) found a similar underconnectivity in brain regions that are part of the DMN in adult *Cntnap2*-null mice compared to WT, but no between-genotype difference was observed in juvenile mice. Additionally, they also reported a reduced connectivity in the left associative area and hippocampus, as well as an increased connectivity in the ventral striatum of adult *Cntnap2*-null mice in comparison to WT (Zerbi et al., 2018).

***Fmr1* knockout mouse model** Zerbi et al. (2018) also investigated the development of FC deficit in a mouse model of FXS. They found that the lateral striatum and auditory/associative cortical networks were underconnected in *Fmr1*-null mice in comparison with WT littermates throughout postnatal development. In a recent paper, Zerbi et al. (2019) additionally reported a decreased DMN and somatosensory network connectivity.

***SynII* knockout mouse model** Mutation in Synapsin genes are associated with ASD and epilepsy in humans (Lakhan et al., 2010; Fassio et al., 2011; Corradi et al., 2014). Michetti et al. (2017) investigated the FC of mice lacking *Syn2*, but observed no global connectivity impairments in *SynII* knockout mice. However, a local decrease in connectivity of the auditory cortex, somatosensory cortex and hippocampus was observed in *SynII*-null mice in comparison to WT mice, as well as a reduced inter-

hemispheric connectivity in the auditory cortex of *SynII*-null mice (Michetti et al., 2017).

BTBR T+tf/J mouse model Two groups investigated the FC of the inbred BTBR T+tf/J (BTBR) mouse strain, which displays ASD-like phenotypes (Dodero et al., 2013; Sforazzini et al., 2016). Dodero et al. (2013) observed a wide-spread cortical underconnectivity in BTBR mice in comparison with control mice. Overconnectivity was observed in the hypothalamus and dorsal hippocampus of BTBR mice (Dodero et al., 2013). Sforazzini et al. (2016) observed that BTBR mice exhibit reduced inter-hemispheric connectivity in rostral cortical regions, but not in sensory regions. They also observed decreased thalamo-cortical and thalamo-subcortical connections, and decreased connectivity of the striatal network (Sforazzini et al., 2016).

16p11.2 microdeletion mice models Bertero et al. (2018) observed a decreased prefrontal connectivity in 16p11.2 deletion carriers, a disorder associated with a high prevalence of ASD and ID. They further reported a similar decreased in prefrontal connectivity in the 16p11.2 microdeletion mouse model (Bertero et al., 2018).

Overall, these resting state studies reported a reduction in FC in mouse models of ASD, mirroring findings of human resting state studies on ASD. Rodent rsfMRI might therefore provide a valuable tool for the study of ASD.

1.7 Aims of this thesis

Given its translatability across species, rsfMRI has potential to be used as a diagnostic tool and to assess therapeutic efficacy in rodent models of ASD. However, to date, no resting state studies have been carried out in rat models of ASD, which provide a better spatial resolution than mice due to their bigger brain size, and are better suited for pharmacological studies as their metabolism is closer to that of humans. In addition, despite promising results in the 16p11.2 microdeletion mice model (Bertero et al., 2018), it remains unclear whether functional connectivity alterations observed in other ASD preclinical models will be comparable to those presented by affected individuals, or whether a pharmacological intervention could restore those deficits.

The overarching aim of this thesis is therefore to determine whether rsfMRI has the potential to improve the translation of therapeutic compounds identified in preclinical FXS studies to the clinics (**Fig. 1.11**). In the first results chapter of this thesis, I established a methodology to acquire and analyse rsfMRI data in WT rats (Chapter 3). I applied this methodology to a rat model of FXS, to test the hypothesis that loss of FMRP leads to a decreased in DMN connectivity in *Fmr1*$^{-/y}$ rats. I further tested the hypothesis that individuals with FXS would have a comparable functional connectivity impairment, by analysing rsfMRI data of FX individuals (Chapter 4). In the final experimental chapter, I tested the hypothesis that lovastatin would restore functional connectivity impairments identified in *Fmr1*$^{-/y}$ rats (Chapter 5).

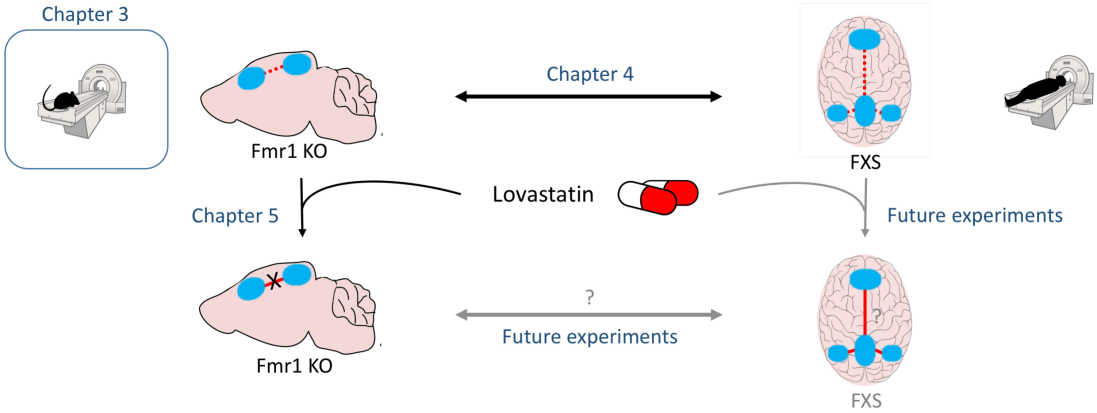


Figure 1.11: Aims of the thesis.

Chapter 3: I established and validated a methodology to acquire and analyse resting state data in WT rats that will be used in later chapters.

Chapter 4: Previous work on idiopathic ASD has suggested that FC is underconnected in individuals with ASD without an intellectual disability. I therefore hypothesise that the DMN connectivity and the brain global FC would be underconnected in *Fmr1*$^{-/y}$ rats. I further hypothesise that the global FC and DMN connectivity would also be decreased in individuals with FXS with an intellectual disability. Using a parallel rsfMRI technique in FX individuals and in a rat model of the disorder, I provide evidence of a similar decrease in DMN and global FC in FXS across species.

Chapter 5: I hypothesise that the development of DMN connectivity would be decreased in *Fmr1*$^{-/y}$ rats compared to WT rats and that lovastatin would restore DMN functional connectivity impairments identified in *Fmr1*$^{-/y}$ rats in Chapter 4. I assessed DMN connectivity throughout development in control and lovastatin-treated WT and *Fmr1*$^{-/y}$ rats. I found that DMN connectivity was underconnected in *Fmr1*$^{-/y}$ rats across development in comparison with WT rats, supporting my first hypothesis. However, my findings did not support my second hypothesis, as I found that the lovastatin treatment was unsuccessful at restoring DMN connectivity in *Fmr1*$^{-/y}$ rats.

Chapter 2

Materials and Methods

2.1 Animals

2.1.1 Housing and breeding

Fmr1$^{-/y}$ rats were group-housed with WT littermates, with food and water available *ad libitum*. Animals were housed in a temperature and humidity controlled environment on a 12 hour light/dark cycle. Rats were maintained as outbred lines. Females heterozygous for *Fmr1* were crossed to WT males from a WT colony, to generate *Fmr1*$^{-/y}$ rats and WT littermate controls. WT colonies were regularly replenished from commercially available colonies. No WT animals used in chapter 4 and 5 came from WT colonies, instead, litters of WT and *Fmr1*$^{-/y}$ rats obtained from this WT x transgenic cross were used. Specifically, litters with a balanced number of animals of each genotype were selected. These litters are 4-7 generations after the generation zero of the SD and LEH *Fmr1* lines. Experiments were performed blind to the animal's genotype and to their diet, when applicable. All experimental procedures were performed in compliance with the University of Edinburgh and the UK Home Office guidelines, under the Animal (Scientific Procedures) Act 1986.

2.1.2 *Fmr1*$^{-/y}$ Sprague Dawley rats

Fmr1$^{-/y}$ Sprague Dawley rats were obtained from Horizon Discovery, previously Sigma Advanced Genetic Engineering (SAGE) Labs (St. Louis, MO, USA). They were generated using zinc-finger nuclease technology to make a 122 base pair deletion across the intron 7 / exon 8 junction resulting in the loss of the Fragile X Mental Retardation Protein (FMRP) (Hamilton et al., 2014).

2.1.3 *Fmr1*$^{-/y}$ Long-Evans hooded rats

Fmr1 Long-Evans hooded (LEH) rats were produced by SAGE Labs (St. Louis, MO, USA). They were generated using zinc-finger nuclease technology to insert an eGFPnlsSV40pA cassette in the coding region of exon 1 resulting in loss of the *FMR1* gene protein product.

2.2 Genotyping

Genotyping was done in-house following the method described below or alternatively, samples were sent to Transnetyx (Memphis, USA) for genotyping using a real-time PCR method.

2.2.1 DNA extraction and isolation

Ear clips or tail clips biopsies were taken at weaning for animal identification and at the end of the experiment for regenotyping.
Tissue samples were digested in 500 μl of tail buffer solution, described in **Table 2.1**, with 5 μl of proteinase K (20 mg/ml) at 55°C overnight.
Digested samples were vigorously mixed and spun for 10 minutes at 13000 x g. 400 μl of the supernatant was transferred to a new Eppendorf tube with an equal volume of isopropanol. Sample were spun again for 10 min at 13000 x g. The supernatant was discarded and the remaining pellet was rinsed with 70% ethanol. The DNA was resuspended in ddH_2O.

Reagents	Concentration
Tris pH 8.5	100mM
NaCl	200mM
SDS	0.2%
EDTA	5mM

Table 2.1: Tail buffer mix

2.2.2 *Fmr1*$^{-/y}$ Sprague Dawley Primers

A single reaction was used for *Fmr1*$^{-/y}$ SD genotyping using the following primers

Fmr1$^{-/y}$ Primers	Sequence - 5'-3'
Forward primer	TGGCATAGACCTTCAGTAGCC
Reverse primer	TATTTGCTTCTCTGAGGGGG

2.2.3 *Fmr1*$^{-/y}$ Long-Evans hooded Primers

A single reaction was used for *Fmr1*$^{-/y}$ LEH genotyping using the following primers

Fmr1$^{-/y}$ Primers	Sequence - 5'-3'
Forward primer	ACGTAAACGGCCACAAGTTC
Reverse primer	ATGCCGTTCTTCTGCTTGTC

2.2.4 Polymerase Chain Reaction (PCR)

The PCR reaction mix listed in **Table 2.2** was used with both the SD and LEH *Fmr1*$^{-/y}$ primers. The thermocycling conditions are shown in **Table 2.3**. The PCR reaction products were run on a 1.0% agarose gel in 1X TBE buffer containing SYBR safe (Thermo Fisher Scientific, MA, USA) at 50V for 35min with a GeneRuler 100bp DNA ladder (Thermo Fisher Scientific, MA, USA).

Reagents	Concentration (μl)
Promega GoTaq master mix	6
DNA	0.5
Forward primer	1
Reverse primer	1
ddH_2O	3.5

Table 2.2: PCR reaction mix

2.3 Preclinical MRI

2.3.1 Habituation

Prior to scanning, animals were handled daily for a week to familiarise them to the experimenter. Animals used in the experiments presented in chapter 4 were also exposed to a recording of the Echo-Planar Imaging (EPI) scans to acclimatize them to the scanning procedure. They were played a recording of the scanning sound while in their home cage for five days, the level of which increased daily by 10-15%. On the

Cycle Step	Temp (°C)	Time	
1	95	5 min	
2	95	30 s	x 35 cycles
3	60	30 s	
4	68	30 s	
5	68	5 min	
6	10	forever	

Table 2.3: Thermocycling conditions used for all *Fmr1*$^{-/y}$ primers

first day, the recording was played at 10% of the level experienced within the scanner, reaching 70% by day five.

2.3.2 Pharmacological intervention

From postnatal week 4 to 9, animals in chapter 5 received either a control diet or a diet of identical appearance and composition but supplemented with 100mg/kg of lovastatin (BioServe, USA), hereafter termed lovachow.

The rats were weighed prior to and for 2 weeks following the diet switch, to ensure that the diet did not adversely affect the animals' development.

2.3.3 Acquisition of MRI scans

2.3.3.1 Agilent scanner

All animals that took part in the experiments presented in chapter 3 and 4 were scanned with a 7T Agilent MRI scanner (Agilent Technologies; formerly Varian, Oxford, UK).

Rats were scanned under isoflurane anaesthesia. Lightly anaesthetized animals were positioned in a 300MHz surface head coil (Rapid Biomedical, Rimpar, Germany) in the 7T MRI scanner, equipped with a 400 mT/m gradient and a 72 mm volume RF coil (Rapid Biomedical, Rimpar, Germany). The surface head coil was used for signal reception and the volume RF coil for signal transmission.

Anaesthesia was maintained throughout the scanning session. Animal physiology was closely monitored throughout the session. Body temperature was monitored using a rectal probe and was maintained at 37°C using a hot hair ventilator. Breathing rate and oxygenation were also monitored using a transducer pad and a pulse oximeter,

respectively (Model 1030 monitoring and gating system, Small Animal Instrument Inc. Stony Brook, NY, USA).

Structural scans Whole brain structural images were acquired in rats under 1% isoflurane, using a Fast Spin Echo sequence. Sequence characteristics are listed in **Table 2.4**.

Sequence characteristics	
Matrix	256x256
Field Of View	30mm
Repetition time (TR)	3000ms
Echo Train Length	8
Echo spacing	12ms
Slice number	26
Slice thickness	1mm

Table 2.4: Agilent structural scan sequence characteristics

EPI Following the structural scan, one to three resting state functional scans were then acquired under 1%, 1.5% or 2.5% isoflurane, as detailed in each experiments. RsfMRI scans were acquired under a two-shot Echo-Planar Imaging (EPI) sequence. The parameters are listed in **Table 2.5**.

Sequence characteristics	
Matrix	60x60
Field Of View	30 mm
Kzero	15
Number of shot	2
Effective TR	2000 ms
Echo time (TE)	12 ms
Slice number	28
Slice thickness	0.8 mm
Spacing	no gap
Volumes	300

Table 2.5: Agilent EPI scan sequence characteristics

2.3.3.2 Bruker scanner

All animals that took part in the experiments presented in chapter 5 were scanned with Bruker scanner electronics (Bruker BioSpin MRI GmbH, Ettlingen, Germany).

Rats were scanned under isoflurane anaesthesia. Lightly anaesthetized animals were positioned in a two-channel phased-array surface head coil (Rapid Biomedical, Rimpar, Germany) in the 7T horizontal bore Biospec ADVANCE neo preclinical imaging system, equipped with a 116 mm bore gradient insert, a 660 mT/m gradient and an 86 mm quadrature volume coil (Bruker BioSpin MRI GmbH, Ettlingen, Germany). A mouse head coil was used for juvenile rats (4 weeks of age) and a rat head coil was used for adults (8 weeks and older). The surface head coil was used for signal reception and the volume RF coil for signal transmission.

Anaesthesia was maintained throughout the scanning session. Animal physiology was closely monitored throughout the session. Body temperature was monitored using a rectal probe and was maintained at 37°C using a hot hair ventilator. Breathing rate and oxygenation were also monitored using a transducer pad and a pulse oximeter, respectively (Model 1030 monitoring and gating system, Small Animal Instrument Inc. Stony Brook, NY, USA).

Structural Whole brain structural images were acquired in rats under 1.5% isoflurane, using a Rapid Imaging with Refocused Echoes (RARE) sequence. Sequence characteristics are listed in **Table 2.6**.

Sequence characteristics	**Juvenile**	**Adult**
Matrix	192 x 192	
Field Of View	30 x 30	
TR	2300 ms	2310 ms
RARE factor	4	
TE	24 ms	
Echo spacing	12 ms	18 ms
Slice number	24	
Slice thickness	0.80 mm	0.85 mm
Number of Averages	4	
Number of Repetitions	1	
Number of Echo Images	1	

Table 2.6: Bruker structural scan sequence characteristics

EPI Resting state functional EPI scans were acquired, under 1.5% isoflurane using a single-shot EPI sequence. Acquisition parameters are reported in **Table 2.7**.

Sequence characteristics	Juvenile	Adult
Matrix	64 x 32	64 x 42
Field Of View	30 x 15	30 x 19.6
Number of shot	1	
Effective TR	2000 ms	
TE	12 ms	
Slice number	24	
Slice thickness	0.80 mm	0.85 mm
Volumes	300	

Table 2.7: Bruker EPI scan sequence characteristics

DTI Diffusion Tensor Imaging (DTI) scans were acquired, under 1.8% isoflurane, using a DTI-EPI sequence. Acquisition parameters can be found in **Table 2.8**.

Sequence characteristics	Juvenile	Adult
Matrix	128 x 128	
Field Of View	30 x 30	
Effective TR	2000 ms	
Number of A0	6	
Diffusion directions	42	
Slice number	24	
Slice thickness	0.80 mm	0.85 mm

Table 2.8: Bruker DTI scan sequence characteristics

2.3.4 Analysis of MRI scans

2.3.4.1 Protocol optimisation

The methods for MRI data analysis used in Chapters 4 and 5 are described in the following sections.

Before adopting these protocols, the author tried alternative ways to analyse MRI data, which are detailed in Chapter 3. Briefly, I first used a protocol relying on SPM8 (Statistical Parametric Mapping, version 8, Functional Imaging Laboratory, UCL, UK) to perform images preprocessing. Seed-based analysis was carried out using Data processing assistant for resting-state fMRI advanced edition (DPARSF A), and ICA was performed using GIFT.

The author also went through different versions of FSL-based protocols (FMRIB Software Library v6.0, Oxford, UK) before adopting the one describe below.

2.3.4.2 File conversion

In order to analyse the MRI scans, raw images obtained from the scanner must first be transformed into a file format that can be read by an imaging software, as depicted in **Fig. 2.1**.

Agilent Images can be transformed from the Agilent .fdf file format into the analyze file format (.hdr/.img), by first renaming the files from the Agilent Scanner name convention sliceXimageXechoXXX.fdf to volumeXsliceXechoXXX.fdf, which the author did using a perl script. Next, the newly renamed .fdf images can be transformed into analyze images using the ImageJ plugin varianfdf_to_analyze_hack. The last step consists in adjusting the header information in MRIcro and saving the images as a 3D analyze image.

Bruker Images can be transformed from the Bruker .2dseq file format into the analyze file format (.hdr/.img) using MRIcro. After opening .2dseq images in MRIcro using the raw header information, an analyze header can be created by filling in the X, Y, Z dimension and size information, and for functional images, the number of volumes. The images can then be transformed and saved as a 3D analyze image.

2.3.4.3 Reorientation

To improve the registration preprocessing step, images were first reoriented to match the template's origin using SPM8 (Statistical Parametric Mapping, version 8, Functional Imaging Laboratory, UCL, UK). Images were also scaled by a factor of 10 in the x, y and z direction to account for difference in size between the rat and human brain.

2.3.4.4 Brain extraction

Registration robustness is also improved by removing non-brain tissues. This was done using the semi-automated software Skullstripper (Delora et al., 2016). The software requires a reference mask and a reference functional image. The reference images were obtained by manually removing non-brain tissues out of a functional image to create a mask.

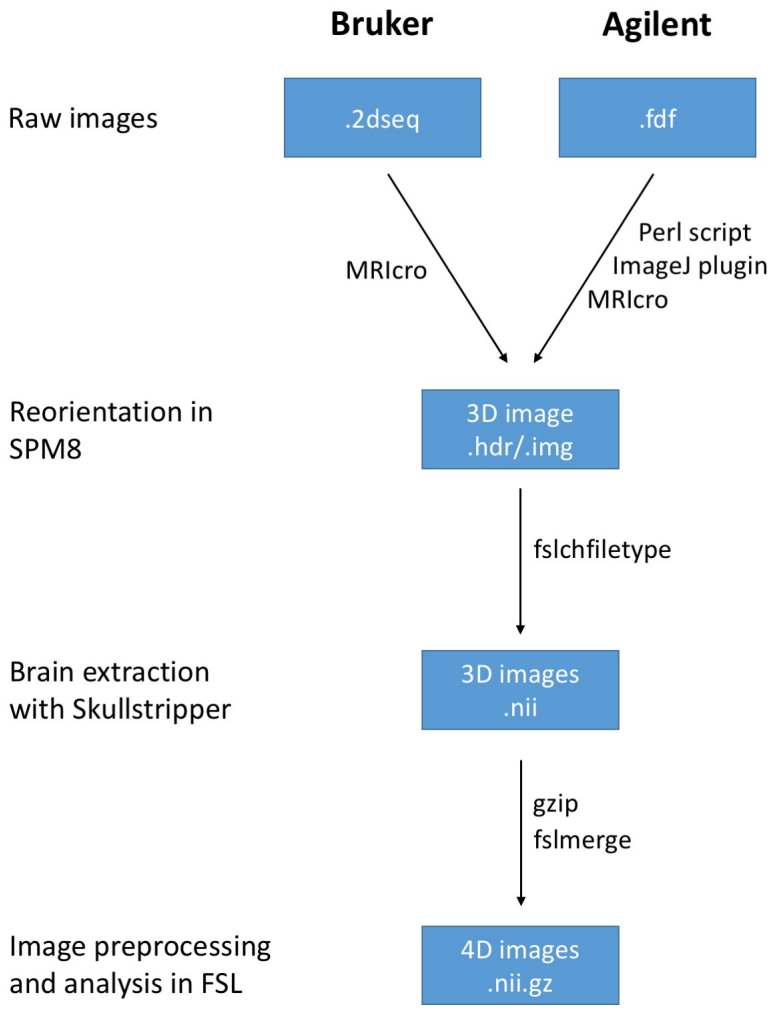


Figure 2.1: Flowchart of the steps required to get the images ready for analysis. First, images need to be transform from the scanner raw file format to the analyze format, which can be read by the SPM8 software. SPM8 is used for image reorientation. Next, non-brain tissues need to be removed. This is done using Skullstripper. In order to use this software, images need to be converted to a nifti format. Finally, preprocessing and data analysis is done with the FSL software, which requires 4D images in a compressed nifti format. It is therefore necessary to merge 3D images and compress them to obtain 4D images in the correct file format.
Each step and software are noted to the left of the image. The required file format for each software is written in the blue rectangles. Arrows show the tools and command lines that can be used to transform the images between file formats.

2.3.4.5 Preprocessing

Functional scans were preprocessed using MELODIC 3.0 (FSL (FMRIB Software Library) v6.0, Oxford, UK).

First, the first 10 volumes were removed from the 4D functional images to allow for T_1 equilibration effects. The images were then motion corrected using MCFLIRT motion correction tool from FSL (FMRIB Software Library v6.0, Oxford, UK), spatially smoothed with a Full Width Half Maximum (FWHM) of 5 mm and temporally filtered with a high pass cut-off of 100 s.

Before multi-subject analysis can be carried out, the filtered and motion-corrected functional images need to be registered with one another in the same space. This was done in two steps, first functional images are registered to the brain-extracted structural images (full search, 12 degrees of freedom (DOF)), and then to the high resolution template (normal search, 12 DOF).

2.3.4.6 ICA

Multi-session temporal concatenation was performed to identify common spatial patterns between registered subjects (**Fig. 2.2**). This analysis is used to identify spatial patterns but does not assume that there is a consistent temporal pattern across subjects. Timecourses were variance-normalised and 20 to 30 components outputted.

2.3.4.7 Seed-based analysis

Alternatively, functional connectivity can be measured between a seed and either the whole brain or a region of interest (ROI). I have done that using a script developed by Wim Otte (UMC Utrecht, The Netherlands) and by using AFNI tools (Analysis of Functional NeuroImages, NIH). Both methods relies on the same steps, described below.

First, a seed had to be created in the functional space of each animal. Next, a 1D file of the mean time series of the seed was extracted. Then, a Pearson correlation was performed between the 1D mean time series previously obtained and every voxel of the brain. The output of this step is the r-score. The r-score needs to be transformed to a z-score to do group analyses, using fisher's z-transformation. The r-score and

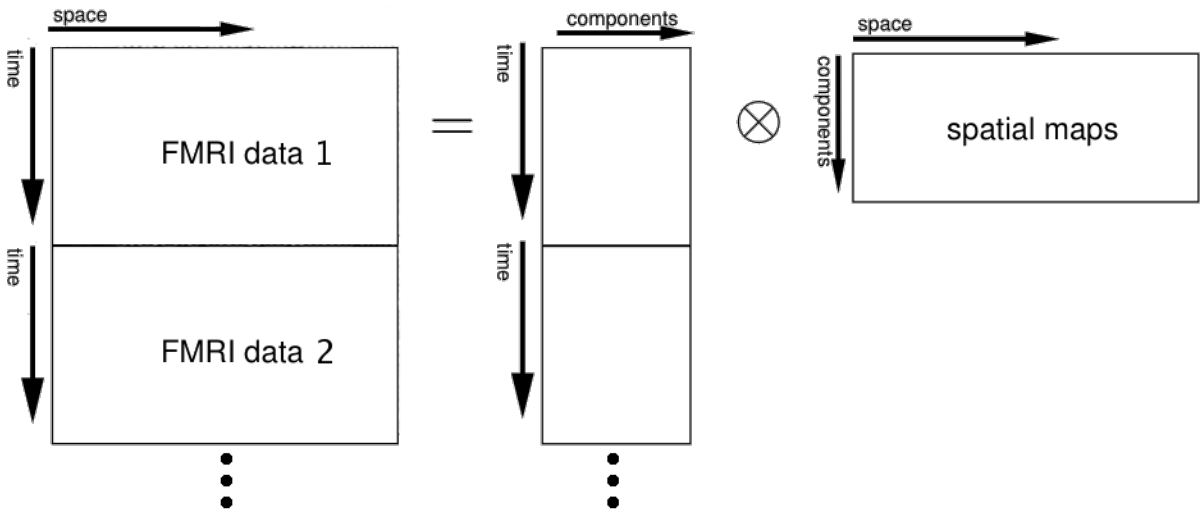


Figure 2.2: Multi-session temporal concatenation ICA.
The input fMRI data (left) is a 2 dimensional time x space matrix obtained by concatenating each subject's 2D time x space matrix together. MELODIC decomposes the concatenated matrix into the time course of components and the group-level spatial map of each component. Dual regression can then be performed to obtain the subject-version of the group-spatial maps. Figure from FSL (FMRIB Software Library v6.0, Oxford, UK).

z-score can be masked with the mask of a network of interest to specifically look at the connectivity of that RSN. Additionally, statistical analysis can be directly carried out on the mean r-score, which allows for advanced statistical analyses that cannot easily be done on whole functional images.

2.3.4.8 Connectograms and functional connectivity matrices

The functional connectivity of the whole brain can be illustrated under the form of matrices or as connectograms. In chapter 4, I selected 34 brain regions of interests (Right and left ACC, primary motor cortex, secondary motor cortex, primary somatosensory cortex (hindlimb region), primary somatosensory cortex (forelimb region), primary somatosensory cortex (other), secondary somatosensory cortex, insular cortex, caudate putamen, nuccleus accumbens, hippocampus, amygdala, thalamus, dorsal raphe nucleus and corpus callosum), I calculated the FC between each combination of brain region pairs (see section 2.3.4.7 above for method) and arranged them as a matrix or a connectogram. The latter was done using Circos (Krzywinski et al., 2009). In a matrix, each square is colour-coded according to the strength of the connectivity between a pair of brain regions, while in a connectogram, the FC strength is represented by the colour of the line connecting two brain regions.

2.3.4.9 Statistical analysis

Group-average spatial maps, obtained from the seed-based analysis and ICA, were dual-regressed to obtain subject-specific version of the spatial maps needed for statistical analysis (FMRIB Software Library v6.0, Oxford, UK). First, the group-average spatial maps were regressed into each subject's 4D dataset. This step outputs a subject-specific timeserie for each group-averaged spatial map. Next, the timeseries obtained in step 1 were regressed into the same 4D space-time dataset, resulting in subject-specific spatial maps for each of the group-average components.

Finally, General linear model (GLM) was applied to test for group differences using FSL's permutation-testing tool randomise (FMRIB Software Library v6.0, Oxford, UK).

2.4 Clinical MRI

Participant recruitment, acclimatisation to the scanner and the acquisition of clinical MRI scans were done by Dr. Andrew McKechanie and Dr. Andrew Stanfield. The author performed the data analysis.

2.4.1 Participants

Participant demographics are given in **Table 2.9**. Subjects were recruited through the Fragile X Society and the Patrick Wild Centre mailing lists. Scotland A Research Ethics Committee reviewed and granted ethical permission for the study. In case where participants were not able to give consent, it was sought from their welfare guardian or nearest relative, in compliance with the Adult With Incapacity (Scotland) Act 2000.

Characteristics	**FXS individuals**	**Controls**	
		Group 1	*Group 2*
Sex, no.			
Male	4	5	12
Female	1	0	0
Age, mean (SD)	18.6 (0.5)	28 (3.08)	44 (10)
IQ, mean (SD)	60.2 (12.53)	114.5 (14.33)	122 (12)
ADOS score	16.2 (4.2)	/	/

Table 2.9: Participant demographics

Controls were split into two groups. Group 1 was composed of 5 age matched individuals and was used to generate group-level spatial functional connectivity maps.

Group 2 was comprised of 12 non-age matched individuals and was used alongside group 1 for statistical analysis.

2.4.2 Participant acclimatisation to the scanning procedure

Given that individuals with FXS often have intellectual disabilities, can suffer from hyperactivity and sensory hypersensitivity and may experience anxiety in new environments or when routine is broken, it is crucial to prepare them for the scanning procedure. To achieve that, individuals with Fragile X Syndrome were gradually introduced to the scanning environment using two mock scanners. First, they practice laying still on a crude replica of a scanner (the table, bore and head coil), while listening to a recording of the scanner sound. Participants were able to visit the mock scanner as many times as it took them to be able to lay still in it. Following this, individuals were able to practice on an accurate replica of the scanner. Once comfortable, FX individuals went on to be scanned on a working scanner unanaesthetised.

2.4.3 Acquisition of MRI scans

Individuals were scanned on a 3T Siemens Magnetom Verio scanner.

Structural Structural images were acquired using a T1-weighted magnetization prepared rapid acquisition gradient echo (MPRAGE) sequence. Acquisition parameters are indicated in **Table 2.10**.

EPI Functional images were acquired using a single-shot EPI sequence. Acquisition parameters are indicated in **Table 2.11**. Individuals were told to keep their eyes open and to look at a visual fixation cross during the scan.

Sequence characteristics	
Field Of View	256 x 256 mm
TR	2300 ms
TE	2.98 ms
Flip angle	9°
Slice number	160
Slice thickness	1 mm

Table 2.10: Siemens structural scan sequence characteristics

Sequence characteristics	
Field Of View	220 x 220 mm
TR	1560 ms
TE	26 ms
TA	7.42 min
Flip angle	66°
Slice number	26 axial
Slice order	interleaved
Voxel size	3.4x3.4x4.0 mm

Table 2.11: Siemens EPI scan sequence characteristics

2.4.4 Analysis of MRI scans

2.4.4.1 File conversion

The files had to be transformed from a DICOM format to a NIFTI format in order to be read by an imaging software. This was done using the dicm2nii matlab tool (Mathworks).

2.4.4.2 Preprocessing

Functional scans were preprocessed using MELODIC 3.0 (FSL (FMRIB Software Library) v6.0, Oxford, UK).

A stringent motion-correction was performed on the subjects, by performing an ICA on each individual subject and regressing out noise and movement components. This involved first preprocessing each individual subject. To do that, the first 10 volumes were removed from the 4D functional images to allow for T_1 equilibration effects. Non-brain tissues were removed from 4D functional images using the FSL tool BET (FMRIB Software Library v6.0, Oxford, UK). Images were then motion corrected using MCFLIRT motion correction tool from FSL (FMRIB Software Library v6.0, Oxford, UK), spatially smoothed with 5 mm FWHM, temporally filtered with a high pass cut-off of 100 s and registered to the template. This last step was done by first registering functional images to the brain-extracted structural images (full search, 12 degrees of freedom (DOF)) and then to the high resolution template (normal search, 12 DOF).

Next, an ICA was performed individually for each preprocessed subject (**Fig. 2.3**). Outputted components were then classified into signal and noise components, and the noise components regressed out from the 4D data.

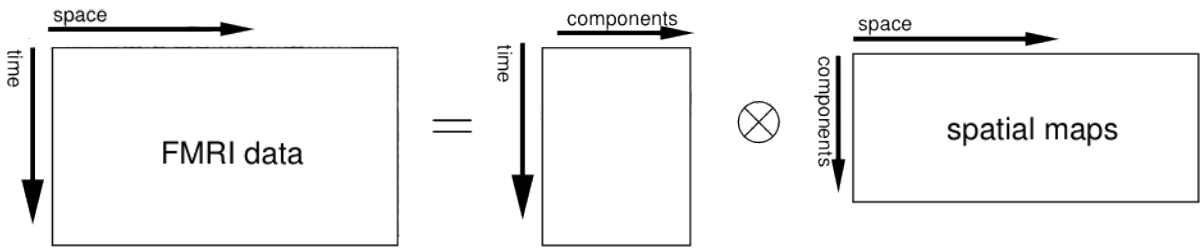


Figure 2.3: Single-session ICA. The input fMRI data (left) is represented as a 2 dimensional time x space matrix. MELODIC decomposes each matrix into the time course of components and the spatial map of each component. Each component spatial map can then be assessed and classified as noise or signal. Figure from FSL (FMRIB Software Library v6.0, Oxford, UK).

2.4.4.3 ICA

Multi-session temporal concatenation was performed on a cohort composed of all the FX individuals and the group 1 of control individuals, to identify common spatial patterns between registered subjects (**Fig. 2.2**). This analysis is used to identify spatial patterns but does not assume that there is a consistent temporal pattern across subjects. Timecourses were variance-normalised and 30-40 components outputted.

2.4.4.4 Seed-based analysis

Functional connectivity can also be directly measured between a seed and either the whole brain or a region of interest (ROI). I performed seed-based analysis on a cohort composed of all the FX individuals and the control group 1 using AFNI tools (Analysis of Functional NeuroImages, NIH).

First, a seed had to be created in the functional space of each individual. Next, a 1D file of the mean time series of the seed was extracted. Then, a Pearson correlation was performed between the 1D mean time series previously obtained and every voxels of the brain. The output of this step is the r-score. The r-score needs to be transformed to a z-score to do group analyses, using fisher's z-transformation. The r-score and z-score can be masked with the mask of a network of interest to specifically look at the connectivity of that RSN. Additionally, statistical analysis can be directly carried out on the mean r-score, which allows for advanced statistical analyses that cannot easily be done on whole functional images.

2.4.4.5 Connectograms

Whole brain connectivity can be illustrated under the form of connectograms. In chapter 4, I selected 26 brain regions of interest (Right and left prefrontal cortex, ACC, primary motor cortex, premotor, primary somatosensory cortex, secondary somatsensory cortex, insula, caudate putamen, nuccleus accumbens, hippocampus, amygdala, thalamus and corpus callosum), I calculated the FC between each combination of brain region pairs (see section 2.4.4.4 above for method) and arranged them as a connectogram. The connectogram was created using the Circos tool (Krzywinski et al., 2009). In a connectogram the FC strength is represented by the colour of the line connecting two brain regions.

2.4.4.6 Statistical analysis

Group-average spatial maps, obtained from the seed-based analysis and ICA, were dual-regressed to obtain subject-specific version of the spatial maps for the whole cohort (FX individuals and control groups 1 and 2) (FMRIB Software Library v6.0, Oxford, UK). First, the group-average spatial maps were regressed into each subject's 4D dataset. With this first step we obtain a subject-specific timeseries for each group-averaged spatial map. Next, the timeseries obtained in step 1 were regressed into the same 4D space-time dataset, resulting in a subject-specific spatial maps for each of the group-average components.

GLM was applied to test for group differences using FSL's permutation-testing tool randomise (FMRIB Software Library v6.0, Oxford, UK).

2.4.4.7 Voxel-based morphometry

Voxel-based morphometry (VBM) was performed to measure changes in local grey matter density using the VBM tool of FSL (FMRIB Software Library v6.0, Oxford, UK).

First, non-brain tissues were removed from the T1-weighted structural images. This was done using BET (FSL v6.0, Oxford, UK). The results were further improved manually. A non-linear registration was then performed to transform the structural images to a standard space to create a study specific grey matter template. Next, the structural images were registered to the study template using an affine registration.

Finally, voxelwise GLM was applied using permutation-testing for statistical analysis.

Chapter 3

Establishing a methodology to study Functional Connectivity in rodents

3.1 Introduction

Preclinical animal models have been an invaluable tool for the study of neurodevelopmental disorders, helping us further our understanding of disease mechanisms and facilitating drug discovery and testing. Recently, advances in genetic engineering techniques have made possible the development of genetically modified rats. They have proven to be particularly useful for the study of neurodevelopmental disorders (Till et al., 2015), as they exhibit a wide range of social and cognitive functions and their larger brains relative to mice facilitate the use of imaging techniques. In addition, they are the animal of choice of the pharmaceutical industry (Iannaccone and Jacob, 2009).

Although predominantly used in clinical studies, MRI offers a platform to bridge the gap between basic science and clinical research, being directly translatable across species. Resting state fMRI is particularly well suited for this endeavour as it is used to study brain activity in a task-free manner, facilitating its application in both animals and clinical populations that may have difficulties with task performance.

In recent years there has been an increase in the number of rsfMRI studies performed on preclinical models, notably in rodents (Lu et al., 2012; Upadhyay et al., 2011; Jonckers et al., 2011). However, the development of rodent resting state studies remains difficult. One reason is that MRI resources have not yet been fully adapted to rodents. Another, is that neuroimaging data is acquired, preprocessed and analysed using a plurality of options, tools and software, with little consensus over their use (Carp, 2012). This

methodological flexibility leads to a substantial variability in results (Gronenschild et al., 2012; Carp, 2012), a difficulty in replicating and assessing results, and an increased rates of false positives (Carp, 2012). Despite the existence of reporting guidelines (Poldrack et al., 2008) and of recommendations to enhance reproducibility for both human (Soares et al., 2016) and rodent studies (Grandjean et al., 2020), crucial details are often misreported in papers (Carp, 2012; Guo et al., 2014), and there still appears to be as many analysis pipelines as there are papers (Carp, 2012).

Taken together, these reasons make it challenging for preclinical scientists to join the field of rodent rsfMRI. Therefore, this first chapter will be dedicated to reviewing how I established a protocol for rat resting state analysis, discussing the underlying methodological choices made at the acquisition, preprocessing and data analysis level. I will further discuss how I tested my methodology, first through an investigation of its translatability across species and second by assessing the impact of anaesthesia on RSNs.

3.2 Results

3.2.1 Methodology troubleshooting

A MRI study is composed of 3 main parts: the acquisition of the scans, the preprocessing of the images obtained and the data analysis. In the following section, I will review a number of options that needs to be decided upon at each of the stages of a MRI study and discuss how these might influence the results obtained. I will also highlight the parameters I selected for my resting state protocol, which I worked out based on a cohort of 12 WT rats.

3.2.1.1 Acquisition of rsfMRI data

Definition of terms
T1* - Longitudinal relaxation time: Decrease in the longitudinal relaxation following the deactivation of radiofrequency pulses.
T2* - Transverse relaxation time: Decrease in the transverse relaxation following the deactivation of radiofrequency pulses.
GRE - Gradient echo: Signal formation algorithm characterised by having a radiofrequency pulse followed by a gradient reversal.
EPI - Echo-planar imaging: Fast method of acquiring MR images.
TR - Repetition time: Time between two radiofrequency excitation pulses.
TE - Echo time: Time between the radiofrequency pulse and the signal echo.

The intensity of a MRI signal is determined by three factors: spin density, longitudinal relaxation time (T1*) and transverse relaxation time (T2*) (Seong-Gi and Bandettini, 2010). T1* is sensitive to modulations in the cerebral blood flow, while T2* is sensitive to changes in paramagnetic content (Seong-Gi and Bandettini, 2010). Functional MRI can be used to look at brain function by applying a contrast that influences T1* or T2*. A commonly used contrast is the BOLD MRI contrast. The BOLD contrast exploits the difference in magnetic properties between oxygenated and deoxygenated haemoglobin (Chen and Glover, 2015). Increased activity induces a transient increase in oxygenated blood, locally changing the paramagnetic content, and therefore T2* (Chen and Glover, 2015).

Pulse sequences are applied to the MRI hardware to obtain MRI images (Seong-Gi and Bandettini, 2010). They must be chosen to maximize the signal to noise ratio (SNR) and the contrast (Seong-Gi and Bandettini, 2010), in our case the BOLD contrast. The pulse sequence used to obtain the resting state data presented in this thesis is a gradient recalled echo echo-planar imaging (GRE-EPI) sequence.

GRE refers to its signal formation algorithms, i.e. the number, frequency and type of signals that need to be applied to the gradient and coil in order to get a MRI signal (Seong-Gi and Bandettini, 2010). GRE is a type of gradient echo pulse, characterised by having a radiofrequency (RF) pulse followed by a gradient reversal (Seong-Gi and Bandettini, 2010). Compared to the alternative spin-echo sequence, the GRE sequence has a higher sensitivity but a lower spatial density (Seong-Gi and Bandettini, 2010). Because of its high sensitivity, it is often chosen for BOLD fMRI.

EPI refers to a fast method of acquiring images. MRI images are acquired under the form of a graphic matrix, called k-space. Each point in k-space holds information about every location of the MRI image. The k-space is then transformed into a MRI image using a Fourier transform (Poustchi-Amin et al., 2001). In EPI, the whole k-space is sampled with either a single or a small number of excitations, defined as shots (**Fig. 3.1**) (Poustchi-Amin et al., 2001). The time resolution of EPI (20-100ms) enables you to study physiological events on a quicker time scale than traditional MRI sequences (Poustchi-Amin et al., 2001).

Pulse sequences are characterised by a series of parameters, a number of which will be described below. The choice of these parameters will determine what trade-off is being made with regards to SNR, spatial resolution, temporal resolution, motion artefacts and contrast.

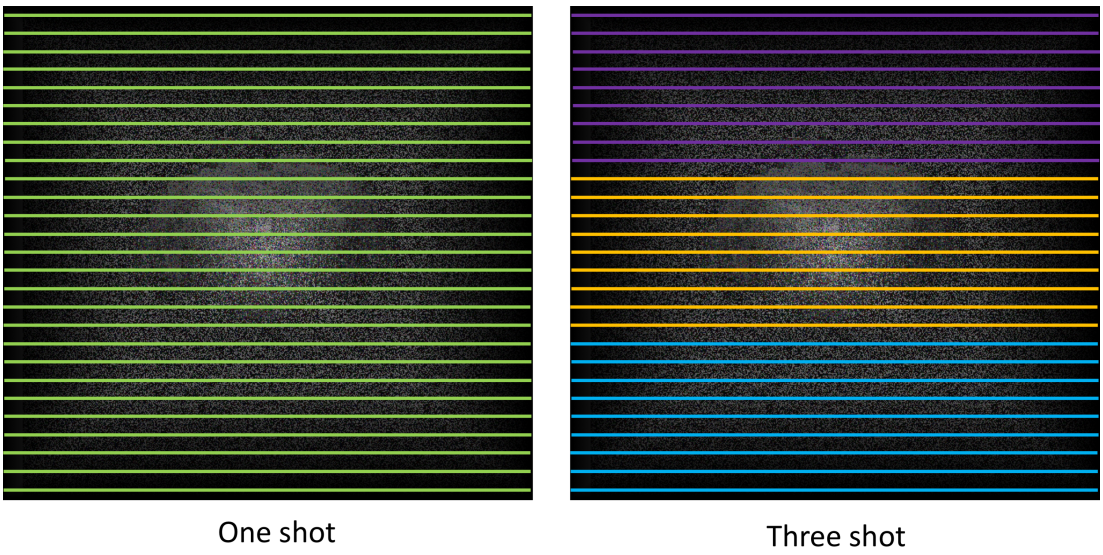


Figure 3.1: K-space sampling during EPI. In the left panel, the k-space is being sampled in one shot (depicted in green). In the right panel, only a portion of the k-space is sampled with each shot. Three shots (depicted in purple, yellow and blue) are needed to acquire the whole the k-space.

Number of shots A quick acquisition time can be achieved by decreasing the number of EPI shots. A small number of shots is also associated with a high SNR and contrast-to-noise ratio (CNR). However, it also leads to greater geometric distortion and off resonance effects (Poustchi-Amin et al., 2001), as seen in **Fig. 3.2**. To maximize SNR while minimizing image distortion, I decided to go with a 2-shot EPI for rsfMRI scans

on the Agilent scanner.

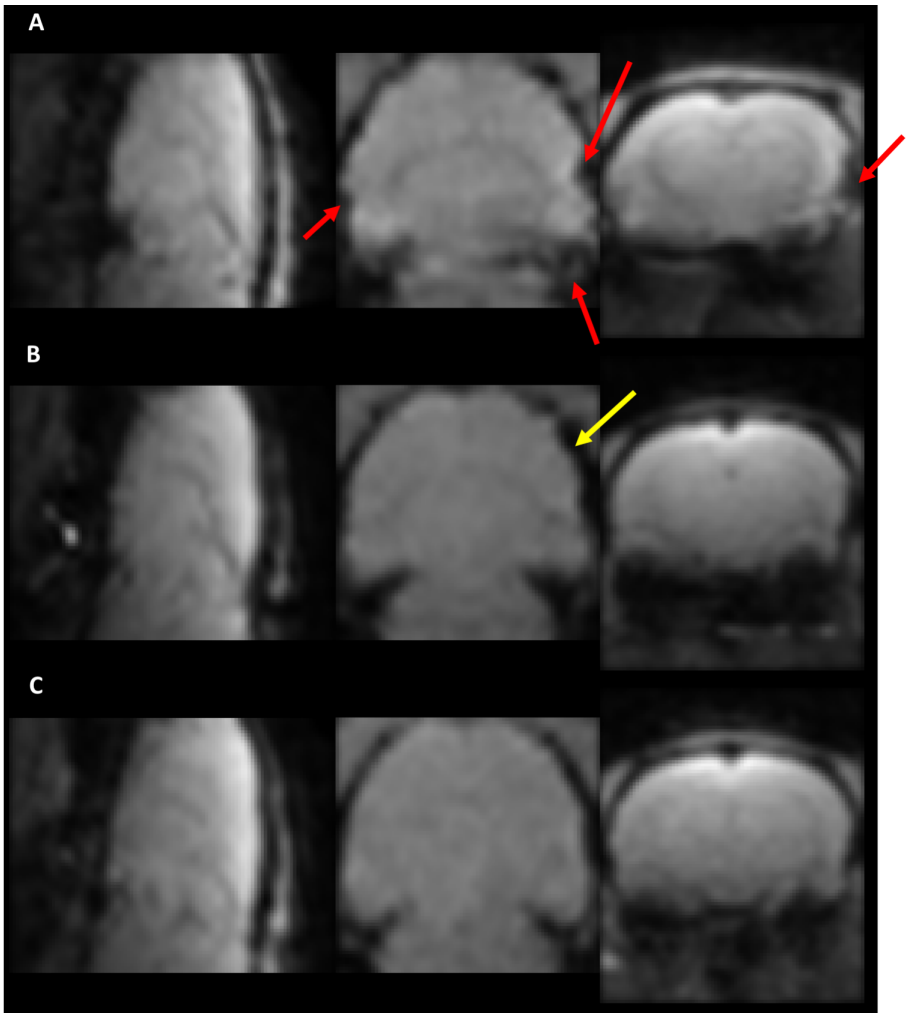


Figure 3.2: Impact of the number of shots on functional images acquired on an Agilent scanner. From left-to-right, the sagittal, axial and coronal planes of a functional image of WT rat brain (example animal) acquired using 1-, 2- or 4-shot EPI. (A) A high number of geometric distortion artefacts, as depicted by the red arrows, can be observed under 1-shot EPI. (B) Mild geometric distortion artefacts, as depicted by the yellow arrow, can be seen under 2-shot EPI. (C) No obvious artefacts are detected under 4-shot EPI.

Another way of reducing distortion effects without compromising on SNR and CNR, is by increasing the gradient strength (Poustchi-Amin et al., 2001). As you can see in **Fig. 3.3**, using the Bruker scanner, equipped with stronger gradient, the amount of distortion observed in functional images obtained by 1-shot and 2-shot EPI is comparable. In such a setting, 1-shot EPI therefore gives you an increased SNR and CNR, without increased distortion. As such, in this set up, I used 1-shot EPI to obtain the resting state scans.

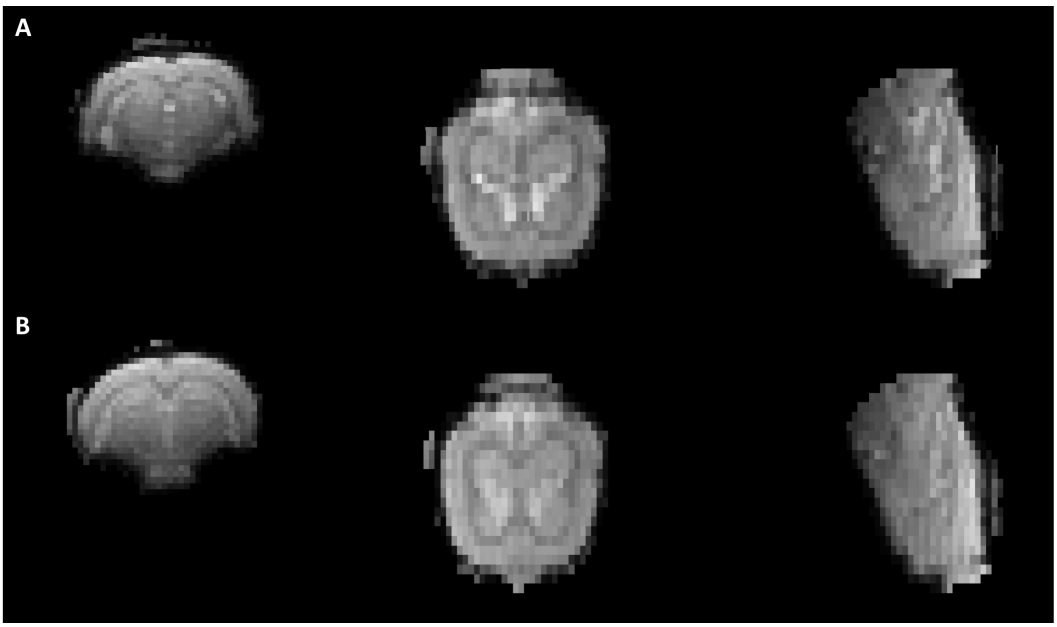


Figure 3.3: Impact of the number of shots on functional images acquired on a Bruker scanner. From left-to-right, the coronal, axial and sagittal planes of WT rat (example animal) functional brain image acquired using 1- or 2-shot EPI, showing no signs of obvious artefacts. (A) 1-shot gradient EPI. (B) 2-shot gradient EPI.

Echo Time and Repetition Time Repetition time (TR) is the time between RF excitation pulses. Echo time (TE) corresponds to the time between an RF pulse and the maximal signal amplitude, termed echo (**Fig. 3.4**).

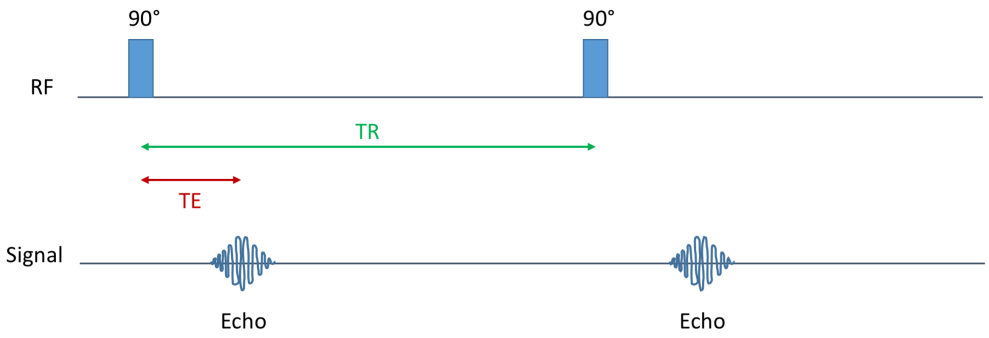


Figure 3.4: GRE sequence parameters TR and TE. On the top line is shown the 90° RF pulses. The gradient echoes are depicted on the bottom line. TR is shown in green and TE is shown in red.

Choosing a TR value comes with a trade-off between temporal and spatial resolution (Soares et al., 2016). A lower TR value improves temporal resolution but can lead to a lower SNR, while a longer TR value will increase spatial resolution but increases the

probability of subject movement within that time. Spatial resolution is often sacrificed for a higher temporal resolution. Increased field strength, faster acquisition protocol or reduced brain coverage can help minimize the downsides of having a low TR.

The TE value should ideally equal the apparent tissue T2* value in order to maximize the T2* contrast. However, long TE values tend to lead to more susceptibility-induced artefacts. TE values must therefore be chosen to maximize the BOLD signal sensitivity while minimizing susceptibility-induced signal loss (Hutton et al., 2002).

The T2* value varies with tissue type and gradient strength. For example, at 7T, the T2* value varies in the human brain between 16.1 ± 1.6 ms in the Putamen, to 33.2 ± 1.3 ms in the cortex (Peters et al., 2007). An optimal TE value at 7T would therefore be around 16ms to 33ms, depending on the brain region of interest.

Fig. 3.5 compares the raw image and the resting state signal obtained in a WT rat with a 12ms TE to those obtained with a 15ms TE. The resting state signal is slightly stronger at 15ms, as this TE value is closer to T2*.

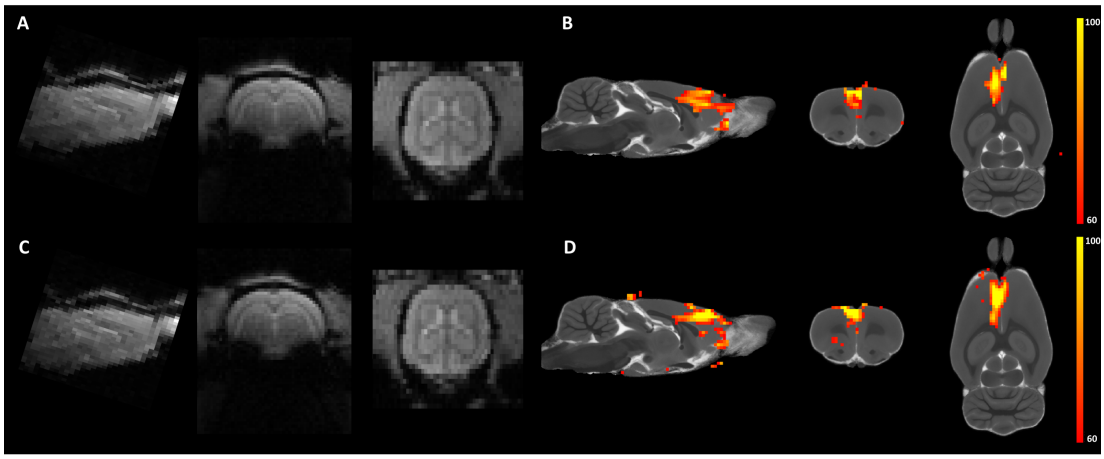


Figure 3.5: Impact of the Echo Time (TE) on functional images. (A) Raw functional image of a WT rat (example animal) acquired with a 12ms TE and (B) the DMN functional connectivity map that was extracted from it. The sagittal, coronal and axial sections are shown from left-to-right. (C) Raw functional image of a WT rat (example animal) acquired with a 15ms TE and (D) the DMN functional connectivity map that was extracted from it. The sagittal, coronal and axial sections are shown from left-to-right. Colour bars (B & D) represent BOLD signal ranging from 0 to 100.

For this study, I wanted to minimize signal loss, as electrophysiological changes have been reported in *Fmr1* KO rats in the amygdala which is at an air/tissue interface (Jackson, 2017). Brain tissues and the air have different magnetic susceptibilities. Nearly all biological tissues apart from bones are weakly diamagnetic, while the air is slightly paramagnetic (Collins, 2016). Difference in susceptibility causes distortions at air/tissue

interfaces, for example near the ear cavity (Collins, 2016). It can for this reason be difficult to study brain regions that are situated near an interface, such as the amygdala. I therefore decided to acquire the data using a 12ms TE, as it is close to the optimal T2* value, but importantly reduces susceptibility artefacts.

Coil RF head coils can also affect the data quality. Specifically, the number of channels in a RF coil can affect the SNR, with 32-channel coil providing a 2-to-3 times higher SNR ratio than those with only 8 channels. However, this increase in SNR is not homogeneous throughout the brain. The SNR is higher on the surface, i.e. over the cortex, but lower in deeper brain structure, leading to an inhomogeneous signal (Blamire, 2008). When looking at group differences, this set up would mean that it will be easy to identify cortical differences in activity, but harder to observe changes in subcortical structures.

Additionally, the image contrast can vary with the type of RF coil (**Fig. 3.6**). While whole-brain coils produce more homogeneous signal throughout the brain and higher image contrast (**Fig. 3.6A**), surface coils produce high SNR in the cortex, but lower SNR with increased depth penetration and a lower image contrast (**Fig. 3.6B**).

It is therefore critical to remain consistent with the choice of coil throughout the study in order to prevent methodological errors (Panman et al., 2019).

Another point worth noting is that a GRE-EPI sequence with a short TR, such as the one selected for this study, is demanding on the MRI scanner hardware. It is therefore important to choose a coil that can withstand such a sequence and thoroughly test it before starting a study to make sure it does not break in the middle of it, like it did during the pilot phase of my project.

Keeping all those requirements in mind, I chose to proceed using a Rapid surface coil, as the cortical SNR obtained with this coil was superior to the whole-brain coil and the SNR in deep brain structures was equivalent to it. Furthermore, it was compatible with the GRE-EPI sequence that I planned to used.

3.2.1.2 Preprocessing

Once the images are acquired, they need to be preprocessed before data analysis can be performed. Preprocessing refers to the series of transformations that must be

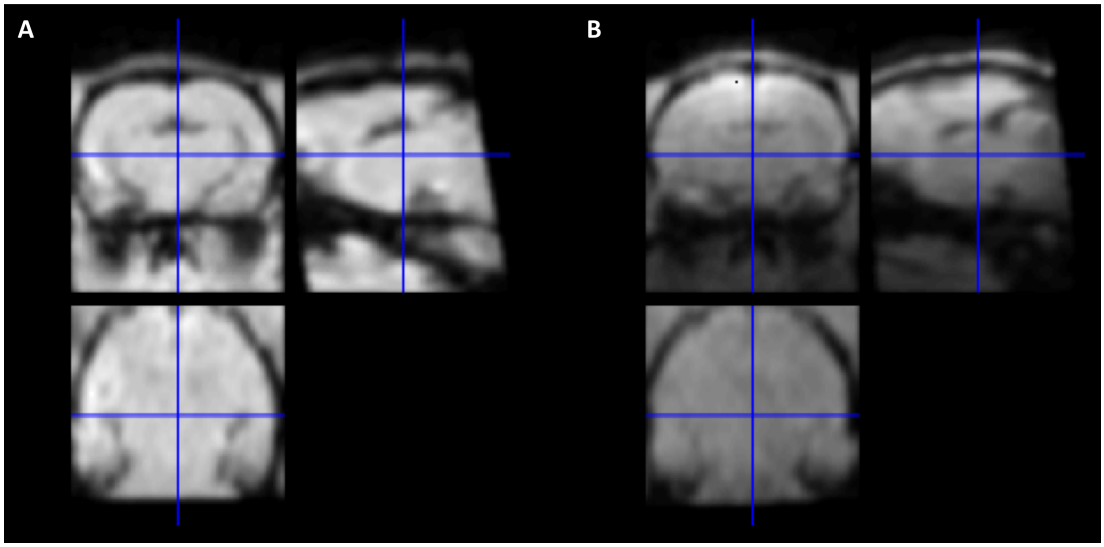


Figure 3.6: Comparison of the effect of head coils on functional image quality. Top left-to-right, the coronal and sagittal sections and bottom the axial section of a WT rat (example animal) functional image acquired using a PulseTEQ or Rapid coil. (A) PulseTEQ coil, a whole brain coil producing high image contrast (brain structures are identifiable). (B) Rapid 72x2 coil, a surface coil producing low image contrast (no brain structures are identifiable) but high SNR.

performed on the images in order to get them ready for data analysis (**Fig. 3.7**) and which I outline below. The same preprocessing steps are used in clinical and preclinical MRI. However, an additional preprocessing step is required with rodent data, which is the scaling of the structural and functional images by a factor of 10 in the x, y and z direction. This is done to account for differences in brain size between rats and humans and to enable us to use clinical MRI analysis software.

1. **Preliminary quality control.** After acquiring the images, while the subject is still in the scanner, it is important to run through the images acquired to check for gross acquisition artefacts, such as movement. It is crucial to do it then as it gives you the opportunity to acquire new scans if needed.

2. **File format conversion.** Each scanner manufacturers have their own data format, although there is some standardization for clinical scanners. Therefore, the next step is to convert the images from the scanner format to a format that can be read by imaging software, namely the analyze format (.hdr/.img) for SPM and the nifti format (.nii) for FSL.

3. **Slice timing.** Slices are typically acquired one after the other, which means that a small lapse of time has passed between the acquisition of the first and of the

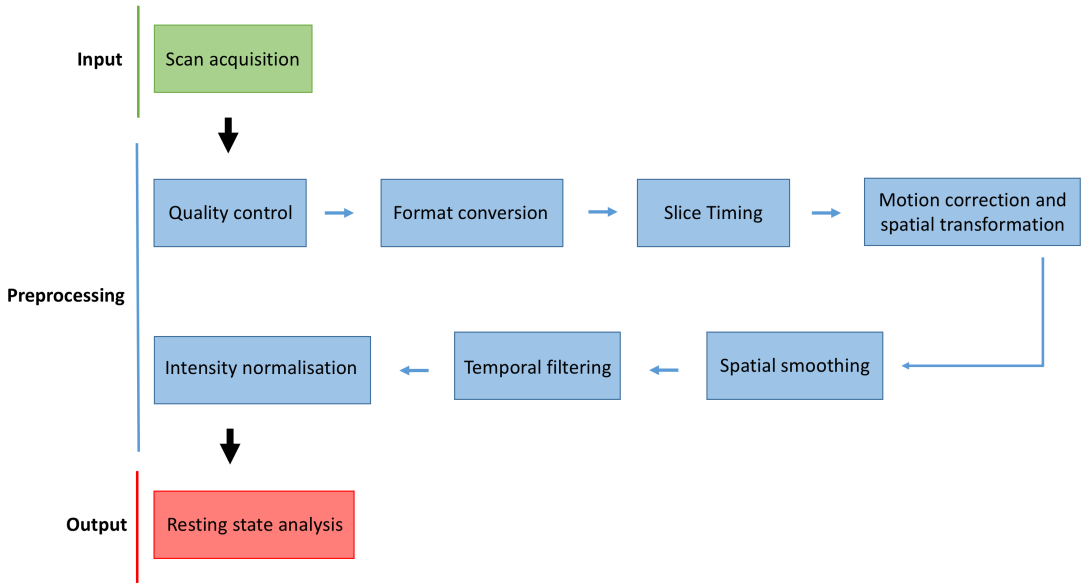


Figure 3.7: Flowchart of preprocessing steps.

last slice. Slices can be acquired sequentially or in an interleaved fashion to limit the impact of acquisition time. This is less of an issue in rodent brains as they are small, but in human brains, it is important to correct for differences in slice acquisition, which is termed slice timing.

Additionally, the first few volumes that are acquired are usually discarded to account for the time needed (approximately 10 seconds) for the scanner to stabilize its gradient and for the tissue being scanned to reach the necessary excitation level (Soares et al., 2016). For this project, the first 10 volumes of each scan were discarded.

4. **Image registration.** Next the functional images need to be registered, first individual volumes to one another, then to the structural image and finally to a high-resolution structural image termed template. Registration of functional images from different subjects to the same template will enable group-analysis by making sure that the voxels being compared are covering the same brain area across subjects.

   Registration of individual volumes of a functional image to one another can be performed using built-in software tools, like the MCFLIRT tool in FSL, to minimize subject motion in the scanner. Simple movement such as gradual rotation of

the head over time can be corrected this way. For better results, additional motion correction steps can be performed, such as regressing out movement components identified through single-subject independent component analysis (ICA).

Registration accuracy can be improved by removing non-brain structures from functional and structural images. Brain extraction tools that are built in pre-processing software are usually only adapted to human brains, that are roughly spherical, and do not perform well on rodent brains that are oblong, without having performed some initial transformations on them. For this reason, I chose to use the brain extraction tool Skullstripper (Delora et al., 2016), as it is designed to be used on data from rodent brains.

Another parameter that can improve registration is the setting of the images bounding box (Yoshino et al., 2014). The bounding box controls what portion of the image is used for registration. Optimal setting of the bounding box can facilitate registration, while an improper setting will lead to an unsuccessful registration (**Fig. 3.8**).

5. **Spatial smoothing.** The following preprocessing step is spatial smoothing, a process during which the voxel's signal is averaged with its neighbour's, typically using a Gaussian kernel. Spatial smoothing increases SNR by reducing anatomical differences and increases the validity of General Linear Model (GLM) statistical tests by ensuring the data fulfils the tests' assumptions. However, smoothing also decreases the image resolution and may smooth out small but meaningful activations (Soares et al., 2016). The kernel size, defined by its FWHM, will determine the extent to which the data is smoothed. Typical values for group analysis is 5-10 mm, for both human data and 10x scaled up rodent data. In this study, a kernel with a 5 mm FWHM was chosen.

6. **Temporal filtering.** A high-pass temporal filtering is typically performed in fMRI studies to remove low-frequency artefacts, such as slow scanner drifts. This step can help increase SNR by decreasing the noise in the data. Since resting state signal is thought to be limited to a low frequency range, it is standard practice to also remove high-frequency signals using a 0.01 - 0.1 Hz band-pass filter (Biswal et al., 1995). However, some studies suggest that frequency signals above 0.1 Hz

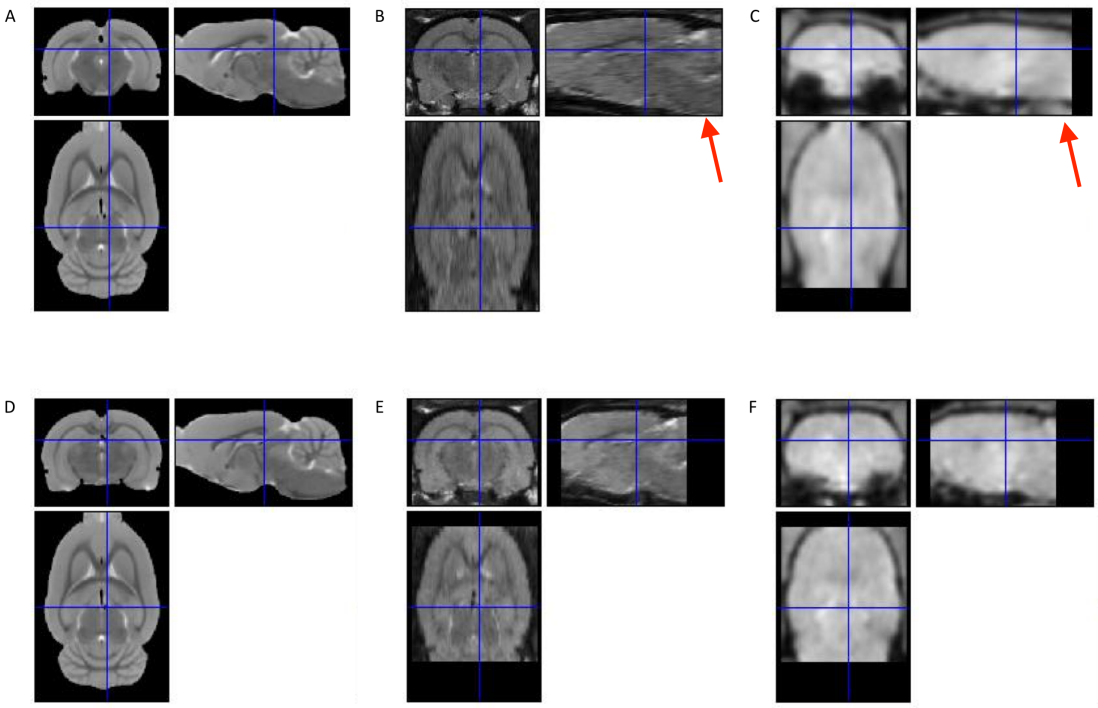


Figure 3.8: Impact of bounding box size on images registration during preprocessing. (A-C) Unsuccessful registration of the anatomical and functional images of an example animal to the template when using the bounding box [-80 -90 -130; 80 108 150]. The template, a high resolution anatomical image is shown in (A). The anatomical image (B) and the functional image (C) are stretched out in comparison to the template, as shown by the red arrows. (D-F) Successful registration of the same anatomical and functional images to the template when using the bounding box [-80 -90 -110; 80 108 50]. The template, a high resolution anatomical image is shown in (D). The anatomical image (E) and the functional image (F) are perfectly aligned with the template.

are also of functional importance (Cordes et al., 2001; Chen and Glover, 2015). Therefore, to avoid discarding frequencies of interest, a 100s high-pass filter was used in this study.

7. **Intensity normalisation.** Finally, global intensity normalisation is performed to ascertain that the signal mean is constant across sessions and individuals. This is done by scaling the 4D dataset to the same group mean by a single factor (FSL (FMRIB Software Library) v6.0, Oxford, UK).

3.2.1.3 Functional connectivity analysis

Once the images have been preprocessed, the next stage is functional connectivity analysis. A number of different methods can be used to extract functional connectivity information from a dataset (**Fig. 3.9**).

Historically, seed-based analysis has been the method of choice to study functional connectivity (Biswal et al., 1995), providing the researcher a map of the connectivity between a region of interest (ROI) and the rest of the brain. Seed-based analysis has evolved into voxel-wise analysis (Dinstein et al., 2011), where every voxel becomes a ROI, which in turn can be summarised using Graph Network Theory measures (Rubinov and Sporns, 2010). ICA provides a data-driven alternative to seed-based analysis (Jung et al., 2001), removing the need to select a specific ROI. It is for this reason that I decided to use ICA in my experiments. I additionally used the seed-based method to specifically probe DMN connectivity.

ICA together with ROI-based methods provide tools to assess functional connectivity at the whole brain scale. There are additional techniques that make it possible to investigate local connectivity, such as the Regional Homogeneity (ReHo) (Zang et al., 2004) and the Amplitude of Low-Frequency Fluctuation (ALFF/fALFF) methods (Wang et al., 2012; Yu-feng et al., 2007).

Additionally, there are multiple software packages which can be used to perform resting-state analysis. It is particularly important to pay attention to the following points when choosing one:

- Availability of the resting state analysis method of your choice, as some software packages are specialised in one analysis method;

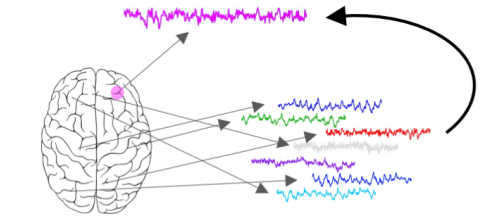
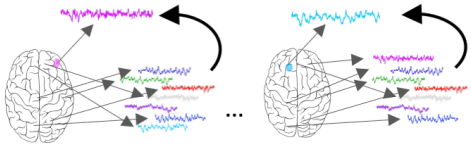
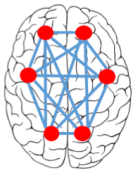
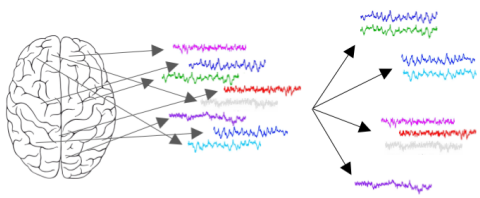
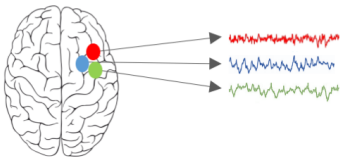
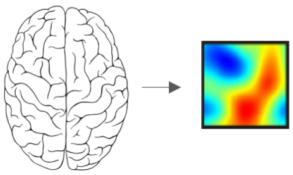
	**Seed-based analysis** Seed-based analysis consists in selecting a predefined seed, your region of interest (pink circle), extracting its average time course and correlating it with the time course of each grey matter voxel or with the averaged time course of another region of interest. The result is a functional connectivity map showing which regions are functionally connected to the seed and the strength of those connections. It therefore only gives information about the selected brain region (Biswal et al., 1995).
	**Voxel-wise analysis** Brain-wide extension of seed-based analysis. Here the time course of every voxel is correlated with the time course of every other voxel in the grey matter, each voxel effectively becoming a seed (pink and blue circles) (Dinstein et al., 2011). This method makes it possible the study functional connectivity at a whole-brain scale, however it produces a large volume of data. It is often summarized using graph network metrics.
	**Graph Network Theory** A network is a mathematical model of a complex system. It is defined as a set of nodes and edges. In large scale brain networks nodes (red circles) represent anatomically defined brain areas and edges (blue lines) the anatomical, functional or effective connections between pairs of nodes. Different network measures can be applied to the network to characterize aspects of local and global brain connectivity (Rubinov and Sporns, 2010).
	**Independent Component Analysis** Independent Component Analysis (ICA) is a data-driven method. It refers to a group of related algorithms that uses the principle of independence to perform blind source separation (Jung et al., 2001). It can be applied to fMRI data to separate time courses of functionally connected brain regions, since they will have similar time courses, distinguishable to those of other networks (Jung et al., 2001).
	**Regional Homogeneity** In the Regional Homogeneity method (ReHo), a Kendall's coefficient of concordance (KCC) is given to a voxel (blue circle) based on this voxel and its neighbours' (red and green circles) time series. It is assumed that neighbouring voxel must have temporally similar time series. An individual KCC map can be generated that way, providing information on the homogeneity of clusters identified (Zang et al., 2004).
	**(Fractional) Amplitude of low-frequency fluctuation** The Amplitude of low-frequency fluctuation (ALFF) method measures the amplitude of low-frequency fluctuation, reflecting the absolute intensity of the brain spontaneous activity. Each voxel's time series is transformed to a frequency domain. The square root is then calculated at each frequency of the power spectrum, and the average is taken across the resting-state frequencies at each voxel. This averaged square root (ALFF) can then be used to generate an individual ALFF map (Wang et al., 2012; Yu-feng et al., 2007). ALFF is sensitive to non-physiological signal fluctuation. To overcome this limitation, a ratio of the power at each frequency at a low-frequency range to the whole frequency range can be calculated (fractional ALFF or fALFF) (Wang et al., 2012).

Figure 3.9: Resting State Functional Connectivity Methods. This figure highlights common approaches that have been developed to study functional connectivity, at both a global and local scale.

- Possibility to preprocess and analyse your data with the same software;
- Ability to perform statistical analysis;
- Ease of use with a non-human dataset.

The strengths and weaknesses, specific to my project, of the different software I used are summarised in **Table 3.1**.

Table 3.1: *Pros and cons of MRI software tested for resting state analysis.*

	SPM	FSL	REST	DPABI	GIFT
Pros	This software has tools for preprocessing MRI data, performing GLM analysis and visualizing results. It is particularly well suited for group analyses. Good documentation available.	This software has tools for pre-processing MRI data, ICA analysis, performing GLM analysis and it has a powerful stand-alone tool for visualizing data and results. It is particularly well suited for group analyses and for ICA. Possibility to write scripts for more advanced options. Good documentation available.	This software has tools for various functional connectivity analysis (seed-based analysis, ReHo, ALFF/fALFF) and statistical analysis. It is automated.	This software has tools for various functional connectivity analysis (seed-based analysis, ReHo, ALFF/fALFF) and statistical analysis. It is automated. There are rodent and non-human primate options.	This software is dedicated to performing ICA and blind source separation. The user has access to a lot of options over how the ICA will be performed.
Cons	No built-in resting state analysis tools. Some community-developed extensions for human rsfMRI analyses. Another option is to preprocess images with SPM and perform FC analyses on another software. It is designed for human data and analyses, and need to be adapted for use with rodent data.	Familiarity with Unix required. Seed-based analysis can only be done through the command line. It is designed for human data and analyses, and need to be adapted for use with rodent data.	Limited documentation available. Little control over the analysis or knowledge on how the analysis is being carried out.	Limited documentation available. Little control over the analysis or knowledge on how the analysis is being carried out.	No built-in preprocessing or statistical analysis tools. Prior knowledge of ICA and blind source separation is required. The documentation available is quite technical. It is designed for human data and analyses, and need to be adapted for use with rodent data.

GLM: General Linear Model, ICA: Independent component analysis, ReHo: Regional Homogeneity, ALFF: Amplitude of low-frequency fluctuation, fALFF: Fractional amplitude of low-frequency fluctuation.

3.2.2 Resting state networks are shared across species

After establishing a resting state protocol (details of the protocol used in chapters 4 and 5, with step-by-step instructions, can be found in **Appendix A**), I set out to test it. The default mode network (DMN) is a highly studied brain network. It is composed of the anterior cingulate cortex (ACC), medial prefrontal cortex (mPFC), posterior cingulate cortex (PCC) and precuneus. Since the ACC/mPFC and the PCC/precuneus are non-adjacent brain structures in humans, this network is easily identifiable. Equivalent brain structures compose the DMN in rodent. There has been some debate regarding what is the homologous structure of the human PCC in rats. It is now generally agreed to be the retrosplenial cortex (Lu et al., 2012), as it has been shown that it is possible to obtain in rats a large-scale network of similar spatial distribution to the human DMN by performing a seed-based analysis using the retrosplenial cortex as a seed (Ash et al., 2016). In contrast to humans, the brain regions that form the DMN are anatomically connected in rodents, making it harder to distinguish it from noise. I therefore decided to first use my protocol in humans to determine whether I could identify the DMN using ICA.

I was able to successfully extract the DMN from human data (**Fig. 3.10A**). With that reassurance, I then confirmed the validity of this approach by successfully identifying the DMN in wild-type (WT) rats (**Fig. 3.10B**).

In addition to highlighting that this protocol can be used to identify resting state networks in both humans and rodents, this experiment also showed that the DMN can be identify in two different species, demonstrating the translational value of this technique.

3.2.3 Effect of anaesthesia on resting state networks

Anaesthesia is commonly used in preclinical rsfMRI studies to minimize movement and distress to the animals. However, anaesthesia has been shown to modulate neural processing and the brain vasculature, and therefore potentially impacts the BOLD signal and RSNs (Masamoto and Kanno, 2012; Bukhari et al., 2017; Grandjean et al., 2014). To counteract this effect, a handful of groups are now developing protocols to perform awake fMRI studies (Upadhyay et al., 2011; Liang et al., 2012; Becerra et al., 2011; Harris et al., 2015; Brydges et al., 2013). Nevertheless, it is possible to identify

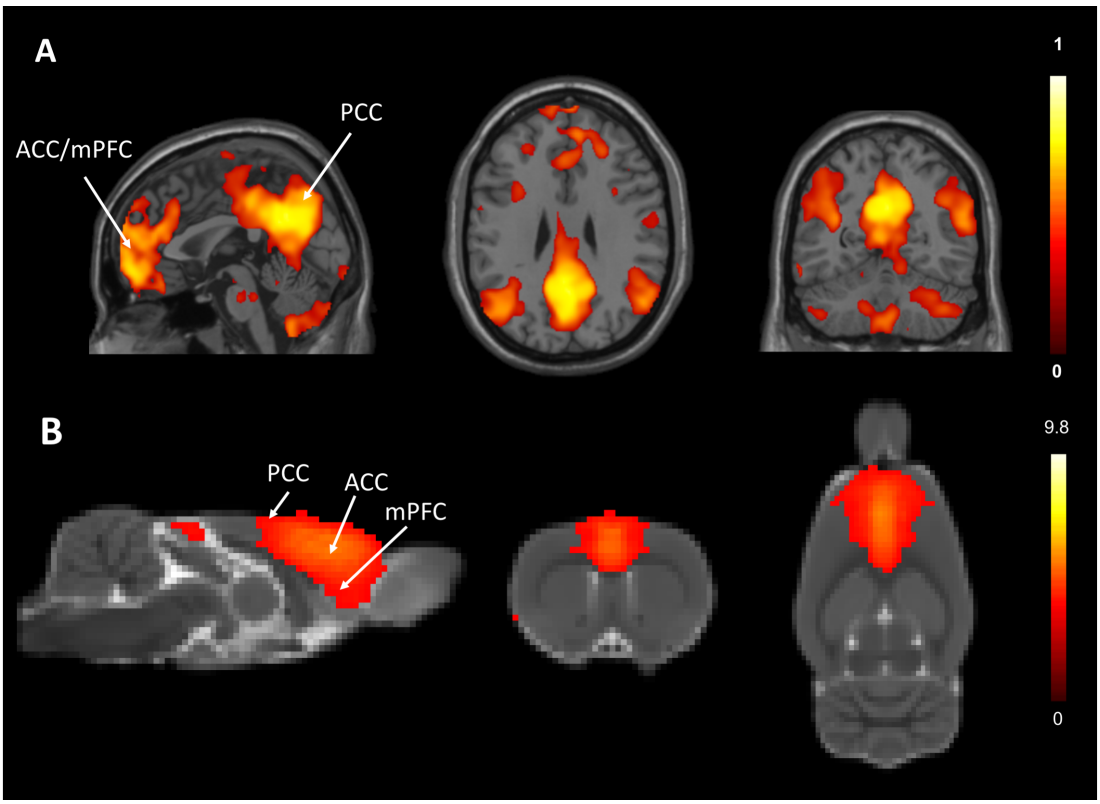


Figure 3.10: Resting state networks are comprised of equivalent brain structures in rats and humans. (A) The Default Mode Network (DMN) resting state network of an example human (sagittal, axial and coronal sections, n=1). (B) The DMN in 3-month old WT Sprague Dawley (SD) rats under 1% of isoflurane anaesthesia (sagittal, coronal and axial sections, n=8). Colour bars represent T-scores.

RSNs under anaesthesia in humans, monkeys, mice and rats (Lu et al., 2012; Vincent et al., 2007; Jonckers et al., 2011; Palanca et al., 2015), as well as during light sleep in humans (Horovitz et al., 2008; Larson-prior et al., 2009). RSNs strength depends on the level of consciousness (You et al., 2013). Specifically, RSNs connectivity decreases with increasing concentration of isoflurane (Wu et al., 2016).

To further test the reliability of my resting state analysis protocol, I took advantage of the ability to modulate RSNs with anaesthetics. First, I asked whether the length of time spent under anaesthesia would influences RSNs, and then I confirmed that RSNs connectivity could be modulated by the concentration of anaesthesia.

3.2.3.1 Resting state networks are unaltered with anaesthesia duration

The set up time, between securing the animal in the scanner and acquiring the first scan, can vary between animals on the order of tens of minutes. It was therefore important to determine whether the amount of time spent under anaesthesia could impact RSNs connectivity.

To do this, I acquired two resting state functional scans in WT Sprague Dawley (SD) rats, 10 minutes apart, anaesthetised with 1% isoflurane. I then compared the strength of the RSNs between the first (**Fig. 3.11A**) and second session (**Fig. 3.11B**). DMN connectivity was not significantly different between the first and second scans (**Fig. 3.11C**), suggesting that a small variation in set up time does not influence the connectivity of this RSN.

3.2.3.2 Increased level of anaesthesia reduces resting state networks connectivity

Next, I assessed whether increasing the concentration of isoflurane would decrease DMN connectivity, as previously demonstrated by Wu and colleagues (Wu et al., 2016). Rats were first scanned under 1% isoflurane anaesthesia (**Fig. 3.12A**). The concentration of isoflurane was then increased to 2.5% and, after waiting 10 min for the concentration to stabilize, the animals were scanned again (**Fig. 3.12B**). The DMN connectivity was significantly decreased under 2.5% isoflurane compared to under 1% isoflurane (**Fig. 3.12C**), indicating that this network can be modulated by anaesthesia strength.

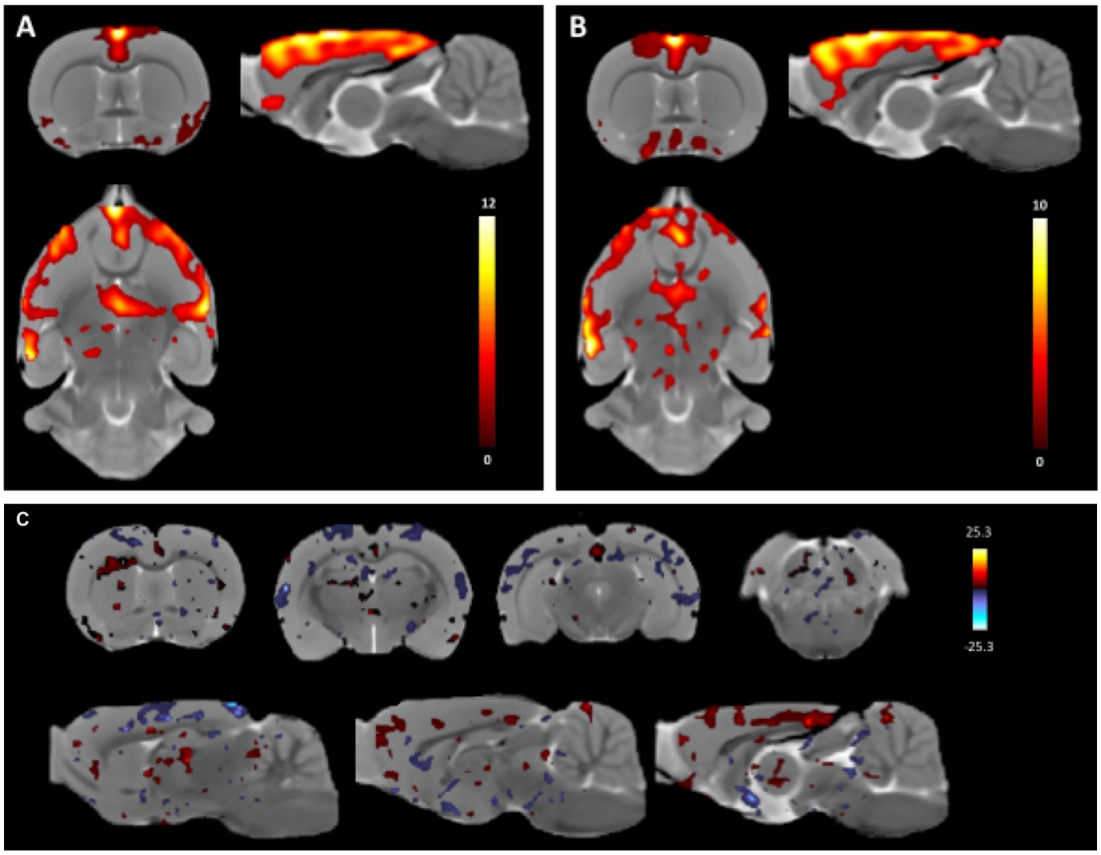


Figure 3.11: Impact of anaesthesia duration on the Default Mode Network connectivity in adult WT Sprague Dawley rats. Map of the DMN resting state network obtained by independent component analysis (ICA) in 3-month old WT Sprague Dawley rats under light anaesthesia (1% isoflurane). (A) Scan acquired at the start of the session (top: coronal and sagittal planes, bottom: axial plane, n=12). (B) Scan acquired 5 minutes after scan A ended (top: coronal and sagittal planes, bottom: axial plane, n=12) under 1% isoflurane anaesthesia (C) No difference in DMN connectivity between the first and second scan obtained under light anaesthesia (top: coronal sections, bottom: sagittal sections). Colour bars represent T-scores.

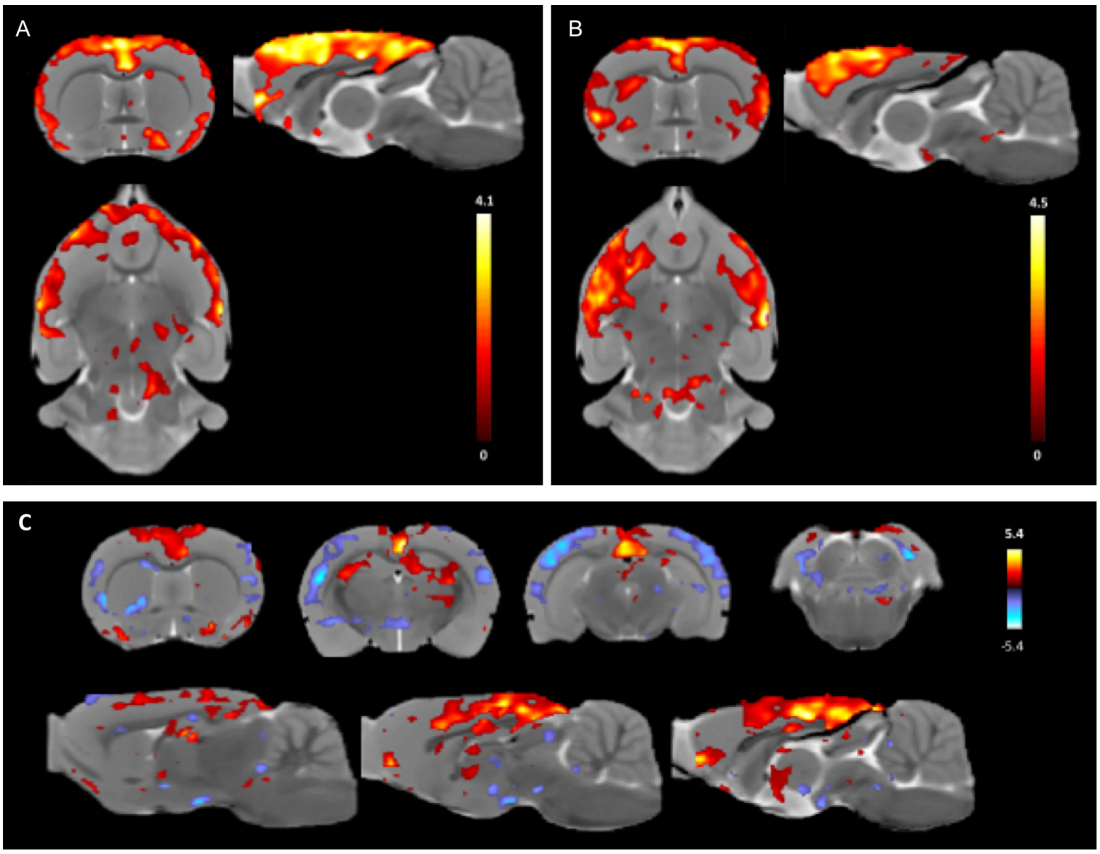


Figure 3.12: Impact of anaesthesia strength on Default Mode Network connectivity in adult WT Sprague Dawley rats. (A) Map of the DMN resting state network obtained in 3-month old WT Sprague Dawley (SD) rats under light anaesthesia (1% isoflurane) by independent component analysis (ICA) (top: coronal and sagittal planes, bottom: axial plane, n=12). (B) Map of the DMN resting state network obtained in 3-month old WT SD rats under moderate anaesthesia (2.5% isoflurane) (top: coronal and sagittal planes, bottom: axial plane, n=12) by ICA. (C) Increased DMN connectivity in rats anaesthetised with 1% isoflurane compared to 2.5% isoflurane (top: coronal sections, bottom: sagittal sections). Colour bars represent T-scores.

3.3 Discussion

3.3.1 Methodological flexibility

As discussed above, there are multiple hardware and preprocessing parameters, software packages and analysis methods that needs to be considered at each stage of a MRI study. This methodological flexibility allows researchers to select acquisition sequences and analysis pipelines that are specific to their research interest (brain area, timing of physiological event, hypothesis) and which maximize the SNR and CNR of the data acquired.

However, one drawback is that custom-made experiments are difficult to compare and assess. Open science has been proposed as a way to address this issue. This allows a thorough examination of the data and results, by enabling other researchers to apply their own analysis pipeline to the data. However, this is a labour-intensive process and cannot resolve any of the design or methodological shortcomings of individual studies (Koslow, 2000; Borghi and Van Gulick, 2018; Van Horn et al., 2004).

The use of different analysis pipelines can also increase the variation in the results and the number of false positives (Carp, 2012). One study that compared the performance of 6912 combinations of preprocessing steps and parameters on a single dataset found a wide variation in the activation strength and localisation with different pipelines (Carp, 2012). This study observed that each preprocessing step affected the activation strength differently across brain regions. Moreover, while peak localisation in specific brain regions was consistent across a number of pipelines, the peak localisation within these regions was found to be highly variable (Carp, 2012). It is therefore possible that the strength and localisation of brain activation reported in this thesis might vary with different preprocessing parameters. However, I am focusing on large-scale brain networks in this thesis and it is therefore unlikely that it would affect my overall conclusions.

3.3.2 Other methodological considerations

There are other considerations while setting up an MRI study that I have not touched upon in this chapter, as I did not select these options but used the ones offered by the preclinical imaging facility. These include the choice of sedation and the scanner

hardware.

In addition to the concentration, the type of anaesthetic or sedative used to induce loss of consciousness in subjects of resting state experiments has been shown to affect functional connectivity (FC) (Grandjean et al., 2014; Paasonen et al., 2018; Williams et al., 2010). Isoflurane was used in all the experiments presented in this thesis, as isoflurane is administered through inhalation and is suitable for longitudinal studies. In addition, stable physiology can be maintained with isoflurane anaesthesia (Grandjean et al., 2014). However, other anaesthetics are also suitable for rodent resting state studies, including α-chloralose, medetomidine, an isoflurane + medetomidine combination, urethane and propofol (Grandjean et al., 2014; Paasonen et al., 2018). Urethane is delivered intraperitoneally, while the other anaesthetics are injected intravenously (i.v). They require anaesthesia to first be induced by an inhalational anaesthetic, such as isoflurane. The use of each of these anaesthetic is discussed below.

Resting-state studies have reported that fronto-cortical connectivity is increased under isoflurane anaesthesia (Paasonen et al., 2018). In addition, thalamo-cortical and subcortical connectivities were found to be suppressed in comparison with awake animals (Paasonen et al., 2018) and medetomidine (Bukhari et al., 2017). Other studies have also reported a less localized connectivity under isoflurane (Williams et al., 2010). Taken together these results suggest that isoflurane may be inducing cortical activity, which would mask naturally occurring FC. However, it is worth noting that these studies used a moderate-to-high-dose of isoflurane. Different groups have reported that these effects are minimized at low-dose, with a connectivity pattern resembling that of awake animals (Grandjean et al., 2014; Liu et al., 2013). Furthermore, the DMN connectivity has been found to be better preserved under isoflurane anaesthesia than under other anaesthetic regimen. Specifically, the prefrontal DMN was found to be suppressed by anaesthetics other than isoflurane (Paasonen et al., 2018).

α-chloralose has typically been the anaesthetic of choice in rodent resting state studies, however researchers are turning to alternatives because it has severe side-effects and is therefore not suitable for longitudinal studies (Weber et al., 2006). FC is globally suppressed with α-chloralose anaesthesia. Nevertheless, it resembles the connectivity pattern observed in awake animals (Paasonen et al., 2018).

Medetomidine is a popular anaesthetic option for resting state experiments as it

is suitable for longitudinal studies. Studies have generally reported a similar-to-better performance compared to other anaesthetics (Grandjean et al., 2014; Paasonen et al., 2018; Bukhari et al., 2017; Williams et al., 2010), even if a few have reported a global suppression of connectivity and notably of the thalamo-cortical connection (Grandjean et al., 2014; Paasonen et al., 2018). However, medetomidine has strong side effects on the cardiovascular system, notably bradycardia, increased blood pressure and vasoconstriction (Grandjean et al., 2014; Paasonen et al., 2018). Grandjean et al. (2014) have also reported that i.v. infusion can induce an epileptic activity.

To limit the systemic effect of medetomidine, some have proposed using a combination of low-doses of isoflurane and medetomidine (Grandjean et al., 2014). Reducing the dose of the individual agents limits undesirable side-effects and dose-dependent effects on connectivity. FC obtained with the isoflurane and medetomidine combination of anaesthesia was found to have a good concordance to that detected in awake rats (Paasonen et al., 2018). Furthermore, their joint administration was reported to lead to greater connectivity than obtained under either agent on its own (Grandjean et al., 2014).

Urethane was reported to have a similar effect on connectivity to isoflurane (Grandjean et al., 2014), and similarly to it, urethane does not have a strong systemic effect on physiology. In addition, FC patterns obtained with urethane anaesthesia were highly similar to those observed in awake animals, making it a good candidate for resting state studies (Paasonen et al., 2018). However, urethane anaesthesia can induce a sleep-like state in rats, which could potentially confound FC results (Zhurakovskaya et al., 2016).

Finally, Paasonen and colleagues have found propofol to be a promising candidate for resting state experiments, as they have shown that FC under propofol is similar to that observed in awake rats (Paasonen et al., 2018). However, physiological conditions are unstable in propofol-anaesthetised animals, affecting the reliability of the data acquired (Grandjean et al., 2014). Therefore, depth and stability of anaesthesia would need to be optimised before propofol can be reliably used.

Fluctuations in physiological parameters can also alter the brain connectivity by providing a non-neuronal contribution to the resting state signal (Pan et al., 2015). It is therefore essential to monitor and control the animals' physiology during an experiment and to ensure that no difference in physiology is observed between groups of animals

being compared. Physiological parameters include body temperature, breathing rate, cardiac rate and blood oxygenation (Pan et al., 2015). In the experiments presented in this thesis, body temperature was monitored using a rectal probe and was maintained at 37°C using a hot hair ventilator. Breathing rate and blood oxygenation were also monitored using a transducer pad and a pulse oximeter, respectively. I found these parameters to be stable throughout the scanning sessions, with no between-genotype differences observed in any experiments presented in this thesis. It is particularly crucial to monitor CO_2 and O_2 levels as the BOLD contrast directly relies on blood oxygenation (Chen and Glover, 2015). Mechanical ventilation can be used to further control CO_2 arterial levels. Freely-breathing anaesthetised animals often exhibit increased CO_2 level in the blood and this can be associated with reduced FC (Biswal et al., 1997). Mechanical ventilation can therefore help prevent hypercapnia and increase FC sensitivity and specificity (Grandjean et al., 2020).

In this chapter, I have also discussed the impact of different acquisition parameters on resting state results. A perhaps more defining characteristic, is the strength of the static magnetic field (B_0) of the scanner. The BOLD CNR is usually very low, but can be increased with increased field strength. B_0 also increases spatial resolution and SNR, but at the cost of increased physiological noise (Van Der Zwaag et al., 2009; Skouras et al., 2014; Wald, 2012; Soares et al., 2016).

3.3.3 Resting state networks or noise?

Before 1995, fMRI studies were exclusively task-based and focused on high-frequency fluctuations of the BOLD signal, because low-frequency oscillations (< 0.1 Hz) were assumed to be noise. In 1995, Biswal and colleagues published a seminal paper, focusing on these low-frequency fluctuations (Biswal et al., 1995). In the brain at rest, they observed that low-frequency fluctuations in regions of the motor cortex associated with hand movement were strongly correlated both within that region and with other brain regions associated with motor function across both hemispheres. The correlation map obtained at rest was similar to the activation detected in a finger tapping experiment. This study therefore suggested that the low frequency oscillations were not exclusively noise but had functional relevance.

However, the need to distinguish between noise and functionally relevant networks

remains in resting state experiments. Furthermore, improper data analysis can lead to false activation, as was described in Bennett and colleagues' infamous salmon study, where they demonstrated that without proper correction, brain activation could be identified in a dead salmon (Bennett et al., 2009). Therefore, before carrying out any experiments, I wanted to confirm that the RSNs obtained with my protocol were not noise.

This was carried out in two ways. First, by testing my protocol on data from humans, where the DMN has been extensively studied and is composed of non-adjacent brain regions. Having successfully identify the human DMN, I then tested the same protocol, adapted to rodent brains, on data from rats. I was able to identify a network composed of equivalent brain regions to those observed in humans and comparable to the rat DMN components described in the literature (Lu et al., 2012). In addition to validating my protocol, my findings also highlight the translational nature of RSNs. The presence of a DMN in humans, rats, mice, monkeys and dogs (Jonckers et al., 2011; Lu et al., 2012; Vincent et al., 2007; Raichle et al., 2001; Kyathanahally et al., 2015), enables inter-species comparisons, including comparisons between animal models of a disorder and their corresponding clinical populations.

Second, by assessing the impact of anaesthesia on RSNs in rats. Since increased anaesthesia concentration has been shown to decrease the connectivity of RSNs (Wu et al., 2016), determining that anaesthesia strength can modulate the DMN helps further support the idea that this is a true RSN and not noise.

3.4 Summary

In summary, this chapter details the protocol I established for the acquisition, preprocessing and data analysis of rat resting state data, highlighting methodological choices that were made at each stage. This protocol was then validated in two species, confirming its ability to identify the DMN in both humans and rats. This experiment also highlighted the translatability of the technique, paving the way to using it a clinical context. The protocol was further assessed through the use of anaesthesia, first by establishing that FC is not affected by variation in the scanner set up time, and second by confirming that DMN connectivity could be decreased with increased anaesthesia.

Chapter 4

Impaired Functional Connectivity in Fragile X Syndrome

4.1 Introduction

Autism Spectrum Disorders (ASD) and intellectual disabilities (ID) are two co-occurring neurodevelopmental disorders that affect approximately 3-5% of the population worldwide (Srivastava and Schwartz, 2014). ASD is characterized by impairments in social communication and interaction, and repetitive patterns of behaviour and interest (Lai et al., 2014) and ID is defined as having significant limitations in adaptive functioning and an IQ below 70 (Kaufman et al., 2010; Ropers and Hamel, 2005). Approximately 40-50% of individuals with ASD also have an intellectual disability, whereas the remainder are of average or above-average intellectual ability (Lai et al., 2014).

Whilst very few studies have investigated functional connectivity alterations in ID (Anderson et al., 2013; Hall et al., 2013), growing evidence suggests that ASD is associated with altered functional connectivity patterns. Studies investigating functional connectivity in individuals with ASD have either reported a global decrease in connectivity in ASD (Anderson et al., 2011; Balsters et al., 2016; Barttfeld et al., 2012; Dinstein et al., 2011; Ebisch et al., 2011; Gotts et al., 2012; Guo et al., 2017; Hahamy et al., 2015; Iidaka, 2014; Itahashi et al., 2014; Jones et al., 2010; Lai et al., 2010; Lee et al., 2016; Long et al., 2016; Rudie and Dapretto, 2013; Spisak et al., 2014) or a mix of long-range underconnectivity and local overconnectivity (Chen and Glover, 2015; Cheng et al., 2015; Cherkassky et al., 2006; Dajani and Uddin, 2015; Di Martino et al., 2010, 2014, 2013; Doyle-thomas et al., 2015; Keown et al., 2013; Murdaugh et al., 2015;

Nair et al., 2013, 2014; von dem Hagen et al., 2013; Itahashi et al., 2015; Ray et al., 2014; Redcay et al., 2013; Venkataraman et al., 2015; Bos et al., 2014; Damarla et al., 2010; Cerliani et al., 2017). Conversely, a handful of groups have also found evidence of whole-brain overconnectivity in ASD (Cerliani et al., 2017; Delmonte et al., 2013; Supekar et al., 2013; Uddin et al., 2013).

Specific networks have also been studied in ASD, notably the default mode network (DMN). The DMN is thought to be involved in interoception and in the continuous acquisition and evaluation of external and internal information, reflecting the brain's basal activity - or its default mode of function. The DMN is composed of the anterior cingulate cortex (ACC), posterior cingulate cortex (PCC), precuneus, medial prefrontal cortex (mPFC), and the lateral parietal cortex. Reports also suggest that the DMN is underconnected in ASD (Assaf et al., 2010; Starck et al., 2013; Jung et al., 2014; Kennedy and Courchesne, 2008c; Weng et al., 2009; Ypma et al., 2016), although one group observed that some DMN subregions are underconnected while others are hyperconnected in ASD (Eilam-stock et al., 2014).

One possible explanation for these discrepancies is the heterogeneity of the disorder itself. Indeed, ASD severity, and the presence and severity of comorbidities can greatly vary between individuals. Furthermore, the majority of cases of ASD/ID are sporadic and are often caused by variants in several genes (Kaufman et al., 2010; Lai et al., 2014). This clinical and neurobiological heterogeneity therefore complicates the identification of, and even challenges the idea that there might be, ASD-specific connectivity patterns.

An alternative approach to studying broadly-defined ASD where heterogeneity in the study population may obscure findings, is to study single-gene disorders associated with a high prevalence of ASD, such as Fragile X Syndrome (FXS). FXS is a leading single-gene cause of both ASD and ID. Clinically, FXS is commonly associated with ASD-like features, cognitive deficits, sensory hypersensitivity, impaired executive function and impulsivity (Garber et al., 2008). A study by Hall et al. (2013) also suggests that the functional connectivity of large scale resting state networks are decreased in individuals with FXS.

Focusing on FXS enables the study of a more biologically homogeneous population. It also facilitates the use of animal models. Preclinical model of FXS can help us gain a better understanding of the underlying neurobiology of FXS and may have importance

for understanding the underpinnings of other forms of autism more generally.

Resting state networks (RSNs) have been shown to be identifiable in multiple species including human, monkeys, rats and mice. Resting state fMRI therefore has the potential to provide a link between preclinical work and the clinics by offering a platform to study a disorder in a comparable way across species. A few resting state studies in mice models of ASD have been carried out, notably in the *Chd8* heterozygous, *Cntnap2* knockout, *Fmr1* knockout, *Syn2* knockout and 16p11.2 microdeletion mice models, which all identified FC abnormalities (Zerbi et al., 2018, 2019; Dodero et al., 2013; Michetti et al., 2017; Suetterlin et al., 2018; Liska et al., 2018; Sforazzini et al., 2016; Bertero et al., 2018). However, despite promising results in 16p11.2 microdeletion (Bertero et al., 2018), it remains unclear whether functional connectivity alterations observed in other ASD preclinical models will translate directly to affected individuals.

In this chapter, I used a parallel resting state fMRI approach in individuals with FXS and in a rat model of FXS and hypothesised that loss of FMRP would lead to similar differences in brain connectivity across species. In the first part of the chapter, I investigated FC abnormalities in *Fmr1*$^{-/y}$ rats. First, by assessing the FC of *Fmr1*$^{-/y}$ Sprague Dawley rats. Then, by studying the global connectivity and the DMN connectivity of *Fmr1*$^{-/y}$ LEH rats. I additionally looked at the impact of the background strain on FC and how anaesthesia affects connectivity in *Fmr1*$^{-/y}$ rats. In the second part of the chapter, I assessed the FC of individuals with FXS. First by determining the feasibility of performing resting state analysis using fMRI data from FX individuals with an intellectual disability. Then, by investigating FXS connectivity both at a global scale and specifically looking at the DMN. Finally, I determined the contribution of grey matter changes to connectivity impairments. I identified a similar decrease in functional connectivity in FX individuals and in the LEH rat model of the disorder, supporting my hypothesis.

4.2 Results

4.2.1 Functional connectivity in a rat model of FXS

Two different lines of *Fmr1*$^{-/y}$ rats were available for these experiments: *Fmr1*$^{-/y}$ rats on a Sprague Dawley (SD) background or on a Long-Evans Hooded (LEH) back-

ground. I chose to investigate the functional connectivity of *Fmr1*$^{-/y}$ rats in both background strains to have the possibility to investigate the effect of background strain on functional connectivity, and to potentially increase the sample size of my experiment. Additionally, functional connectivity was assessed under different concentrations of anaesthesia.

4.2.1.1 Functional connectivity in *Fmr1*$^{-/y}$ Sprague Dawley rats

Functional images were acquired in *Fmr1*$^{-/y}$ SD rats and WT littermates under 1% isoflurane (n=9, and n=11, respectively). ICA was then performed to explore the connectivity patterns of the group. 30 group-level components were successfully extracted (**Fig. 4.1**). Of those components, some were identified as noise, such as component **16**, while others were identified as true networks. The identification of noise *versus* a signal component is discussed in **Appendix B**. The DMN can be seen in component **1**. The posterior DMN can be further identified in component **5**. This network split is due to the high number of components extracted during ICA.

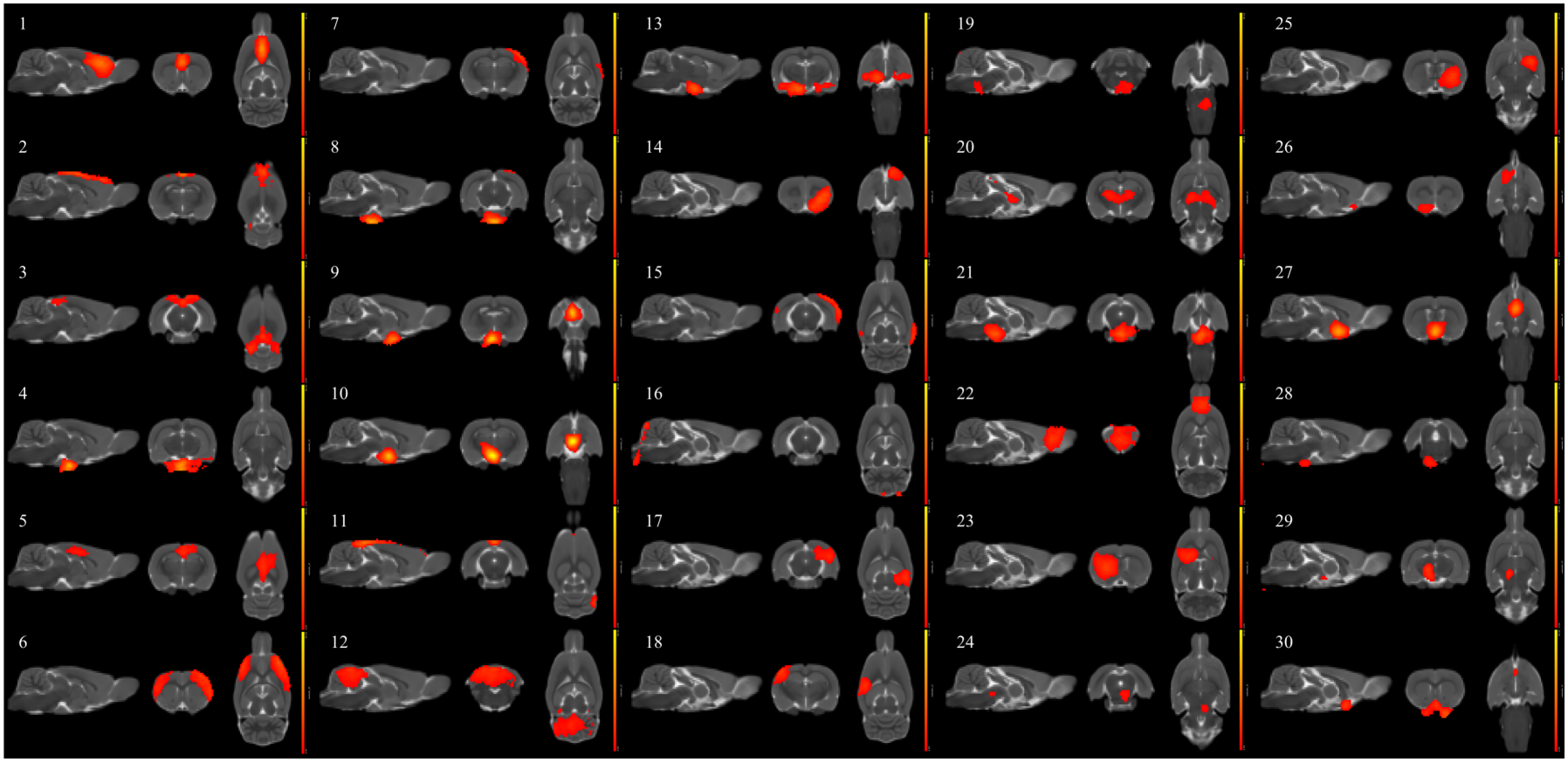


Figure 4.1: Resting State Networks identified in adult WT and *Fmr1*$^{-/y}$ Sprague Dawley using Independent Component Analysis. 1-30 represent the spatial maps of different networks, each shown from left-to-right in the sagittal, coronal and axial planes, obtained by ICA in the cohort of adult rats (3-4 months old; mixed genotype, n=20, 11 WT and 9 KO) scanned under light anaesthesia (1% isoflurane). These maps are overlayed on a high resolution anatomical template. (1) Default Mode Network. (2) Cingulate cortex. (3) Noise. (4) Supramammillary nucleus. (5) Retrospenial cortex. (6) Sensory Network. (7) Primary sensory cortex. (8) Pons. (9) Hypothalamus. (10) Hypothalamic nucleus. (11) Retrospenial cortex. (12) Cerebellar cortex. (13) Hypothalamus. (14) Left caudate putamen. (15) Left visual network. (16) noise. (17) Visual cortex. (18) Right Primary Sensory Cortex. (19) Pons. (20) Thalamic nucleus (21) Pons. (22) Prefrontal cortex (23) Right Caudate Putamen. (24) Pontine nuclear. (25) Left thalamus. (26) Nucleus accumbens (27) Paraventricular thalamic nucleus (28) Pons (29) Medial geniculate body. (30) Nucleus accumbens. Colour bar represent Z-score, ranging from 4.95-36.5.

I next performed a between-genotype comparison of the networks identified by ICA (**Fig. 4.2**). In order to do that, the group-average spatial maps were dual-regressed to obtain the subject-specific versions of the spatial map, which are required for statistical analysis.

I found statistically significant between-genotype differences in 2 networks. The connectivity of the cerebellar network (**Fig. 4.2A**) was found to be decreased in *Fmr1*$^{-/y}$-SD rats compared to WT-SD (**Fig. 4.2B**, non-parametric permutation testing of 2-sample t-test GLM, n=11 WT-SD and 9 *Fmr1*$^{-/y}$-SD, p<0.05). Similarly, a between-genotype comparison performed on the right caudate putamen network (**Fig. 4.2C**), revealed that the caudate putamen was underconnected in *Fmr1*$^{-/y}$-SD rats compared to their WT-SD littermates (**Fig. 4.2D**, GLM of a 2-sample t-test, n=11 WT-SD and 9 *Fmr1*$^{-/y}$-SD, p<0.05).

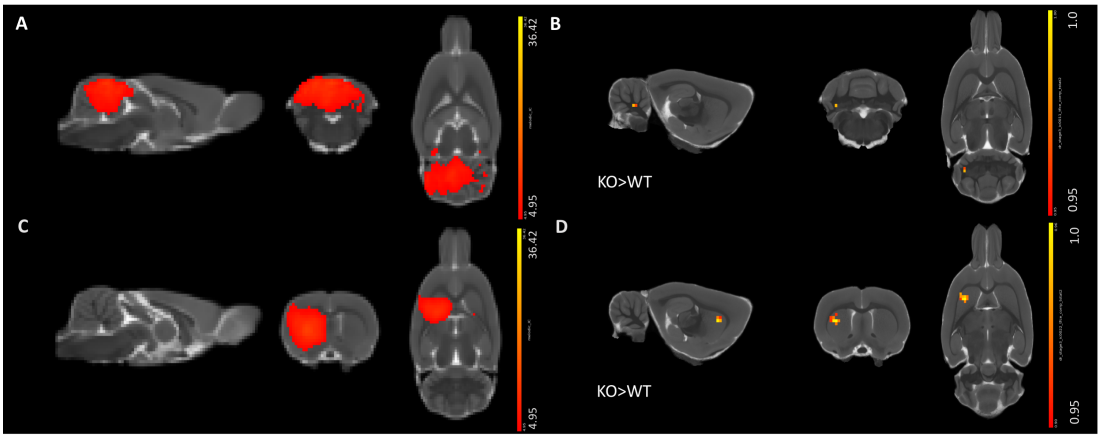


Figure 4.2: Between genotypes comparison of the Resting State Networks identified by ICA in *Fmr1*$^{-/y}$ Sprague Dawley rats and WT littermates. Network spatial maps and statistical maps are shown from left-to-right in the sagittal, coronal and axial planes, overlayed on a high resolution anatomical template. (A) Cerebellar Network component obtained by ICA in the cohort of *Fmr1*$^{-/y}$-SD and WT rats. (B) Decreased connectivity in the Cerebellar Network in *Fmr1*$^{-/y}$-SD. (C) Caudate putamen component obtained by ICA in the cohort of *Fmr1*$^{-/y}$-SD and WT rats. (D) Decreased connectivity in the caudate putamen of *Fmr1*$^{-/y}$-SD rats. Statistical parametric maps were obtained using the Threshold-Free Cluster Enhancement method and were corrected for multiple comparisons. Colour bars represent Z-score ranging from 4.95-36.5 (A & C) and 1-P-values ranging from 0.95-1 (B & D).

No other between-genotype differences in FC were observed in ICA networks. A seed-based analysis of the DMN was additionally performed using a seed in the right ACC (**Fig. 4.3**). Connectivity maps comprised of voxels that were found to be significantly connected to the ACC in WT-SD and in KO-SD (**Fig. 4.3A** and **Fig. 4.3B** respectively, non-parametric permutation testing of one-sample t-test GLM, n=11 WT-SD and

9 *Fmr1*$^{-/y}$-LEH respectively, (p<0.005)) suggest a greater spatial extent of DMN connectivity in WT-SD animals than in *Fmr1*$^{-/y}$-SD. Between-genotype analysis indicated a trend towards decreased DMN connectivity in *Fmr1*$^{-/y}$-SD rats compared to WT-SD rats (**Fig. 4.3C**, non-parametric permutation testing of two-sample t-test GLM, n=11 WT-SD and 9 *Fmr1*$^{-/y}$-LEH, (p<0.30)).

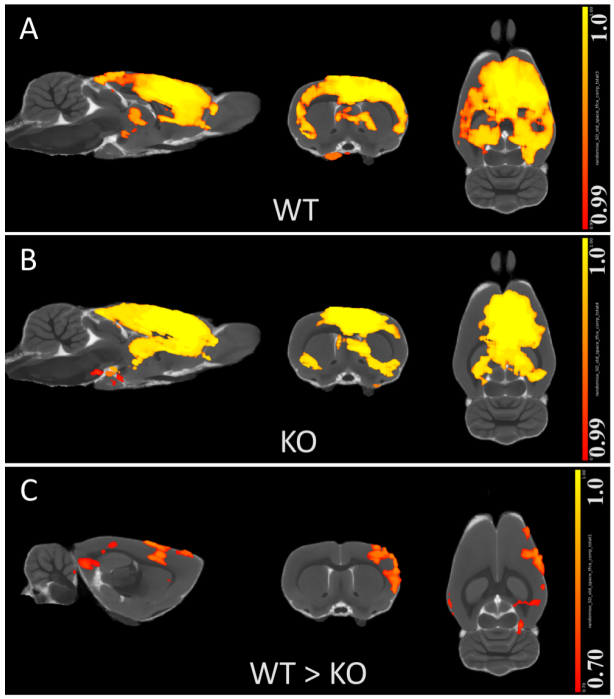


Figure 4.3: Between genotype comparison of the Default Mode Network identified by seed-based analysis in *Fmr1*$^{-/y}$ Sprague Dawley rats and WT littermates. Seed-based functional connectivity of the right anterior cingulate cortex prefrontal cortex (A) in WT-SD rats. (B) In *Fmr1*$^{-/y}$-SD rats. (C) Trend towards greater functional connectivity to the seed in WT-SD compared to *Fmr1*$^{-/y}$-SD rats. All colour bars represent 1-P-value ranging, corrected for multiple comparisons.

4.2.1.2 Functional connectivity in *Fmr1*$^{-/y}$ Long-Evans Hooded rats

To further investigate whether the lack of FMRP results in alterations of the brain functional connectivity, I assessed resting state networks connectivity in adult *Fmr1*$^{-/y}$ LEH rats and WT-LEH littermates under 1% isoflurane (n=11, and n=13, respectively).

A global decrease in functional connectivity has been extensively reported in both individuals with ASD and in preclinical models of ASD (Di Martino et al., 2014). I therefore first wanted to probe whether connectivity patterns were affected at a global scale in FXS. To test that, I selected 34 regions of interest (ROI) spread across

both brain hemispheres and measured functional connectivity strength between each ROI combination by calculating their r-scores. FC between pairs of brain regions is represented in **Fig. 4.4** in the form of connectograms, where each line represents the connectivity between the ROIs it connects and the colour indicates its strength. This analysis revealed a global decrease in functional connectivity in *Fmr1*$^{-/y}$-LEH animals (**Fig. 4.4B**) compared to WT-LEH controls (**Fig 4.4A**).

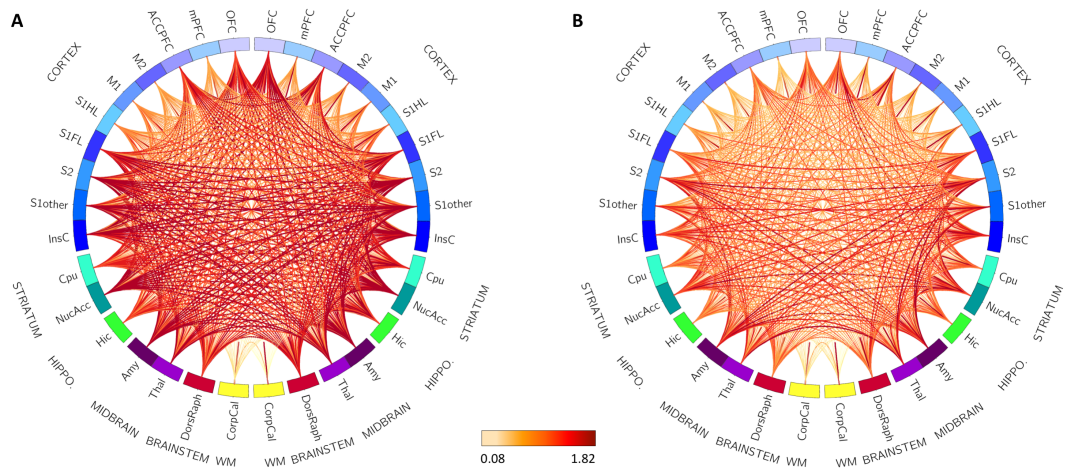


Figure 4.4: Global decrease in functional connectivity in *Fmr1*$^{-/y}$-LEH rats (A-B) Functional connectograms showing strength of connectivity between 34 brain regions across both hemispheres in (A) WT-LEH rats (n=13) and (B) *Fmr1*$^{-/y}$-LEH rats (n=11). The 34 brain regions are represented by rectangles of different colours forming a circle around the connectogram lines. Each line represents the functional connectivity between the two brain regions it links. Greater functional connectivity is represented by thicker and darker lines, as indicated by the r-score colour bar which ranging from 0.08-1.82.

I next probed RSN connectivity by performing an ICA on the dataset. **Fig. 4.5** illustrates the 20 components that were obtained with ICA. 20 components were chosen instead of 30 to limit the number of split components (**Fig. 4.6**). This resulted in the extraction of networks that were more symmetrical across hemisphere, as can be seen in component **C**. Known RSNs, such as the DMN (**Fig. 4.5A**) and the sensory network (**Fig. 4.5C**) were successfully extracted, with few noise components (**Fig. 4.5S & T**).

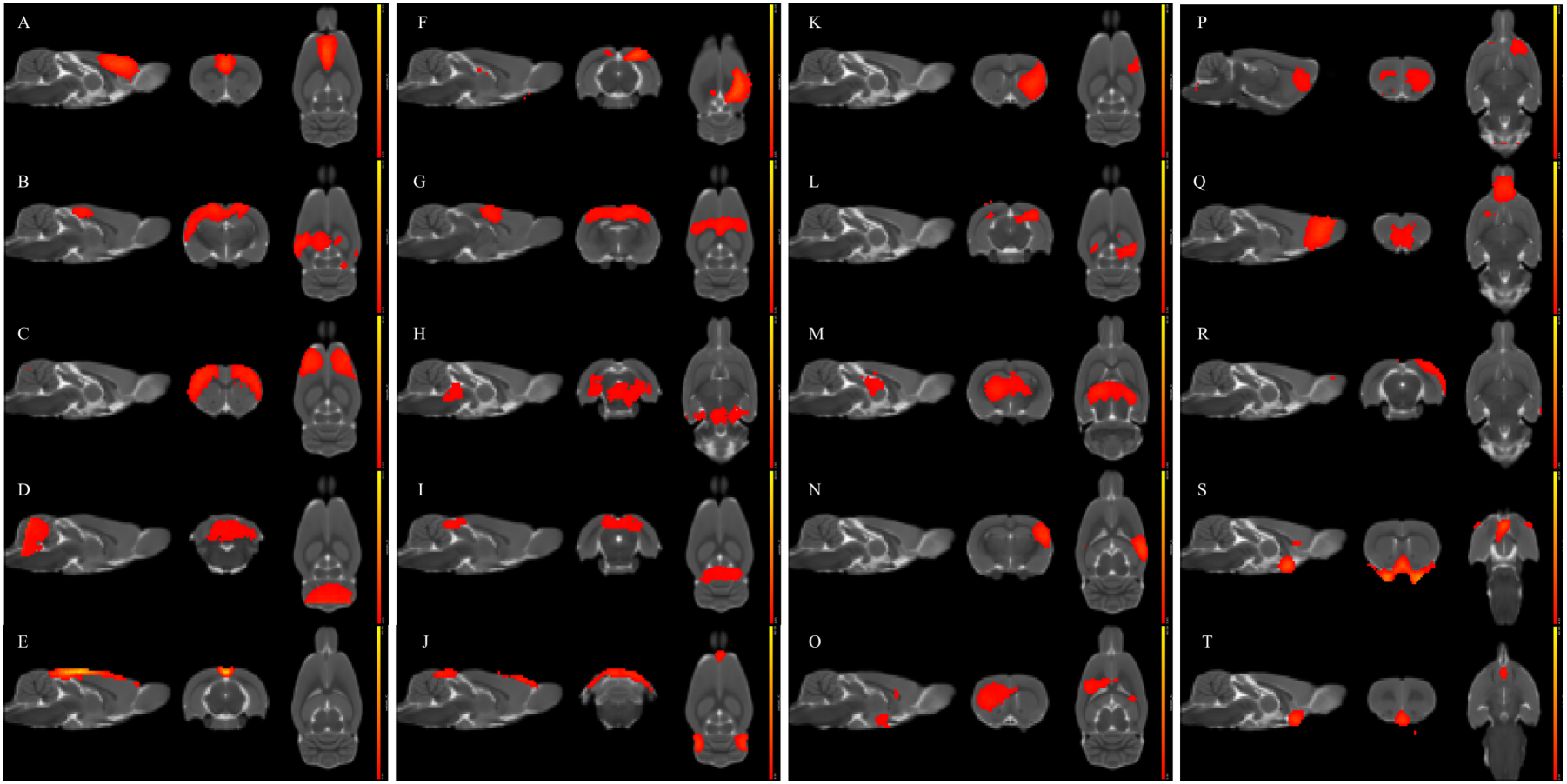


Figure 4.5: Resting State Networks identified in adult WT and *Fmr1*$^{-/y}$ Long Evans hooded rats using Independent Component Analysis. A-T represent the spatial maps of different networks, each shown from left-to-right in the sagittal, coronal and axial planes, obtained by ICA in the adult rat cohort (3-4 months; mixed genotype, n=24, 13 WT-LEH and 11 KO-LEH) scanned under light anaesthesia (1% isoflurane). These maps are overlayed on a high resolution anatomical template. (A) Default Mode Network. (B) Right Somatomotor Network. (C) Sensory Network. (D) Cerebellar Network. (E) Retrospenial and Cingulate Cortex. (F) Left Visual Network. (G) Sensorimotor Network. (H) Dorsal Raphe Nucleus. (I) Retrospenial Cortex. (J) Cerebellar Network. (K) Left Caudate Putamen. (L) Left Dorsal Subiculum. (M) Thalamus Network. (N) Right Primary Sensory Cortex. (O) Right Caudate Putamen. (P) Left Caudate Putamen. (Q) Medial Prefrontal Cortex. (R) Left Visual Network. (S) Noise. (T) Noise. Statistical parametric maps were obtained using a 0.5 Threshold. Colour bars represent Z-score ranging from 4.95-60.1.

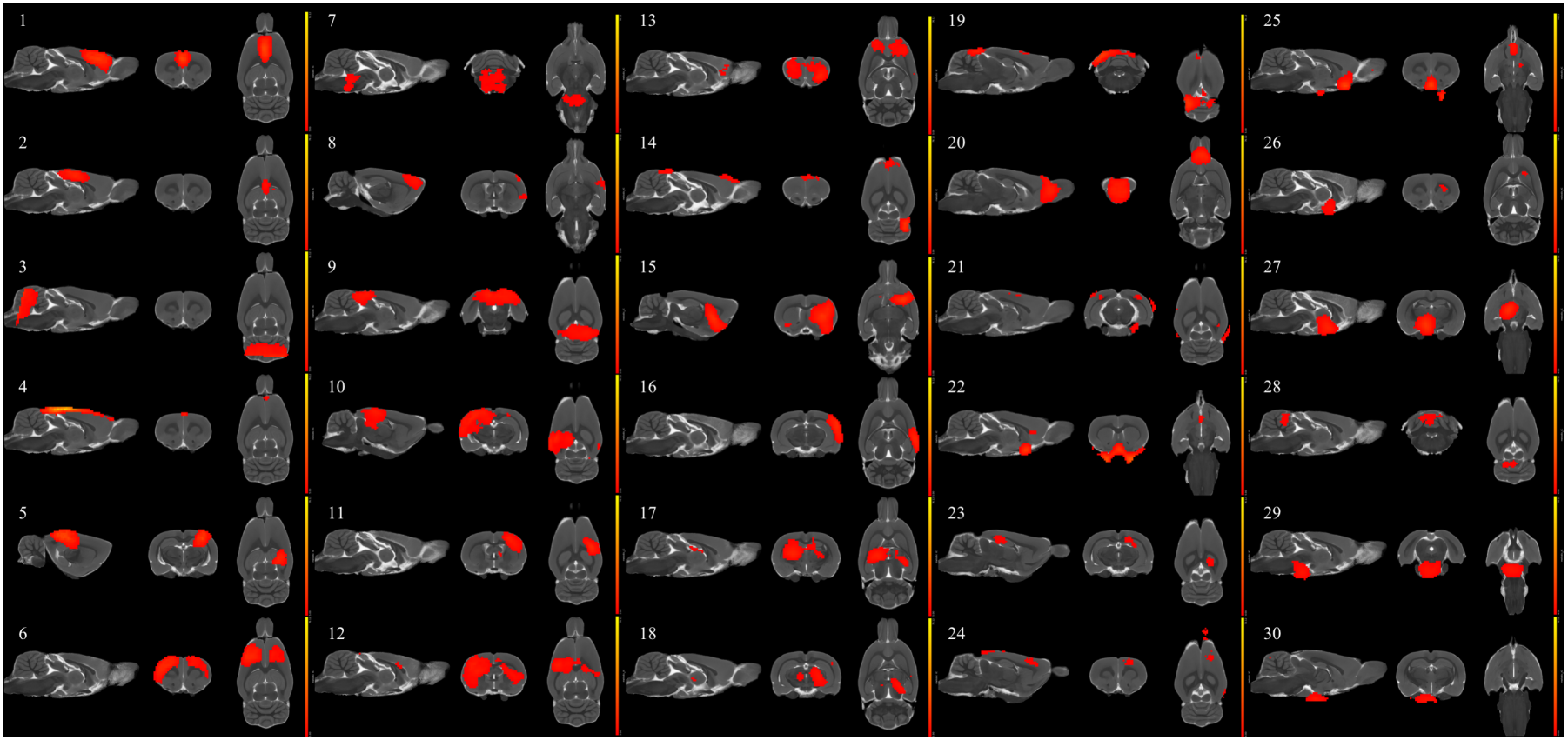


Figure 4.6: Resting State Networks identified in adult WT and *Fmr1*$^{-/y}$ Long Evans hooded rats using Independent Component Analysis. 1-30 represent the spatial maps of different networks, each shown from left-to-right in the sagittal, coronal and axial planes, obtained by ICA in the adult rat cohort (3-4 months; mixed genotype, n=24, 13 WT-LEH and 11 KO-LEH) scanned under light anaesthesia (1% isoflurane). These maps are overlayed on a high resolution anatomical template. (1) Default Mode Network. (2) Retrosplenial cortex. (3) Cerebellum. (4) Retrosplenial and Cingulate Cortex. (5) Left Hippocampal network. (6) Motor Network. (7) Pons. (8) Left Sensory cortex (9) Visual network. (10) Right hippocampal and somatosensory network. (11) Left somatosensory network. (12) Caudate putamen. (13) Caudate putamen. (14) Noise. (15) Left caudate putamen. (16) Left Primary sensory cortex. (17) Hippocampus. (18) Periaqueductal gray. (19) Cerebellum. (20) Medial Prefrontal Cortex. (21) Noise. (22) Nuccleus accumbens. (23) Left Hippocampus. (24) Left Motor cortex. (25) Medial prefrontal cortex. (26) Left Caudate putamen. (27) Hypothalamic nucleus. (28) Cerebellum. (29) Pons. (30) Noise. Statistical parametric maps were obtained using a 0.5 Threshold. Colour bars represent Z-score ranging from 4.95-76.15.

I wanted to further analyse the connectivity of the DMN, as changes in the DMN connectivity has been extensively reported in individuals with ASD. Many resting state studies on autism have reported a hypoconnected DMN in ASD. I therefore set out to test whether a similar impairment could be observed in our rat model of FXS.

First, I performed a between-genotype comparison of the DMN component obtained with the data-driven ICA approach (**Fig. 4.7A**). This revealed that the DMN was hypoconnected in *Fmr1*$^{-/y}$-LEH compared to control littermates (**Fig. 4.7B**, non-parametric permutation testing of 2-sample t-test GLM, n=13 WT and 11 *Fmr1*$^{-/y}$-LEH, $p<0.05$).

Next, using a seed-based approach, I measured the functional connectivity between the right ACC, as it is part of the DMN, and the rest of the brain in WT-LEH and *Fmr1*$^{-/y}$-LEH rats (**Fig. 4.8**). Connectivity maps comprised of voxels that were found to be significantly connected to the ACC in WT-LEH and in KO-LEH (**Fig. 4.8A** and **Fig. 4.8B** respectively, non-parametric permutation testing of one-sample t-test GLM, n=13 WT-LEH and 11 *Fmr1*$^{-/y}$-LEH respectively, ($p<0.05$)) suggest a greater DMN connectivity in WT-LEH animals than in *Fmr1*$^{-/y}$-LEH. Between-genotype analysis confirmed that the DMN connectivity was significantly decreased in *Fmr1*$^{-/y}$-LEH rats compared to WT-LEH rats (**Fig. 4.8C**, non-parametric permutation testing of two-sample t-test GLM, n=13 WT-LEH and 11 *Fmr1*$^{-/y}$-LEH, ($p<0.05$)), corroborating the ICA approach.

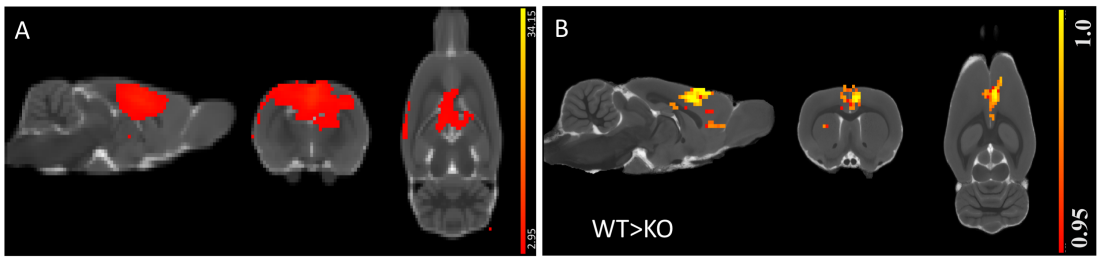


Figure 4.7: Between-group Default Mode Network functional connectivity obtained by Independent Component Analysis. (A) Represents the spatial map of the Default Mode Network obtained by ICA in the cohort, overlaid on a high resolution anatomical template shown in the sagittal, coronal and axial planes (from left-to-right). Colour bars represent Z-score ranging from 4.95-60.1. (B) Greater functional connectivity in the DMN in WT-LEH compared to their *Fmr1*$^{-/y}$-LEH littermates. Statistical map is overlaid on a high resolution anatomical template shown in the sagittal, coronal and axial planes (from left-to-right). Colour bars represent 1-P-value, ranging from 0.95-1, TFCE corrected for multiple comparison.

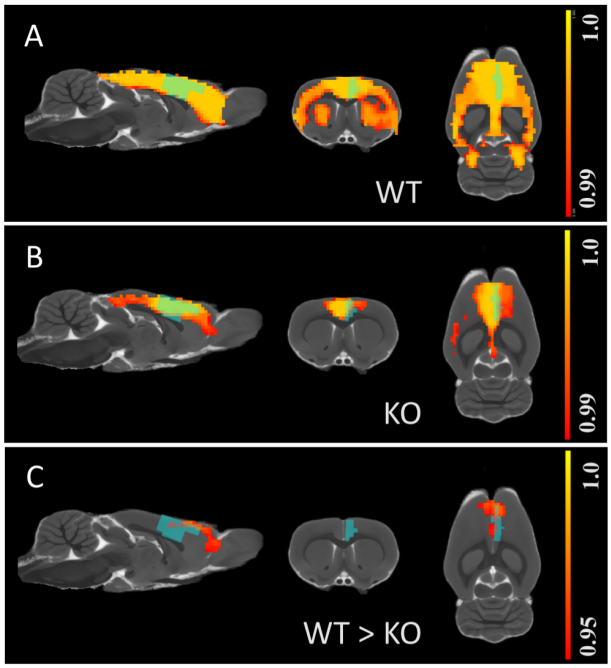


Figure 4.8: Between-group Default Mode Network functional connectivity Seed-based functional connectivity of the right anterior cingulate cortex prefrontal cortex (rACCPFC) (A) in WT-LEH rats. (B) In *Fmr1*$^{-/y}$-LEH rats. (C) Greater functional connectivity to the seed in WT-LEH compared to *Fmr1*$^{-/y}$-LEH rats. The rACCPFC seed is represented in blue. All colour bars represent 1-P-value ranging from 0.95-1, corrected for multiple comparisons.

4.2.1.3 Impact of background strains on functional connectivity

Having investigated functional connectivity in rat models of FXS on SD and LEH rats background separately, I wanted to assess whether it would be beneficial to analyse the two groups as a single cohort. This could increase the power of my study, however having multiple background strains might introduce a large between-subject variability.

To test this, I carried out an ICA on both the SD and the LEH data together (**Fig. 4.9**). This enabled me to review the group components obtained in this mixed dataset. The RSNs in the mixed dataset closely resembled those obtained in the single-strain ICA. The DMN can be observed in component **1** and the sensory network in component **7**. A few noise components were also extracted from the dataset (components **25** and **26**).

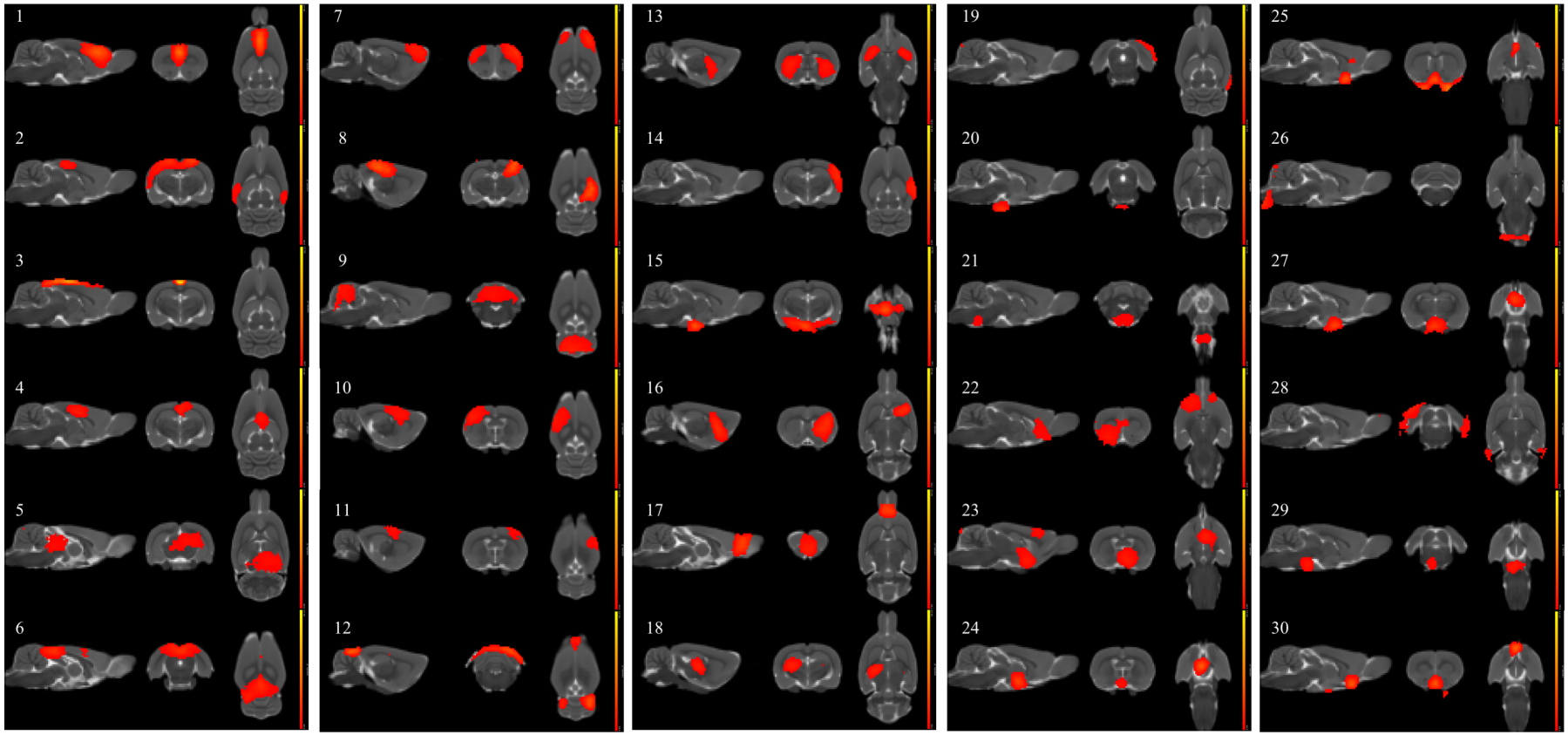


Figure 4.9: Resting State Networks identified in WT and *Fmr1*$^{-/y}$ rats on a Sprague Dawley or Long Evans Hooded background, using Independent Component Analysis 1-30 represent the spatial maps of different networks, each shown from left-to-right in the sagittal, coronal and axial planes, obtained by ICA in the cohort of 3-4 months old rats scanned under light anaesthesia (1% isoflurane) (SD: n=20, 11 WT and 9 KO; LEH: n=24, 13 WT and 11 KO). These maps are overlayed on a high resolution anatomical template. (1) Default Mode Network. (2) Right Somatomotor Network. (3) Noise. (4) Retrospenial cortex. (5) Periaqueductal gray. (6) Retrospenial cortex. (7) Sensory cortex. (8) Visual cortex. (9) Cerebellar cortex. (10) Primary Sensory Cortex. (11) Sensory Cortex. (12) Cerebellar cortex. (13) Caudate Putamen. (14) Sensory and Auditory cortex. (15) Hypothalamus. (16) Left Caudate Putamen. (17) Medial Prefrontal Cortex. (18) Thalamus. (19) Visual cortex. (20) Noise. (21) Pons. (22) Caudate Putamen. (23) Thalamus. (24) Hypothalamus. (25) Noise. (26) Noise. (27) Hypothalamus. (28) Visual cortex. (29) Pons. (30) Accumbens Nucleus. Colour bars represent Z-score ranging from 4.95-63.3.

I next performed a general linear model statistical analysis on the mixed-strain components (**Fig. 4.10**) to determine whether the background strain impacts the FC of specific components or even whether some components are specific to one strain. This between-strain comparison revealed that the hypothalamus was hypoconnected in LEH rats compared to SD rats (**Fig. 4.10B & D**, non-parametric permutation testing of ANOVA GLM, n=11 WT-SD, n=9 *Fmr1*$^{-/y}$-SD, n=13 WT-LEH and 11 *Fmr1*$^{-/y}$-LEH, $p<0.05$ and $p<0.15$, respectively). This decrease in connectivity in LEH rats was detected in two separate networks encompassing the hypothalamus (**Fig. 4.10A & C**).

Interestingly, no between-genotype differences were observed in this mixed-strain group.

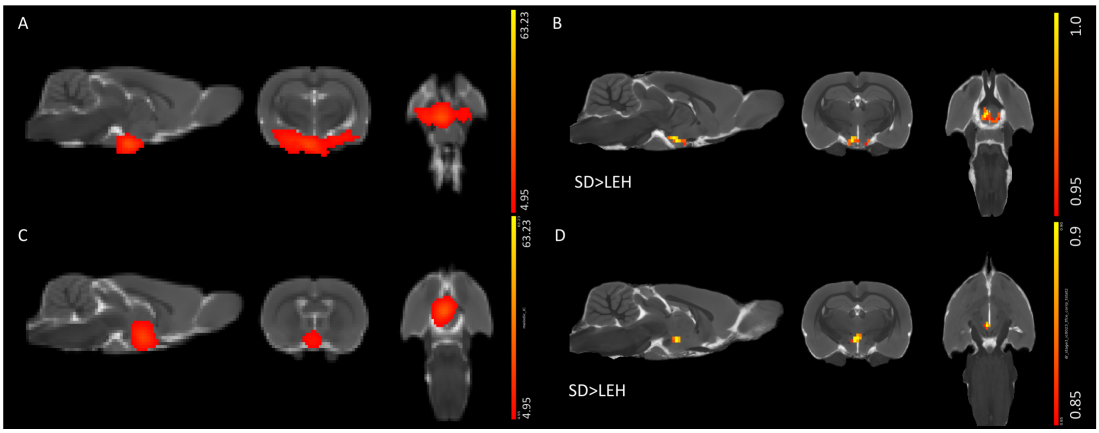


Figure 4.10: The hypothalamus is hyperconnected in LEH compared to SD rats. Network spatial maps and statistical maps are shown from left-to-right in the sagittal, coronal and axial planes, overlaid on a high resolution anatomical template. (A & C) Spatial maps of the hypothalamus obtained by ICA in the mixed cohort. Colour bars represent Z-score ranging from 4.95-63.3. (B & D) Between-strain comparison of Resting State Networks obtained by ICA reveals greater functional connectivity in the hypothalamus in SD compared to the LEH. Colour bars represent 1-P-value, ranging from 0.95-1 (B) and 0.85-0.9 (D), TFCE corrected for multiple comparisons.

4.2.1.4 Effect of anaesthesia on functional connectivity

To assess the effect of anaesthesia on *Fmr1*$^{-/y}$ rats, two additional resting state scans were acquired under 1.5% and 2.5% isoflurane in WT-LEH and *Fmr1*$^{-/y}$ LEH rats, following the initial functional scan acquired under 1% isoflurane. In the previous chapter I showed that the strength of anaesthesia modulates FC in WT rats (**Fig. 3.12**). However, it remains unclear whether anaesthesia modulates FC similarly in *Fmr1*$^{-/y}$ rats. Indeed, a study by Goncalves and colleagues suggest that *Fmr1*$^{-/y}$ mice have a

different sensitivity to anaesthesia than their WT littermates (Goncalves et al., 2013). I therefore wanted to determine if this finding translates to rats as well and whether it could confound any of the between-genotype comparisons.

Fmr1$^{-/y}$-LEH rats and WT-LEH control were scanned under 3 different levels of anaesthesia with a 5 min waiting period between each scan to allow the isoflurane level to reach the desired concentration (**Fig. 4.11A**). To test the impact of anaesthesia on the FC of the DMN, a correlation coefficient was calculated between a seed within the ACC and the DMN for each genotype and at each concentration of anaesthesia (**Fig. 4.11B**). The DMN connectivity differed significantly between genotypes (Two-way repeated measures ANOVA, n=11 WT-LEH and 9 *Fmr1*$^{-/y}$-LEH, Genotype $F_{(1,63)}$=3.86, $p<0.05$) and with the concentration of isoflurane (Two-way repeated measures ANOVA, n=11 WT-LEH and 9 *Fmr1*$^{-/y}$-LEH, Isoflurane $F_{(2,63)}$=13.66, $p<0.001$). Furthermore, anaesthesia affected DMN connectivity differently across genotypes (Two-way repeated measures ANOVA, n=11 WT-LEH and 9 *Fmr1*$^{-/y}$-LEH, Isoflurane*genotype $F_{(2,63)}$=4.85, $p<0.05$). Post hoc analysis revealed that the strength of DMN connectivity decreased with increasing isoflurane concentration in WT-LEH rats, as demonstrated in the previous chapter ($p<0.001$). However, the DMN connectivity was not significantly different between 1% and 2.5% isoflurane in *Fmr1*$^{-/y}$-LEH animals ($p>0.05$). Moreover, the DMN connectivity at 1% isoflurane was found to be significantly decreased in *Fmr1*$^{-/y}$-LEH rats compared to WT-LEH, mirroring my ICA and seed-based connectivity findings ($p<0.05$).

Additionally, the effect of anaesthesia on FC in *Fmr1*$^{-/y}$-LEH and WT-LEH rats was assessed at a global scale. To do that, 34 brain regions of interest were chosen and a correlation coefficient was calculated between pairs of brain regions. This was done for both genotypes at each isoflurane level (**Fig. 4.11C**). Anaesthesia appears to modulate FC at a global scale similarly to what I observed in the DMN. Indeed, the FC appears to be decreased with increasing anaesthesia concentration in WT-LEH, but the decrease was not as marked in *Fmr1*$^{-/y}$-LEH rats.

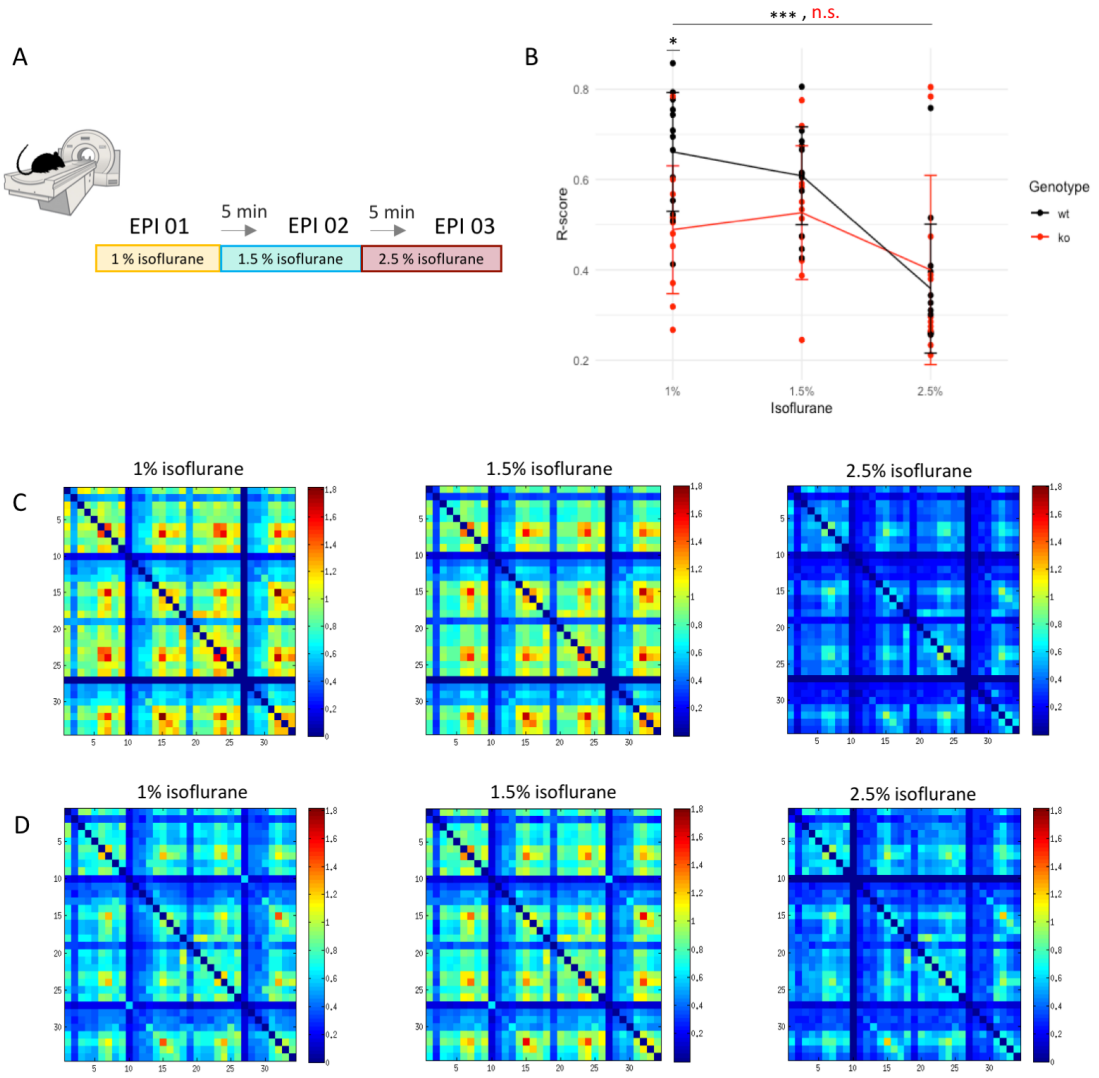


Figure 4.11: Functional connectivity correlation in adult LEH rats under three different levels of anaesthesia (1%, 1.5%, 2.5% isoflurane). (A) Schematic of scanning protocol (B) Functional connectivity strength, calculated as an r-score, in the DMN of LEH *Fmr1*$^{-/y}$ (n=11) and WT-LEH rats (n=13) under 3 levels of anaesthesia. In WT-LEH, r-score is significantly greater at 1% than at 2.5% isoflurane ($p<0.001$), but was non significant in *Fmr1*$^{-/y}$-LEH. Under 1% isoflurane, r-score was significantly greater in WT-LEH than in *Fmr1*$^{-/y}$-LEH ($p=0.05$). Dots represent r-score of individual animals coloured by genotype, WT-LEH is shown in black and *Fmr1*$^{-/y}$-LEH is shown in red. Bars represent standard deviation. *** $p<0.001$ difference between timepoints in WT-LEH animals, n.s $p>0.05$ between timepoints in *Fmr1*$^{-/y}$-LEH, * $p<0.05$ between-genotype difference. (C-D) Functional connectivity correlation matrices between 34 seeds (*1. right orbitofrontal cortex, 2 right mPFC, 3. right ACC, 4. right caudate putamen 5. right hippocampus, 6. right nucleus accumbens, 7. right amygdala, 8. right dorsal raphe nucleus, 9. right insular cortex, 10. right corpus callosum, 11. right secondary motor cortex, 12. right primary motor cortex, 13. right primary somatosensory cortex (hindlimb region), 14. right primary somatosensory cortex (forelimb region), 15. right thalamus, 16. right secondary somatosensory cortex, 17. right primary somatosensory cortex (other), 18. left orbitofrontal cortex, 19. left mPFC, 20. left ACC, 21. left caudate putamen, 22. left hippocampus, 23. left nucleus accumbens, 24. left amygdala, 25. left dorsal raphe nucleus, 26. left insular cortex, 27. left corpus callosum, 28. left secondary motor cortex, 29. left primary motor cortex, 30. left primary somatosensory cortex (hindlimb region), 31. left primary somatosensory cortex (forelimb region), 32. right thalamus, 33. left secondary somatosensory cortex, 34. left primary somatosensory cortex (other)*) in in WT-LEH rats (C) and *Fmr1*$^{-/y}$-LEH rats (D), under 3 levels of anaesthesia.

4.2.1.5 Summary of results

In this section, I have looked at the FC pattern of *Fmr1*$^{-/y}$ rats, in two different background strains. I have observed that *Fmr1*$^{-/y}$ rats on the SD background had an underconnected caudate putamen and cerebellum. In contrast, *Fmr1*$^{-/y}$ rats on the LEH background were found to have a decreased DMN connectivity, also observed as a trend in *Fmr1*$^{-/y}$-SD rats. To determine whether the strain difference is caused by a difference in the number of animals, that is a difference in the power of the experiment, or by a direct effect of the background strain, I performed a group-analysis on a mixed-strain dataset. This revealed that there are some underlying differences in hypothalamic connectivity between strains.

Additionally, I acquired resting state images at increasing isoflurane concentrations in the LEH cohort. I used this data to assess the impact of anaesthesia on FC in both *Fmr1*$^{-/y}$-LEH and WT-LEH controls. This experiment revealed that *Fmr1*$^{-/y}$-LEH rats have a different sensitivity to anaesthesia to WT rats. In WT-LEH animals, I observed a decrease in the global and DMN connectivity with increased concentration of anaesthesia. This finding was not observed in *Fmr1*$^{-/y}$-LEH rats, suggesting that special care should be taken when comparing FC at high dose anaesthesia. However, this is unlikely to explain the differences in FC observed between WT-LEH and *Fmr1*$^{-/y}$-LEH rats as a low concentration of isoflurane was used during scanning and if anaesthesia sensitivity was solely driving the between-genotype difference, FC would be expected to be increased in *Fmr1*$^{-/y}$-LEH rats compared to WT-LEH rats, which is the reversed of what I observed.

4.2.2 Functional connectivity in individuals with FXS

4.2.2.1 Feasibility of functional connectivity analysis using rsfMRI data from FX individuals with an intellectual disability

Despite the translational potential of rsfMRI, it remains unclear whether connectivity abnormalities identified in preclinical models would translate back to human disorders. To date, in the field of autism, only one resting state study on autism-associated 16p11.2 microdeletion has reported a correspondence between a decrease in prefrontal connectivity in 16p11.2 deletion carriers and in a mouse model of the disorder (Bertero et al., 2018). Therefore, in parallel to investigating FC in *Fmr1*$^{-/y}$ rats, I assessed the

FC of individuals with FXS.

First, I wanted to map functional networks in individuals with Fragile X Syndrome. However, the scanning procedure involves laying still in a scanner, which is a novel and loud environment, and FXS is associated with a high prevalence of ASD and ID. FX individuals might therefore struggle to understand that they need to lay in the scanner and might have difficulty staying still. They might also find stressful being in an unfamiliar environment and might be hypersensitive to sounds. Together, this makes scanning a complicated and highly stressful procedure for FX individuals. To overcome these challenges, individuals with FXS went through several rounds of mock-scanning habituation prior to scanning in order to acclimatize them to the scanning procedure (**Fig. 4.12A**). This protocol was devised and implemented by Dr Andrew McKechanie and Dr Andrew Stanfield. They further acquired the resting state images, which I then analysed.

I assessed whether individuals that underwent scanner acclimatization remained still in the scanner, as resting state studies are particularly sensitive to movement, which can confound existing networks and create artefactual between-group differences. Within-subject spatial registration of functional images revealed that individuals with FXS did not move more than typically developing (TD) controls (**Fig. 4.12B**). In addition, I was able to extract known RSNs from this dataset using ICA (**Fig. 4.12C**).

4.2.2.2 Functional connectivity of FXS

Having established the feasibility of performing resting state studies in low-functioning individuals with FXS, I moved on to investigating FXS connectivity.

I first wanted to probe whether connectivity patterns were affected at a global scale in FX individuals, similarly to what has been reported in ASD and to what I observed in *Fmr1*$^{-/y}$ rats. For that, a correlation coefficient was calculated between each pairing of 26 brain regions in typically developing and Fragile X individuals (n=5 and 5) (**Fig. 4.13**). Controls were matched for age but not for intellectual ability or severity of ASD symptoms, to allow for investigation of how those factors influence functional connectivity. This analysis revealed a decrease in cortico-cortical connectivity in FX individuals (**Fig. 4.13B**) compared to TD (**Fig. 4.13A**), as observed in the rat model, but in contrast to it, also highlighted an increase in thalamo-cortical connectivity in

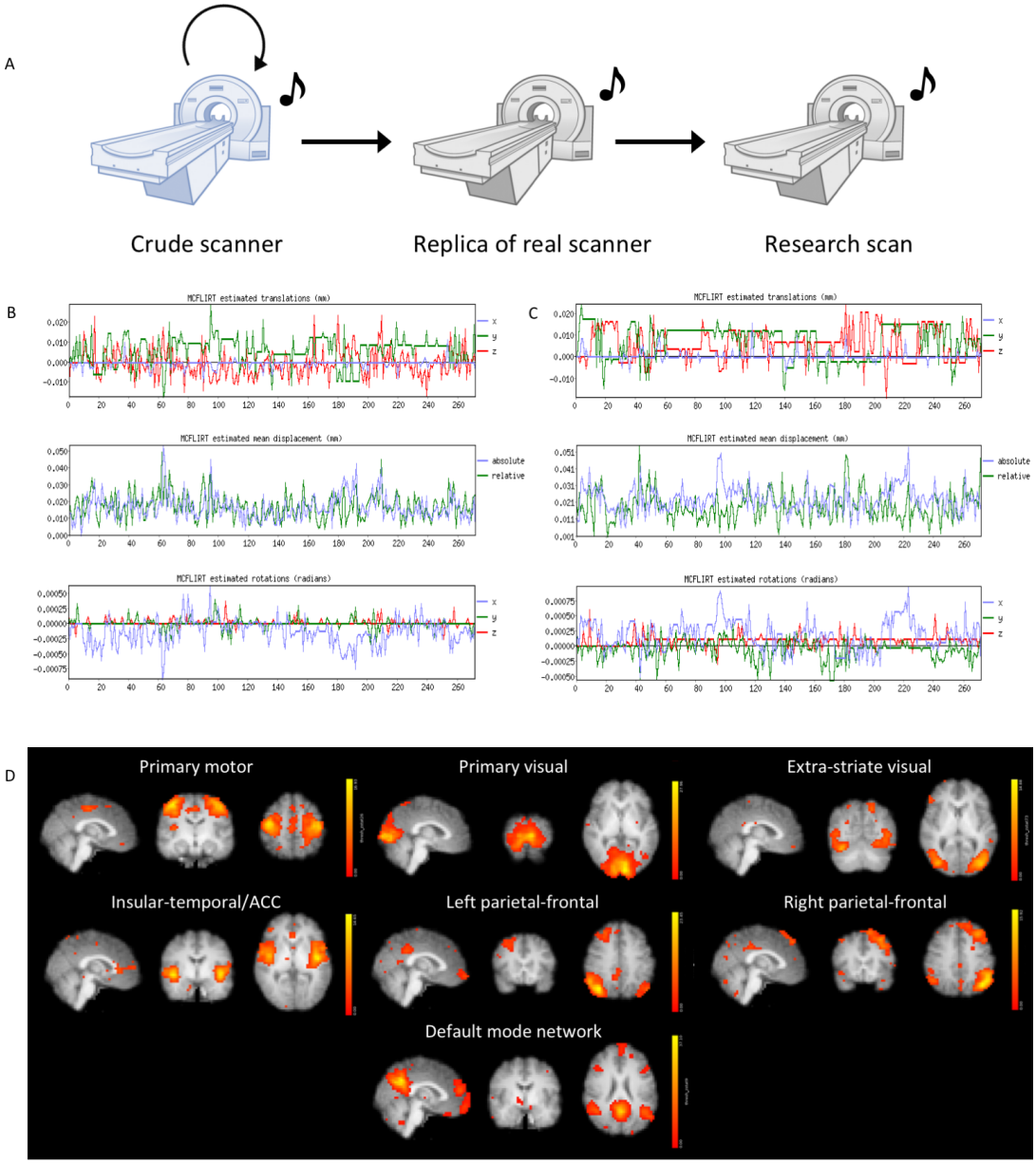


Figure 4.12: Resting state fMRI scanning in individuals with Fragile X Syndrome. (A) Schematic of acclimatization protocol for FX individuals. To habituate themselves to the scanning procedure, participants practice laying still on a crude replica of the scanner as many time as it took them to be comfortable. They next had an habituation session on an accurate replica of the scanner and finally had the research scan. (B) Representative motion traces of a typically developing individual. From top-to-bottom, traces of the estimated translation in mm in the x, y, and z directions, of the absolute and relative estimated mean displacement in mm and of the estimated rotation in radians in the x, y and z directions. (C) Representative motion traces of a FX individual. From top-to-bottom, traces of the estimated translation in mm in the x, y, and z directions, of the absolute and relative estimated mean displacement in mm and of the estimated rotation in radians in the x, y and z directions. (D) Resting State Networks (overlaid on a high resolution anatomical template shown in the sagittal, coronal and axial planes) in individuals with severe FXS, identified by ICA. From left to right: Primary Motor Network, Primary Visual Network, Extra-Striate Visual Network, Insular-Temporal / ACC Network, Left Parietal-Frontal Network, Right Parietal-Frontal Network, Default Mode Network. Colour bars represent Z-score, ranging from 4-43.

individual with FXS compared to controls.

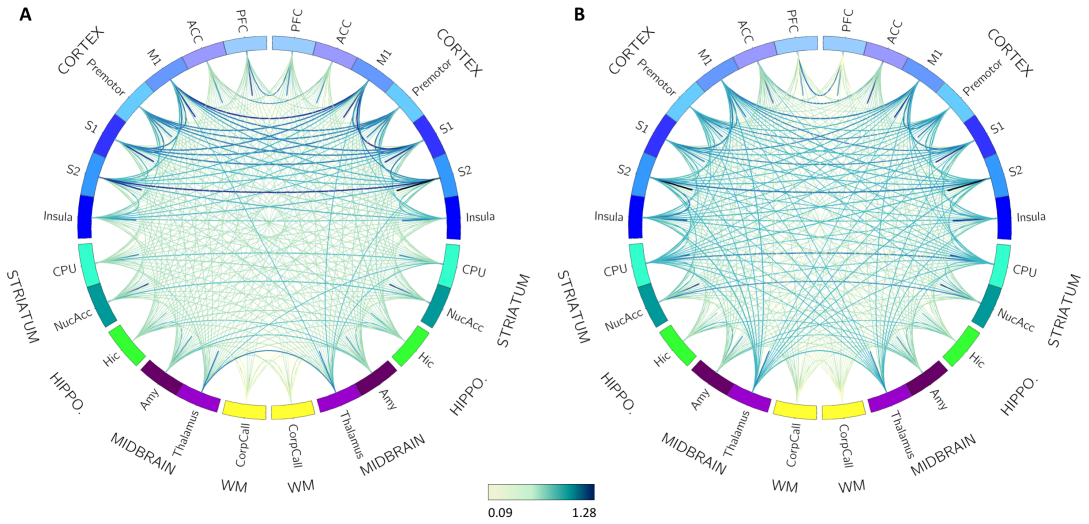


Figure 4.13: Decreased cortico-cortical connectivity and increased thalamo-cortical connectivity in individuals with FXS (A-B) Functional connectograms between 26 brain regions across both hemispheres, in typically developing individuals (A) (n=5) and individuals with Fragile X Syndrome (B) (n=5). The 26 brain regions are represented by rectangles of different colours forming a circle around the connectogram lines. Each line represents the functional connectivity between the two brain regions it links. Greater functional connectivity is represented by thicker and darker lines, as indicated by the r-score colour bar ranging from 0.09-1.28.

Next, I moved on to specifically study the DMN. Using an ICA approach, I found that a frontal component encompassing the dorsal ACC and the superior frontal gyrus was hyperconnected in FXS compared to controls (**Fig. 4.14A**, non-parametric permutation testing of 2-sample t-test GLM, n=5 TD for dual-regression, n=17 TD for permutation testing and 5 FXS, $p<0.05$), while in controls it was hyperconnected to the mPFC and frontal ACC, key components of the DMN (**Fig. 4.14B**, non-parametric permutation testing of 2-sample t-test GLM, n=5 TD for dual-regression, n=17 TD for permutation testing and 5 FXS, $p<0.05$). This finding was also observed when removing the low-functioning female individual (**Fig. 4.15**, non-parametric permutation testing of 2-sample t-test GLM, n=4 TD for dual-regression, n=17 TD for permutation testing and 4 FXS, $p<0.1$ and $p<0.05$ for testing controls > FXS and FXS > controls, respectively.)

I then carried out a correlation analysis, where I calculated the connectivity strength within the dorsal ACC and between the dorsal ACC and the PCC (**Fig. 4.14C**), another

key region of the DMN. This analysis confirmed that the effect of genotype on connectivity was dependent on the brain region studied (Repeated measures two-way ANOVA, n=5 TD for dual-regression, n=17 TD for ANOVA testing and 5 FXS, Region*Genotype $F_{(1,42)}$=12.916, p<0.001). Specifically, I observed a trend of hyperconnectivity in the dorsal ACC in FXS (p<0.1) and a decreased connectivity between the PCC and the dorsal ACC in FX individuals compared to controls (p<0.05). These two analyses both indicate that the DMN is underconnected in individuals with FXS in comparison with controls, while the dorsal ACC and superior frontal gyrus is hyperconnected.

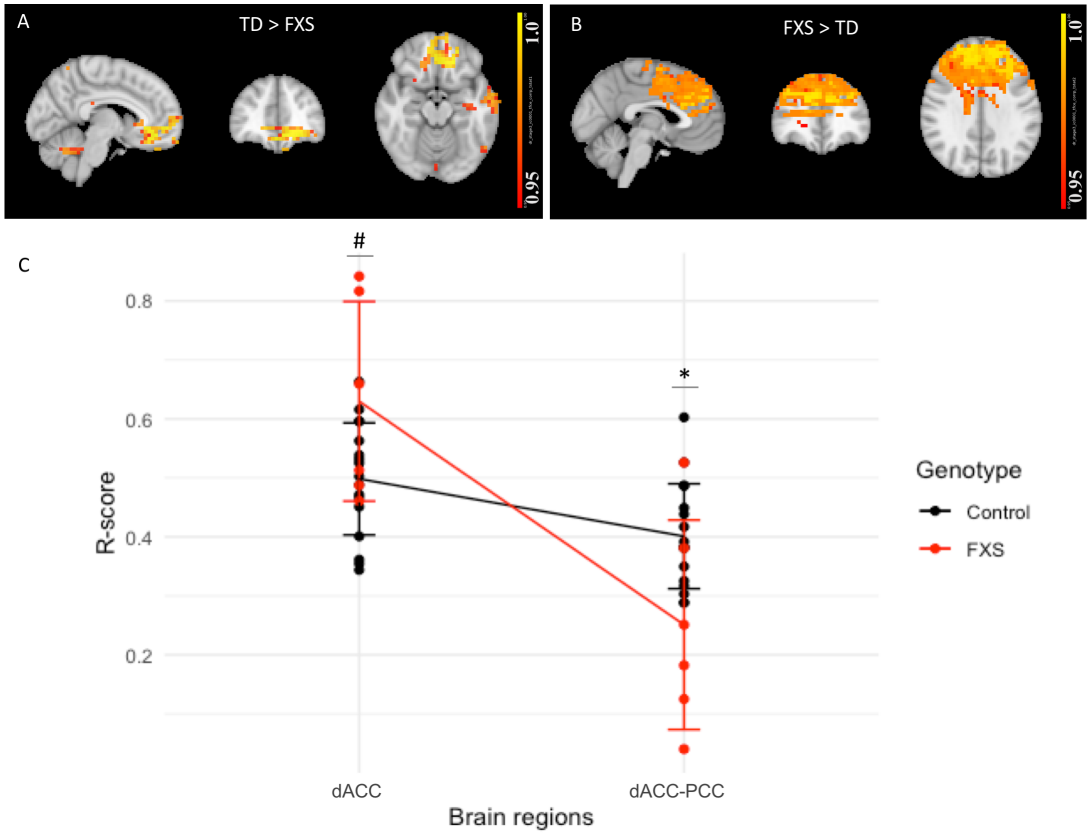


Figure 4.14: Increased frontal connectivity and decreased DMN connectivity in individuals with FXS. (A) Between-group ICA showing greater connectivity in typically developing individuals compared to FX individuals. Statistical map is shown from left-to-right in the sagittal, coronal and axial planes, overlaid on a high resolution anatomical template. Colour bars represent TFCE-corrected 1-P-values, ranging from 0.95-1. (B) Between-group ICA showing greater connectivity in individuals with FXS compared to typically developing individuals. Statistical map is shown from left-to-right in the sagittal, coronal and axial planes, overlaid on a high resolution anatomical template. Colour bars represent TFCE-corrected 1-P-values, ranging from 0.95-1. (C) R-score of functional connectivity within the dorsal ACC and between the dorsal ACC and the PCC in typically developing and FX individuals. Dots represent individual r-scores coloured by genotype, control is shown in black and FXS individuals is shown in red. Bars represent standard deviation. # p<0.1 difference between genotypes, * p<0.05 difference between genotypes.

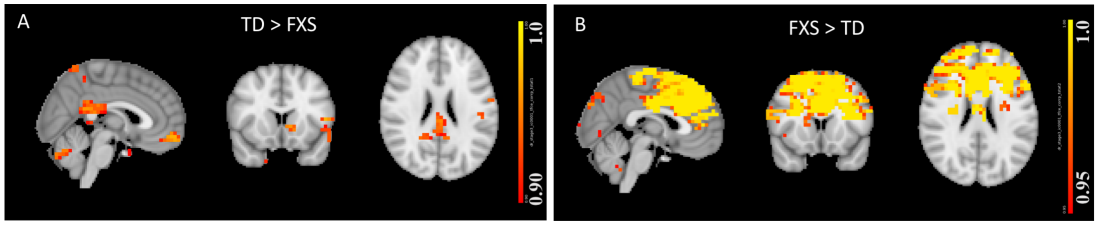


Figure 4.15: Increased frontal connectivity and decreased DMN connectivity in males with FXS. (A) Between-group ICA showing greater connectivity in typically developing individuals compared to male FX individuals. Statistical map is shown from left-to-right in the sagittal, coronal and axial planes, overlaid on a high resolution anatomical template. Colour bars represent TFCE-corrected 1-P-values, ranging from 0.90-1. (B) Between-group ICA showing greater connectivity in male individuals with FXS compared to typically developing individuals. Statistical map is shown from left-to-right in the sagittal, coronal and axial planes, overlaid on a high resolution anatomical template. Colour bars represent TFCE-corrected 1-P-values, ranging from 0.95-1.

In addition, a seed-based analysis was performed to further probe the DMN connectivity, with the seed placed in the ACC (shown in blue on **Fig. 4.16**). Here, again I observed a trend towards a decrease in connectivity between the ACC and the PCC in FXS (**Fig. 4.16**, non-parametric permutation testing of 2-sample t-test GLM, n=5 TD for dual-regression, n=17 TD for permutation testing and 5 FXS, $p<0.2$), supporting my ICA findings.

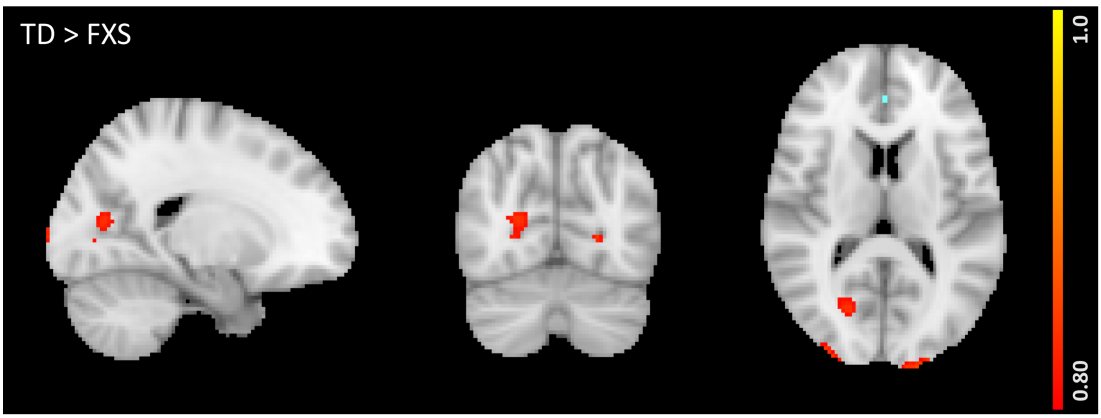


Figure 4.16: Seed-based functional connectivity of the anterior cingulate cortex. Greater functional connectivity to the anterior cingulate cortex seed (blue) in typically developing (n=5) compared to Fragile X individuals (n=5). Statistical map is shown from left-to-right in the sagittal, coronal and axial planes, overlaid on a high resolution anatomical template. Colour bar represents 1-P-value ranging from 0.8-1, corrected for multiple comparison. .

Having established that the DMN connectivity is decreased in FXS, I wanted to determine whether changes in grey matter (GM) could be underlying it. To determine this, I performed a voxel-based morphometry (VBM) on the FX individuals and TD controls. This analysis showed that there was a trend towards a decrease in local GM in

the PCC of FX individuals compared to TD (**Fig. 4.17**, non-parametric permutation testing of 2-sample t-test GLM, n=5 TD for dual-regression and 5 FXS, p<0.4).

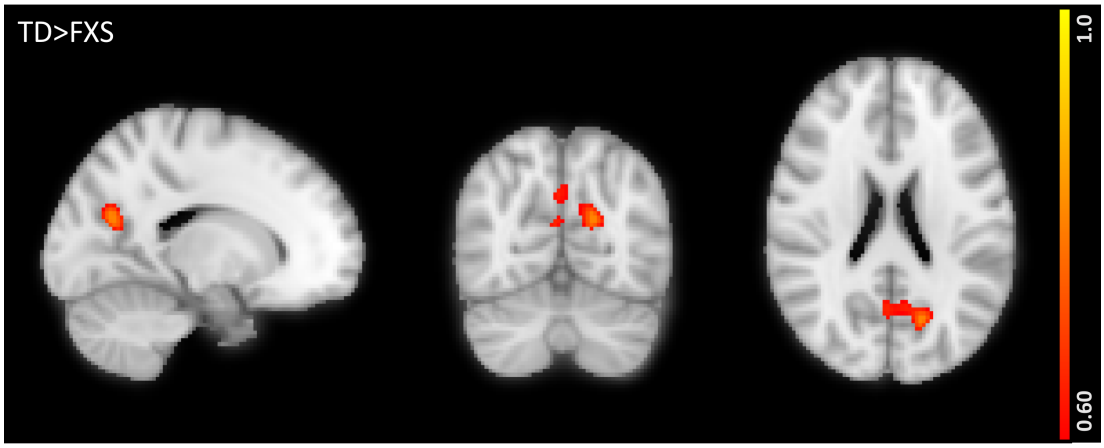


Figure 4.17: Between genotype voxel-wise differences in local grey matter. Trend of voxel-wise decrease in local grey matter in Fragile X individuals (n=5) compared to TD individuals (n=5) obtained by voxel-based morphometry. Statistical map is shown from left-to-right in the sagittal, coronal and axial planes, overlaid on a high resolution anatomical template. Colour bar represents 1-P-value ranging from 0.6-1, corrected for multiple comparison.

4.2.2.3 Summary of results

In the second part of this chapter, I tried to assess whether FC impairments observed in *Fmr1*$^{-/y}$ rats are conserved across species. First, I assessed the feasibility of performing rsfMRI in low functioning individuals with FXS. I found that FX individuals were able to lay still in the scanner following the acclimatization protocol put in place by Dr Andrew McKechanie and Dr Andrew Stanfield. Furthermore, I was able to extract known RSNs from images acquired this way, allowing me to start investigating between-group differences.

At a whole-brain scale, I observed a global decrease in cortico-cortical connectivity in FXS. Surprisingly, thalamo-cortical connectivity was found to be increased in FX individuals compared to TD individuals. Additionally, the long-range connection of the DMN was found to be specifically underconnected in FXS, which may be associated with decreased GM in the PCC, although this was not statistically significant. In contrast, the dorsal ACC and the superior frontal gyrus were found to be hyperconnected in FX individuals compared to controls.

4.3 Discussion

In this chapter, the functional connectivity of FXS was explored using a common imaging approach in individuals with FXS and rats that model the disorder, enabling me to directly compare findings across species. Investigation of the brain's intrinsic activity in anaesthetised *Fmr1*$^{-/y}$ rats revealed a global decrease in functional connectivity and specifically, a decrease in their DMN connectivity. This decrease in DMN connectivity was observed in *Fmr1*$^{-/y}$ rats on a LEH background and a seed-based analysis suggests it could also be present in *Fmr1*$^{-/y}$ rats on a SD background. Furthermore, DMN connectivity was found to decrease with increased anaesthesia concentration in WT rats but not in *Fmr1*$^{-/y}$-LEH rats. In addition, I demonstrated the feasibility of identifying differences in resting state networks using fMRI data from FX individuals with moderate to severe ID and ASD. As observed in textcolormagenta*Fmr1*$^{-/y}$-LEH rats, loss of FMRP resulted in a global decrease of cortico-cortical connectivity and of DMN connectivity in FX individuals. Interestingly, I found that thalamo-cortical connections and two brain regions that are anatomically connected (Li et al., 2013), the dorsal ACC and the superior frontal gyrus, were hyperconnected in FX individuals.

4.3.1 FXS connectivity across species

4.3.1.1 Global connectivity

My observations of a global decrease in functional connectivity in *Fmr1*$^{-/y}$-LEH rats and of a cortico-cortical underconnectivity and a thalamo-cortical hyperconnectivity in FX individuals adds to the existing body of literature pointing towards altered whole-brain connectivity in ASD. My preclinical finding agrees with the handful of resting state fMRI studies that have been carried out in mice models of ASD/ID, including a developmental study on *Cntnap2* and *Fmr1* knockout mice (Zerbi et al., 2018; Dodero et al., 2013; Michetti et al., 2017; Suetterlin et al., 2018; Liska et al., 2018). Apart from Suetterlin et al. (2018), all those studies found a similar overall underconnectivity trend to what I observed, with some local overconnectivity also observed in the *Cntnap2*$^{-/-}$ and BTBR models (Zerbi et al., 2018; Dodero et al., 2013).

Consistently with my findings in individuals with FXS, Hall et al. (2013) reported that functional connectivity in cortical networks was decreased in FX individuals, while a thalamic network was increased. In addition, a number of human rsfMRI studies

on ASD have reported underconnectivity at the whole brain scale (Anderson et al., 2011; Balsters et al., 2016; Barttfeld et al., 2012; Dinstein et al., 2011; Ebisch et al., 2011; Gotts et al., 2012; Guo et al., 2017; Hahamy et al., 2015; Iidaka, 2014; Itahashi et al., 2014; Jones et al., 2010; Lai et al., 2010; Lee et al., 2016; Long et al., 2016; Rudie and Dapretto, 2013; Spisak et al., 2014), while others have reported a mix of underconnectivity in long-range connections and increased local connectivity (Chen and Glover, 2015; Cheng et al., 2015; Cherkassky et al., 2006; Dajani and Uddin, 2015; Di Martino et al., 2010, 2014, 2013; Doyle-thomas et al., 2015; Keown et al., 2013; Murdaugh et al., 2015; Nair et al., 2013, 2014; von dem Hagen et al., 2013; Itahashi et al., 2015; Ray et al., 2014; Redcay et al., 2013; Venkataraman et al., 2015; Bos et al., 2014; Damarla et al., 2010; Cerliani et al., 2017), mirroring my findings in FX individuals. As those latter studies were often carried out on large multi-centre cohorts, it is possible that my preclinical findings were not sufficiently powered to detect the limited increase in connectivity present in ASD brains, therefore only revealing an underconnectivity phenotype.

4.3.1.2 DMN connectivity

The DMN is known to be commonly affected in psychiatric disorders. Most ASD-related studies report a decrease in DMN connectivity, both in humans (Barttfeld et al., 2012; Jung et al., 2014; Kennedy and Courchesne, 2008c; Weng et al., 2009; Ypma et al., 2016; Starck et al., 2013; Nebel et al., 2014) and in mouse models (Michetti et al., 2017; Suetterlin et al., 2018; Liska et al., 2018; Zerbi et al., 2019). These findings are consistent with my observations; in a rat model of FXS, connectivity was decreased in all components of the DMN, while in FX individuals, the mPFC and ACC seemed to be specifically underconnected with a trend of decreased connectivity between the ACC and precuneus/PCC also observed. Consistent with my observations, Hall et al. (2013) also reported that the precuneus network was underconnected in individuals with FXS. In addition, my VBM analysis, although underpowered, suggests that changes in local grey matter in the PCC may underlie altered DMN connectivity. The cross-species discrepancy in DMN connectivity I observed could be linked to differences in brain anatomy. While the DMN is composed of the same brain regions in both species, the ACC and PCC are anatomically separated in humans, while they are in contiguous in

rodents (Lu et al., 2012). This anatomical difference could explain why I only detected a general underconnectivity phenotype in the rodent DMN. The limited power of my experiment due to the small sample size of my human cohort might also explain the difference observed between species. My experiment might have been underpowered to detect a general DMN underconnectivity in FX individuals, as observed in the rats. Indeed, the DMN underconnectivity was observed on a ICA component encompassing two networks, one composed of the DMN and one of the dorsal ACC and superior frontal gyrus, but not on the component only encompassing the anterior DMN. Similarly, the seed-based analysis indicated a trend of decreased DMN connectivity that was not statistically significant. It is therefore possible that the deficit in DMN connectivity observed in FX individuals might be restricted by the power of this experiment both in terms of activation strength and spatial extent.

Prefrontal cortex (PFC) impairments have been implicated in the pathophysiology of FXS. As a part of the DMN, impairments in the PFC may therefore be underlying the DMN connectivity deficits observed in FXS. Deficits in attention, inhibitory control and cognitive flexibility are common phenotypes reported in FX individuals that are associated with PFC function (Royall et al., 2002). Loss of FMRP in *Fmr1*$^{-/y}$ mice has been reported to lead to robust PFC-related behavioural impairments, including reduced cognitive flexibility in a visuospatial discrimination task (Krueger et al., 2011), impaired acquisition of the PFC-dependent trace eyeblink conditioning task (Siegel et al., 2017), exaggerated instrumental extinction response (Sidorov et al., 2014) and increased perseverance in a 5-choice serial reaction time task (Kramvis et al., 2013), and to decreased neuronal activity and synaptic complexity in the PFC (Krueger et al., 2011), suggesting that FMRP plays a key role in PFC function. Synaptic plasticity deficits, such as reduced LTP, have also been reported in several subregions of the PFC in mouse and rat models of FXS, notably the ACC and mPFC (Meredith et al., 2007; Zhao et al., 2005; Asiminas et al., 2019). In addition, Asiminas, Jackson and colleagues reported that *Fmr1*$^{-/y}$ rats show specific deficits in two mPFC-dependent novelty discrimination tasks, but not in ones which do not require it (Asiminas et al., 2019). Neuroimaging studies have also reported abnormal PFC activation in FXS. One group reported that while individuals with FXS performed similarly to the TD group on a Go/NoGo task, several brain regions were found to be differently activated during the

task in FX individuals, including the PFC (Menon et al., 2004). Interestingly, reduced PFC activation was associated with reduced FMRP levels (Menon et al., 2004), further supporting the importance of FMRP for PFC function.

4.3.1.3 Local overconnectivity in FX individuals

I identified a frontal brain network composed of the dorsal ACC and of the superior frontal gyrus which was overconnected in FX individuals compared to TD individuals. Consistent with my findings, neuroimaging studies have also reported that the superior frontal gyrus is hyperconnected in ASD (Xu et al., 2019; Westeinde et al., 2020). Xu et al. (2019) observed that low-functioning children with ASD had a hyperconnected superior frontal gyrus. In addition, one group reported that increased cortical thickness in the frontal superior gyrus was found to be associated with restricted and repetitive behaviours and interests in ASD-discordant female twins, but not in ASD-discordant male twins (Westeinde et al., 2020). This would suggest that the overconnectivity I observed may be driven by the female FX individual and/or could be linked to the FXS cohort being composed of low-functioning individuals and could explain why no local overconnectivity was observed in $Fmr1^{-/y}$ rat. To assess whether the female participant with FXS could be driving the overconnectivity observed in the dorsal ACC and superior frontal gyrus, I ran the same ICA test having removed the female individual and found that this component was still overconnected in male FX individuals. This additional analysis suggests that gender is not driving the between-species difference in functional connectivity observed. The analysis of functional connectivity data from a bigger group of participants that can be stratified by gender and intellectual ability would help further decipher this question.

4.3.1.4 Link with ASD and ID

The majority of ASD imaging studies are carried out on high-functioning individuals. In contrast, the human cohort I analysed was comprised of low-functioning individuals which is more representative of the spread of severity encountered in FXS. Common RSNs were identifiable in individuals with an intellectual disability proving the feasibility of obtaining analysable data from scanning low-functioning individuals. Similar acclimatization protocols will hopefully be used in future studies on ASD to better

characterise the full breadth of the autisms and not only individuals of average or above-average intellectual functioning.

Nonetheless, the fact that the FX individuals were found to have a similar impairment in DMN and global connectivity to individuals with ASD of average or above-average intellectual functioning, suggests that the altered DMN connectivity observed in FXS is common to ASD, and independent of intellectual ability.

4.3.2 Inter-strain differences in brain connectivity in rat models of FXS

Between-strains differences were discovered while investigating FXS connectivity in SD and LEH rats. *Fmr1*$^{-/y}$ SD rats were found to have an underconnected caudate putamen and cerebellum, while in *Fmr1*$^{-/y}$ LEH rats the DMN was underconnected.

As described in the previous section, the DMN of individuals with ASD, including FX individuals, have been widely found to be underconnected, as I observed in *Fmr1*$^{-/y}$ LEH rats. However, caudate putamen and cerebellar abnormalities, as observed in *Fmr1*$^{-/y}$ SD rats, have also been implicated with ASD. Enlargement of the caudate and putamen volumes has been reported in individuals with FXS and in individuals with ASD (Hazlett et al., 2009; Reiss et al., 1995; Hoeft et al., 2008; Hall et al., 2013). In addition, fractional amplitude in the 0.01 to 0.1 Hz frequency range, an indicator of local connectivity, was found to be decreased in the caudate head of FXS individuals (Hall et al., 2013).

Cerebellar abnormalities have been extensively reported in ASD and FXS. A neuroanatomical study of monozygotic twins with a full mutation in *Fmr1* but with discordant intellectual ability, one twin having an IQ of 105, the other of 47, revealed that the volume of the ventricles, caudate and cerebellar vermis were enlarged in the twin with intellectual disability (Reiss et al., 1995). Cerebellum and cerebellar vermis volumes were also reported to differ between young boys with FXS and both typically developing and developmentally delayed boys of matched age (Hoeft et al., 2008). In addition to neuroanatomical studies, individuals with cerebellar malformation syndromes provide further evidence of the cerebellum's involvement in ASD. Indeed, up to 40% of individuals with Joubert Syndrome, which is characterized by brainstem malformations and cerebellar vermis hypoplasia, are diagnosed with ASD (Fatemi et al., 2012). Fur-

thermore, cerebellum injury during preterm birth is also associated with early signs of autism features (Limperopoulos et al., 2014). Moreover, functional connectivity studies have reported decreased connectivity in parts of the cerebellum involved in supramodal function, while cerebellar area involved in sensorimotor function are hyperconnected in individuals with ASD (Khan et al., 2015).

Several factors could explain the difference in connectivity observed between SD and LEH rats. First, the SD cohort was composed of fewer animals than the LEH one. The SD experiment might therefore be underpowered and unable to detect impairments in DMN connectivity. This is likely to be a contributing factor as a seed-based analysis revealed a trend towards a decreased DMN connectivity in $Fmr1^{-/y}$-SD rats. However, no between-genotype differences in caudate putamen or cerebellum connectivity were detected in the LEH cohort. Those connectivity impairments were restrained to a few voxels in the SD cohort and could therefore be false positives, although those brain regions have been implicated in the pathophysiology of FXS and ASD and stringent multiple comparisons correction has been used.

An alternative explanation is that the background strain affects the FC of brain networks, obscuring genotype differences. This would explain why the ICA performed on both cohorts together did not reveal any between-genotype impairments. Increased sample size would be needed to detect smaller FXS-linked connectivity changes. Evidence of strain differences in rats has been well documented. Differences in the visual system has been widely reported. The albino SD strain was found to be more sensitive to light than LEH rats. In addition, they were reported to have a lower visual acuity, resolution and adaptation to dark than LEH rats (Prusky et al., 2002; Behn et al., 2003). Furthermore, a study has indicated that these two strains have a different sensitivity to anaesthesia, LEH being more sensitive to isoflurane than SD (Russel and Graybeal, 1995), which we know affects FC. Moreover, strain differences in cognitive performance have been extensively investigated, with LEH rats exhibiting higher cognitive function than SD rats (Tonkiss et al., 1992; Harker and Whishaw, 2002). Motor function was also reported to be different across strains of rats (Whishaw et al., 2003), and so was their exploratory behaviour (Meyerson et al., 2006). Furthermore, they also differ in their response to stress, both at a behavioural level and physiological level (Faraday, 2002; Pardon et al., 2002). Chronic mild stress does not increase corticosterone levels in SD rats, but does in LEH rats (Bielajew et al., 2002). Moreover, deactivation of

the limbic system, including the hypothalamus, has been reported in response to stress (Dedovic et al., 2009). Between-strain differences in the hypothalamus connectivity revealed by the mixed cohort analysis, could therefore be highlighting differences in stress response between LEH and SD rats. Despite habituation to the scanner sound prior to the scanning session, and the use of anaesthesia, scanning may remain stressful for rodents. Since enhanced activation of RSNs has been reported with acclimatization to the scanning procedure, indicated by a lower respiratory rate and reduced motion (Upadhyay et al., 2011), it could be well perceived that a higher stress response in LEH might be preventing the observation of smaller FC impairments detected in *Fmr1*$^{-/y}$ SD rats. It therefore seems possible that both inter-strain differences and difference in sample size could account for the difference in FC patterns observed between the SD and LEH cohorts.

4.3.3 Impact of anaesthesia on functional connectivity

I have shown in this chapter that the effect of anaesthesia on FC differs between genotypes. With increasing concentration of anaesthesia, FC decreases in WT rats. This trend is observed both globally and in the DMN. However, DMN connectivity was not significantly different under 1% and 2.5% isoflurane in textcolormagenta*Fmr1*$^{-/y}$-LEH rats. This suggests that textcolormagenta*Fmr1*$^{-/y}$-LEH rats have a diminished sensitivity to isoflurane.

My findings are consistent with previous research on *Fmr1*$^{-/y}$ mice. Goncalves et al. (2013) examined ensemble network activity in layer 2/3 neurons in *Fmr1*$^{-/y}$ mice and WT littermates. They found that the correlation coefficient between cells were unaffected by isoflurane in *Fmr1*$^{-/y}$ mice, contrary to WT animals. Furthermore, they found that anaesthesia did not affect neuronal firing in *Fmr1*$^{-/y}$ mice, but did in WT animals (Goncalves et al., 2013). Altered sensitivity to anaesthesia has also been reported in another mouse model of ASD. The minimum alveolar concentration needed for anaesthesia was found to be significantly lower in a mouse model of *Shank3* haploinsufficiency than in WT mice (Li et al., 2017). Furthermore, they observed that the concentration of isoflurane needed to prevent a *Shank3* haploinsufficient mouse put on his back to return onto all four paws under 1 minute (righting reflex), was significantly lower than in WT mice (Li et al., 2017). Together these findings suggest that genetic alterations in *Shank3* leads to an increased sensitivity to isoflurane.

In addition, ASD individuals have been reported to have different anaesthesia requirements in the context of dental treatment. Patients with ASD were found to require a higher dose of anaesthesia during dental treatment than patients with only intellectual disability. Furthermore, they were more likely to need a bolus injection of propofol after anaesthesia induction (Asahi et al., 2009). Altogether, this would indicate that sensitivity to anaesthesia is altered in ASD, albeit in different ways across single-gene disorders.

Isoflurane acts presynaptically and postsynaptically to inhibit excitatory neurotransmission. At the presynapse, isoflurane blocks the release of five neurotransmitters (Glutamate, γ-aminobutyric acid (GABA), norepinephrine, dopamine et acetylcholine), inhibiting excitatory and inhibitory postsynaptic currents (EPSC and IPSC) (Wu et al., 2004; Westphalen et al., 2013). It is an especially potent inhibitor of glutamate release. It also decreases the presynaptic action potential amplitude, which may contribute to the EPSC inhibition (Wu et al., 2004). In addition, isoflurane acts as a non-specific antagonist of postsynpatic glutamate receptors (Carla and Moroni, 1992). Alterations in glutamate receptor function in FXS might therefore be underlying the decreased sensitivity to isoflurane observed.

Evidence suggests that the metabotropic glutamate receptor 5 (mGluR_5) function may be affected in *Fmr1*$^{-/y}$ mice. Giuffrida et al. (2005) demonstrated that mGluR_5 association with the postsynpatic density is altered in *Fmr1*$^{-/y}$ mice, with mGluR_5 being less associated with long-form Homer proteins and more associated with Homer1a. Interaction with Homer proteins regulates the constitutive activity of mGluR_5 (Ango et al., 2001). This change in Homer isoforms binding partners could therefore lead to an increased constitutive activity of mGluR_5 (Giuffrida et al., 2005). An increase in constitutively active mGluR_5 could therefore explain the decreased sensitivity to isoflurane observed in *Fmr1*$^{-/y}$ rats, including in the DMN, as isoflurane would not impact their activity. It would further explain the decreased sensitivity to isoflurane in the DMN of *Fmr1*$^{-/y}$ rats, as mGluR_5 is highly expressed in layer 5 pyramidal neurons of the mPFC (Muly et al., 2003), a key brain region of the DMN. It is however worth noting that no direct action of isoflurane on mGluRs have been reported, its effect on glutamate receptors having been found to be mostly targeted at N-methyl-D-aspartate (NMDA) and α-amino-3-hydroxy-5-methyl-4-isoxazolepropionic acid (AMPA) receptors

(Carla and Moroni, 1992).

Loss of FMRP in FXS has also been shown to reduce NMDA receptors and to lead to an increased internalization of AMPA receptors (Nakamoto et al., 2007; Gocel and Larson, 2012; Yau et al., 2019). However, the resulting decrease in AMPA and NMDA receptors in FXS neurons would make them more sensitive to isoflurane inhibition. The decreased sensitivity to anaesthesia observed in this experiment therefore suggests that the differential sensitivity to isoflurane observed between *Fmr1*$^{-/y}$ and WT rats would be mainly it driven by $mGluR_5$ activity, rather than through NMDA or AMPA receptors.

FMRP also regulates the expression of $GABA_A$ receptor subunits (Curia et al., 2009). As isoflurane is a positive modulator of GABA, this could be another way through which isoflurane may differently impact functional connectivity in *Fmr1*$^{-/y}$ and WT rats. However, GABA currents are largely unaffected in *Fmr1*$^{-/y}$ neurons (Curia et al., 2009), suggesting it may not significantly contribute to the differential sensitivity to isoflurane observed between genotype.

The reduced functional connectivity of *Fmr1*$^{-/y}$-LEH compared to WT rats observed under 1% isoflurane both at a global scale and when looking at the DMN, may provide an alternative explanation to the reduced anaesthesia sensitivity observed in *Fmr1*$^{-/y}$-LEH rats. It is possible that the functional connectivity decrease cause by the loss of FMRP is such that isoflurane may not be able to impact functional connectivity further in *Fmr1*$^{-/y}$-LEH, as suggested by the stable DMN functional connectivity across anaesthesia concentration observed in *Fmr1*$^{-/y}$-LEH rats. In contrast, as WT-LEH functional connectivity under 1% isoflurane is higher than in *Fmr1*$^{-/y}$-LEH rats, isoflurane would be able to decrease it with increasing isoflurane concentration, as observed in the experiment. Future experiments carried out at higher isoflurane concentration are needed to determine whether functional connectivity in WT would plateau after a certain isoflurane concentration and/or whether the apparent plateau observed in *Fmr1*$^{-/y}$-LEH rats is in fact a true plateau or not.

4.3.4 Methodological limitations

4.3.4.1 General limitations

First, although the alterations in functional connectivity I identified in FXS are strengthened by the similar results obtained in my individuals with FXS and in a rat model of the disorder, it is possible that the limited sample size of my human cohort and, to lesser degree, of my preclinical cohorts, may prevent the observation of subtle functional connectivity abnormalities present between genotypes. Thirion et al. (2007) demonstrated that a sample size of 20-25 individuals should be used for sufficient sensitivity and reliability. However, the recruitment of participants from a rare disease population is challenging, which is why the human pilot experiment presented in this chapter was based on 5 FX individuals and why neuroimaging studies are increasingly pooling data acquired at multiple sites to increase sample size (Di Martino et al., 2014; Biswal et al., 2010). Therefore, the sample sizes used in this thesis are likely to preclude the detection of FC changes of low effect size, such as those limited to a few voxels within a brain region.

Motion can also confound rsfMRI studies as increased movement in one group can create artefactual differences in connectivity between groups. However, it is unlikely to be the case here, as all rats were anaesthetised and no difference in movement was observed between groups in the human cohort. Furthermore, I corrected for motion artefacts by performing ICA at the individual level and regressing out noise artefacts, including those caused by movement, as well as by performing a motion correction.

4.3.4.2 Preclinical limitations

It should also be noted that all preclinical experiments were performed under light anaesthesia to minimize movement and distress to the animals. While anaesthesia is known to influence RSNs (Masamoto and Kanno, 2012; Bukhari et al., 2017; Grandjean et al., 2014), the dose of isoflurane used in these experiments has been shown to have a limited impact on FC (Grandjean et al., 2014; Liu et al., 2013), enabling me to observe reliable RSNs.

Differences in sensitivity to anaesthesia between genotypes could also affect the validity of my findings. Since anaesthesia dampens FC and $Fmr1^{-/y}$ rats have a decreased sensitivity to anaesthesia, $Fmr1^{-/y}$ rats would be expected to exhibit an inflated connectivity.

However, I observed the opposite, thereby strengthening my underconnectivity results. It further suggests that the difference in connectivity between group might be greater than observed. An awake rsfMRI study would have to be performed to confirm this hypothesis.

Additionally, factors that affect cerebral blood are known to confound resting state studies. In particular, the arterial partial pressure of CO_2 and O_2 have been shown to influence the BOLD signal (Nasrallah et al., 2015). Between-genotype differences in physiology, notably hypercapnia and hyperoxia, could therefore be confounding my FC findings. Blood sampling should therefore be performed to compare basal blood gas values between groups.

Finally, our preclinical cohorts were comprised only of males. As gender has been found to impact functional connectivity (Biswal et al., 2010), and as our human cohort is comprised of both men and women, it would have been interesting to study the impact of loss of FMRP in both male and female rats. However, as FXS is an X-linked disorder, females have a mosaic expression of *Fmr1*. A mix-gender cohort would therefore be more variable than an all male cohort that would uniformly be lacking FMRP. This would make the identification of functional connectivity deficits specific to the loss of FMRP more challenging, especially in small cohorts.

4.3.4.3 Clinical limitations

Gender has been reported to affect functional connectivity, with gender-specific increases in connectivity observed across brain regions (Biswal et al., 2010). Functional connectivity was specifically found to be higher in females with ASD compare to males with ASD (Alaerts et al., 2016; Ypma et al., 2016). As the FXS group included one female, but the TD group was solely composed of males, the increase in thalamo-cortical and local connectivity may be partly driven by the female FX individual. It would therefore be good to recruit female controls to determine whether the observed difference in FC are due to gender or genotype.

Finally, medication is often prescribed in ASD to manage behavioural symptoms. In the UK, approximately 29% of individuals with ASD are under medication, antidepressant and antipsychotics being the most common medication taken, with evidence of polypharmacy (Murray et al., 2014). Crucially, the likelihood of remaining under

medication over time is very high in individuals with ASD (Esbensen et al., 2009). It is therefore important to take the medication status of the participant under account, since they could have an effect on the vasculature, which in turn would affect the BOLD signal and the connectivity patterns, similarly to anaesthesia. Unfortunately, no information on the medication status of the participants analysed in this chapter was available. However, a study reported that the difference in FC observed between ASD and TD participants remained when excluding individuals using certain class of medications, although the medication did modulate the strength of functional connectivity within certain brain areas (Monk et al., 2009). Similarly, several studies found that their original finding remained when excluding individuals under medication from the dataset (Lee Wiggins et al., 2010, 2013; Weng et al., 2009). This would suggest that it is unlikely that the difference in connectivity I discovered between genotypes would solely be an effect of medication.

4.4 Summary

In conclusion, in this chapter I have shown that individuals with moderate to severe FXS and a rat model of the disorder exhibit similar global and DMN functional connectivity impairments, highlighting the potential translational value of this technique. Further experiments are now needed to assess whether therapeutic efficacy in a rodent model predicts outcome in humans, paving the way to using resting state fMRI as a biomarker for clinical trials.

Chapter 5

Impact of early lovastatin treatment on Default Mode Network connectivity of *Fmr1*$^{-/y}$ rats across development

5.1 Introduction

Preclinical studies have shown that loss of FMRP affect early neurodevelopmental processes crucial for normal brain development (Gholizadeh et al., 2015; Harlow et al., 2010; Lu et al., 2004; Wijetunge et al., 2014; Harlow et al., 2010; Testa-silva et al., 2012; Meredith et al., 2012; Zerbi et al., 2018). Clinical and neuroimaging studies have also reported that individuals with FXS present signs of cognitive delay and global cognitive impairments (Cornish et al., 2008; Skinner et al., 2005; Bailey Jr et al., 1998; Hatton et al., 2009; Baranek et al., 2008; Roberts et al., 2009). When looking at adult phenotypes of FXS, the developmental nature of the disorder may render it difficult to distinguish between direct effects of loss of FMRP, compensatory mechanisms and altered developmental experience. It has therefore been suggested that therapeutic intervention prior to the emergence of major symptoms might maximize chances of therapeutic success (Meredith, 2015). This would however require a good understanding of the developmental progression of the pathophysiological process being targeted.

In recent years, a series of potential drug treatment for FXS has arisen from preclinical research, one of them being lovastatin. Lovastatin is a 3-hydroxy-3-methylglutaryl coenzyme A reductase inhibitor, which is used to treat hypercholesterolemia. Li et al. (2005) have shown that lovastatin can also correct cognitive deficits resulting from ex-

cess Ras activity in a mouse model of neurofibromatosis 1 (NF1). Pathological changes observed in FXS is thought to arise from an increased sensitivity to extracellular signal-regulated kinase (ERK1/2) activation, within the mGluR5-ERK1/2 pathway (Osterweil et al., 2010). At the head of the ERK1/2 pathway is the GTPase Ras. In an original study, Osterweil et al. (2013) showed that lovastatin can correct excessive protein synthesis, exagerated mGluR-LTD and mGluR-mediated epileptogenesis in the hippocampus of *Fmr1*$^{-/y}$ mice and provided evidence that this effect was mediated through dampening of the Ras-ERK1/2 activation. Lovastatin also normalized visual cortex hyperexcitibility and audiogenic seizures susceptibility.

Asiminas, Jackson and colleagues (2019) examined the emergence of associative memory circuits using spontaneous exploration tasks in *Fmr1*$^{-/y}$ rats and WT rats and assessed whether early treatment with lovastatin can prevent deficits in associative memory. They found that treatment with lovastatin prior to the emergence of the ability to perform those tasks, between 4 weeks and 9 weeks of age, successfully restored the performance of *Fmr1*$^{-/y}$ rats on associative memory tasks. Additionally, they demonstrated that lovastatin further prevented the emergence of plasticity deficits in the mPFC of *Fmr1*$^{-/y}$ rats. Surprisingly, the benefits of early lovastatin treatment were found to persist 14 weeks after the end of treatment. This study supports the idea that early treatment, before major deficits emerges, improves therapeutic success.

Since I have shown in chapter 4 that similar DMN connectivity impairments are identifiable in *Fmr1*$^{-/y}$-LEH rats and affected human, I hypothesised that rsfMRI could be used to assess therapeutic efficacy in rodent models. First, I investigated the developmental profile of DMN connectivity in WT and *Fmr1*$^{-/y}$-LEH rats to better understand the nature and the timing of the deficits observed in adults. Second, I assessed the hypothesis that early lovastatin treatment would enhance DMN connectivity in *Fmr1*$^{-/y}$-LEH rats, by giving *Fmr1*$^{-/y}$-LEH rats and WT littermates a lovastatin-enriched or control diet between week 4 and 9 of age. This time window was chosen as Asiminas et al. (2019) have shown that it is a critical time period for the emergence of circuits, including some involving the mPFC, that underlie associative memory and of mPFC-LTD. I provide evidence that early lovastatin treatment was unsuccessful at restoring DMN connectivity in *Fmr1*$^{-/y}$-LEH rats. However, as a recent clinical trial found no clear benefit of lovastatin over placebo in individuals with FXS, rsfMRI may be a good tool in predicting therapeutic success in clinical trials, supporting my main

hypothesis.

5.2 Results

5.2.1 Developmental trajectory of DMN connectivity

To examine the developmental trajectory of DMN connectivity in LEH *Fmr1*$^{-/y}$ and WT rats, I performed rsfMRI experiments on *Fmr1*$^{-/y}$-LEH and WT rats at four different timepoints across postnatal development: 4 weeks, 8 weeks, 12 weeks and 15 weeks of age (**Fig. 5.1**). The 4 week scan was the earliest timepoint, which occurred immediately prior to treatment administration. From 4 weeks to 9 weeks, the rodent diet was changed, with half of the cohort receiving a control diet and the other half receiving the control diet enriched with lovastatin, similarly to what Asiminas et al. (2019) did in their study. The 8 week scan therefore took place while the animals were on the experimental diet. From week 9 onwards, the rats were switched back to a standard diet, on which they remained until the end of the experiment, including during the 12 week and 15 week scans.

This experimental design allowed me both to investigate the developmental trajectory of RSNs, as well as to determine the effect of early therapeutic intervention on functional connectivity.

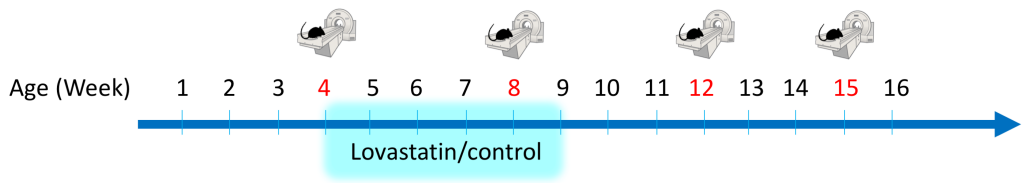


Figure 5.1: Experimental timeline. *Fmr1*$^{-/y}$-LEH rats and WT littermates were scanned at multiple timepoints across postnatal development; at 4 weeks, 8 weeks, 12 weeks and 15 weeks of age. The rats were put on either a control diet or a lovastatin-enriched diet following the first scan on week 4 until week 9.

To look at how DMN connectivity develops over time, I first compared *Fmr1*$^{-/y}$-LEH and WT littermates on a control diet. I identified the DMN by performing an ICA on all animals having received a control diet, grouping all timepoints. I then, measured the functional connectivity strength of the DMN across development, by calculating the correlation value between voxels within the DMN and the rest of the DMN for each animal at each timepoint. The DMN connectivity differed between *Fmr1*$^{-/y}$-LEH and

WT (2-way repeated measures ANOVA, n=27 WT and n=25 *Fmr1*$^{-/y}$-LEH, Genotype $F_{(1,118)}$=4.39, p=0.03; **Fig. 5.2**), with the DMN connectivity being higher in WT animals than in *Fmr1*$^{-/y}$-LEH.

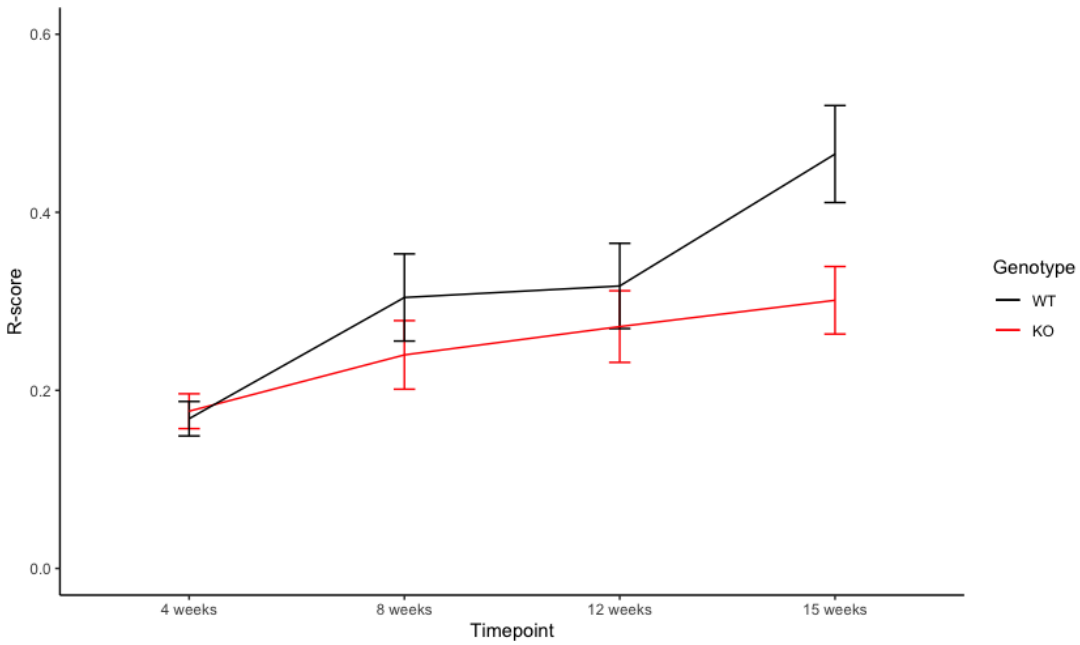


Figure 5.2: Developmental trajectory of DMN connectivity in *Fmr1*$^{-/y}$-LEH and WT rats on a control diet. DMN connectivity is decreased in *Fmr1*$^{-/y}$-LEH rats (KO) (red) compared to WT littermates (black) (Genotype $F_{(1,118)}$=4.39, p<0.05). It further appears that DMN connectivity between genotypes depends on the developmental stage (Genotype*Timepoint $F_{(3,118)}$=2.30, p=0.08). Graph indicates mean DMN connectivity, as indicated by r-score, ± SE across 4 timepoints (age).

Furthermore, I identified a trend towards a difference in the developmental trajectory of DMN connectivity between genotypes (Repeated measures 2-way ANOVA, n=27 WT and n=25 *Fmr1*$^{-/y}$-LEH, Genotype*Timepoint $F_{(3,118)}$=2.30 , p=0.08; **Fig. 5.2**). At 4 weeks of age, DMN connectivity is comparable in juvenile *Fmr1*$^{-/y}$-LEH and control rats, as indicated by within-DMN r-score of 4-weeks old rats (2-sample t-test, n=27 WT and n=25 *Fmr1*$^{-/y}$, $t_{(50)}$=-0.31, p>0.05; **Fig. 5.3A**), and comparable mean maps of the DMN component across genotypes (**Fig. 5.3B**). While there was only a trend to significance in the developmental trajectory between genotypes, analysis of drug treatment at subsequent timepoints shows a significant difference in DMN connectivity between genotypes from 8 weeks onward (see below).

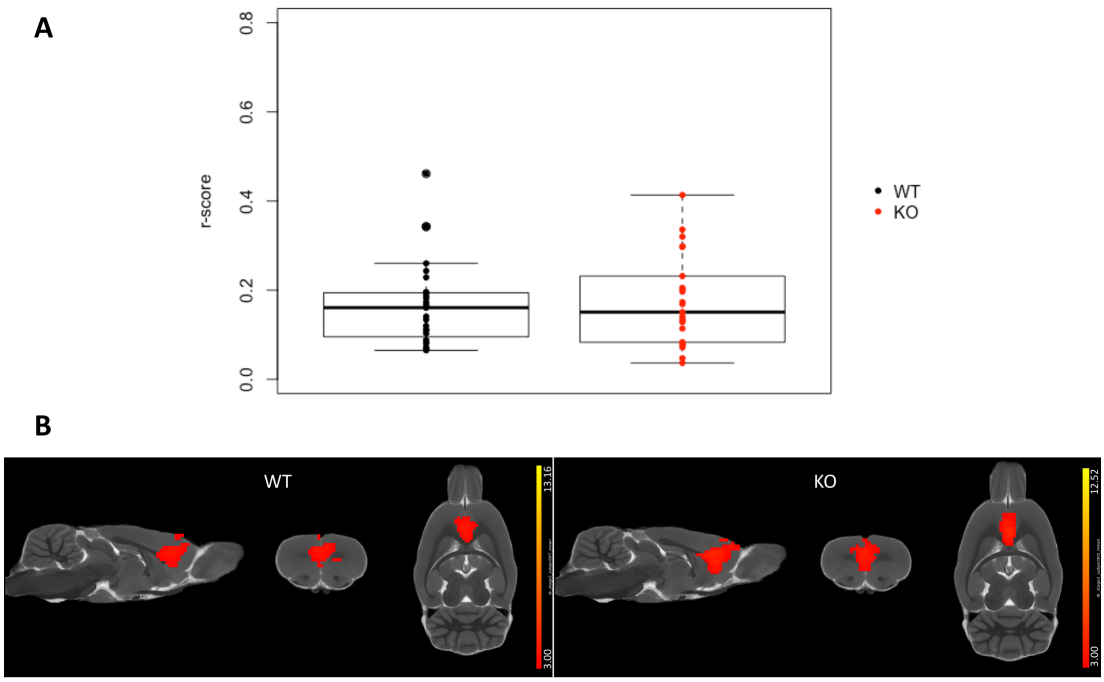


Figure 5.3: No between-group difference in DMN connectivity in 4-week old *Fmr1*$^{-/y}$-LEH rats and WT littermates. (A) Boxplot of DMN connectivity (r-score) in 4-week old WT (black) and *Fmr1*$^{-/y}$-LEH rats (KO, red). No between-genotype difference was observed (p>0.05). (B) DMN z-score in 4-week old rats, averaged by groups; WT group-averaged is shown on the left panel and *Fmr1*$^{-/y}$-LEH on the right. DMN spatial maps are shown from left-to-right in the sagittal, coronal and axial planes, overlaid on a high resolution anatomical template. Colour bars represent z-score, ranging from 3.00 to 13.00.

5.2.2 Can Lovastatin enhance DMN connectivity in *Fmr1*$^{-/y}$ rats?

To assess whether early lovastatin treatment would restore DMN connectivity, all rats were transferred to a new diet immediately following the baseline MRI scan at 4 weeks of age, with half receiving a diet enriched with lovastatin and the other half a control diet. After receiving 4 weeks of either the control or lovastatin diet, *Fmr1*$^{-/y}$-LEH and control rats were scanned at 8 weeks of age. DMN connectivity was again identified by performing an ICA, followed with a dual-regression on the ICA components to obtain subject-specific version of the DMN component. Those were then averaged by group to obtain a mean DMN component for each genotype and diet combination. The strength of DMN connectivity was further calculated by correlating resting state time course between voxels in the ACC and the rest of the DMN.

At 8 weeks of age, DMN connectivity was significantly decreased in *Fmr1*$^{-/y}$-LEH rats compared to WT (Repeated measures 2-way ANOVA, n=13 WT-control, n=14 WT-lovastatin, n=13 *Fmr1*$^{-/y}$-control and n=25 *Fmr1*$^{-/y}$-lovastatin, Genotype ($F_{(1,48)}$=4.37, p=0.042); **Fig. 5.4A**), which is also seen on the mean DMN group maps (**Fig. 5.4B**). However, no drug effect or drug x genotype interaction were identified (Repeated measures 2-way ANOVA, n=13 WT-control, n=14 WT-lovastatin, n=13 *Fmr1*$^{-/y}$-control and n=25 *Fmr1*$^{-/y}$-lovastatin, Drug ($F_{(1,48)}$=0.05, p>0.05), Genotype*Drug ($F_{(1,48)}$=0.30, p>0.05)). This would suggest that at 8 weeks, the DMN of *Fmr1*$^{-/y}$-LEH rats is underconnected, and that 4 weeks of lovastatin treatment does not to enhance DMN connectivity in 8 weeks old *Fmr1*$^{-/y}$-LEH or WT rats.

The cohort was next scanned at 12 weeks and 15 weeks of age, having completed the 5 week treatment and having been off lovastatin or control diet for an additional 3 weeks and 6 weeks, respectively. Similarly to the 8-week timepoint, mean DMN component maps were obtained by performing an ICA, followed with a dual-regression. The strength of DMN connectivity was measured by correlating fluctuations in the BOLD signal between voxels in the ACC and the DMN.

At 12 weeks of age, DMN connectivity was found to be underconnected in *Fmr1*$^{-/y}$-LEH rats compared to WT rats at this age as well (Repeated measures 2-way ANOVA, n=13 WT-control, n=14 WT-lovastatin, n=13 *Fmr1*$^{-/y}$-control and n=25 *Fmr1*$^{-/y}$-lovastatin, Genotype $F_{(1,48)}$=4.05, p=0.049; **Fig. 5.5A**), which can also be seen on the mean DMN component maps (**Fig. 5.5B**). Similar to findings at 8 weeks of age, lovast-

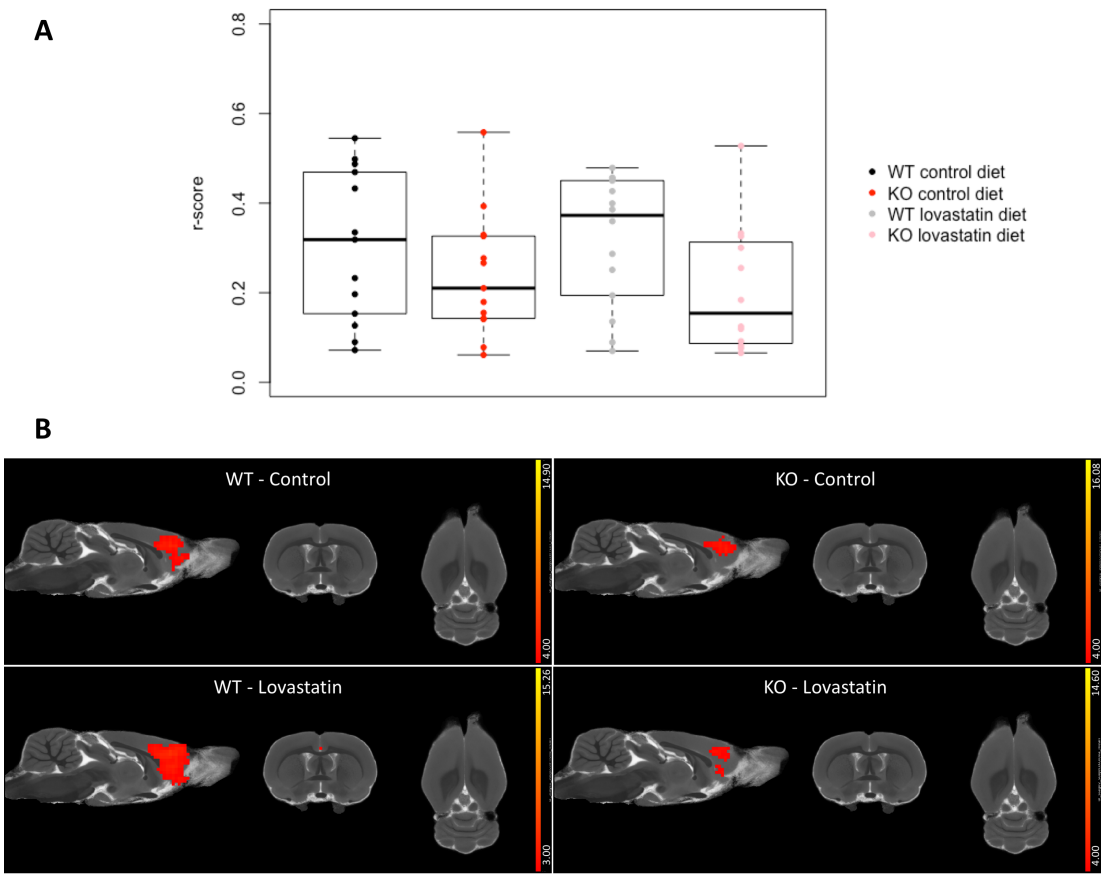


Figure 5.4: DMN connectivity in 8 week old *Fmr1*$^{-/y}$-LEH rats and WT littermates on lovastatin or control diet. (A) Boxplot comparing mean DMN connectivity (r-score) in 8-weeks old WT rats on a control diet (black), WT rats on a lovastatin-enriched diet (grey), *Fmr1*$^{-/y}$-LEH (KO) rats on a control diet (red) and *Fmr1*$^{-/y}$-LEH (KO) rats on a lovastatin-enriched diet (pink). A genotype effect was detected ($F_{(1,48)}$=4.37, p=0.042), but no drug effect or drug x genotype interaction (p>0.05). (B) Mean map of DMN z-score in 8-weeks old rats, averaged by groups. WT on a control diet group is shown on the top left panel and *Fmr1*$^{-/y}$-LEH on a control diet is shown on the top right. WT and *Fmr1*$^{-/y}$-LEH rats on lovastatin enriched diets are shown in the bottom left and right panels, respectively. DMN spatial maps are shown from left-to-right in the sagittal, coronal and axial planes, overlaid on a high resolution anatomical template. Colour bars represent z-score, ranging from 4.00 to 16.00.

atin showed no evidence of correcting this decrease in DMN connectivity (Repeated measures 2-way ANOVA, n=13 WT-control, n=14 WT-lovastatin, n=13 *Fmr1*$^{-/y}$-control and n=25 *Fmr1*$^{-/y}$-lovastatin, Drug $F_{(1,48)}$=0.01, p>0.05) and no drug x genotype interaction was observed (Repeated measures 2-way ANOVA, n=13 WT-control, n=14 WT-lovastatin, n=13 *Fmr1*$^{-/y}$-control and n=25 *Fmr1*$^{-/y}$-lovastatin, Genotype*Drug ($F_{(1,48)}$=1.06, p>0.05). This indicates that a 5 week regimen of lovastatin, from 4 weeks to 9 weeks of age, does not alter DMN connectivity in 12 weeks old WT or *Fmr1*$^{-/y}$-LEH rats.

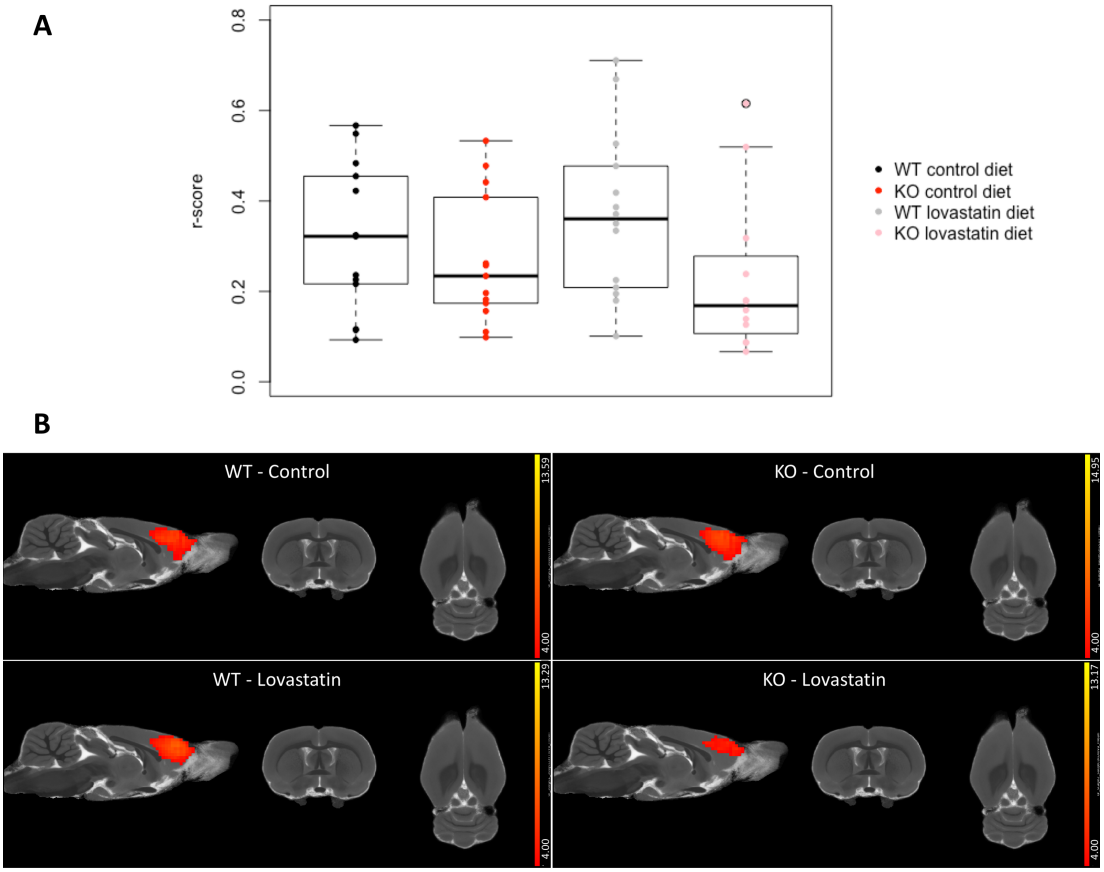


Figure 5.5: DMN connectivity in 12 week old *Fmr1*$^{-/y}$-LEH rats and WT littermates treated with a lovastatin or control diet. Boxplot comparing mean DMN connectivity (r-score) between 12-weeks old WT rats on a control diet (black), WT rats having received a lovastatin-enriched diet (grey), *Fmr1*$^{-/y}$-LEH (KO) rats on a control diet (red) and *Fmr1*$^{-/y}$-LEH (KO) rats on a lovastatin-enriched diet (pink). A genotype effect was detected ($F_{(1,48)}$=4.05, p=0.049), but no drug effect or drug x genotype interaction (p>0.05). (B) Mean map of DMN z-score in 12-weeks old rats, averaged by groups. WT on a control diet group is shown on the top left panel and textitFmr1$^{-/y}$-LEH on a control diet is shown on the top right. On the bottom left panel is shown WT rats on a lovastatin diet, and bottom right, *Fmr1*$^{-/y}$-LEH on a lovastatin-enriched diet. DMN spatial maps are shown from left-to-right in the sagittal, coronal and axial planes, overlaid on a high resolution anatomical template. Colour bars represent z-score, ranging from 4.00 to 15.00.

Finally, I also identified a decrease in within DMN connectivity in 15 weeks old *Fmr1*$^{-/y}$-LEH rats (Repeated measures 2-way ANOVA, n=13 WT-control, n=14 WT-lovastatin, n=13 *Fmr1*$^{-/y}$-control and n=25 *Fmr1*$^{-/y}$-lovastatin, Genotype $F_{(1,48)}$=4.05, p=0.038; **Fig. 5.5A**), which can be observed in the group components (**Fig. 5.5B**). This finding supports my previous observation of a DMN underconnectivity in adult *Fmr1*$^{-/y}$-LEH rats, reported in chapter 4. No drug or interaction effect was detected (Repeated measures 2-way ANOVA, n=13 WT-control, n=14 WT-lovastatin, n=13 *Fmr1*$^{-/y}$-control and n=25 *Fmr1*$^{-/y}$-lovastatin, Drug $F_{(1,48)}$=0.17, p>0.05; drug*Genotype $F_{(1,48)}$=1.02, p>0.05). This further suggests that the particular lovastatin treatment that this cohort received does not affect DMN connectivity in 8 weeks old, 12 weeks or 15 weeks old rats.

5.3 Discussion

5.3.1 The Default Mode Network development

I have shown in this chapter that the development of DMN connectivity follows a different trajectory in WT rats and in *Fmr1*$^{-/y}$-LEH rats. At 4 weeks of age, DMN connectivity is comparable across genotypes, but still immature. By 15 weeks of age, DMN connectivity is significantly higher in WT animals than in *Fmr1*$^{-/y}$-LEH, with a mean WT DMN connectivity roughly twice that observed at 4 weeks.These findings suggest that prior to 4 weeks of age, the processes underlying DMN connectivity might be unaffected by the loss of FMRP in *Fmr1*$^{-/y}$-LEH rat. Following that timepoint, FMRP presence appears to be required for the effective development of DMN connectivity.

The time period between 4 weeks and 8 weeks of age is one of pronounced developmental changes for rats. They reach their sexual maturity around 6 weeks of age, and transition into adulthood at around 8 weeks of age (Sengupta, 2013). Critical changes underlying the DMN connectivity maturation would therefore be happening during rats' late juvenile and adolescence period. Childhood and early adolescence is a period of important neuronal development, with substantial changes in the brain's functional and structural organisation (Blakemore et al., 2010; Dennis and Thompson, 2013). Human and rodent brains are organised into large functional RSNs. These networks can be identified during childhood and even infancy, but in an immature version character-

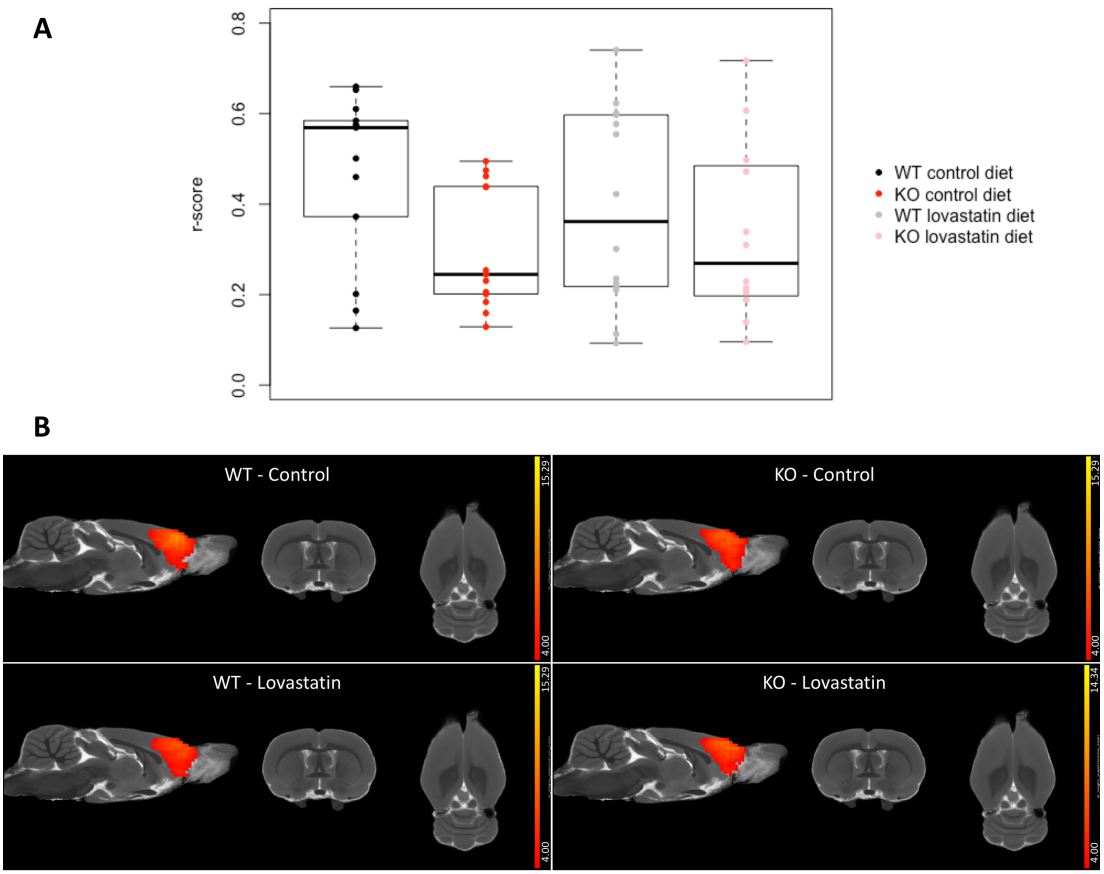


Figure 5.6: DMN connectivity in 15 week old *Fmr1*$^{-/y}$-LEH rats and WT littermates fed with lovastatin or control diet. (A) Boxplot of DMN connectivity (r-score) in 15-weeks old WT rats treated with a control diet (black), WT rats on a lovastatin-enriched diet (grey), *Fmr1*$^{-/y}$-LEH (KO) rats on a control diet (red) and *Fmr1*$^{-/y}$-LEH (KO) rats on a lovastatin-enriched diet (pink). A genotype effect was detected ($F_{(1,48)}$=4.54, p=0.038), but no drug effect or drug x genotype interaction (p>0.05). (B) DMN z-score in 15-weeks old rats, averaged by groups. WT on a control diet group is shown on the top left panel and *Fmr1*$^{-/y}$-LEH on a control diet is shown on the top right. On the bottom left panel is shown the WT on a lovastatin diet group , and bottom right, *Fmr1*$^{-/y}$-LEH on a lovastatin-enriched diet group. DMN spatial maps are shown from left-to-right in the sagittal, coronal and axial planes, overlaid on a high resolution anatomical template. Colour bars represent z-score, ranging from 4.00 to 15.50.

ised by weaker connectivity between the different brain regions that form the networks (Dennis and Thompson, 2013; Bajic et al., 2016).

DMN maturation from childhood to adulthood has been investigated by Supekar et al. (2010). They showed that DMN functional connectivity was weaker in children aged 7 to 9 than in young adults. Furthermore, the long-range connectivity between the mPFC and PCC was specifically underconnected, a result that has also been reported by other groups (Sherman et al., 2014; Fair et al., 2008). This was accompanied by white matter changes. Specifically, fibre density and mean fractional anisotropy (FA) was decreased between the mPFC and PCC in children compared to young adults. In addition, Superkar and colleagues showed that grey matter density was higher in the mPFC and in the PCC of children, while lower WM was found in the dorsal cingulum tract which connects the mPFC and PCC (Supekar et al., 2010). Greater GM could be indicative of exuberant synaptic connectivity in children, which would later be corrected through synaptic pruning (Gogtay and Thompson, 2010). Finally, functional connectivity between the mPFC and PCC showed a weak but non-significant correlation with structural connectivity in children, while the correlation was significant in adult (Supekar et al., 2010). These findings suggest that the mPFC - PCC connectivity within the DMN becomes more stable with age.

Synaptic pruning and changes in WM microstructure and myelination in the WM tract connecting the mPFC and PCC might therefore be underlying DMN maturation. There is evidence from the literature that these processes are affected by the loss of FMRP. FMRP has been suggested to promote pruning of cell-to-cell connections. Connections between L5A pyramidal neurons in the somatosensory cortex have been found to decrease between the 3rd and 5th postnatal week in WT mice (Patel et al., 2014). However, decreased pruning was observed in *Fmr1*$^{-/y}$ mice, leading to a higher connection frequency and a state of hyperconnectivity in *Fmr1*$^{-/y}$ mice (Patel et al., 2014). This would indicate that, at least during this time period, cell-to-cell connection pruning in L5A somatosensory cortex is altered, which could affect circuit development. Similar connection pruning deficits in the mPFC, where a transient hyperconnectivity in L5 is observed in *Fmr1*$^{-/y}$ mice around postnatal week 3 (Testa-silva et al., 2012), or in the PCC might be sufficient to impair maturation of the DMN in *Fmr1*$^{-/y}$ mice, and even in rats, if the same processes are affected by the loss of FMRP in mice and

rats.

Abnormal white matter tract development has also been reported in FXS, as well as abnormal structural networks (Bruno et al., 2017; La Fata et al., 2014). A decrease in FA in white matter pathways has been reported in male and female infants with FXS from 6 months to 24 months of age (Swanson et al., 2018). In young adults, FA was found to be increased in male and female FX individuals in comparison to age, gender and IQ-matched controls (mean IQ: controls 71.0 and FXS 74.2), and radial diffusivity was found to be decreased (Green et al., 2015), indicative of alterations in WM microstructure that are independent of cognitive abilities. Higher FA and lower radial diffusivity was specifically identified in the cingulum tract which links the mPFC/ACC to the PCC (Green et al., 2015). Loss of FMRP was further found to have a direct effect on myelin and oligodendrocyte development in mice. A delay in myelination was reported in the cerebellum of *Fmr1*$^{-/y}$ mice compared to WT, with fewer myelinated axons and reduced myelin thickness observed in the cerebellum of *Fmr1*$^{-/y}$ mice at postnatal day 7, which normalises as the brain matures (Pacey et al., 2013). This is accompanied by a reduction in the number of olygodendrocyte precursor cells, which could be responsible for the reduced myelination in *Fmr1*$^{-/y}$ mice (Pacey et al., 2013). Additionally, La Fata et al. (2014) have reported that FMRP regulates the positioning of neurons in the cortical plate during embryonic development, via its interaction with N-cadherin (Cdh2) mRNA, and that a delay can be observed in *Fmr1*$^{-/y}$ mice. They have shown that this migration delay was associated with abnormal WM fibers projection and abnormal structural connectivity in *Fmr1*$^{-/y}$ mice. A delay in neuronal migration and in the myelination of the cingulum tract between the ACC/mPFC and PCC during early development could therefore be underlying the reduced DMN maturation observed in *Fmr1*$^{-/y}$ rats.

Spontaneous neuronal activity may also be involved in DMN maturation. Honey et al. (2007) have shown in a computational model that the presence of spontaneous activity is sufficient for complex temporal and spatial pattern of synchronized activity to develop over time. Similarly, it has been hypothesised that the co-fluctuation of BOLD signal over time between brain regions, and the resulting coactivation of those brain regions, may lead to a Hebbian strengthening of their functional connectivity over time (Fair et al., 2008). Abnormal neuronal and network activity has been extensively

reported in a mouse model of FXS. Persistent neocortical circuit activity, or UP states, was reported to be prolonged in cortical pyramidal neurons of *Fmr1*$^{-/y}$ mice (Gibson et al., 2008). Additionally, an increase in the probability of neuronal firing during UP states was observed in *Fmr1*$^{-/y}$ mice (Goncalves et al., 2013), further supporting the idea of a cortical network hyperexcitibility in FXS. Recently, Domanski et al. (2019) also showed using a predictive network model that single-cell physiological alterations, such as neuronal hyperexcitibility in the *Fmr1-KO* model, can lead to connectivity and plasticity changes and circuit dysfunction. Increases in firing rates during spontaneous activity have also been observed in rodent models of FXS. Notably, Goncalves et al. (2013) reported a 3-fold increase in the firing rate of L2/3 cortical neurons of P14-16 *Fmr1*$^{-/y}$ mice but only when the animals were at rest. They further showed that cortical circuit activity was increased in *Fmr1*$^{-/y}$ mice and that neuronal ensemble firing synchronicity was also elevated throughout the first postnatal month. Increased neuronal firing rates during spontaneous activity or an increase in the proportion of neurons recruited during network activity, could obscure the specific coactivation of brain regions within a RSN, hampering its strengthening over time. This could be an additional mechanism through which DMN connectivity is reduced across development in *Fmr1*$^{-/y}$ rats.

5.3.2 Lovastatin and FXS

There are currently no disease-modifying therapies that have been approved for the treatment of FXS, and current therapeutic intervention focuses on the clinical management of symptoms and on behavioural therapies. In the last decade, researchers have identified several potential treatments that target neurobiological mechanisms that are altered in preclinical models of FXS (Berry-kravis et al., 2018). Many are clinically available drugs that have been repurposed as treatments for FXS and are currently undergoing randomized controlled trials (Protic et al., 2019; Tranfaglia et al., 2019). Repurposing drugs is one avenue to bring treatment options to rare diseases, circumventing the cost-benefit issue of developing a new drug for a small patient population. Off-label use of drugs is less expensive than de novo drug development and it speeds up the delivery of medications to patients (Tranfaglia et al., 2019).

Lovastatin has been the subject of a repurposing effort in the Fragile X field. In addition to speeding up and reducing the cost of clinical trials, lovastatin presents the

advantage of having already been extensively tested for safety in children, allowing for chronic treatment even in infancy. Lovastatin has been used in clinical trials for NF1 (Li et al., 2005; Acosta et al., 2011; Payne et al., 2016), which included children. In addition, it has also been approved for use in children with hypercholesterolemia (Clauss et al., 2005; Lambert et al., 1996; Stein et al., 1999), making it possible for clinical trials on lovastatin to be carried out in children with FXS.

Osterweil et al. (2013) first showed that lovastatin could correct FXS pathophsyiology. They observed that lovastatin reduced the amount of active Ras and reduces ERK1/2 activation, which was sufficient to restore protein synthesis to WT levels in hippocampal slices from *Fmr1*$^{-/y}$ mice. These findings have since been confirmed by another group (Pellerin et al., 2016). They also found that lovastatin restored to WT level exaggerated mGlur-LTD observed in *Fmr1*$^{-/y}$ mice. Lovastatin additionally prevented epileptiform activity in hippocampal slices from *Fmr1*$^{-/y}$ mice and reduced cortical hyperexcitibility in *Fmr1*$^{-/y}$ mice. Finally, they demonstrated that lovastatin reduced audiogenic seizure incidence and severity in *Fmr1*$^{-/y}$ mice, both following injection of lovastatin and chronic oral administration of lovastatin with lovachow.

In contrast to Osterweil and colleagues' findings (2013) and to a study by Asiminas et al. (2019) which reported that early lovastatin treatment restored associative memory in *Fmr1*$^{-/y}$ rats, I have shown in this chapter that transient lovastatin treatment between 4 and 9 weeks of age was unsuccessful at restoring DMN connectivity to WT level. It therefore suggests that cellular phenotypes and different behaviours may respond differently to lovastatin treatment. Lovastatin has indeed been shown to have mixed results in correcting behaviours, and especially cognitive deficits, suggesting that it may have a specific effect on certain brain circuitries. Lovastatin was successful in correcting audiogenic seizure (Osterweil et al., 2013). Asiminas et al. (2019) also showed that lovastatin improved *Fmr1*$^{-/y}$ rats' performance in the object-place and object-place-context associative memory tasks. These tasks are dependent on the lateral entorhinal cortex (LEC) and mPFC for the object-place memory and on the LEC, mPFC and hippocampus for the object-place-context memory. In contrast, chronic lovastatin treatment from postnatal day 30 to 60 was unsuccessful at reducing exaggerated instrumental extinction in *Fmr1*$^{-/y}$ mice, a behaviour that requires the PFC (Sidorov et al., 2014). Additionally, lovastatin also failed to correct heightened responses evoked by optogenetic stimulation in L2/3 of auditory cortex slices from *Fmr1*$^{-/y}$ mice

(Goswami et al., 2019). Lovastatin was further unable to reduce the increase in gamma power observed in L2/3 or in L5 auditory cortex slices from *Fmr1*$^{-/y}$ mice (Goswami et al., 2019). Taken together these findings suggest that lovastatin might have a localized effect on specific brain regions and circuitries in FXS, possibly some involving the hippocampus and LEC. Investigation of the FC of those brain regions would tell us whether their connectivity differ between *Fmr1*$^{-/y}$ and WT rats, and second whether lovastatin has a localized impact on FC in *Fmr1*$^{-/y}$ rats.

In addition to preclinical studies, an open-label study was undertaken to assess the safety and efficacy of lovastatin in FXS (Caku et al., 2014). It showed that the treatment had minimal side effects and significantly improved aberrant behaviour, which was their primary outcome measure, as well as 12 secondary outcome measures. A follow-up study failed to replicate the findings of the open-label study conducted by Çaku and colleagues, with no clear benefit of lovastatin over placebo observed in the language-focused primary outcome measure or any of the secondary outcome measures, some of which were comparable to primary and secondary outcome measures of the open-label study (Thurman et al., 2020). In addition, lovastatin was found not to have an effect on a set of biomarkers, including *Fmr1* methylation and ERK level (Thurman et al., 2020). This discrepancy could be explained by a difference in outcome measures, supporting a circuit specific action of lovastatin. It may also reflect a difference in the age of the participants, the open-label study of Çaku and colleagues having younger participants. Disease-modifying treatments may be more efficient in young individuals, when the brain plasticity is maximal. Finally, due to its open-label study design, it is possible that additional unaccounted for factors might have affected the results presented by Çaku et al. Additional follow-up studies are still ongoing (NCT02680379 and NCT02998151) and might provide clarity on this discrepancy.

Without having performed a behavioural assay assessing DMN function on my cohort, I cannot rule out that early chronic lovastatin treatment may also lead to a compensatory reorganisation of neural processing, potentially rescuing DMN function without rescuing its underlying connectivity. Perhaps more crucially, without having performed a positive control experiment, such as testing that enhanced novel protein synthesis in *FMR1*$^{-/y}$ rats or that the emergence of object-place-context task can be rescued by a 5-week lovastatin treatment, as has been shown by Asiminas et al. (2019), I also cannot rule out that the lovastatin given to animals in this experiment could have

been inactive. These positive control experiments would also enable us to assess whether genetic drift in the rat colony could be underlying the lack of effectiveness of lovastatin observed in the present experiment. However, such a finding would be surprising as the LEH colony has recently undergone extensive testing when the rats stopped being able to perform a behavioural task, to ascertain that genetic abnormalities were not driving this result. A complete behavioural characterization of the colony was made, in addition, new WT breeders from a commercially available line were introduced to the colony and the line was also bred to a Lister hooded background (Dr Antonis Asiminas and Dr Anjanette Harris, University of Edinburgh, personal communication). No whole genome sequencing was performed to address this question directly as the behaviour was recovered beforehand by changing the luminosity during the task, suggesting that environmental rather than genetic factors were likely to have been responsible for the altered performance on the behavioural task even if genetic drift cannot be ruled out (Dr Antonis Asiminas and Dr Anjanette Harris, University of Edinburgh, personal communication). It is however worth noting that as the LEH *FMR1* colony is an outbred line, checking for genetic drift by sequencing might not be straightforward.

Finally, when considering using lovastatin as a treatment option for FXS, it is important to note that individuals with FXS were reported to have lower levels of total cholesterol, low density lipoprotein (LDL) and high density lipoprotein (HDL) (Berry-kravis et al., 2014). Low cholesterol levels were observed in children, adolescent and adults with FXS. Cholesterol levels would therefore need to be monitored in individuals with FXS when receiving a statin-based treatment. Special care will have to be taken when starting treatment in children as low cholesterol level can affect myelination of the central nervous system (Werner et al., 2013) and myelination has already been reported to be delayed in mice model of FXS (Pacey et al., 2013). As impairments in myelination can impact structural and functional connectivity, it would be worth investigating whether early lovastatin treatment affect structural connectivity. This in turn would impact the maturation of functional connectivity, which could also explain why I did not observe a positive effect of lovastatin on DMN connectivity in *Fmr1*$^{-/y}$-LEH rats.

5.3.3 Timing of the intervention

The timing of therapeutic intervention is key to maximizing its success. The brain might be more susceptible to treatment during specific time-window during development where plasticity is higher (Meredith et al., 2012), which might lead to treatment failing if started at a later timepoint. Supporting that idea, it is thought that clinical trials of mGlur5 inhibitors for FXS may have been unsuccessful despite promising preclinical results (Michalon et al., 2012; Dölen et al., 2007), due in part to it not including young patients (Berry-kravis et al., 2018).

Clinical studies on the ontogeny of RSNs have shown that they are already established in foetuses, neonates and infants (Fransson et al., 2007; Gao and Ji, 2010; Doria et al., 2010; Wylie et al., 2014; Thomason et al., 2015), but will undergo maturation and refinement as the brain matures. This suggests that RSNs develop before birth, during the period of intense neural growth (Doria et al., 2010). In rodents, Bajic and colleagues Bajic et al. (2016) have demonstrated that RSNs can be identified in 2-weeks old infant rats. They were able to specifically identified the DMN, although it was separated between an anterior and posterior component. This indicates that the long-range connection between the ACC and PCC is not yet mature at 2-weeks of age. This finding mirrors human studies, which show that a primitive DMN, split into an anterior and posterior component, can already be observed during foetal life and in neonates (Thomason et al., 2015; Gao and Ji, 2010; Doria et al., 2010). DMN becomes anatomically comparable to the one observed in adults by 2 years of age (Gao and Ji, 2010).

Since RSNs and DMN connectivity develop at an early age, prior to complex associative memory (Asiminas et al., 2019), therapeutic intervention might need to be started earlier than 4 weeks of age. However, a clinical study that examined the effect of lovastatin on NF1, showed that lovastatin treatment started around 11 year of age increased DMN connectivity (Chabernaud et al., 2012). Future experiments will have to be conducted to determine whether starting lovastatin treatment earlier, possibly around 2-weeks of age when the long-range connection between the ACC and PCC is still immature, can restore the development of DMN connectivity in $Fmr1^{-/y}$ rats.

5.4 Summary

In summary, in this chapter I have demonstrated that DMN connectivity follows a different developmental trajectory in *Fmr1*$^{-/y}$-LEH rats and WT littermates. DMN connectivity is comparable in *Fmr1*$^{-/y}$-LEH and control rats at 4 weeks of age and then differs as the brain matures, with *Fmr1*$^{-/y}$-LEH rats exhibiting a lower DMN connectivity than WT rats. Furthermore, I have shown that treatment with lovastatin from 4 to 9 week of age was unsuccessful at restoring DMN connectivity to WT levels in *Fmr1*$^{-/y}$-LEH rats.

Chapter 6

Discussion

6.1 Concluding remarks

In this thesis, I have shown that resting state fMRI can be used to assess functional connectivity changes in rats associated with drug or anaesthetic administration, postnatal development and a neurodevelopmental disorder. My main findings are:

1. The functional connectivity of *Fmr1*$^{-/y}$ rats is decreased at a global scale and when specifically looking at the DMN;

2. Similar functional connectivity phenotypes are observed in affected human;

3. A 5-week lovastatin treatment appears to be unsuccessful at restoring impaired DMN connectivity in *Fmr1*$^{-/y}$ rats.

6.1.1 Can preclinical rsfMRI be used to predict therapeutic success?

Large clinical trials in individuals with FXS have been carried out to assess the therapeutic efficacy of mGlur5 antagonists and GABA receptor activators, and smaller trials were recently conducted for lovastatin (Berry-kravis et al., 2018). Controlled trials on basimglurant and mavoglurant, two mGlur5 inhibitors, did not show any sign of therapeutic efficacy (Jacquemont et al., 2011; Berry-Kravis et al., 2016), despite encouraging results from a pilot study (Berry-Kravis et al., 2009). Similarly, a randomized controlled trial assessing the efficacy of lovastatin in FXS did not show any clear benefit of lovastatin over placebo (Thurman et al., 2020), despite findings from an open-label study, which showed significant improvement in aberrant behaviour and in 12 other secondary outcome measures (Caku et al., 2014). Finally, no therapeutic efficacy was

demonstrated in phase III studies for the $GABA_B$ agonist arbaclofen, although a phase III study carried out in children showed signs of improvement which just failed to reach significance (Berry-Kravis et al., 2017).

The FXS clinical trials failure despite promising preclinical drug studies could be attributed to several factors. First, therapeutic success in the *Fmr1* knockout mouse or rat model of FXS might not predict therapeutic success in affected humans, due to species differences or model limitations. Second, evidence from studies in mice suggests that drug tolerance can develop with prolonged mGluR5 antagonists administration (Yan et al., 2005; McCamphill et al., 2020), offsetting its benefits. Third, the age at which treatments were started and treatment duration differed between preclinical and clinical trials. Preclinical studies were largely carried out in juvenile animals that had not yet reached sexual maturity (Chuang et al., 2005; Osterweil et al., 2010, 2013; Min et al., 2009; Aschrafi et al., 2005; Michalon et al., 2012; Yan et al., 2005), while clinical trials only included adults and adolescents. There might therefore be a critical time window during which the brain is more amenable to disease-modifying therapeutic intervention. Disease-modifying compounds may only be effective during that time period, and trials taking place after that window might show little to no therapeutic effect. Finally, different outcome measures were used to assess therapeutic success in humans and rodents. Preclinical studies mainly relied on measures of core biochemical and synaptic phenotypes, such as mGluR-LTD and protein synthesis, which are too difficult or invasive to obtain in humans. Instead, clinical trials relied on behavioural readouts, often reported by parents and care givers. This resulted in a high inherent variability and a strong placebo response. Jones et al. (2017) demonstrated that participation in a trial alone is sufficient to elicit a strong placebo response, with parents reporting a marked improvement in their child's behaviour even in the absence of treatment or of interaction with medical professionals.

The overarching aim of this thesis was to find out whether rsfMRI has the potential to improve the translation of therapeutic compounds identified in preclinical studies to the clinics.

As rsfMRI is directly translatable across species and the absence of a task facilitates the study of individuals with an ID, which may have difficulties learning a task, identical protocols can be used to investigate functional connectivity in rodents and in humans,

regardless of their intellectual ability. In chapter 4, I used a comparable resting state fMRI analysis protocol on data from *Fmr1*$^{-/y}$ rats and FX individuals, and identified similar functional connectivity impairments in both species, both in the DMN and at a global scale, indicating that functional connectivity is likely to be a good outcome measure to assess therapeutic success across species. In addition, it could provide a quantifiable clinical endpoint and might potentially limit the placebo response. Bertero et al. (2018) also found that 16p11.2 deletion carriers had similar prefrontal functional connectivity impairments to 16p11.2 mice model, further highlighting the potential of functional connectivity as an outcome measure for therapeutic efficacy in ASD.

It remains to be answered whether functional connectivity strength can be restored by therapeutic agents and whether restoring FC in a rodent model of FXS predicts efficacy in affected individuals. In addition, it is also unclear whether FC improvement is associated with an amelioration of behavioural deficits, which is a major objective of treatment. To start answering these questions, I carried out a developmental experiment with chronic administration of lovastatin from 4 weeks to 9 weeks of age in *Fmr1*$^{-/y}$ and WT rats (chapter 5). However, this administration protocol was unsuccessful at restoring DMN FC deficits in *Fmr1*$^{-/y}$ rats. As Zerbi et al. (2019) showed that an mGluR5 antagonist was also unsuccessful at improving DMN connectivity deficits in *Fmr1*$^{-/y}$ mice, but did rescue the FC of the sensorimotor network, further experiments are needed to determine whether the DMN connectivity can be rescued, if DMN connectivity is related to clinically relevant behaviours, or whether the FC of other RSNs might provide a better clinical endpoint.

If it is found that therapeutic success in FXS animal models predicts therapeutic outcome in affected individuals, it will be possible to use preclinical resting state studies to screen for new therapeutic compounds. It will further be possible to use rodent resting state studies to identify the age of participants and treatment duration that maximizes treatment outcome, to inform design of clinical trials. In addition, as tolerance could have been a factor limiting the success of clinical trials carried out to date, this phenomenon could also be investigated in longitudinal preclinical rsfMRI experiments.

6.2 Future Directions

Further experiments are needed to dissect the effect of lovastatin on FXS functional connectivity. First, as the long-range DMN connection between the ACC and the PCC starts maturing prior to 4 weeks of age (Bajic et al., 2016), it would be worth determining whether starting lovastatin treatment earlier can restore FC deficits in *Fmr1*$^{-/y}$ rats and therefore whether there is a critical window for connectivity rescue. As findings from Bajic et al. (2016) suggest that the DMN long-range connection is immature at 2 weeks of age in rats, this could be a good timepoint to start treatment.

An mGluR5 antagonist has been shown to rescue the somatosensory RSN in *Fmr1*$^{-/y}$ mice (Zerbi et al., 2019) and lovastatin has been reported to restore associative memory brain circuitry (Asiminas et al., 2019). FC of these networks should be investigated in our developmental cohort that received the lovastatin or controlled diet to determine whether the 5-week lovastatin treatment can enhance RSNs connectivity, and whether it has a specific action on certain brain networks.

In addition to carrying out additional FC experiments, it would be interesting to determine whether the effect of therapeutic intervention on FC is accompanied by and/or predicts improvement of behavioural deficits, although it is worth noting that FXS behaviours have been found to be expressed differently across species (Till et al., 2015; Dahlhaus, 2018). Moreover, it is important to determine whether the FC changes observed in *Fmr1*$^{-/y}$ rats are accompanied by structural connectivity changes, and whether lovastatin acts on structural connectivity. This would allow us to uncover the mechanism through which FC alterations develops in *Fmr1*$^{-/y}$ rats, and it would provide us with insight into lovastatin's mechanism of action in FXS. As lovastatin reduces blood lipid levels and it has been reported that FX individuals have low cholesterol levels (Berry-kravis et al., 2014), this would also allow us to determine whether lovastatin treatment has a deleterious effect on the white matter of FX individuals.

Finally, the effect of other potential FXS treatment on FC can be assessed in *Fmr1*$^{-/y}$ rats. If found to be successful, it would be important to determine whether the disease-modifying agent has a similar effect on the FC of individuals with FXS, opening the door to using resting state fMRI as a clinical endpoint in clinical trials.

Appendix A

Resting state protocol

File version required by different resting state analysis programs

SPM8 3D *.img/.hdr* images

Skullstripper 3D *.nii* images

FSL 4D *.nii.gz* images

A.1 FMRI file conversion

Images that are obtained from a Bruker scanner are in a Bruker format and are called <2dseq>. In order to perform resting state data analysis on some images, you first need to convert them into a file format that is read by the software you are going to use.

A.1.1 Create .hdr/.img files in MRIcro

The first software we are planning on using is **SPM8**. **SPM8** requires 3D images, in an analyze format (*.img/.hdr*). This first step transforms the <2dseq> file into an analyze format with the correct header, using **MRIcro**.

In **MRIcro** (PC only):

1. Open a functional image using the 'header info [RAW]': select the <2dseq> image.
2. In the header info edit X, Y, Z dimension and size, and for the functional, the number of volumes. *You can find the dimension information in your scan notes.*

3. 'Save as' → 'save intel' → 'save 4D'

4. 'Open image' <`2dseq`>

5. 'Save as' → 'save intel' → 'save segment padded'

We now have new functional files called <`2dseqx.hdr/.img`> and <`x2dseqxXXX.hdr/.img`>.

Repeat steps 1-3 with the structural images, to obtain new structural files called <`2dseq.hdr/.img`>.

A.1.2 Reorientation in SPM8

Reorient the images (both structural and functional) so they match the template. This step will help improve registration and will increase the image size by a factor 10.

In **SPM8**:

1. In Matlab type `spm fmri` to start **SPM8**

2. Using 'display' open the structural image <`2dseq.hdr/.img`>.

3. Resize (x,y,z) the brain by a factor 10, and adjust the other parameters so the orientation and the origin matches the template's one (**Fig. A.1**)

   - The top left image is the coronal view with top (superior) of head displayed at the top and the left shown on the left, as if subject is viewed from behind
   - The top right image is the sagittal view with the front (anterior) of head at the left and the top on top
   - The bottom image is the axial view with the front of head at the top and the left on the left, as if viewed from above.

4. Once you are happy with the parameters press 'reorient images' and select the structural converted image.

5. Next do the same for the functional images:

   → In 'display' open any one of the <`x2dseqxXXX.hdr/.img`> files

   → Apply the same parameter values as the structural image. *Typically, values are same as the structural image, but double check that the origin is at the correct place*

→ Select 'reorient images' and select all the <x2dseqxXXX.hdr/.img> files

6. 'Check reg' to verify that the structural and functional images are well aligned to one another.

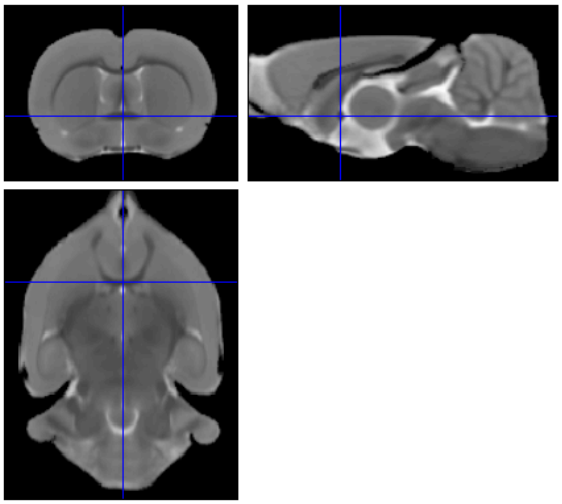


Figure A.1: High resolution image set at the template's origin.

A.2 FMRI file preparation for FSL

First, we need to transform the files to a nifti (*.nii*) format for **Skullstripper**. Next, the brain extracted files need to be converted to a 4D image, in a zipped nifti (*nii.gz*) format for **FSL**.

A.2.1 Conversion to nifti

A.2.1.1 Anatomical

In terminal, type:

`fslchfiletype NIFTI <x2dseq.hdr>`

Check that the images are converted to nifti (*.nii*). If they are converted to *nii.gz*, unzip the images with the command line:

`gunzip <x2desq.nii.gz>`

A.2.1.2 Functional

In terminal, use this command line to batch convert the functional images to nifti format:

```
for i in $(ls <x2desqx???.hdr>); do fslchfiletype NIFTI ${i} ratX_n_${i};
done
```

A.2.2 Brain extraction with skullstriper

In this step, we remove non-brain tissue from our images.

To go faster on this step, you can copy (`cp`) each `<ratX_n_x2dseqx001.nii>` from every animal to the same folder to run **Skullstripper** on all animals at once (shown below). Alternatively, you can perform **Skullstripper** on one animal at a time (see anatomical for the one file at the time command line).

A.2.2.1 Functional

In the folder you are going to run **Skullstripper**, add the Skullstripper software (skullstripper_v2.py), a reference mask and a reference 3D volume in *.nii* format.

To obtain the reference mask and volume, you need to manually extract the brain from non-brain tissue in one of your image. This will serve as a reference for every scan obtained with the same scanning protocol. Manual extraction can be done in **FSLeyes** in the 'edit mode'. Once done, a mask (<BET_ref_mask>) of your brain extracted image (<BET_ref>) can be obtained with the command line:

```
fslmaths <BET_ref> –bin <BET_ref_mask>
```

To run Skullstripper (batch):

```
for f in *.nii; do python skullstripper_v2.py –in $f –ref <BET_ref>
–refmask <BET_ref_mask> –out $f_mask –thr 0.5; done
```

Two folders are created, one with each volume's mask and one with each volume's brain extracted image. You can now use the masks to create a brain extracted image for each animal. To do that, first we need to create a 4D image in *.nii.gz* format and then apply this mask (in *.nii.gz* format) to the 4D image:

1. Convert mask to *nii.gz*.
   In the newly created mask folder, do:
   `gzip <rat*_mask>`

2. Apply the mask to your original 4D *.nii.gz* image to get your 4D brain extracted image.

   (a) Convert your 3D *.nii* images to *.nii.gz* format

   `gzip *.nii`

   (b) Create a 4D image by merging the 3D functional images together

   `fslmerge –tr <4D image output> <3D images input> <TR value>`

   (c) Apply mask to create a 4D brain extracted image

   `fslmaths <4D image input> –mas <mask> <brain extracted 4D image output>`

   (d) Check TR value of your 4D image in its header

   `fslinfo <brain extracted 4D image>`

   Check that the TR value is correct (pixdim4). Melodic will not work if the TR value is not correct!

Make sure that you check that **Skullstripper** worked well using **FSLeyes** before moving on to the next step.

A.2.2.2 Anatomical

You now follow similar steps for the anatomical images.

In the folder you are going to run **Skullstripper**, add the Skullstripper software (skullstripper_v2.py), a reference anatomical mask and a reference brain extracted anatomical 3D image in *.nii* format.

To obtain the reference mask and brain extracted anatomical image, you need to manually extract the brain from non-brain tissue in one of your image. This will serve as a reference for every scan obtained with the same scanning protocol. Manual extraction can be done in **FSLeyes** in the 'edit mode'. Once done, a mask <BET_struct_ref_mask> of your brain extracted image <BET_struct_ref> can be obtained with the command line:

`fslmaths <BET_struct_ref> –bin <BET_struct_ref_mask>`

To run Skullstripper (single line method):

```
python ./skullstripper_v2.py –in $f –ref <BET_struct_ref> –refmask
<BET_struct_ref_mask> –out <anatomical_masked.nii> –thr 0.5
```

You obtain a mask for each animal in a new folder called masks. You can now apply this mask to your original 4D image:

1. Convert mask to *nii.gz*.
   In the newly created mask folder, do:
   `gzip <rat*_mask>`
2. Apply the mask to your original anatomical *.nii.gz* image to get your brain extracted image.
   (a) Convert your anatomical *.nii* image to *.nii.gz* format
   `gzip <x2dseq.nii>`
   (b) Apply mask to create a brain extracted image
   `fslmaths <anatomical image input> –mas <mask> <brain extracted anatomical image output>`

Make sure that you check that **Skullstripper** worked well using **FSLeyes** before moving on to the next step.

You are now ready to perform preprocessing and resting state analysis in FSL.

For human data, use the **dicm2nii matlab tool** to transform dicom files to nifti. Use the **FSL BET tool** with f=0.5 to get brain extracted images. For anatomical images you might have to crop the neck first. This can be done using the following command line: `robustfov –i <MPRAGE.nii.gz> –r <MPRAGE_crop.nii.gz>`

A.3 Resting state analysis using MELODIC

You can perform an ICA using the MELODIC tool of FSL. You can either use the gui or set up the analysis via the command line. If you are using the gui you will need to set up:

A.3.1 Data

- Input the 4D brain extracted functional images obtained above.
- Select the output directory.
- Discard the first 10 volumes (for data with around 300 volumes).
- Select a high pass filter cutoff of 100s.
- Check that the number of volumes and TR value are correct.

A.3.2 Pre-Stats

This is where you decide the preprocessing options.

- Select the MCFLIRT motion correction.
- Select a 5mm FWHM for spatial smoothing.
- Select a high pass filtering.
- If you have not performed a brain extraction, select BET, otherwise unselect this option.
- If you have need to perform a slice timing correction, select this option, otherwise unselect it.
- If you acquired a B0 map during scanning, select this B0 unwarping option, otherwise deselect it.
- Do not select intensity normalization or alternative reference image.

A.3.3 Registration

You need to register your image to the main structural image and to the standard space template.

Main structural image. Select a structural image for each functional image selected in the data section, in the same order. Perform a linear registration with a full search and 12 DOF.

Standard space image. Select your template. Perform a linear registration with a normal search and 12 DOF.

Make sure to check the registration. If images are poorly aligned to one another, you might need to change the search, the DOF used or add a non-linear registration.

A.3.4 Stats

- Variance-normalise the timecourses.
- For a group analysis perform a multi-session temporal concatenation. Select the number of components to be outputed (for rats, try 20 components).
- For an individual analysis perform a single-session ICA, and automatically estimate the number of components ('dimensionality').

A.3.5 Post-Stats

- Threshold the independent component maps at 0.5.
- Select standard space template for background, to obtain ICA components in the standard space.
- Make sure all the stats are saved.

If using the command line, equivalent parameters will have to be selected.

A.4 Dual regression

Statistical analysis of independent components obtained with MELODIC can be carried out through performing a dual regression.

1. First, you need to set up a general liner model design, on which your statistical analysis will be based. This can be done through the GLM tool of **FSL**.
2. Next, perform the dual regression:

   ```
   dual_regression <groupICA.gica/groupmelodic.ica/melodic_IC.nii.gz>
   1 <GLM.mat> <GLM.con> 500 <output_directory_name>
   `cat <groupICA.gica/.filelist>`
   ```

- <groupICA.gica/groupmelodic.ica/melodic_IC.nii.gz> : The <melodic_IC.nii.gz> file is created during MELODIC. It is comprised of the different independent components obtained by ICA as volumes.
- <GLM.mat> and <GLM.con>: GLM matrix and contrast. These are obtained when saving your GLM design (step 1).
- <‘cat groupICA.gica/.filelist‘> : <.filelist> is a list of all the 4D functional images that were used to obtain <melodic_IC.nii.gz> in MELODIC. This file is automatically created when you run MELODIC. `cat` is a command to read a text file. So by doing <‘cat groupICA.gica/.filelist‘>, you are simply telling terminal to read all the images present on the <.filelist>. This saves you from having to write it manually, but if you prefer you can input it manually.
- <output_directory_name>: Selects the name of the folder that will be created to contain the dual regression results.

A dual regression run creates 3 types of files in your output directory: dr_stage1, dr_stage2 and dr_stage3 files.

- **dr_stage1:** timeseries of each subject
- **dr_stage2:** Images of all the independent components with subjects as volume, and images of all the subjects with independent components as volumes.
- **dr_stage3:** GLM results. Tfce_corrp_tstat has been corrected for multiple comparison, while tstat has not. The tstat number corresponds to the order of tests set up in GLM.

GLM results example

If you set up a GLM for a paired t-test with:

test 1: WT>KO

test 2: KO>WT

test 3: mean WT

test 4: mean KO

Tstat1 will give you the result of the WT>KO statistical analysis.

A.5 Seed-based analysis

1. Create a seed in each rat's functional image space. This can be done by creating a seed in the template's standard space and transforming it to each individual's functional space using the `FLIRT` command line.

2. In **AFNI**:

   (a) First, we need to extract the seed's mean time series:

   `3dROIstats −mask <seed_in_ratX_functional_space.nii.gz>`
   `−1Dformat <preprocessed_BET_4D_functional_image.nii.gz> >`
   `<outputname_stepA.1D>`

   The output is a 1D file of the time series.

   (b) Next, we need to perform a Pearson correlation between the mean time series of the seed (obtained step A) and of every voxel of the brain.

   `3dTcorr1D −pearson −prefix <outputname_stepB.Tcorr1D.nii>`
   `<preprocessed_BET_4D_functional_image.nii.gz>`
   `<outputname_stepA.1D>`

   (c) We need to perform a r−to−z Fisher's transform, for use in group analysis.

   `3dcalc −a <outputname_stepB.Tcorr1D.nii> −expr`
   `'atanh(a)' −prefix <outputname_stepC.z.nii>`

   `<outputname_stepC.z.nii>` is your seed-based functional connectivity map.

3. The seed-based functional connectivity maps can be further processed:

   ⇒ Dual regression analysis can be performed on them (see section A.4).

   ⇒ To look at a specific network, we can apply a mask to only look at this network of interest:

   `fslmaths <outputname_stepB.Tcorr1D.nii> −mas <mask>`
   `<output_filename>`

   or

   `fslmaths <outputname_stepC.z.nii> −mas <mask>`
   `<output_filename>`

The network mean functional connectivity can be calculated and advanced statistical analysis can be performed on it.

$\Rightarrow$ These three steps can be repeated for multiple pairs of brain regions, which can be visualised in the form of a matrix or of a connectogram.

Appendix B

Classification of signal and noise components

Whether running a single-subject ICA to clean the subject's data or a group ICA, you will have to identify and, in the case of a single-subject ICA, remove non-signal components.

This can be done by analysing the spatial map, the power spectrum and the timeseries of the components obtained by ICA. If the spatial map, power spectrum or timeseries is identified as bad/noise, the whole component should be classified as noise, regardless of whether the other parameters have been identified as noise or not.

B.1 Spatial maps

Looking at the spatial maps can help you distinguish signal components from noise components. Noise components can be further classified into motion components, cardiac components, white matter components, susceptibility artefacts and MRI acquisition-related issues.

B.1.1 Signal components

The signal of a true signal component will always be in the GM (**Fig. B.1**).

B.1.2 Cardiac components

A component can be classified as cardiac noise, if the activation signal is in the ventricles (**Fig. B.2**).

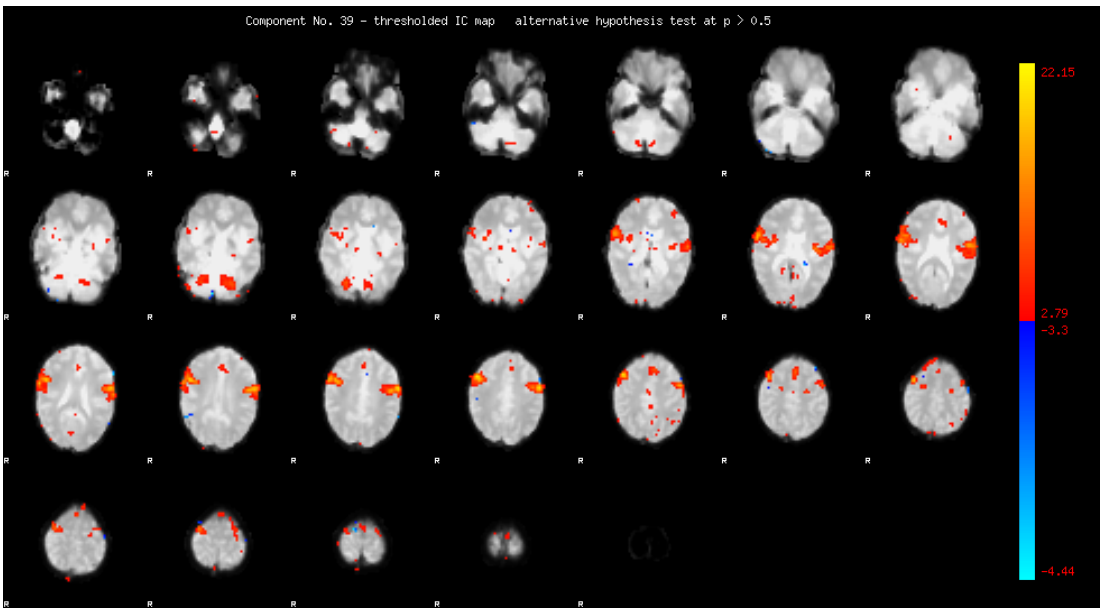


Figure B.1: Signal component.

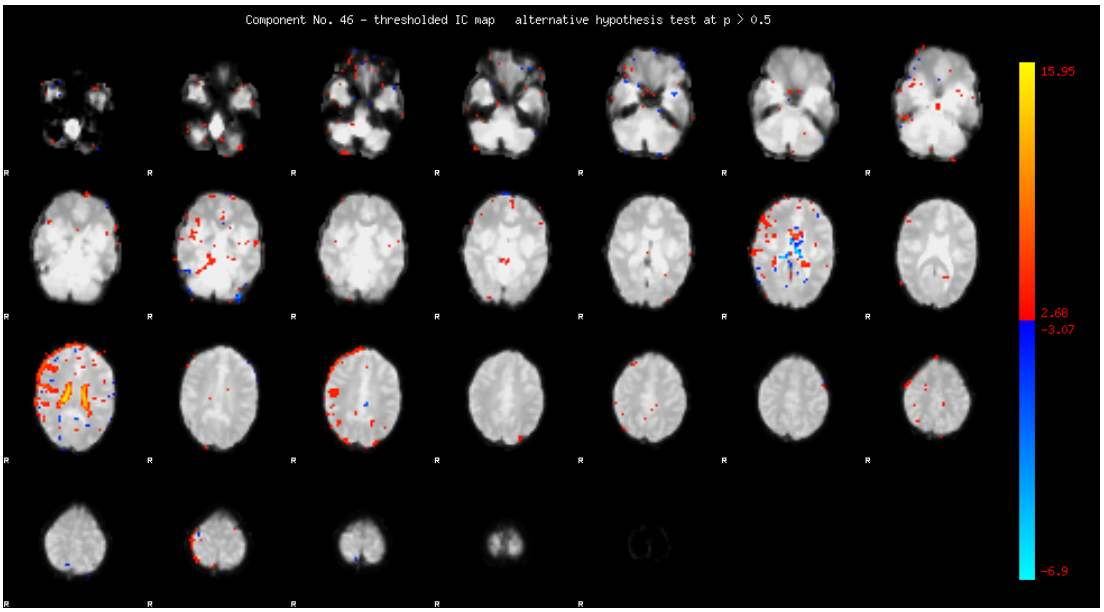


Figure B.2: Cardiac component.

B.1.3 Motion components

Motion components can be easily identified, as they often present themselves as a circle of activation around the brain (**Fig. B.3**).

B.1.4 White matter component

The signal activation of a WM noise component is in the WM (**Fig. B.4**).

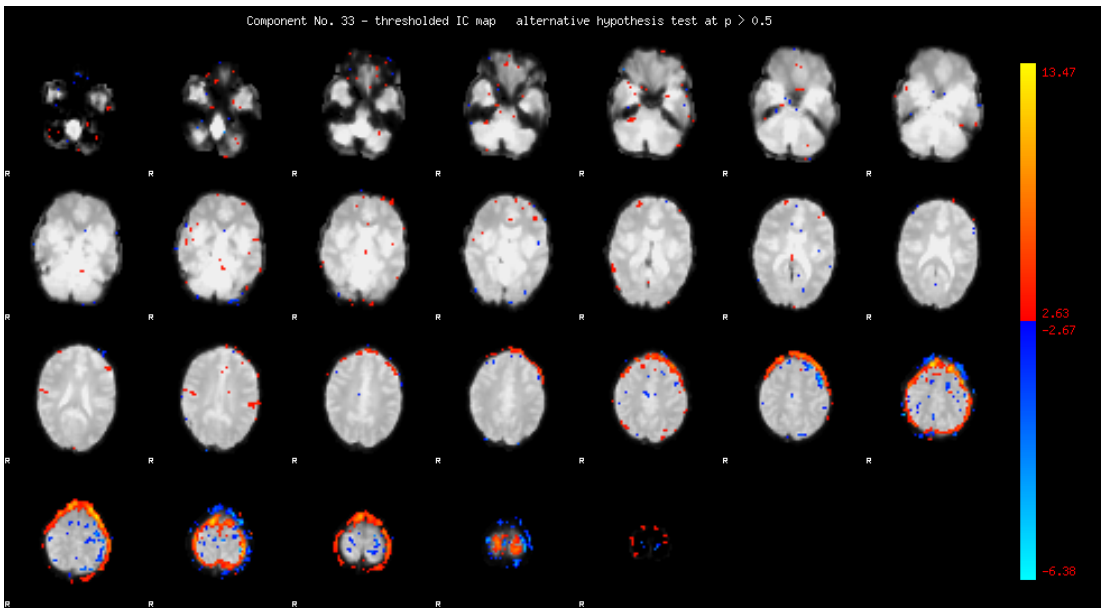


Figure B.3: Motion component.

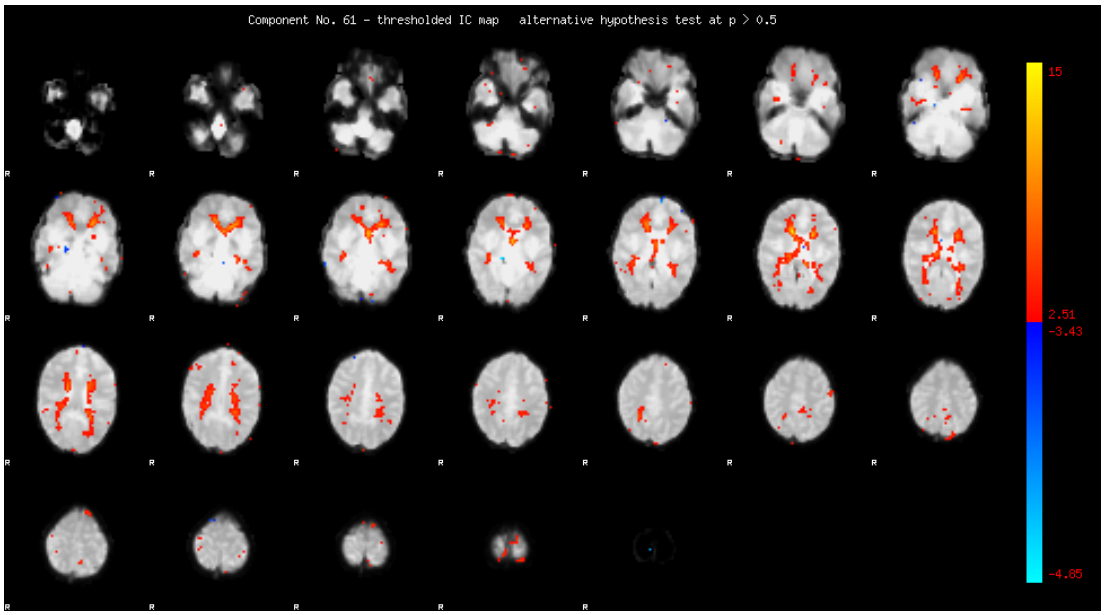


Figure B.4: White matter component.

B.2 Timecourses

In addition to looking at the spatial maps, it is important to look at the timeseries of each component. Timecourses should be regular, with no abrupt changes in the timecourse pattern or rapid modulation of amplitudes (**Fig. B.5**).

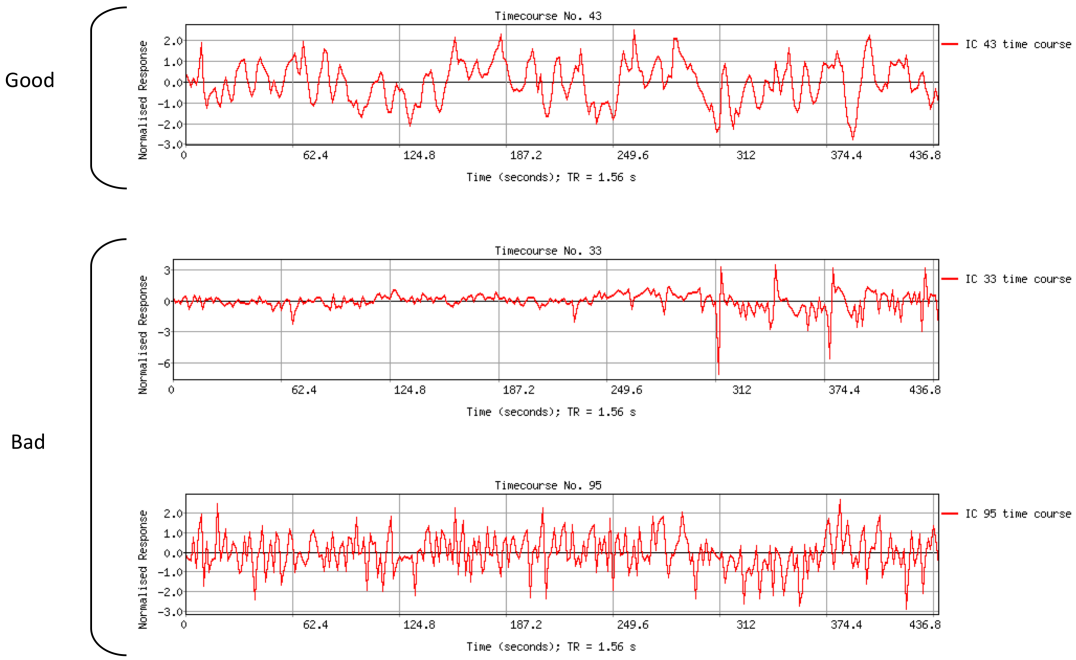


Figure B.5: Independent component timecourses. The figure shows the timecourses of three separate components. Top shows a timecourse that is considered 'good'. Bottom two timecourses are considered 'bad'.

B.3 Powerspectra

Finally, in addition to looking at the spatial map and at the timecourses, it is important to inspect the powerspectra. As resting state signal is thought to be a low frequency signal, a 'good' powerspectrum will have a defined low frequency peak (**Fig. B.6**), while a 'bad' powerspectrum will either have a peak at a high frequency or no defined peaks (**Fig. B.6**).

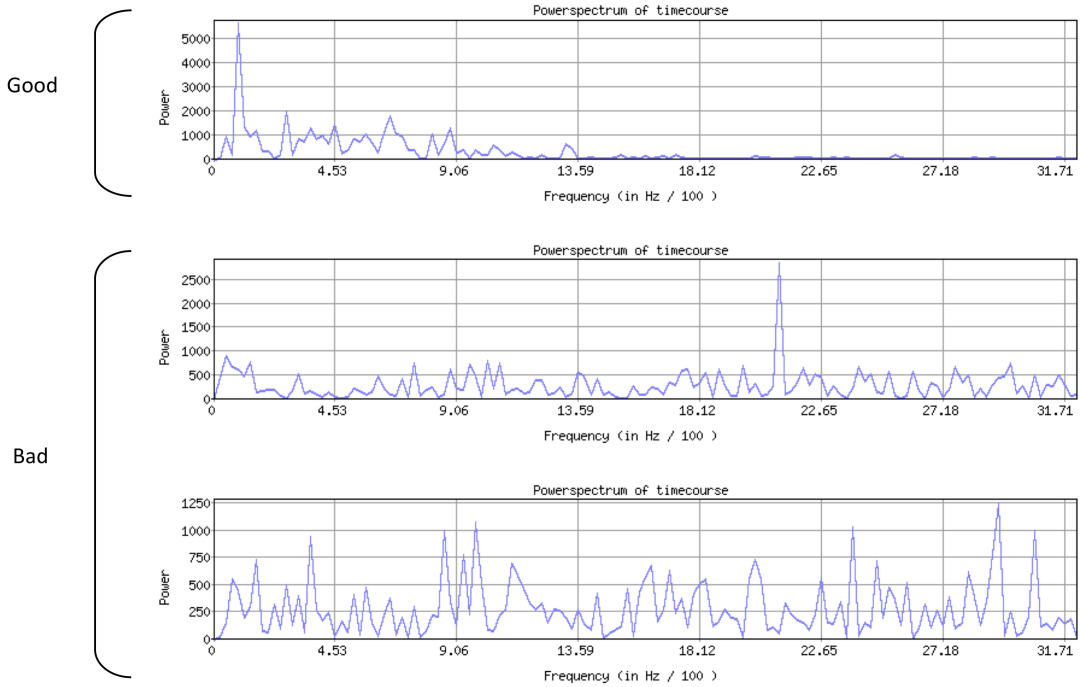


Figure B.6: Independent component powerspectra. The figure shows the timecourses of three separate components. Top shows a powerspectrum that is considered 'good'. Bottom two powerspectra are considered 'bad'.

Bibliography

Abrams DA, Lynch CJ, Cheng KM, Phillips J, Supekar K, Ryali S (2013) Underconnectivity between voice-selective cortex and reward circuitry in children with autism. *PNAS* 110:12060–12065.

Acosta MT, Kardel PG, Walsh KS, Rosenbaum KN, Gioia GA, Packer RJ (2011) Lovastatin as Treatment for Neurocognitive Deficits in Neurofibromatosis Type 1 : Phase I Study. *Pediatric Neurology* 45:241–245.

Akins MR, Berk-Rauch HE, Kwan KY, Mitchell ME, Shepard KA, Korsak LIT, Stackpole EE, Warner-Schmidt JL, Sestan N, Cameron HA, Fallon JR (2017) Axonal ribosomes and mRNAs associate with fragile X granules in adult rodent and human brains. *Human Molecular Genetics* 26:192–209.

Alaerts K, Nayar K, Kelly C, Raithel J, Milham MP, Martino AD (2015) Age-related changes in intrinsic function of the superior temporal sulcus in autism spectrum disorders. *SCAN* 10:1413–1423.

Alaerts K, Swinnen SP, Wenderoth N (2016) Sex differences in autism : a resting-state fMRI investigation of functional brain connectivity in males and females. *Social Cognitive and Affective Neuroscience* 11:1002–1016.

Alaerts K, Woolley DG, Steyaert J, Martino AD, Swinnen SP, Wenderoth N (2014) Underconnectivity of the superior temporal sulcus predicts emotion recognition deficits in autism. *SCAN* 9:1589–1600.

Alarcon M, Abrahams BS, Stone JL, Duvall JA, Perederiy JV, Bomar JM, Sebat J, Wigler M, Martin CL, Ledbetter DH, Nelson SF, Cantor RM, Geschwind DH (2008) Linkage, association, and gene-expression analyses identify CNTNAP2 as an autism-susceptibility gene. *American Journal of Human Genetics* 82:150.

Alpatov R, Lesch Bj, Nakamoto-Kinoshita M, Blanco A, Chen S, Stützer A, Armache Kj, Simon Md, Xu C, Ali M, Murn J, Prisic S, Kutateladze Tg, Vakoc Cr (2014) A Chromatin-Dependent Role of the Fragile X Mental Retardation Protein FMRP in the DNA Damage Response. *Cell* 157:869–881.

Anderson JS, Druzgal TJ, Froehlich A, Dubray MB, Lange N, Alexander AL (2011) Decreased Interhemispheric Functional Connectivity in Autism. *Cerebral Cortex* 21:1134–1146.

Anderson JS, Nielsen JA, Ferguson MA, Burback MC, Cox ET, Dai L, Gerig G, Korenberg JR (2013) Abnormal brain synchrony in Down Syndrome. *NeuroImage: Clinical* 2:703–715.

Anderson JS, Nielsen JA, Froehlich AL, Dubray MB, Druzgal TJ, Cariello AN, Cooperrider JR, Zielinski BA, Ravichandran C, Fletcher PT, Alexander AL (2011) Functional connectivity magnetic resonance imaging classification of autism. *Brain* 134:3742–3754.

Ango F, Prezeau L, Muller T, Tu JC, Xiao B, Worley P, PIn JP, Bockaert J, Fagni L (2001) Agonist-independent activation of metabotropic glutamate receptors by the intracellular protein Homer. *Nature* 411:962–965.

Asahi Y, Kubota K, Omichi S (2009) Dose requirements for propofol anaesthesia for dental treatment for autistic patients compared with intellectually impaired patients. *Anaesth Intensive Care* 37:70–73.

Aschrafi A, Cunningham BA, Edelman GM, Vanderklish PW (2005) The fragile X mental retardation protein and group I metabotropic glutamate receptors regulate levels of mRNA granules in brain. *Proceedings of the National Academy of Sciences of the United States of America* 102:2180.

Ash JA, Lu H, Taxier LR, Long JM, Yang Y, Stein EA, Rapp PR (2016) Functional connectivity with the retrosplenial cortex predicts cognitive aging in rats. *Proceedings of the National Academy of Sciences* 113:12286 LP – 12291.

Ashley CT, Wilkinson KD, Reines D, Warren ST (1993) FMR1 protein: conserved RNP family domains and selective RNA binding. *Science* 262:563 LP – 566.

Asiminas A, Jackson AD, Louros SR, Till SM, Spano T, Dando O, Bear MF, Chattarji S, Hardingham GE, Osterweil EK, Wyllie DJA, Wood ER, Kind PC (2019) Sustained correction of associative learning deficits after brief, early treatment in a rat model of Fragile X Syndrome. *Science translational medicine* 11:1–10.

Assaf M, Jagannathan K, Calhoun VD, Miller L, Stevens MC, Sahl R, Boyle JGO, Schultz RT, Pearlson GD (2010) Abnormal functional connectivity of default mode sub-networks in autism spectrum disorder patients. *NeuroImage* 53:247–256.

Attwell D, Laughlin SB (2001) An energy budget for signaling in the grey matter of the brain. *Journal of cerebral blood flow and metabolism : official journal of the International Society of Cerebral Blood Flow and Metabolism* 21:1133–1145.

Auerbach BD, Osterweil EK, Bear MF (2011) Mutations causing syndromic autism define an axis of synaptic pathophysiology. *Nature* 480:63–68.

Bagni C, Greenough WT (2005) From mRNP trafficking to spine dysmorphogenesis: the roots of fragile X syndrome. *Nature Reviews Neuroscience* 6:376.

Bailey Jr DB, Hatton DD, Skinner M (1998) Early Developmental Trajectories of Males With Fragile X Syndrome. *American Journal on Mental Retardation* 103:29–39.

Bajic D, Craig MM, Borsook D, Becerra L, Sullivan RM (2016) Probing Intrinsic Resting-State Networks in the Infant Rat Brain. *Frontiers in Behavioral Neuroscience* 10:1–13.

Baker KB, Wray SP, Ritter R, Mason S, Lanthorn TH, Savelieva KV (2010) Male and female Fmr1 knockout mice on C57 albino background exhibit spatial learning and memory impairments. *Genes, brain, and behavior* 9:562–574.

Bakker CE, Kooy RF, D'Hooge R, Tamanini F, Willemsen R, Nieuwenhuizen I, De Vries BBA, Reyniers E, Hoogeveen AT, Willems PJ, De Deyn PP, Oostra BA (2000) Introduction of a FMR1 transgene in the fragile X knockout mouse. *Neuroscience Research Communications* 26:265–277.

Bakker C, Verheij C, Willemsen R, van der Helm R, Oerlemans F, Vermey M, Bygrave a, Hoogeveen A, Reyniers E, De Boulle K, D'Hooge R, Cras P, van Velzen D, Nagels G, Martin J, De Deyn P, Darby J, Oostra B, Willems P (1994) Fmrl Knockout M ice : A Model to Study Fragile X Mental Retardation. *Cell* 78:23–33.

Balsters JH, Mantini D, Apps MAJ, Eickhoff SB, Wenderoth N (2016) Connectivity-based parcellation increases network detection sensitivity in resting state fMRI : An investigation into the cingulate cortex in autism. *Neuroimage Clin.* 11:494–507.

Baranek GT, Danko CD, Skinner ML, Jr DBB, Hatton DD, Roberts JE, Mirrett PL (2005) Video Analysis of Sensory-Motor Features in Infants with Fragile X Syndrome at 9 – 12 Months of Age. *Journal of autism and developmental disorders* 35:645–656.

Baranek GT, Roberts JE, David FJ, Sideris J, Penny L, Hatton DD, Bailey DB, Baranek GT, Roberts JE, David FJ, Sideris J, Penny L, Hatton DD, Bailey DB, Trajectories D, Roberts JE, David FJ, Mirrett PL, Hatton DD, Bailey DB (2008) Developmental Trajectories and Correlates of Sensory Processing in Young Boys with Fragile X Syndrome. *Physical & Occupational Therapy In Pediatrics* 28:79–98.

Barnes SA, Wijetunge LS, Jackson AD, Katsanevaki D, Osterweil EK, Komiyama NH, Grant SGN, Bear MF, Nagerl UV, Kind PC, Wyllie DJA (2015) Convergence of Hippocampal Pathophysiology in Syngap+/- and Fmr1-/y Mice. *Journal of Neuroscience* 35:15073–15081.

Barttfeld P, Wicker B, Cukier S, Navarta S, Lew S, Sigman M, Leiguarda R (2012) Neuropsychologia State-dependent changes of connectivity patterns and functional brain network topology in autism spectrum disorder. *Journal of Neuropsychologia* 50:3653–3662.

Bassell GJ, Warren ST (2008) Fragile X Syndrome: Loss of Local mRNA Regulation Alters Synaptic Development and Function. *Neuron* 60:201–214.

Baxter AJ, Brugha TS, Erskine HE, Scheurer RW, Vos T, Scott JG (2015) The epidemiology and global burden of autism spectrum disorders. *Psychological Medicine* 45:601–613.

Bear MF, Huber KM, Warren ST (2004) The mGluR theory of fragile X mental retardation. *Trends in Neurosciences* 27:370–377.

Becerra L, Pendse G, Chang Pc, Bishop J, Borsook D (2011) Robust Reproducible Resting State Networks in the Awake Rodent Brain. *PloS one* 6:1–10.

Beckmann CF, DeLuca M, Devlin JT, Smith SM (2005) Investigations into resting-state connectivity using independent component analysis. *Philosophical transactions of the Royal Society of London. Series B, Biological sciences* 360:1001–1013.

Behn D, Doke A, Racine J, Casanova C, Chemtob S (2003) Dark adaptation is faster in pigmented than albino rats. *Documenta Ophthalmologica* 106:153–159.

Belliveau AJW, Kennedy DN, Mckinstry RC, Buchbinder BR, Weisskoff RM, Cohen MS (1991) Functional mapping of the human visual cortex by magnetic resonance imaging. *Science* 254:716–719.

Bennett CM, Baird AA, Miller MB, Wolford GL (2009) Neural correlates of interspecies perspective taking in the post-mortem Atlantic Salmon : An argument for multiple comparisons correction. *15th Annual Meeting of the Organization for Human Brain Mapping. San Francisco, CA* .

Bernier R, Golzio C, Xiong B, Stessman HA, Coe BP, Penn O, Witherspoon K, Gerdts J, Baker C, Vulto-van Silfhout AT, Schuurs-Hoeijmakers JH, Fichera M, Bosco P, Buono S, Alberti A, Failla P, Peeters H, Steyaert J, Vissers LELM, Francescatto L, Mefford HC, Rosenfeld JA, Bakken T, O'Roak BJ, Pawlus M, Moon R, Shendure J, Amaral DG, Lein E, Rankin J, Romano C, de Vries BBA, Katsanis N, Eichler EE (2014) Disruptive CHD8 Mutations Define a Subtype of Autism Early in Development. *Cell* 158:263.

Berry-Kravis E, Hessl D, Coffey S, Hervey C, Schneider A, Yuhas J, Hutchison J, Snape M, Tranfaglia M, Nguyen DV, Hagerman R (2009) A pilot open label, single dose trial of fenobam in adults with fragile X syndrome. *Journal of Medical Genetics* 46:266.

Berry-Kravis E, Des Portes V, Hagerman R, Jacquemont S, Charles P, Visootsak J, Brinkman M, Rerat K, Koumaras B, Zhu L, Barth GM, Jaecklin T, Apostol G, von Raison F (2016) Mavoglurant in fragile X syndrome: Results of two randomized, double-blind, placebo-controlled trials. *Science translational medicine* 8:321ra5.

Berry-Kravis E, Hagerman R, Visootsak J, Budimirovic D, Kaufmann WE, Cherubini M, Zarevics P, Walton-Bowen K, Wang P, Bear MF, Carpenter RL (2017) Arbaclofen in fragile X syndrome: results of phase 3 trials. *Journal of neurodevelopmental disorders* 9:3.

Berry-kravis E, Levin R, Shah H, Mathur S, Darnell JC, Ouyang B (2014) Cholesterol Levels in Fragile X Syndrome. *American Journal of medical genetics* Part A:379–384.

Berry-kravis EM, Lindemann L, Jønch AE, Apostol G, Bear MF, Carpenter RL, Crawley JN, Curie A, Portes VD, Hossain F, Gasparini F, Gomez-mancilla B (2018) Drug development for neurodevelopmental disorders : lessons learned from fragile X syndrome. *Nature Publishing Group* 17:280–299.

Bertero A, Liska A, Pagani M, Parolisi R, Masferrer ME, Gritti M, Pedrazzoli M, Galbusera A, Sarica A, Cerasa A, Buffelli M, Tonini R, Buffo A, Gross C, Pasqualetti M, Gozzi A (2018) Autism-associated 16p11.2 microdeletion impairs prefrontal functional connectivity in mouse and human. *Brain* 141:1–11.

Bielajew C, Konkle ATM, Merali Z (2002) The effects of chronic mild stress on male Sprague-Dawley and Long Evans rats I. Biochemical and physiological analyses. *Behavioural Brain Research* 136:583–592.

Biswal B, Yetkin FZ, Haughton VM, Hyde J (1995) Functional Connectivity in the Motor Cortex of Resting Human Brain Using Echo-Planar MRI. *MRM* 34:537–541.

Biswal BB, Mennes M, Zuo Xn, Gohel S, Kelly C, Smith SM, Beckmann CF, Adelstein JS, Buckner RL, Colcombe S, Dogonowski Am, Ernst M, Fair D, Hampson M,

Hoptman MJ, Hyde JS, Kiviniemi VJ, Kötter R, Li Sj, Lin Cp, Lowe MJ, Mackay C, Madden DJ, Madsen KH, Margulies DS, Mayberg HS, Mcmahon K, Monk CS, Mostofsky SH, Nagel BJ, Pekar JJ, Peltier SJ, Petersen SE, Riedl V, Rombouts SARB, Rypma B, Schlaggar BL, Schmidt S, Seidler RD, Siegle GJ, Sorg C, Teng Gj, Veijola J, Villringer A, Walter M, Wang L, Weng Xc, Whit S, Williamson P, Windischberger C, Zang Yf, Zhang Hy, Castellanos FX, Milham MP (2010) Toward discovery science of human brain function. *PNAS* 107:4734–4739.

Biswal BB, Van Kylen J, Hyde JS (1997) Simultaneous Assessment of Flow and BOLD Signals in Resting-State Functional Connectivity Maps. *NMR in biomedicine* 10:165–170.

Blakemore Sj, Burnett S, Dahl RE (2010) The Role of Puberty in the Developing Adolescent Brain. *Human brain mapping* 31:926–933.

Blamire A (2008) The technology of MRI — the next 10 years ? *The British Journal of Radiology* 81:601–617.

Bolduc FV, Bell K, Cox H, Broadie KS, Tully T (2008) Excess protein synthesis in Drosophila Fragile X mutants impairs long-term memory. *Nature Neuroscience* 11:1143.

Bontekoe CJ, de Graaff E, Nieuwenhuizen IM, Willemsen R, Oostra BA (1997) FMR1 Premutation Allele (CGG)(81) Is Stable in Mice. *European Journal of Human Genetics* 5:293–298.

Booker SA, Simões de Oliveira L, Anstey NJ, Kozic Z, Dando OR, Jackson AD, Baxter PS, Isom LL, Sherman DL, Hardingham GE, Brophy PJ, Wyllie DJ, Kind PC (2020) Input-Output Relationship of CA1 Pyramidal Neurons Reveals Intact Homeostatic Mechanisms in a Mouse Model of Fragile X Syndrome. *Cell Reports* 32.

Borghi JA, Van Gulick AE (2018) Data management and sharing in neuroimaging : Practices and perceptions of MRI researchers. *PLoS ONE* 13:1–18.

Bos DJ, Raalten TRV, Oranje B, Smits AR, Kobussen NA, Belle JV, Rombouts SARB, Durston S (2014) Developmental differences in higher-order resting-state networks in Autism Spectrum Disorder. *Neuroimage Clin.* 4:820–827.

Brookes MJ, Woolrich M, Luckhoo H, Price D, Hale JR, Stephenson MC, Barnes GR, Smith SM, Morris PG (2011) Investigating the electrophysiological basis of resting state networks using magnetoencephalography. *PNAS* 108:16783–8.

Bruno JL, Hosseini SMH, Saggar M, Quintin Em, Raman MM, Reiss AL (2017) Altered Brain Network Segregation in Fragile X Syndrome Revealed by Structural Connectomics. *Cerebral cortex* 27:2249–2259.

Brydges NM, Whalley HC, Jansen MA, Merrifield GD, Wood ER, Lawrie SM, Wynne Sm, Day M, Fleetwood-Walker S, Steele D, Marshall I, Hall J, Holmes MC (2013) Imaging Conditioned Fear Circuitry Using Awake Rodent fMRI. *PLoS ONE* 8:e54197.

Buckner RL, Sepulcre J, Talukdar T, Krienen FM, Liu H, Hedden T, Andrews-hanna JR, Sperling RA, Johnson KA (2009) Cortical Hubs Revealed by Intrinsic Functional Connectivity : Mapping , Assessment of Stability , and Relation to Alzheimer's Disease. *The journal of Neuroscience* 29:1860–1873.

Buckner RL, Snyder AZ, Shannon BJ, Larossa G, Sachs R, Fotenos AF, Sheline YI, Klunk WE, Mathis CA, Morris JC, Mintun MA (2005) Molecular , Structural , and Functional Characterization of Alzheimer ' s Disease : Evidence for a Relationship between Default Activity , Amyloid , and Memory. *The journal of Neuroscience* 25:7709–7717.

Bukhari Q, Schroeter A, Cole DM, Rudin M (2017) Resting State fMRI in Mice Reveals Anesthesia Specific Signatures of Brain Functional Networks and Their Interactions. *Frontiers in Neural Circuits* 11:1–11.

Caku A, Pellerin D, Bouvier P, Riou E, Corbin F (2014) Effect of Lovastatin on Behavior in Children and Adults with Fragile X Syndrome : An Open-Label Study. *American Journal of medical genetics* Part A:2834–2842.

Campbell DB, Li C, Sutcliffe JS, Persico AM, Levitt P (2008) Genetic evidence implicating multiple genes in the MET receptor tyrosine kinase pathway in autism spectrum disorder. *Autism Research* 1:159–168.

Campbell DB, Warren D, Sutcliffe JS, Lee EB, Levitt P (2010) Association of MET with social and communication phenotypes in individuals with autism spectrum disorder. *American journal of medical genetics. Part B, Neuropsychiatric genetics : the official publication of the International Society of Psychiatric Genetics* 153B:438.

Cardinale F, Chinnici G, Bramerio M, Mai R, Sartori I, Cossu M, Lo Russo G, Castana L, Colombo N, Caborni C, De Momi E, Ferrigno G (2014) Validation of FreeSurfer-Estimated Brain Cortical Thickness: Comparison with Histologic Measurements. *Neuroinformatics* pp. 535–542.

Carla V, Moroni F (1992) General anaesthetics inhibit the responses induced by glutamate receptor agonists in the mouse cortex. *Neuroscience Letters* 146:21–24.

Carp J (2012) The secret lives of experiments : Methods reporting in the fMRI literature. *NeuroImage* 63:289–300.

Castellanos FX, Margulies DS, Kelly C, Uddin LQ, Ghaffari M, Kirsch A, Shaw D, Shehzad Z, Di Martino A, Biswal B, Sonuga-Barke EJ, Rotrosen J, Adler LA, Milham MP (2008) Cingulate-Precuneus Interactions: A New Locus of Dysfunction in Adult Attention-Deficit/Hyperactivity Disorder. *Biological Psychiatry* 63:332–337.

Cerliani L, Mennes M, Thomas RM, Martino AD, Thioux M, Keysers C (2017) Increased Functional Connectivity Between Subcortical and Cortical Resting-State Networks in Autism Spectrum Disorder. *JAMA Psychiatry* 72:767–777.

Chabernaud C, Mennes M, Kardel PG, Gaillard WD, Kalbfleisch ML, VanMeter JW, Packer RJ, Milham MP, Castellanos FX, Acosta MT (2012) Lovastatin regulates brain spontaneous low-frequency brain activity in Neurofibromatosis type 1. *Neuroscience Letters* 515:28–33.

Chabernaud C, Mennes M, Kardel PG, Gaillard WD, Kalbfleisch ML, VanMeter JW, Packer RJ, Milham MP, Castellanos FX, Acosta MT (2013) Lovastatin regulates brain spontaneous low-frequency brain activity in Neurofibromatosis type 1. *Neuroscience Letters* 515:28–33.

Chang S, Bray SM, Li Z, Zarnescu DC, He C, Jin P, Warren ST (2008) Identification of small molecules rescuing fragile X syndrome phenotypes in Drosophila. *Nature Chemical Biology* 4:256.

Chen B, Xu T, Zhou C, Wang L, Yang N, Wang Z (2015) Individual Variability and Test-Retest Reliability Revealed by Ten Repeated Resting-State Brain Scans over One Month. *PLOS ONE* 10:1–21.

Chen JE, Glover GH (2015) Functional Magnetic Resonance Imaging Methods. *Neuropsychology Review* 25:289–313.

Cheng W, Rolls ET, Gu H, Zhang J, Feng J (2015) Autism : reduced connectivity between cortical areas involved in face expression , theory of mind , and the sense of self. *Brain* 138:1382–1393.

Cherkassky VL, Kana RK, Keller TA, Just MA (2006) Functional connectivity in a baseline resting-state network in autism. *NeuroReport* 17:1687–1690.

Choe AS, Jones CK, Joel SE, Muschelli J, Belegu V, Caffo BS, Lindquist MA, van Zijl PCM, Pekar JJ (2015) Reproducibility and Temporal Structure in Weekly Resting-State fMRI over a Period of 3.5 Years. *PloS one* 10:e0140134.

Chou YH, Panych LP, Dickey CC, Petrella JR, Chen NK (2012) Investigation of long-term reproducibility of intrinsic connectivity network mapping: A resting-state fMRI study. *American Journal of Neuroradiology* 33:833–838.

Chuang SC, Zhao W, Bauchwitz R, Yan Q, Bianchi R, Wong RKS (2005) Prolonged epileptiform discharges induced by altered group I metabotropic glutamate receptor-mediated synaptic responses in hippocampal slices of a fragile X mouse model. *The Journal of neuroscience : the official journal of the Society for Neuroscience* 25:8048.

Clauss SB, Holmes KW, Hopkins P, Stein E, Cho M, Tate A, Johnson-Levones AO, Kwiterovich PO (2005) Efficacy and Safety of Lovastatin Therapy in Adolescent Girls With Heterozygous Familial Hypercholesterolemia. *Pediatrics* 116:682–688.

Coffee B, Zhang F, Warren ST, Reines D (1999) Acetylated histones are associated with FMR1 in normal but not fragile X-syndrome cells. *Nature genetics* 22:98.

Collins C (2016) *Electromagnetics in magnetic resonance imaging: Physical principles, related applications, and ongoing developments* IOP Publishing Ltd.

Cordes D, Haughton VM, Arfanakis K, Carew JD, Turski PA, Moritz CH, Quigley MA, Meyerand ME (2001) Frequencies Contributing to Functional Connectivity in the Cerebral Cortex in " Resting-state " Data. *AJNR* 22:1326–1333.

Cornish K, Turk J, Hagerman R (2008) The fragile X continuum : new advances and perspectives. *Journal of Intellectual Disability Research* 52:469–482.

Corradi A, Fadda M, Piton A, Patry L, Marte A, Rossi P, Cadieux-Dion M, Gauthier J, Lapointe L, Mottron L, Valtorta F, Rouleau GA, Fassio A, Benfenati F, Cossette P (2014) SYN2 is an autism predisposing gene: loss-of-function mutations alter synaptic vesicle cycling and axon outgrowth. *Human Molecular Genetics* 23:90–103.

Crossley NA, Mechelli A, Vértes PE, Toby T, Patel AX, Ginestet CE, Crossley NA, Mechelli A, Vértes PE, Winton-brown TT, Patel AX, Ginestet CE (2013) Cognitive relevance of the community structure of the human brain functional coactivation network. *PNAS* 110:11583–8.

Curia G, Papouin T, Seguela P, Avoli M (2009) Downregulation of Tonic GABAergic Inhibition in a Mouse Model of Fragile X Syndrome. *Cerebral Cortex* 19:1515–1520.

Currie S, Hoggard N, Craven IJ, Hadjivassiliou M, Wilkinson ID (2013) Understanding MRI : basic MR physics for physicians. *Postgrad Med J* 89:209–223.

Dahlhaus R (2018) Of men and mice: modeling the fragile X syndrome. *Frontiers in Molecular Neuroscience* 11.

Dajani DR, Uddin LQ (2015) Local Brain Connectivity Across Development in Autism Spectrum Disorder : A Cross-Sectional Investigation. *Autism Research* 00:1–12.

Dale BM, Brown MA, Semelka RC (2015) *MRI : basic principles and applications* Chichester, West Sussex, Chichester, West Sussex, fifth edit edition.

Damarla SR, Keller TA, Kana RK, Cherkassky VL (2010) Cortical underconnectivity coupled with preserved visuospatial cognition in autism: Evidence from an fMRI study of an embedded figures task. *Autism Research* 3:273–279.

Damoiseaux JS, Rombouts SARB, Barkhof F, Scheltens P, Stam CJ, Smith SM, Beckmann CF (2006) Consistent resting-state networks across healthy subjects. *PNAS* 103:13848–13853.

Daniel L. Schacter, Donna Rose Addis (2007) Constructive memory: The ghosts of past and future. *Nature* 445:27.

Darnell Jc, Van driesche Sj, Zhang C, ying sharon Hung K, Mele A, Fraser Ce, Stone Ef, Chen C, Fak Jj, wook Chi S, Licatalosi Dd (2011) FMRP Stalls Ribosomal Translocation on mRNAs Linked to Synaptic Function and Autism. *Cell* 146:247–261.

de Vries BB, Wiegers AM, Smits AP, Mohkamsing S, Duivenvoorden HJ, Fryns JP, Curfs LM, Halley DJ, Oostra BA, van Den Ouweland AM, Niermeijer MF (1996) Mental status of females with an FMR1 gene full mutation. *American journal of human genetics* 58:1025.

de Vrij FMS, Levenga J, van der Linde HC, Koekkoek SK, De Zeeuw CI, Nelson DL, Oostra BA, Willemsen R (2008) Rescue of behavioral phenotype and neuronal protrusion morphology in Fmr1 KO mice. *Neurobiology of Disease* 31:127–132.

Dedovic K, Aguiar CD, Pruessner JC (2009) What Stress Does to Your Brain : A Review of Neuroimaging Studies. *La Revue canadienne de psychiatrie* 54:6–15.

Delmonte S, Gallagher L, Hanlon EO, Mcgrath J, Balsters JH (2013) Functional and structural connectivity of frontostriatal circuitry in Autism Spectrum Disorder. *Frontiers in Human Neuroscience* 7:1–14.

Delora A, Gonzales A, Medina CS, Mitchell A, Faheem A, Jacobs RE, Bearer EL (2016) A simple rapid process for semi-automated brain extraction from magnetic resonance images of the whole mouse head. *Journal of Neuroscience Methods* 257:185–193.

den Broeder MJ, van der Linde H, Brouwer JR, Oostra BA, Willemsen R, Ketting RF (2009) Generation and Characterization of Fmr1 Knockout Zebrafish (Fmr1 Mutant Zebrafish). *PLoS ONE* 4:e7910.

Dennis EL, Thompson PM (2013) Mapping connectivity in the developing brain. *International Journal of Developmental Neuroscience* 31:525–542.

Detre JA, Leigh JS, Williams DS, Koretsky AP (1992) Perfusion Imaging. *Magnetic Resonance in Medecine* 23:37–45.

Di Martino A, Yan Cg, Li Q, Denio E, Castellanos FX, Alaerts K, Anderson JS, Assaf M, Bookheimer SY, Sunaert S, Thioux M (2014) The autism brain imaging data exchange : towards a large-scale evaluation of the intrinsic brain architecture in autism. *Molecular Psychiatry* 19:659–667.

Di Martino A, Kelly C, Grzadzinski R, Zuo Xn, Mennes M, Mairena MA, Lord C, Castellanos FX, Milham MP (2010) Aberrant Striatal Functional Connectivity in Children with Autism. *Biological Psychiatry* 69:847–856.

Di Martino A, Zuo Xn, Kelly C, Grzadzinski R, Mennes M, Schvarcz A, Rodman J, Lord C, Castellanos FX, Milham MP (2013) Shared and Distinct Intrinsic Functional Network. *Biological Psychiatry* 74:623–632.

Didiot MC, Tian Z, Schaeffer C, Subramanian M, Mandel JL, Moine H (2008) G-quartet containing FMRP binding site in FMR1 mRNA is a potent exonic splicing enhancer. *Nucleic acids research* 36:4902–4912.

Dinstein I, Pierce K, Eyler L, Solso S, Malach R, Behrmann M (2011) Disrupted Neural Synchronization in Toddlers with Autism. *Neuron* 70:1218–1225.

Dodero L, Damiano M, Galbusera A, Bifone A, Tsaftsaris SA, Scattoni ML, Gozzi A (2013) Neuroimaging Evidence of Major Morpho-Anatomical and Functional Abnormalities in the BTBR T+TF/J Mouse Model of Autism. *PLOS ONE* 8:1–10.

Dölen G, Osterweil E, Rao BS, Smith GB, Auerbach BD, Chattarji S, Bear MF (2007) Correction of Fragile X Syndrome in Mice. *Neuron* 56:955–962.

Domanski APF, Booker SA, Wyllie DJA, Isaac JTR, Kind PC (2019) Cellular and synaptic phenotypes lead to disrupted information processing in Fmr1-KO mouse layer 4 barrel cortex. *Nature Communications* 10:4814.

Doria V, Beckmann CF, Arichi T, Merchant N, Groppo M, Turkheimer FE (2010) Emergence of resting state networks in the preterm human brain. *PNAS* 107:20015–20020.

Doyle-thomas KAR, Lee W, Foster NEV, Tryfon A, Ouimet T, Hyde KL, Evans AC, Lewis J, Zwaigenbaum L, Anagnostou E (2015) Atypical Functional Brain Connectivity during Rest in Autism Spectrum Disorders. *Ann Neurol* 77:866–876.

Drozd M, Bardoni B, Capovilla M (2018) Modeling Fragile X Syndrome in. *Frontiers in molecular neuroscience* 11:124.

Durand E, Moortele VD, Pachot-clouard M, Bihan DL (2001) Artifact Due to B0 Fluctuations in fMRI : Correction Using the k- Space Central Line. *Magnetic Resonance in Medecine* 201:198–201.

Eberhart DE, Malter HE, Feng Y, Warren ST (1996) The fragile X mental retardation protein is a ribonucleoprotein containing both nuclear localization and nuclear export signals. *Human molecular genetics* 5:1083.

Ebisch SJH, Gallese V, Willems RM, Mantini D, Groen WB, Romani GL, Buitelaar JK, Bekkering H (2011) Altered Intrinsic Functional Connectivity of Anterior and Posterior Insula Regions in High-Functioning Participants With Autism Spectrum Disorder. *Human brain mapping* 32:1013–1028.

Eilam-stock T, Xu P, Cao M, Gu X, Dam NTV, Anagnostou E, Kolevzon A, Soorya L, Park Y, Siller M, He Y, Hof PR, Fan J (2014) Abnormal autonomic and associated brain activities during rest in autism spectrum disorder. *Brain* 137:153–171.

El-Fishawy P, State MW (2011) The Genetics of Autism: Key Issues, Recent Findings and Clinical Implications. *Psychiatry Clin North Am.* 33:83–105.

Engineer CT, Centanni TM, Im KW, Rahebi KC, Buell EP, Kilgard MP (2014) Degraded speech sound processing in a rat model of fragile X syndrome. *Brain Research* 1564:72–84.

Entezam A, Biacsi R, Orrison B, Saha T, Hoffman GE, Grabczyk E, Nussbaum RL, Usdin K (2007) Regional FMRP deficits and large repeat expansions into the full mutation range in a new Fragile X premutation mouse model. *Gene* 395:125–134.

Erickson C, Davenport M, Schaefer T, Wink L, Pedapati E, Sweeney J, Fitzpatrick S, Brown W, Budimirovic D, Hagerman R, Hessl D, Kaufmann W, Berry-Kravis E (2017) Fragile X targeted pharmacotherapy: lessons learned and future directions. *Journal Of Neurodevelopmental Disorders* 9:7.

Esbensen AJ, Greenberg JS, Seltzer MM, G AM (2009) A Longitudinal Investigation of Psychotropic and Non-Psychotropic Medication Use Among Adolescents and Adults with Autism Spectrum Disorders. *J Autism Dev Disor* 39:1339–1349.

Estes PS, O'shea M, Clasen S, Zarnescu DC (2008) Fragile X protein controls the efficacy of mRNA transport in Drosophila neurons. *Molecular and Cellular Neuroscience* 39:170–179.

Fair DA, Cohen AL, Dosenbach NUF, Church JA, Miezin FM, Barch DM, Raichle ME, Petersen SE, Schlaggar BL (2008) The maturing architecture of the brain ' s default network. *PNAS* 105:4028–4032.

Faraday MM (2002) Rat sex and strain differences in responses to stress. *Physiology & Behavior* 75:507–522.

Fassio A, Patry L, Congia S, Onofri F, Piton A, Gauthier J, Pozzi D, Messa M, Defranchi E, Fadda M, Corradi A, Baldelli P, Lapointe L, St-Onge J, Meloche C, Mottron L, Valtorta F, Khoa Nguyen D, Rouleau GA, Benfenati F, Cossette P (2011) SYN1 loss-of-function mutations in autism and partial epilepsy cause impaired synaptic function. *Human Molecular Genetics* 20:2297–2307.

Fatemi SH, Aldinger KA, Blaha CD, Blatt GJ, Chauhan A, Kemper TL, King BH, Martin LA, Millen KJ, Mittleman G, Sweeney JA, Webb SJ, Welsh JP (2012) Consensus Paper : Pathological Role of the Cerebellum in Autism. *Cerebellum* 11:777–807.

Feng Y, Gutekunst CA, Eberhart DE, Yi H, Warren ST, Hersch SM (1997) Fragile X mental retardation protein: nucleocytoplasmic shuttling and association with somatodendritic ribosomes. *The Journal of neuroscience : the official journal of the Society for Neuroscience* 17:1539.

Fishman I, Keown CL, Lincoln AJ, Pineda JA, Muller RA (2014) Atypical Cross Talk Between Mentalizing and Mirror Neuron Networks in Autism Spectrum Disorder. *JAMA Psychiatry* 71:751–760.

Fleming K, Riser D, Kumari D, Usdin K (2003) Instability of the fragile X syndrome repeat in mice: the effect of age, diet and mutations in genes that affect DNA replication, recombination and repair proficiency. *Cytogenetic and Genome Research* 100:140–146.

Fox MD, Raichle ME (2007) Spontaneous fluctuations in brain activity observed with functional magnetic resonance imaging. *Nature reviews. Neuroscience* 8:700–711.

Frank LR, Buxton RB, Wong EC (2001) Estimation of Respiration-Induced Noise Fluctuations From Undersampled Multislice fMRI Data. *Magnetic Resonance in Medecine* 644:635–644.

Fransson P, Skiold B, Horsch S, Nordell A, Blennow M, Lagercrantz H, Åden U (2007) Resting-state networks in the infant brain. *PNAS* 104:15531–15536.

Gantois I, Pop AS, de Esch CE, Buijsen RA, Pooters T, Gomez-Mancilla B, Gasparini F, Oostra BA, D'Hooge R, Willemsen R (2013) Chronic administration of AFQ056/Mavoglurant restores social behaviour in Fmr1 knockout mice. *Behavioural Brain Research* 239:72–79.

Gao YJ, Ji RR (2010) Light touch induces ERK activation in superficial dorsal horn neurons after inflammation: involvement of spinal astrocytes and JNK signaling in touch-evoked central sensitization and mechanical allodynia. *Journal of Neurochemistry* 115:505–514.

Garber KB, Visootsak J, Warren ST (2008) Fragile X syndrome. *Eur J Hum Genet.* 16:666–672.

Gholizadeh S, Kumar S, Hampson DR (2015) Expression of fragile X mental retardation protein in neurons and glia of the developing and adult mouse brain. *Brain Research* 1596:22–30.

Gibson JR, Bartley AF, Hays SA, Huber KM (2008) Imbalance of Neocortical Excitation and Inhibition and Altered UP States Reflect Network Hyperexcitability in the Mouse Model of Fragile X Syndrome. *Journal of neurophysiology* 100:2615–2626.

Giuffrida R, Musumeci S, Antoni SD, Bonaccorso CM, Giuffrida-stella AM, Oostra BA, Catania MV (2005) A Reduced Number of Metabotropic Glutamate Subtype 5 Receptors Are Associated with Constitutive Homer Proteins in a Mouse Model of Fragile X Syndrome. *The journal of Neuroscience* 25:8908–8916.

Glover GH (2011) Overview of functional magnetic resonance imaging. *Neurosurgery Clinics of North America* 22:133–139.

Gocel J, Larson J (2012) Synpatic NMDA Receptor-Mediated Currents in Anterior Piriform Cortex Are Reduced in the Adult Fragile X Mouse. *Neuroscience* 221:170–181.

Gogtay N, Thompson PM (2010) Mapping gray matter development : Implications for typical development and vulnerability to psychopathology. *Brain and Cognition* 72:6–15.

Goncalves JT, Anstey JE, Golshani P, Portera-Cailliau C (2013) Circuit level defects in the developing neocortex of fragile X mice. *Nature Neuroscience* 16:903–909.

Goswami S, Cavalier S, Sridhar V, Huber KM, Gibson JR (2019) Local cortical circuit correlates of altered EEG in the mouse model of Fragile X syndrome. *Neurobiology of Disease* 124:563–572.

Gotts SJ, Simmons WK, Milbury LA, Wallace GL, Cox RW, Martin A (2012) Fractionation of social brain circuits in autism spectrum disorders. *Brain* 135:2711–2725.

Grandjean J, Canella C, Anckaerts C, Ayranc G, Bougacha S, Bienert T, Buehlmann D, Coletta L, Garin M, Abhay N, Gallino D, Gass N, Hübner NS, Karatas M, Komaki Y, Kreitz S, Mandino F, Mechling AE, Sato C, Sauer K, Shah D, Strobelt S, Takata N, Wank I, Wu T, Yahata N, Yun L, Yee Y, Aoki I, Chakravarty MM, Chang Wt, Dhenain M, Elverfeldt DV, Harsan La, Hess A, Jiang T, Keliris GA, Lerch JP, Meyerlindenberg A, Okano H, Rudin M, Sartorius A, Linden AVD, Verhoye M, Weber-fahr W, Wenderoth N, Zerbi V, Gozzi A (2020) Common functional networks in the mouse brain revealed by multi-centre resting-state fMRI analysis. *NeuroImage* 205:1–11.

Grandjean J, Schroeter A, Batata I, Rudin M (2014) Optimization of anesthesia protocol for resting-state fMRI in mice based on differential effects of anesthetics on functional connectivity patterns. *NeuroImage* 102:838–847.

Green T, Barnea-goraly N, Raman M, Hall SS, Lightbody AA, Bruno JL, Quintin Em, Reiss AL (2015) Specific effect of the fragile-X mental retardation-1 gene (FMR1) on white matter microstructure. *The British Journal of Psychiatry* 207:143–148.

Greenough WT, Klintsova AY, Irwin SA, Galvez R, Bates KE, Weiler IJ (2002) Synaptic regulation of protein synthesis and the fragile X protein. *Proceedings of the National Academy of Sciences of the United States of America* 98:7101.

Greicius MD, Flores BH, Menon V, Glover GH, Solvason HB, Kenna H, Reiss AL, Schatzberg AF (2007) Resting-State Functional Connectivity in Major Depression: Abnormally Increased Contributions from Subgenual Cingulate Cortex and Thalamus. *Biological Psychiatry* 62:429–437.

Greicius MD, Krasnow B, Reiss AL, Menon V (2003) Functional connectivity in the resting brain : A network analysis of the default mode hypothesis. *PNAS* 100.

Greicius MD, Supekar K, Menon V, Dougherty RF (2009) Resting-state functional connectivity reflects structural connectivity in the default mode network. *Cerebral cortex (New York, N.Y. : 1991)* 19:72–78.

Gronenschild EHBM, Habets P, Jacobs HIL, Mengelers R, Rozendaal N, Os JV, Marcelis M (2012) The Effects of FreeSurfer Version , Workstation Type , and Macintosh Operating System Version on Anatomical Volume and Cortical Thickness Measurements. *PLoS ONE* 7:1–13.

Guo Q, Parlar M, Truong W, Hall G, Thabane L, Mckinnon M, Goeree R, Pullenayegum E (2014) The Reporting of Observational Clinical Functional Magnetic Resonance Imaging Studies : A Systematic Review. *PLoS ONE* 9:1–11.

Guo X, Chen H, Long Z, Duan X, Zhang Y, Chen H (2017) Atypical developmental trajectory of local spontaneous brain activity in autism spectrum disorder. *Scientific reports* 7:1–10.

Guo X, Duan X, Long Z, Chen H, Wang Y, Zheng J (2016) Decreased amygdala functional connectivity in adolescents with autism: A resting-state fMRI study. *Psychiatry Research: Neuroimaging* 257:47–56.

Hagerman PJ, Hagerman RJ (2007) Fragile X-associated tremor/ataxia syndrome—an older face of the fragile X gene. *Nature Clinical Practice Neurology* 3:107.

Hagerman RJ (1997) Fragile X syndrome. Molecular and clinical insights and treatment issues. *The Western journal of medicine* 166:129.

Hagerman RJ, Berry-Kravis E, Hazlett HC, Bailey DB, Moine H, Kooy RF, Tassone F, Gantois I, Sonenberg N, Mandel JL, Hagerman PJ (2017) Fragile X syndrome. *Nature reviews. Disease primers* 3:17065.

Hahamy A, Behrmann M, Malach R (2015) The idiosyncratic brain : distortion of spontaneous connectivity patterns in autism spectrum disorder. *Nature Neuroscience* 18:302–309.

Hall SS, Jiang H, Reiss AL, Greicius MD (2013) Identifying Large-Scale Brain Networks in Fragile X Syndrome. *JAMA Psychiatry* 70:1215–1223.

Hamilton SM, Green JR, Veeraragavan S, Yuva L, McCoy A, Wu Y, Warren J, Little L, Ji D, Cui X, Weinstein E, Paylor R (2014) Fmr1 and Nlgn3 knockout rats: novel tools for investigating autism spectrum disorders. *Behavioral neuroscience* 128:103–9.

Hansen BH, Oerbeck B, Skirbekk B, Petrovski BÉ, Kristensen H (2018) Neurodevelopmental disorders: prevalence and comorbidity in children referred to mental health services. *Nordic Journal of Psychiatry* 72:285–291.

Harker KT, Whishaw IQ (2002) Place and matching-to-place spatial learning affected by rat inbreeding (Dark-Agouti, Fischer 344) and albinism (Wistar, Sprague-Dawley) but not domestication (wild rat vs. Long-Evans, Fischer-Norway). *Behavioural Brain Research* 134:467–477.

Harlow EG, Till SM, Russell TA, Wijetunge LS, Kind P, Contractor A (2010) Critical Period Plasticity Is Disrupted in the Barrel Cortex of Fmr1 Knockout Mice. *Neuron* 65:385–398.

Harris AP, Lennen RJ, Marshall I, Jansen MA, Pernet CR, Brydges NM, Duguid IC, Holmes MC (2015) Imaging learned fear circuitry in awake mice using fMRI. *European Journal of Neuroscience* 42:2125–2134.

Hatton DD, Wheeler A, Sideris J, Sullivan K, Reichardt A, Roberts J, Clark R, Bailey Jr DB (2009) Developmental Trajectories of Young Girls With Fragile X Syndrome. *American Association on Intellectual and Developmental Disabilities* 114:161–171.

Hazlett HC, Poe MD, Lightbody AA, Gerig G, Macfall JR, Ross AK, Provenzale J, Martin A, Reiss AL, Piven J (2009) Teasing apart the heterogeneity of autism : Same behavior , different brains in toddlers with fragile X syndrome and autism. *J Neurodevelop Disord* 1:81–90.

He Y, Wang J, Wang L, Chen ZJ, Yan C, Yang H, Tang H, Zhu C, Gong Q, Zang Y, Evans AC (2009) Uncovering intrinsic modular organization of spontaneous brain activity in humans. *PLoS ONE* 4:23–25.

Hildebrandt IJ, Su H, Weber WA (2008) Anesthesia and other considerations for in vivo imaging of small animals. *ILAR journal* 49:17–26.

Hoeft F, Lightbody AA, Hazlett HC, Patnaik S, Piven J, Reiss AL (2008) Morphometric Spatial Patterns Differentiating Boys With Fragile X Syndrome, Typically Developing Boys, and Developmentally Delayed Boys Aged 1 to 3 Years. *Arch Gen Psychiatry* 65:1087–1097.

Honey CJ, Sporns O, Cammoun L, Gigandet X, Thiran JP, Meuli R, Hagmann P (2009) Predicting human resting-state functional connectivity from structural connectivity. *PNAS* 106:1–6.

Honey CJ, Breakspear M, Sporns O, Ko R (2007) Network structure of cerebral cortex shapes functional connectivity on multiple time scales. *PNAS* 104:10240–10245.

Horovitz SG, Fukunaga M, Zwart JAD, Gelderen PV, Fulton SC, Balkin TJ, Duyn JH (2008) Low Frequency BOLD Fluctuations During Resting Wakefulness and Light Sleep : A Simultaneous EEG-fMRI Study. *Human brain mapping* 29:671–682.

Huber KM, Gallagher SM, Warren ST, Bear MF (2002) Altered synaptic plasticity in a mouse model of fragile X mental retardation. *PNAS* 59:7746–7750.

Huijbers W, Schultz AP, Vannini P, McLaren DG, Wigman SE, Ward AM, Hedden T, Sperling RA (2013) The Encoding/Retrieval Flip: Interactions between Memory Performance and Memory Stage and Relationship to Intrinsic Cortical Networks. *Journal of cognitive neuroscience* 25:1163–1179.

Hull JV, Jacokes ZJ, Torgerson CM, Irimia A, Van Horn JD, Aylward E, Bernier R, Bookheimer S, Dapretto M, Gaab N, Geschwind D, Jack A, Nelson C, Pelphrey K, State M, Ventola P, Webb SJ (2017) Resting-state functional connectivity in autism spectrum disorders: A review. *Frontiers in Psychiatry* 7.

Hull L, Petrides KV, Mandy W (2020) The Female Autism Phenotype and Camouflaging: a Narrative Review. *Review Journal for Autism and Developmental Disorders* .

Hutton C, Bork A, Josphes O, Deichmann R, Ashburner J, Turner R (2002) Image Distortion Correction in fMRI : A Quantitative Evaluation. *NeuroImage* 16:217–240.

Iannaccone PM, Jacob HJ (2009) Rats ! *Disease Models & Mechanisms* 210:206–210.

Iida T, Nakahori Y, Tsutsumi O, Taketani Y, Nakagome Y (1994) The CpG island of the FMR-1 gene is methylated differently among embryonic tissues: implication for prenatal diagnosis. *Human reproduction (Oxford, England)* 9:1471.

Iidaka T (2014) ScienceDirect Resting state functional magnetic resonance imaging and neural network classified autism and control. *CORTEX* 63:55–67.

Itahashi T, Yamada T, Watanabe H, Nakamura M, Jimbo D (2014) Altered Network Topologies and Hub Organization in Adults with Autism : A Resting-State fMRI Study. *PLOS ONE* 9:1–15.

Itahashi T, Yamada T, Watanabe H, Nakamura M, Ohta H, Kanai C, Iwanami A, Kato N, Hashimoto Ri (2015) Alterations of local spontaneous brain activity and connectivity in adults with high-functioning autism spectrum disorder. *Molecular Autism* 6:1–14.

Jackson A (2017) Cellular and synaptic pathophysiology in a rat model of Fragile X syndrome Ph.D. diss., The University of Edinburgh.

Jacquemont S, Curie A, Des Portes V, Torrioli M, Berry-Kravis E, Hagerman R, Ramos F, Cornish K, He Y, Paulding C, Neri G, Chen F, Hadjikhani N, Martinet D, Meyer J, Beckmann J, Delange K, Brun A, Bussy G, Gasparini F, Hilse T, Floesser A, Branson J, Bilbe G, Johns D, Gomez-Mancilla B (2011) Epigenetic Modification of the FMR1 Gene in Fragile X Syndrome Is Associated with Differential Response to the mGluR5 Antagonist AFQ056. *Science Translational Medicine* 3:64ra1.

Jonckers E, Audekerke JV, Visscher GD, Linden AVD (2011) Functional Connectivity fMRI of the Rodent Brain : Comparison of Functional Connectivity Networks in Rat and Mouse. *PloS one* 6:1–9.

Jones RM, Carberry C, Hamo A, Lord C (2017) Placebo-like response in absence of treatment in children with Autism. *Autism Research* 10:1567–1572.

Jones TB, Bandettini PA, Kenworthy L, Case LK, Milleville SC, Martin A, Birn RM (2010) Sources of group differences in functional connectivity : An investigation applied to autism spectrum disorder. *NeuroImage* 49:401–414.

Jung M, Kosaka H, Saito DN, Ishitobi M, Morita T, Inohara K, Asano M, Arai S, Munesue T, Tomoda A, Wada Y, Sadato N, Okazawa H, Iidaka T (2014) Default mode network in young male adults with autism spectrum disorder : relationship with autism spectrum traits. *Mol Autism* 5:1–11.

Jung Tp, Makeig S, Mckeown MJ, Bell AJ, Lee Tw, Sejnowski TJ (2001) Imaging Brain Dynamics Using Independent Component Analysis. *Proceedings of the IEEE* 89:1007–1122.

Just MA, Cherkassky VL, Keller TA, Minshew NJ (2004) Cortical activation and synchronization during sentence comprehension in high-functioning autism : evidence of underconnectivity. *Brain* 127:1811–1821.

Kaufman L, Ayub M, Vincent JB (2010) The genetic basis of non-syndromic intellectual disability : a review. *J Neurodevelop Disord* 2:182–209.

Kaufmann WE, Abrams MT, Chen W, Reiss AL (1999) Genotype, molecular phenotype, and cognitive phenotype: Correlations in fragile X syndrome. *American Journal of Medical Genetics* 83:286–295.

Kaufmann WE, Kidd SA, Andrews HF, Budimirovic DB, Esler A, Haas-Givler B, Stackhouse T, Riley C, Peacock G, Sherman SL, Brown WT, Berry-Kravis E (2017) Autism Spectrum Disorder in Fragile X Syndrome: Cooccurring Conditions and Current Treatment. *Pediatrics* 139:S194.

Kelley WM, Macrae CN, Wyland CL, Caglar S, Inati S, Heatherton TF (2002) Finding the Self? An Event-Related fMRI Study. *Journal of Cognitive Neuroscience* 14:785–794.

Kennedy DP, Courchesne E (2008a) Functional abnormalities of the default network during self- and other-reflection in autism. *Soc Cogn Affect Neurosci* 3:177–190.

Kennedy DP, Courchesne E (2008b) Functional abnormalities of the default network during self- and other-reflection in autism. *Soc Cogn Affect Neurosci* 3:177–190.

Kennedy DP, Courchesne E (2008c) The intrinsic functional organization of the brain is altered in autism. *NeuroImage* 39:1877–1885.

Kennedy DP, Redcay E, Courchesne E (2006) Failing to deactivate : Resting functional abnormalities in autism. *PNAS* 103:8275–8280.

Keown CL, Shih P, Nair A, Peterson N, Mulvey ME (2013) Local Functional Overconnectivity in Posterior Brain Regions Is Associated with Symptom Severity in Autism Spectrum Disorders. *Cell Reports* 5:567–572.

Khan AJ, Nair A, Keown CL, Datko MC, Lincoln AJ, Müller Ra (2015) Archival Report Connectivity in Children and Adolescents with Autism Spectrum Disorder. *Biological Psychiatry* 78:625–634.

Khandjian EW, Huot ME, Tremblay S, Davidovic L, Mazroui R, Bardoni B (2004) Biochemical evidence for the association of fragile X mental retardation protein with brain polyribosomal ribonucleoparticles. *Proceedings of the National Academy of Sciences of the United States of America* 101:13357.

Kim SH, Markham JA, Weiler IJ, Greenough WT (2008) Aberrant early-phase ERK inactivation impedes neuronal function in fragile X syndrome. *PNAS* 105:4429–4434.

Koch MA, Norris DG, Hund-Georgiadis M (2002) An investigation of functional and anatomical connectivity using magnetic resonance imaging. *NeuroImage* 16:241–250.

Konishi M, McLaren DG, Engen H, Smallwood J (2015) Shaped by the past: The default mode network supports cognition that is independent of immediate perceptual input. *PLoS ONE* 10:1–18.

Koslow SH (2000) Should the neuroscience community make a paradigm shift to sharing primary data ? *Nature Neuroscience* 3:863–865.

Kramvis I, Mansvelder HD, Loos M, Meredith R (2013) Hyperactivity , perseveration and increased responding during attentional rule acquisition in the Fragile X mouse model. *Frontiers in Behavioral Neuroscience* 7:1–13.

Krueger DD, Osterweil EK, Chen SP, Tye LD, Bear MF (2011) Cognitive dysfunction and prefrontal synaptic abnormalities in a mouse model of fragile X syndrome. *PNAS* 108:2587–2592.

Krzywinski M, Schein J, Birol I, Connors J, Gascoyne R, Jones SJ, Marra MA (2009) Circos : an Information Aesthetic for Comparative Genomics. *Genome Res* 19:1639–1645.

Kyathanahally SP, Jia H, Pustovyy OM, Waggoner P (2015) Anterior – posterior dissociation of the default mode network in dogs. *Brain Struct Funct* 220:1063–1076.

La Fata G, Gärtner A, Domínguez-iturza N, Dresselaers T, Dawitz J, Poorthuis RB, Averna M, Himmelreich U, Meredith RM, Achsel T, Dotti CG, Bagni C (2014) FMRP regulates multipolar to bipolar transition affecting neuronal migration and cortical circuitry. *Nature Neuroscience* 17:1693–1700.

Lai Mc, Lombardo MV, Baron-Cohen S (2014) Autism. *The Lancet* 383:896–910.

Lai Mc, Lombardo MV, Chakrabarti B, Sadek SA, Pasco G, Wheelwright SJ, Bullmore ET, Baron-cohen S, Consortium MRCA (2010) A Shift to Randomness of Brain Oscillations in People with Autism. *Biological Psychiatry* 68:1092–1099.

Lakhan R, Kalita J, Misra UK, Kumari R, Mittal B (2010) Association of intronic polymorphism rs3773364 A>G in synapsin-2 gene with idiopathic epilepsy. *Synapse* 64:403–408.

Lambert M, Lupien PJ, Gagne C, Levy E, Blaichman S, Langlois S (1996) Treatment of familial hypercholesterolemia in children and adolescents : effect of lovastatin. *Pediatrics* 97.

Larson-prior LJ, Zempel JM, Nolan TS, Prior FW, Snyder AZ, Raichle ME (2009) Cortical network functional connectivity in the descent to sleep. *PNAS* 106:4489–4494.

Laufs H, Krakow K, Sterzer P, Eger E, Beyerle A, Kleinschmidt A (2003) Electroencephalographic signatures of attentional and cognitive default modes in spontaneous brain activity fluctuations at rest. *PNAS* 100.

Laumann TO, Gordon EM, Adeyemo B, Jeanette A, Poldrack RA, Petersen E, Laumann TO, Gordon EM, Adeyemo B, Snyder AZ, Joo SJ, Chen My (2015) Functional System and Areal Organization of a Highly Sampled Individual Human Brain. *Neuron* 87:657–670.

Lavedan CN, Garrett L, Nussbaum RL (1997) Trinucleotide repeats (CGG) 22 TGG(CGG) 43 TGG(CGG) 21 from the fragile X gene remain stable in transgenic mice. *Human Genetics* 100:407–414.

Lee JM, Kyeong S, Kim E, Cheon Ka (2016) Abnormalities of Inter- and Intra-Hemispheric Functional Connectivity in Autism Spectrum Disorders : A Study Using the Autism Brain Imaging Data Exchange Database. *Front. Neurosci.* 10:191:1–11.

Lee Wiggins J, Peltier SJ, Ashinoff S, Weng Sj, Carrasco M, Welsh RC, Lord C, Monk CS (2010) Using a self-organizing map algorithm to detect age-related changes in functional connectivity during rest in autism spectrum disorders. *Brain Research* 1380:187–197.

Lee Wiggins J, Peltier SJ, Bedoyan JK, Carrasco M, Welsh RC, Martin DM, Lord C, Monk CS (2013) The impact of serotonin transporter genotype on default network connectivity in children and adolescents with autism spectrum disorders. *Neuroimage Clin.* 2:17–24.

Leonard H, Wen X (2002) The epidemiology of mental retardation: Challenges and opportunities in the new millennium. *Mental Retardation and Developmental Disabilities Research Reviews* 8:117–134.

Leopold DA, Murayama Y, Logothetis NK (2003) Very slow activity fluctuations in monkey visual cortex: Implications for functional brain imaging. *Cerebral Cortex* 13:422–433.

Leyfer OT, Folstein SE, Bacalman S, Davis NO, Dinh E, Morgan J, Tager-Flusberg H, Lainhart JE (2006) Comorbid Psychiatric Disorders in Children with Autism: Interview Development and Rates of Disorders. *Journal of Autism and Developmental Disorders* 36:849–861.

Li C, Schaefer M, Gray C, Yang Y, Furmanski O, Worley P, Mintz CD, Tao F, Johns RA (2017) Sensitivity to isoflurane anesthesia increases in autism spectrum disorder Shank3+/Δc mutant mouse model. *Neurotoxicol Teratol.* 60:69–74.

Li W, Qin W, Liu H, Fan L, Wang J, Jiang T, Yu C (2013) Subregions of the human superior frontal gyrus and their connections. *NeuroImage* 78:46–58.

Li W, Cui Y, Kushner Sa, Brown RaM, Jentsch JD, Frankland PW, Cannon TD, Silva AJ (2005) The HMG-CoA reductase inhibitor lovastatin reverses the learning and attention deficits in a mouse model of Neurofibromatosis Type 1. *Current Biology* 15:1961–1967.

Liang M, Zhou Y, Jiang T, Liu Z, Tian L, Liu H, Hao Y (2006) Widespread functional disconnectivity in schizophrenia with resting-state functional magnetic resonance imaging. *NeuroReport* 17:209–213.

Liang Z, King J, Zhang N (2011) Uncovering Intrinsic Connectional Architecture of Functional Networks in Awake Rat Brain. *The Journal of Neuropsychiatry and Clinical Neurosciences* 31:3776–3783.

Liang Z, King J, Zhang N (2012) Anticorrelated resting-state functional connectivity in awake rat brain. *NeuroImage* 59:1190–1199.

Limperopoulos C, Chilingaryan G, Sullivan N, Guizard N, Robertson RL, Plessis AJ (2014) Injury to the Premature Cerebellum : Outcome is Related to Remote Cortical Development. *Cerebral Cortex* 24:728–736.

Liska A, Bertero A, Gomolka R, Sabbioni M, Galbusera A, Barsotti N, Panzeri S, Scattoni ML, Pasqualetti M, Gozzi A (2018) Homozygous Loss of Autism-Risk Gene CNTNAP2 Results in Reduced Local and Long-Range Prefrontal Functional Connectivity. *Cerebral cortex* 28:1141–1153.

Liu X, Yi XhZ, Chen W (2013) The Change of Functional Connectivity Specificity in Rats Under Various Anesthesia Levels and its Neural Origin. *Brain Topogr* 26:363–377.

Loesch DZ, Huggins RM, Hagerman RJ (2004) Phenotypic variation and FMRP levels in fragile X. *Mental Retardation and Developmental Disabilities Research Reviews* 10:31–41.

Long Z, Duan X, Mantini D, Chen H (2016) Alteration of functional connectivity in autism spectrum disorder : effect of age and anatomical distance. *Scientific reports* 6:1–8.

Lowe MJ, Phillips MD, Lurito JT, Mattson D, Dzemidzic M, Mathews VP (2002) Multiple sclerosis: low-frequency temporal blood oxygen level-dependent fluctuations indicate reduced functional connectivity initial results. *Radiology* 224:184.

Lu H, Zou Q, Gu H, Raichle ME, Stein EA, Yang Y (2012) Rat brains also have a default mode network. *PNAS* 109:3979–3984.

Lu R, Wang H, Liang Z, Ku L, Donnell WTO, Li W, Warren ST, Feng Y (2004) The fragile X protein controls microtubule-associated protein 1B translation and microtubule stability in brain neuron development. *PNAS* 101:15201–15206.

Ludwig AL, Espinal GM, Pretto DI, Jamal AL, Arque G, Tassone F, Berman RF, Hagerman PJ (2014) CNS expression of murine fragile X protein (FMRP) as a function of CGG-repeat size. *Human Molecular Genetics* 23:3228–3238.

Lund TE (2001) fcMRI — Mapping Functional Connectivity or Correlating Cardiac-Induced Noise ? *Magnetic Resonance in Medecine* 628:2650.

Lynch CJ, Uddin LQ, Supekar K, Khouzam A, Phillips J (2012) Default Mode Network in Childhood Autism : Relationship with Social Deficits. *Biological Psychiatry* 74:212–219.

Mantini D, Perrucci MG, Gratta CD, Romani GL, Corbetta M (2007) Electrophysiological signatures of resting state networks in the human brain. *PNAS* 104:13170–13175.

Marchitelli R, Minati L, Marizzoni M, Bosch B, Bernhard WM, Wiltfang J, Fiedler U, Roccatagliata L, Picco A, Nobili F, Blin O, Payoux P, Caulo M (2016) Test-Retest Reliability of the Default Mode Network in a Multi-Centric fMRI Study of Healthy Elderly : Effects of Data-Driven Physiological Noise Correction Techniques. *Human brain mapping* 2132:2114–2132.

Martin HGS, Lassalle O, Brown JT, Manzoni OJ (2016) Age-Dependent Long-Term Potentiation Deficits in the Prefrontal Cortex of the Fmr1 Knockout Mouse Model of Fragile X Syndrome. *Cerebral cortex (New York, N.Y. : 1991)* 26:2084–2092.

Masamoto K, Kanno I (2012) Anesthesia and the quantitative evaluation of neurovascular coupling. *Journal of Cerebral Blood Flow & Metabolism* 32:1233–1247.

Maximo JO, Keown CL, Nair A, Müller Ra (2013) Approaches to local connectivity in autism using resting state functional connectivity MRI. *Frontiers in Human Neuroscience* 7:1–13.

Mcbride SM, Choi CH, Wang Y, Liebelt D, Braunstein E, Ferreiro D, Sehgal A, Siwicki KK, Dockendorff TC, Nguyen HT, Mcdonald TV, Jongens TA (2005) Pharmacological Rescue of Synaptic Plasticity, Courtship Behavior, and Mushroom Body Defects in a Drosophila Model of Fragile X Syndrome. *Neuron* 45:753–764.

McCamphill PK, Stoppel LJ, Senter RK, Lewis MC, Heynen AJ, Stoppel DC, Sridhar V, Collins KA, Shi X, Pan JQ, Madison J, Cottrell JR, Huber KM, Scolnick EM, Holson EB, Wagner FF, Bear MF (2020) Selective inhibition of glycogen synthase kinase 3α corrects pathophysiology in a mouse model of fragile X syndrome. *Science Translational Medicine* 12:eaam8572.

Menon V, Leroux J, White CD, Reiss AL (2004) Frontostriatal deficits in fragile X syndrome : Relation to FMR1 gene expression. *PNAS* 101:3615–3620.

Meredith RM (2015) Sensitive and critical periods during neurotypical and aberrant neurodevelopment : A framework for neurodevelopmental disorders. *Neuroscience and Biobehavioral Reviews* 50:180–188.

Meredith RM, Dawitz J, Kramvis I (2012) Sensitive time-windows for susceptibility in neurodevelopmental disorders. *Trends in Neurosciences* 35:335–344.

Meredith RM, Holmgren CD, Weidum M, Burnashev N (2007) Increased Threshold for Spike-Timing-Dependent Plasticity Is Caused by Unreliable Calcium Signaling in Mice Lacking Fragile X Gene Fmr1. *Neuron* 54:627–638.

Meyerson BJ, Augustsson H, Berg M, Roman E (2006) The Concentric Square Field : A multivariate test arena for analysis of explorative strategies. *Behavioural Brain Research* 168:100–113.

Michalon A, Sidorov M, Ballard TM, Ozmen L, Spooren W, Wettstein JG, Jaeschke G, Bear MF, Lindemann L (2012) Chronic Pharmacological mGlu5 Inhibition Corrects Fragile X in Adult Mice. *Neuron* 74:49–56.

Michetti C, Caruso A, Pagani M, Sabbioni M, Medrihan L, David G, Galbusera A, Morini M, Gozzi A, Benfenati F, Scattoni ML, Neuroscience S, Italiano I (2017) The Knockout of Synapsin II in Mice Impairs Social Behavior and Functional Connectivity Generating an ASD-like Phenotype. *Cerebral cortex* 27:5014–5023.

Min WW, Yuskaitis CJ, Yan Q, Sikorski C, Chen S, Jope RS, Bauchwitz RP (2009) Elevated glycogen synthase kinase-3 activity in Fragile X mice: Key metabolic regulator with evidence for treatment potential. *Neuropharmacology* 56:463–472.

Mines MA, Yuskaitis CJ, King MK, Beurel E, Jope RS (2010) GSK3 Influences Social Preference and Anxiety-Related Behaviors during Social Interaction in a Mouse Model of Fragile X Syndrome and Autism. *PLOS ONE* 5:e9706.

Mitchell JP, Banaji MR, Macrae CN (2005) The link between social cognition and self-referential thought in the medial prefrontal cortex. *Journal of Cognitive Neuroscience* 17:1306–1315.

Monk CS, Peltier SJ, Lee J, Weng Sj, Carrasco M, Risi S, Lord C (2009) Abnormalities of intrinsic functional connectivity in autism spectrum disorders. *NeuroImage* 47:764–772.

Muly EC, Maddox M, Smith Y (2003) Distribution of mGluR1a and mGluR5 Immunolabeling in Primate Prefrontal Cortex. *The journal of comparative neurology* 467:521–535.

Murdaugh DL, Maximo JO, Kana RK (2015) Changes in Intrinsic Connectivity of the Brain ' s Reading Network following Intervention in Children With Autism. *Human brain mapping* 36:2965–2979.

Murdaugh DL, Shinkareva SV, Deshpande HR, Wang J, Pennick MR, Kana RK (2012) Differential Deactivation during Mentalizing and Classification of Autism Based on Default Mode Network Connectivity. *PLoS ONE* 7:1–11.

Murray ML, Hsia Y, Glaser K (2014) Pharmacological treatments prescribed to people with autism spectrum disorder (ASD) in primary health care. *Psychopharmacology* 231:1011–1021.

Nair A, Carper RA, Abbott AE, Chen CP, Solders S, Nakutin S, Datko MC, Fishman I (2015) Regional Specificity of Aberrant Thalamocortical Connectivity in Autism. *Human brain mapping* 36:4497–4511.

Nair A, Keown CL, Datko M, Shih P (2014) Impact of Methodological Variables on Functional Connectivity Findings in Autism Spectrum Disorders. *Human brain mapping* 35:4035–4048.

Nair A, Treiber JM, Shukla DK, Shih P, Mu Ra (2013) Impaired thalamocortical connectivity in autism spectrum disorder : a study of functional and anatomical connectivity. *Brain* 136:1942–1955.

Nair S, Keehn RJJ, Berkebile MM, Maximo JO (2018) Local resting state functional connectivity in autism : site and cohort variability and the effect of eye status. *Brain Imaging and Behavior* 12:168–179.

Nakamoto M, Nalavadi V, Epstein MP, Narayanan U, Bassell GJ, Warren ST (2007) Fragile X mental retardation protein deficiency leads to excessive mGluR5-dependent internalization of AMPA receptors. *PNAS* 104:15537–15542.

Narayanan U, Nalavadi V, Nakamoto M, Thomas G, Ceman S, Bassell G, Warren S (2008) S6K1 phosphorylates and regulates fragile X mental retardation protein (FMRP) with the neuronal protein synthesis-dependent mammalian target of rapamycin (mTOR) signaling cascade. *Journal Of Biological Chemistry* 283:18478–18482.

Nasrallah FA, Yun L, Biswal B, Chuang Kh (2015) Dependence of BOLD signal fluctuation on arterial blood CO2 and O2 : Implication for resting-state functional connectivity. *NeuroImage* 117:29–39.

Nathan Spreng R (2012) The fallacy of a "task-negative" network. *Frontiers in Psychology* 3:1–5.

Nebel MB, Joel SE, Muschelli J, Barber AD, Caffo BS, Pekar JJ, Mostofsky SH (2014) Disruption of Functional Organization Within the Primary Motor Cortex in Children With Autism. *Human brain mapping* 35:567–580.

Nielsen JA, Zielinski BA, Fletcher PT, Alexander AL, Lange N (2014) Abnormal lateralization of functional connectivity between language and default mode regions in autism. *Molecular Autism* 5:1–11.

Nielsen JA, Zielinski BA, Fletcher T, Alexander AL (2013) Multisite functional connectivity MRI classification of autism : ABIDE results. *Frontiers in Human Neuroscience* 7:1–12.

Nir Y, Mukamel R, Dinstein I, Privman E, Harel M, Fisch L, Gelbard-sagiv H, Kipervasser S, Andelman F, Neufeld MY, Kramer U, Arieli A, Fried I, Malach R (2008) Interhemispheric correlations of slow spontaneous neuronal fluctuations revealed in human sensory cortex. *Nature neuroscience* 11.

Obrig H, Neufang M, Wenzel R, Kohl M, Steinbrink J, Einhäupl K, Villringer A (2000) Spontaneous low frequency oscillations of cerebral hemodynamics and metabolism in human adults. *NeuroImage* 12:623–639.

Ogawa S, Lee TM, Kay AR, Tank DW (1990) Brain magnetic resonance imaging with contrast dependent on blood oxygenation. *Proceedings of the National Academy of Sciences of the United States of America* 87:9868–9872.

Olivito G, Clausi S, Laghi F, Tedesco AM, Baiocco R, Mastropasqua C, Molinari M, Cercignani M, Bozzali M, Leggio M (2016) Resting-State Functional Connectivity Changes Between Dentate Nucleus and Cortical Social Brain Regions in Autism Spectrum Disorders. *The Cerebellum* 16:283–292.

Olmos-Serrano JL, Paluszkiewicz SM, Martin BS, Kaufmann WE, Corbin JG, Huntsman MM (2010) Defective GABAergic neurotransmission and pharmacological rescue of neuronal hyperexcitability in the amygdala in a mouse model of fragile X syndrome. *The Journal of neuroscience : the official journal of the Society for Neuroscience* 30:9929–9938.

Osterweil EK, Chuang Sc, Chubykin AA, Sidorov M, Bianchi R, Wong RK, Bear MF (2013) Lovastatin Corrects Excess Protein Synthesis and Prevents Epileptogenesis in a Mouse Model of Fragile X Syndrome. *Neuron* 77:243–250.

Osterweil EK, Krueger DD, Reinhold K, Bear MF (2010) Hypersensitivity to mGluR5 and ERK1/2 Leads to Excessive Protein Synthesis in the Hippocampus of a Mouse Model of Fragile X Syndrome. *Journal of Neuroscience* 30:15616–15627.

Paakki Jj, Rahko J, Long X, Moilanen I, Tervonen O, Nikkinen J, Starck T, Remes J, Hurtig T, Haapsamo H (2009) Alterations in regional homogeneity of resting-state brain activity in autism spectrum disorders. *Brain Research* 1321:169–179.

Paasonen J, Stenroos P, Salo RA, Kiviniemi V (2018) Functional connectivity under six anesthesia protocols and the awake condition in rat brain. *NeuroImage* 172:9–20.

Pacey LKK, Xuan ICY, Guan S, Sussman D, Henkelman RM, Chen Y, Thomsen C, Hampson DR (2013) Delayed myelination in a mouse model of fragile X syndrome. *Human Molecular Genetics* 22:3920–3930.

Palanca BJA, Mitra A, Larson-prior L, Snyder AZ, Avidan MS, Raichle ME (2015) Resting-state Functional Magnetic Resonance Imaging Correlates of Sevoflurane-induced Unconsciousness. *Anaesthesiology* 123:346–356.

Pan L, Broadie KS (2007) Drosophila fragile X mental retardation protein and metabotropic glutamate receptor A convergently regulate the synaptic ratio of ionotropic glutamate receptor subclasses. *The Journal of neuroscience : the official journal of the Society for Neuroscience* 27:12378.

Pan L, Woodruff E, Liang P, Broadie K (2008) Mechanistic relationships between Drosophila fragile X mental retardation protein and metabotropic glutamate receptor A signaling. *Molecular and Cellular Neuroscience* 37:747–760.

Pan Wj, Billings JCW, Grooms JK, Shakil S (2015) Considerations for resting state functional MRI and functional connectivity studies in rodents. *Frontiers in Neuroscience* 9:1–17.

Panman JL, To YY, Ende ELVD, Poos JM, Jiskoot LC, Meeter LHH, Dopper EGP, Bouts MJRJ, Grond JVD, Papma JM, Hafkemeijer A (2019) Bias Introduced by Multiple Head Coils in MRI Research : An 8 Channel and 32 Channel Coil Comparison. *Frontiers in Neuroscience* 13:1–9.

Pardon MC, Gould GG, Garcia A, Phillips L, Cook MC, Miller SA, Mason PA, Morilak DA (2002) Stress reactivity of the brain noradrenergic system in three rat strains differing in their neuroendocrine and behavioral responses to stress: Implications for susceptibility to stress-related neuropsychiatric disorders. *Neuroscience* 115:229–242.

Patel AB, Loerwald KW, Huber KM, Gibson JR (2014) Postsynaptic FMRP Promotes the Pruning of Cell-to-Cell Connections among Pyramidal Neurons in the L5A Neocortical Network. *Journal of Neuroscience* 34:3413–3418.

Payne JM, Barton B, Ullrich NJ, Cantor A, Hearps SJC, Walsh KS, Gioia GA, Wolters PL, Tonsgard J, Schorry E, Fisher M, Gutmann DH, Silva AJ, Hunter SJ, Reycasserly C, Byars AW, Stavinoha PL, Ackerson JD, Armstrong CL, Isenberg J, Neil SHO, Packer RJ, North KN (2016) Randomized placebo-controlled study of lovastatin in children with neurofibromatosis type 1. *American Academy of Neurology* B7:2575–2584.

Peier AM, McIlwain KL, Kenneson A, Warren ST, Paylor R, Nelson DL (2000) (Over)correction of FMR1 deficiency with YAC transgenics: behavioral and physical features. *Human molecular genetics* 9:1145–1159.

Pellerin D, Artuela C, Fradet M, Dub J (2016) Lovastatin corrects ERK pathway hyperactivation in fragile X syndrome : potential of platelet's signaling cascades as new outcome measures in clinical trials. *Biomarkers* 21:497–508.

Peters AM, Brookes MJ, Hoogenraad FG, Gowland PA, Francis ST, Morris PG, Bowtell R (2007) T2 * measurements in human brain at 1.5 , 3 and 7 T. *Magnetic resonance imaging* 25:748–753.

Petersen SE, Fox PT, Posner MI, Minton M, Raichle ME (1988) Positron emission tomographic studies of the cortical anatomy of single-word processing. *Nature* 331:585–589.

Philippi CL, Tranel D, Duff M, Rudrauf D (2015) Damage to the default mode network disrupts autobiographical memory retrieval. *Social Cognitive and Affective Neuroscience* 10:318–326.

Pieretti M, Zhang F, Fu YH, Warren ST, Oostra BA, Caskey C, Nelson DL (1991) Absence of expression of the FMR-1 gene in fragile X syndrome. *Cell* 66:817–822.

Plitt M, Anne K, Martin A (2015) Functional connectivity classification of autism identifies highly predictive brain features but falls short of biomarker standards. *Neuroimage Clin.* 7:359–366.

Plitt M, Anne K, Wallace GL, Kenworthy L, Martin A (2015) Resting-state functional connectivity predicts longitudinal change in autistic traits and adaptive functioning in autism. *PNAS* 112:E6699–E6706.

Poerio GL, Sormaz M, Wang Ht, Margulies D, Jefferies E, Smallwood J (2017) The role of the default mode network in component processes underlying the wandering mind. *Social Cognitive and Affective Neuroscience* pp. 1047–1062.

Poldrack RA, Fletcher PC, Henson RN, Worsley KJ, Brett M, Nichols TE (2008) Guidelines for reporting an fMRI study. *NeuroImage* 40:409–414.

Poustchi-Amin M, Mirowitz SA, Brown JJ, Mckinstry RC, Li T (2001) Principles and Applications of Echo-planar Imaging : A Review for the General Radiologist. *Imaging & Therapeutic Technology* 21:767–779.

Price T, Wee Cy, Gao W, Shen D (2014) Multiple-Network Classification of Childhood Autism Using Functional Connectivity Dynamics. *Med Image Comput Comput Assist Interv* 17:177–184.

Protic D, Salcedo-arellano MJ, Dy JB, Potter LA, Hagerman RJ, X KF (2019) New Targeted Treatments for Fragile X Syndrome. *Current Pediatric Reviews* 15:251–258.

Pruett JR, Kandala S, Hoertel S, Snyder AZ, Elison JT, Nishino T, Feczko E, Dosenbach NUF, Nardos B, Power JD, Adeyemo B, Botteron KN, Mckinstry RC, Evans AC, Hazlett HC, Dager SR, Paterson S, Schultz RT, Collins DL, Fonov VS, Styner M, Gerig G, Das S, Kostopoulos P, Constantino JN, Estes AM, Network TI, Petersen SE, Schlaggar BL, Piven J (2015) Accurate age classification of 6 and 12 month-old infants based on resting-state functional connectivity magnetic resonance imaging data. *Developmental Cognitive Neuroscience* 12:123–133.

Prusky GT, Harker KT, Douglas RM, Whishaw IQ (2002) Variation in visual acuity within pigmented , and between pigmented and albino rat strains. *Behavioural Brain Research* 136:339–348.

Raichle ME (2010) Two views of brain function. *Trends in cognitive sciences* 14:180–190.

Raichle ME, Macleod AM, Snyder AZ, Powers WJ, Gusnard DA, Shulman GL (2001) A default mode of brain function. *PNAS* 98:676–682.

Rauch A, Wieczorek D, Graf E, Wieland T, Endele S, Schwarzmayr T, Albrecht B, Bartholdi D, Beygo J, Di Donato N, Dufke A, Cremer K, Hempel M, Horn D, Hoyer J, Joset P, Röpke A, Moog U, Riess A (2012) Range of genetic mutations associated with severe non-syndromic sporadic intellectual disability: an exome sequencing study. *The Lancet* 380:1674–1682.

Ray S, Miller M, Karalunas S, Robertson C, Grayson DS, Cary RP, Hawkey E, Painter JG, Kriz D, Fombonne E, Nigg JT, Fair DA (2014) Structural and Functional Connectivity of the Human Brain in Autism Spectrum Disorders and Attention-Deficit / Hyperactivity Disorder : A Rich Club-Organization Study. *Human brain mapping* 6048:6032–6048.

Redcay E, Moran JM, Mavros PL, Tager-flusberg H, Gabrieli JDE, Whitfield-gabrieli S (2013) Intrinsic functional network organization in high-functioning adolescents with autism spectrum disorder. *Front. Hum. Neurosci.* 7:1–11.

Reiss AI, Abrams MT, Greenlaw R, Freund L, Denckla MB (1995) Neurodevelopmental effects of the FMR-1 full mutation in humans. *Nature Medicine* 1:159–167.

Renoux AJ, Sala-Hamrick KJ, Carducci NM, Frazer M, Halsey KE, Sutton MA, Dolan DF, Murphy GG, Todd PK (2014) Impaired sensorimotor gating in Fmr1 knock out and Fragile X premutation model mice. *Behavioural brain research* 267:42–45.

Repicky S, Broadie K (2009) Metabotropic glutamate receptor-mediated use-dependent down-regulation of synaptic excitability involves the fragile X mental retardation protein. *Journal of neurophysiology* 101:672.

Restivo L, Ferrari F, Passino E, Sgobio C, Bock J, Oostra BA, Bagni C, Ammassari-Teule M (2005) Enriched environment promotes behavioral and morphological recovery in a mouse model for the fragile X syndrome. *Proceedings of the National Academy of Sciences of the United States of America* 102:11557–11562.

Roberts JE, Mankowski JB, Sideris J, Goldman BD, Hatton DD, Mirrett PL, Baranek GT, Reznick JS, Long ACJ, Bailey DB (2009) Trajectories and Predictors of the Development of Very Young Boys with Fragile X Syndrome. *Journal of Pediatric Psychology* 34:827–836.

Rolfe DF, Brown GC (1997) Cellular energy utilization and molecular origin of standard metabolic rate in mammals. *Physiological reviews* 77:731–758.

Ropers HH, Hamel BCJ (2005) X-linked mental retardation. *Nature Reviews Genetics* 6:46.

Rotschafer SE, Trujillo MS, Dansie LE, Ethell IM, Razak KA (2012) Minocycline treatment reverses ultrasonic vocalization production deficit in a mouse model of Fragile X Syndrome. *Brain research* 1439:7–14.

Royall DR, Lauterbach EC, Cummings JL, Reeve A, Rummans TA, Kaufer DI, Lafrance WC, Coffey CE (2002) Executive Control Function : A Review of Its Promise and Challenges for Clinical Research. *The Journal of Neuropsychiatry and Clinical Neurosciences* 14:377–405.

Rubinov M, Sporns O (2010) Complex network measures of brain connectivity : Uses and interpretations. *NeuroImage* 52:1059–1069.

Rudie JD, Hernandez LM, Brown JA, Beck-pancer D, Colich NL, Gorrindo P, Thompson PM, Geschwind DH, Bookheimer SY, Levitt P, Dapretto M (2012) Autism-Associated Promoter Variant in MET Impacts Functional and Structural Brain Networks. *Neuron* 75:904–915.

Rudie JD, Dapretto M (2013) Convergent Evidence of Brain Overconnectivity in Children with Autism ? *Cell Reports* 5:565–566.

Russel G, Graybeal J (1995) Differences in Anesthetic Potency between Sprague-Dawley and Long-Evans Rats for Isoflurane but Not Nitrous Oxide. *Pharmacology* 50:162–167.

Saxena K, Webster J, Hallas-Potts A, Mackenzie R, Spooner PA, Thomson D, Kind P, Chattarji S, Morris RGM (2018) Experiential contributions to social dominance in a rat model of fragile-X syndrome. *Proceedings. Biological sciences* 285:20180294.

Scheeringa R, Fries P, Petersson KM, Oostenveld R, Grothe I, Norris DG, Hagoort P, Bastiaansen MCM (2011) Neuronal dynamics underlying high- and low-frequency EEG oscillations contribute independently to the human BOLD signal. *Neuron* 69:572–583.

Seeley WW, Carlin DA, Allman JM, Macedo MN, Bush C, Miller BL, Dearmond SJ (2006) Early frontotemporal dementia targets neurons unique to apes and humans. *Annals of Neurology* 60:660–667.

Sengupta P (2013) The Laboratory Rat : Relating Its Age With Human's. *International journal of preventive medicine* 4:624–630.

Seong-Gi K, Bandettini PA (2010) *Bold fMRI* Springer.

Sforazzini F, Bertero A, Dodero L, David G, Galbusera A, Luisa M, Pasqualetti M, Gozzi A (2016) Altered functional connectivity networks in acallosal and socially impaired BTBR mice. *Brain Structure and Function* 221:941–954.

Shehzad Z, Kelly AMC, Reiss PT, Gee G, Gotimer K, Uddin LQ, Lee SH, Margulies DS, Roy AK, Biswal BB, Petkova E, Castellanos FX, Milham MP (2009) The Resting Brain : Unconstrained yet Reliable. *Cerebral Cortex* 19:2209–2229.

Shen MD, Li DD, Keown CL, Lee A, Johnson RT, Angkustsiri K, Rigers SJ, Muller RA, Amaral DG, Nordahl CW (2016) Functional Connectivity of the Amygdala Is Disrupted in Preschool-Aged Children with Autism Spectrum Disorder. *Journal of the American Academy of Child & Adolescent Psychiatry* 55:817–824.

Sherman LE, Rudie JD, Pfeifer JH, Masten CL, Mcnealy K, Dapretto M (2014) Development of the Default Mode and Central Executive Networks across early adolescence : A longitudinal study. *Developmental Cognitive Neuroscience* 10:148–159.

Shmuel A, Leopold DA (2008) Neuronal correlates of spontaneous fluctuations in fMRI signals in monkey visual cortex: Implications for functional connectivity at rest. *Human Brain Mapping* 29:751–761.

Shukla DK, Keehn B, Muller RA (2010) Regional homogeneity of fMRI time series in autism spectrum disorders. *Neuroscience Letters* 476:46–51.

Sidorov MS, Krueger DD, Taylor M, Gisin E, Osterweil EK, Bear MF (2014) Extinction of an instrumental response: A cognitive behavioral assay in Fmr1 knockout mice. *Genes, Brain and Behavior* 13:451–458.

Siegel XJJ, Chitwood XRA, Ding JM, Payne XC, Taylor W, Gray XR, Zemelman XBV, Johnston XD (2017) Prefrontal Cortex Dysfunction in Fragile X Mice Depends on the Continued Absence of Fragile X Mental Retardation Protein in the Adult Brain. *The journal of Neuroscience* 37:7305–7317.

Skinner M, Hooper S, Hatton DD, Roberts J, Mirrett P, Schaaf J, Sullivan K, Wheeler A, Jr DBB (2005) Mapping Nonverbal IQ in Young Boys With Fragile X Syndrome. *American Journal of medical genetics* 132A:25–32.

Skouras S, Gray M, Critchley H, Koelsch S (2014) Superficial amygdala and hippocampal activity during affective music listening observed at 3 T but not 1.5 T fMRI. *NeuroImage* 101:364–369.

Smallwood J, Tipper C, Brown K, Baird B, Engen H, Michaels JR, Grafton S, Schooler JW (2013) Escaping the here and now: Evidence for a role of the default mode network in perceptually decoupled thought. *NeuroImage* 69:120–125.

Smitha KA, Akhil Raja K, Arun KM, Rajesh PG, Thomas B, Kapilamoorthy TR, Kesavadas C (2017) Resting state fMRI: A review on methods in resting state connectivity analysis and resting state networks. *Neuroradiology Journal* 30:305–317.

Soares JM, Magalhães R, Moreira PS, Sousa A (2016) A Hitchhiker's Guide to Functional Magnetic Resonance Imaging. *Frontiers in Neuroscience* 10:1–35.

Sokoloff L, Mangold R, Wechsler RL, Kennedy C, Kety SS (1955) The effect of mental arithmetic on cerebral circulation and metabolism. *The Journal of clinical investigation* 34:1101–1108.

Song H, Zou Z, Kou J, Liu Y, Yang L, Zilverstand A (2015) Love-related changes in the brain : a resting-state functional magnetic resonance imaging study. *Front. Hum. Neurosci.* 9:1–13.

Spisak T, Jakab A, Kis SA, Opposits G, Aranyi C, Berenyi E, Emri M (2014) Voxel-Wise Motion Artifacts in Population-Level Whole- Brain Connectivity Analysis of Resting-State fMRI. *PLOS ONE* 9:1–19.

Srivastava AK, Schwartz CE (2014) Intellectual disability and autism spectrum disorders: causal genes and molecular mechanisms. *Neuroscience and biobehavioral reviews* 46 Pt 2:161–174.

Starck T, Nikkinen J, Rahko J, Remes J, Hurtig T, Haapsamo H, Jussila K, Kuusikko-gauffin S, Mattila Ml, Jansson-verkasalo E (2013) Resting state fMRI reveals a default mode dissociation between retrosplenial and medial prefrontal subnetworks in ASD despite motion scrubbing. *Front. Hum. Neurosci.* 7:1–10.

Stein EA, Illingworth DR, Kwiterovich, Jr PO, Liacouras CA, Siimes MA, Jacobson MS, Brewster TG, Hopkins P, Davidson M, Graham K, Arensman F, Knopp RH, DuJovne C, Williams CL, Isaacsohn JL, Jacobsen CA, Laskarzewski PM, Ames S, Gormley GJ (1999) Efficacy and Safety of Lovastatin in Adolescent Males With Heterozygous Familial Hypercholesterolemia. A randomized Controlled Trial. *JAMA* 281:137–144.

Suetterlin P, Hurley S, Mohan C, Riegman KLH, Pagani M, Caruso A, Ellegood J, Galbusera A, Crespo-enriquez I, Michetti C, Yee Y, Ellingford R, Brock O, Delogu A, Francis-west P, Lerch JP, Scattoni ML, Gozzi A, Fernandes C, Basson MA (2018) Altered Neocortical Gene Expression, Brain Overgrowth and Functional Over-Connectivity in Chd8 Haploinsufficient Mice. *Cerebral cortex* 28:2192–2206.

Supekar K, Uddin LQ, Khouzam A, Phillips J, Gaillard WD, Kenworthy LE, Yerys BE, Vaidya CJ (2013) Brain hyper-connectivity in children with autism and its links to social deficits. *Cell Reports* 5:738–747.

Supekar K, Uddin LQ, Prater K, Amin H, Michael D, Menon V (2010) Development of functional and structural connectivity within the default mode network in young children. *NeuroImage* 52:290–301.

Sutcliffe JS, Nelson DL, Zhang F, Pieretti M, Caskey CT, Saxe D, Warren ST (1992) DNA methylation represses FMR-1 transcription in fragile X syndrome. *Human molecular genetics* 1:397.

Swanson MR, Wolff JJ, Shen MD, Styner M, Estes A, Gerig G, Mckinstry RC, Botteron KN, Piven J (2018) Development of White Matter Circuitry in Infants With Fragile X Syndrome. *JAMA Psychiatry* 75:505–513.

Tan W, Schauder C, Naryshkina T, Minakhina S, Steward R (2016) Zfrp8 forms a complex with fragile-X mental retardation protein and regulates its localization and function. *Developmental Biology* 410:202–212.

Tassone F, Hagerman RJ, Taylor AK, Hagerman PJ (2001) A majority of fragile X males with methylated, full mutation alleles have significant levels of FMR1 messenger RNA. *Journal of medical genetics* 38:453–456.

Testa-silva G, Loebel A, Giugliano M, Kock CPJD, Mansvelder HD, Meredith M (2012) Hyperconnectivity and Slow Synapses during Early Development of Medial Prefrontal Cortex in a Mouse Model for Mental Retardation and Autism. *Cerebral cortex* 22:1333–1342.

Thapar A, Cooper M, Rutter M (2017) Neurodevelopmental disorders. *The Lancet Psychiatry* 4:339–346.

Thirion B, Pinel P, Mériaux S, Roche A, Dehaene S, Poline Jb (2007) Analysis of a large fMRI cohort : Statistical and methodological issues for group analyses. *NeuroImage* 35:105–120.

Thomason ME, Grove LE, Lozon TA, Vila AM, Ye Y, Nye MJ, Manning JH, Pappas A, Hernandez-andrade E, Yeo L, Mody S, Berman S, Hassan SS, Romero R (2015) Age-related increases in long-range connectivity in fetal functional neural connectivity networks in utero. *Developmental Cognitive Neuroscience* 11:96–104.

Thurman AJ, Potter LA, Kim K, Tassone F, Banasik A, Potter SN, Bullard L, Nguyen V, Mcduffie A, Hagerman R, Abbeduto L (2020) Controlled trial of lovastatin combined with an open-label treatment of a parent- implemented language intervention in youth with fragile X syndrome. *Journal of Neurodevelopmental Disorders* 12:1–17.

Tian Y, Yang C, Shang S, Cai Y, Deng X, Zhang J, Feng Shao, Desheng Zhu, Yunbo Liu, Guiquan Chen, Jing Liang, Qiang Sun, Zilong Qiu, Chen Zhang (2017) Loss of FMRP Impaired Hippocampal Long-Term Plasticity and Spatial Learning in Rats. *Frontiers in molecular neuroscience* 10:269.

Till SM, Asiminas A, Jackson AD, Katsanevaki D, Barnes SA, Osterweil EK, Bear MF, Chattarji S, Wood ER, Wyllie DJ, Kind PC (2015) Conserved hippocampal cellular pathophysiology but distinct behavioural deficits in a new rat model of FXS. *Human Molecular Genetics* 24:5977–5984.

Tomson SN, Schreiner MJ, Narayan M, Rosser T, Enrique N, Silva AJ, Allen GI, Bookheimer SY, Bearden CE (2015) Resting State Functional MRI Reveals Abnormal Network Connectivity in Neurofibromatosis 1. *Human brain mapping* 36:4566–4581.

Tonkiss J, Shultz P, Galler JR (1992) Long-Evans and Sprague-Dawley Rats Differ in Their Spatial Navigation Performance During Ontogeny and at Maturity. *Developmental Psychobiology* 25:567–579.

Tordjman S, Gutknecht L, Carlier M, Spitz E, Antoine C, Slama F, Carsalade V, Cohen DJ, Ferrari P, Roubertoux PL, Anderson GM (2001) Role of the serotonin transporter gene in the behavioral expression of autism. *Molecular Psychiatry* 6:434.

Tranfaglia MR, Thibodeaux C, Mason DJ, Brown D, Roberts I, Smith R, Guilliams T, Cogram P (2019) Repurposing available drugs for neurodevelopmental disorders : The fragile X experience. *Neuropharmacology* 147:74–86.

Tucker B, Richards RI, Lardelli M (2005) Contribution of mGluR and Fmr1 functional pathways to neurite morphogenesis, craniofacial development and fragile X syndrome. *Human Molecular Genetics* 15:3446–3458.

Uddin LQ, Supekar K, Lynch CJ, Khouzam A, Phillips J, Feinstein C, Ryali S, Menon V (2013) Salience Network–Based Classification and Prediction of Symptom Severity in Children With Autism. *JAMA Psychiatry* 70:869–879.

Upadhyay J, Baker SJ, Chandran P, Miller L, Lee Y, Marek GJ, Sakoglu U, Chin Cl, Luo F, Fox GB, Day M (2011) Default-Mode-Like Network Activation in Awake Rodents. *PloS one* 6:1–8.

van den Heuvel MP, Hulshoff Pol HE (2010) Exploring the brain network: A review on resting-state fMRI functional connectivity. *European Neuropsychopharmacology* 20:519–534.

van den Heuvel MP, Mandl RCW, Kahn RS, Hulshoff Pol HE (2009) Functionally linked resting-state networks reflect the underlying structural connectivity architecture of the human brain. *Human brain mapping* 30:3127–3141.

Van Der Zwaag W, Francis S, Head K, Peters A, Gowland P, Morris P, Bowtell R (2009) fMRI at 1.5 , 3 and 7 T : Characterising BOLD signal changes. *NeuroImage* 47:1425–1434.

Van Horn JD, Grafton ST, Rockmore D, Gazzaniga MS (2004) Sharing neuroimaging studies of human cognition. *Nature Neuroscience* 7:473–481.

Vanhoutte G, Verhoye M, Van Der Linden A (2006) Changing body temperature affects the T 2 * signal in the rat brain and reveals hypothalamic activity. *Magnetic Resonance in Medicine* 55:1006–1012.

Venkataraman A, Duncan JS, Yang DY, Pelphrey KA (2015) An unbiased Bayesian approach to functional connectomics implicates social-communication networks in autism. *NeuroImage: Clinical* 8:356–366.

Verkerk AJM, Pieretti M, Sutcliffe JS, Fu YH, Kuhl DPA, Pizzuti A, Reiner O, Richards S, Victoria MF, Zhang F, Eussen BE, van Ommens GJB, Blonden LAJ, Riggins GJ, Chastain JL, Kunst CB, Gaijaard H, Caskey CT, Nelson DL, Oostra BA, Warren ST (1991) Identification of a Gene (FMR-1) Containing a CGG Repeat Coincident with a Breakpoint Cluster Region Exhibiting Length Variation in Fragile X Syndrome. *Cell* 65:905–914.

Verly M, Verhoeven J, Zink I, Mantini D, Peeters R, Deprez S, Emsell L, Boets B, Noens I, Steyaert J, Lagae L, Cock PD, Rommel N, Sunaert S (2014) Altered functional connectivity of the language network in ASD : Role of classical language areas and cerebellum. *NeuroImage: Clinical* 4:374–382.

Vincent JL, Patel GH, Fox MD, Snyder AZ, Baker JT, Essen DCV, Zempel JM, Snyder LH, Corbetta M, Raichle ME (2007) Intrinsic functional architecture in the anaesthetized monkey brain. *Nature* 447:83–86.

von dem Hagen EAH, Stoyanova RS, Baron-cohen S, Calder AJ (2013) Reduced functional connectivity within and between 'social' resting state networks in autism spectrum conditions. *SCAN* 8:694–701.

Wald LL (2012) The future of acquisition speed, coverage, sensitivity, and resolution. *NeuroImage* 62:1221–1229.

Wang D, Yan L, Hu Q, Sucheston LE, Higgins MJ, Ambrosone CB, Johnson CS, Smiraglia DJ, Liu S (2012) IMA: An R package for high-throughput analysis of Illumina's 450K Infinium methylation data. *Bioinformatics* 28:729–730.

Washington SD, Gordon EM, Brar J, Warburton S, Sawyer AT, Wolfe A, Mease-ference ER, Girton L, Hailu A, Mbwana J, Gaillard WD, Kalbfleisch ML, Vanmeter JW (2014) Dysmaturation of the Default Mode Network in Autism. *Human brain mapping* 35:1284–1296.

Waterston RH, Lindblad-Toh K, Birney E, Rogers J, Abril JF, Agarwal P, Agarwala R, Ainscough R, Alexandersson M, An P, Antonarakis SE, Attwood J, Baertsch R, Bailey J, Barlow K, Beck S, Berry E, Birren B, Bloom T, Bork P, Botcherby M, Bray N, Brent MR, Brown DG, Brown SD, Bult C, Burton J, Butler J, Campbell RD, Carninci P, Cawley S, Chiaromonte F, Chinwalla AT, Church DM, Clamp M, Clee C, Collins FS, Cook LL, Copley RR, Coulson A, Couronne O, Cuff J, Curwen V, Cutts T, Daly M, David R, Davies J, Delehaunty KD, Deri J, Dermitzakis ET, Dewey C, Dickens NJ, Diekhans M, Dodge S, Dubchak I, Dunn DM, Eddy SR, Elnitski L, Emes RD, Eswara P, Eyras E, Felsenfeld A, Fewell GA, Flicek P, Foley K, Frankel WN, Fulton LA, Fulton RS, Furey TS, Gage D, Gibbs RA, Glusman G, Gnerre S, Goldman N, Goodstadt L, Grafham D, Graves TA, Green ED, Gregory S, Guigo R, Guyer M, Hardison RC, Haussler D, Hayashizaki Y, Hillier LW, Hinrichs A, Hlavina W, Holzer T, Hsu F, Hua A, Hubbard T, Hunt A, Jackson I, Jaffe DB, Johnson LS, Jones M, Jones TA, Joy A, Kamal2 M, Karlsson EK, Karolchik D, Kasprzyk A, Kawai J, Keibler E, Kells C, Kent WJ, Kirby A, Kolbe DL, Korf I, Kucherlapati RS, Kulbokas EJ, Kulp D, Landers T, Leger JP, Leonard S, Letunic I, Levine R, Li J, Li M, Lloyd C, Lucas S, Ma B, Maglott DR, Mardis ER, Matthews L, Mauceli E, Mayer JH, McCarthy M, McCombie WR, McLaren S, McLay K, McPherson JD, Meldrim J, Meredith B, Mesirov, Miller P, Webb J, Miner TL, Mongin E, Montgomery KT, Morgan M, Mott R, Mullikin JC, Muzny DM, Nash WE, Nelson JO, Nhan MN, Nicol R, Ning Z, Nusbaum C, O'Connor MJ, Okazaki Y, Oliver K, Overton-Larty E, Pachter L, Parra G, Pepin KH, Peterson J, Pevzner P, Plumb R, Pohl CS, Poliakov A, Ponce TC, Ponting CP, Potter S, Quail M, Reymond A, Roe BA, Roskin KM, Rubin EM, Rust AG, Santos R, Sapojnikov V, Schultz B, Schultz J, Schwartz MS, Schwartz S, Scott C, Seaman S, Searle S, Sharpe T, Sheridan A, Shownkeen R, Sims S, Singer JB, Slater G, Smit A, Smith DR, Spencer B, Stabenau A, Stange-Thomann N, Sugnet C, Suyama M, Tesler G, Thompson J, Torrents D, Trevaskis E, Tromp J, Ucla C, Ureta-Vidal A, Vinson JP, Von Niederhausern AC, Wade CM, Wall M, Weber RJ, Weiss RB, Wendl MC, West AP, Wetterstrand K, Wheeler R, Whelan S, Wierzbowski J, Willey D, Williams S, Wilson RK, Winter E, Worley KC, Wyman D, Yang S, Yang SP, Zdobnov EM, Zody MC, Lander ES (2002) Initial sequencing and comparative analysis of the mouse genome. *Nature* 420:520.

Weber R, Ramos-cabrer P, Wiedermann D, Camp NV, Hoehn M (2006) A fully noninvasive and robust experimental protocol for longitudinal fMRI studies in the rat. *NeuroImage* 29:1303–1310.

Wee Cy, Yap Pt, Shen D (2016) Diagnosis of Autism Spectrum Disorders Using Temporally Distinct Resting-State Functional Connectivity Networks. *CNS Neuroscience & Therapeutics* 22:212–219.

Weiler IJ, Irwin SA, Klintsova AY, Spencer CM, Brazelton AD, Miyashiro K, Comery TA, Patel B, Eberwine J, Greenough WT (1997) Fragile X mental retardation protein

is translated near synapses in response to neurotransmitter activation. *Proceedings of the National Academy of Sciences* 94:5395–5400.

Weng Sj, Lee J, Peltier SJ, Carrasco M, Risi S, Lord C, Monk CS (2009) Alterations of resting state functional connectivity in the default network in adolescents with autism spectrum disorders. *Brain Research* 1313:202–214.

Werner HB, Amer-albers EmKR, Tenzer S, Ohno-iwashita Y, Monasterio-schrader PDE (2013) A Critical Role for the Cholesterol-Associated Proteolipids PLP and M6B in Myelination of the Central Nervous System. *Glia* 61:567–586.

Westeinde AV, Cauvet É, Toro R, Kuja-halkola R, Neufeld J, Mevel K, Bölte S (2020) Sex differences in brain structure : a twin study on restricted and repetitive behaviors in twin pairs with and without autism. *Molecular Autism* 11:1–20.

Westphalen RI, Desai KM, Jr HCH (2013) Presynaptic inhibition of the release of multiple major central nervous system neurotransmitter types by the inhaled anaesthetic isoflurane. *British Journal of Anaesthesia* 110:592–599.

Whishaw IQ, Gorny B, Foroud A, Kleim JA (2003) Long–Evans and Spragu –Dawley rats have similar skilled reaching success and limb representations in motor cortex but different movements : some cautionary insights into the selection of rat strains for neurobiological motor research. *Behavioural Brain Research* 145:221–232.

Wijetunge LS, Angibaud J, Frick A, Kind PC, Nagerl UV (2014) Stimulated Emission Depletion (STED) Microscopy Reveals Nanoscale Defects in the Developmental Trajectory of Dendritic Spine Morphogenesis in a Mouse Model of Fragile X Syndrome. *Journal of Neuroscience* 34:6405–6412.

Williams KA, Magnuson M, Majeed W, Laconte SM, Peltier SJ, Hu X, Keilholz SD (2010) Comparison of α -chloralose , medetomidine and isoflurane anesthesia for functional connectivity mapping in the rat. *Magnetic resonance imaging* 28:995–1003.

Wu Tl, Mishra A, Wang F, Yang Pf, Gore JC, Chen LM (2016) Effects of isoflurane anesthesia on resting-state fMRI signals and functional connectivity within primary somatosensory cortex of monkeys. *Brain and Behavior* 6:1–12.

Wu Xs, Ph D, Sun Jy, Ph D, Evers AS, Crowder M, Ph D (2004) Isoflurane Inhibits Transmitter Release and the Presynaptic Action Potential. *Anaesthesiology* 100:663–670.

Wylie KP, Rojas DC, Ross RG, Hunter SK (2014) Reduced brain resting-state network specificity in infants compared with adults. *Neuropsychiatric Disease and Treatment* 10:1349–1359.

Xu S, Li M, Yang C, Fang X, Ye M, Wei L (2019) Altered Functional Connectivity in Children With Low-Function Autism Spectrum Disorders. *Frontiers in Neuroscience* 13:1–9.

Yan QJ, Asafo-Adjei PK, Arnold HM, Brown RE, Bauchwitz RP (2004) A phenotypic and molecular characterization of the fmr1-tm1Cgr fragile X mouse. *Genes, brain, and behavior* 3:337–359.

Yan Q, Rammal M, Tranfaglia M, Bauchwitz R (2005) Suppression of two major Fragile X Syndrome mouse model phenotypes by the mGluR5 antagonist MPEP. *Neuropharmacology* 49:1053–1066.

Yau Sy, Bettio L, Chiu J, Chiu C, Christie BR, Christie BR (2019) Fragile-X Syndrome Is Associated With NMDA Receptor Hypofunction and Reduced Dendritic Complexity in Mature Dentate Granule Cells. *Frontiers in molecular neuroscience* 11:1–10.

Yoshino M, Kin T, Saito T (2014) Optimal setting of image bounding box can improve registration accuracy of diffusion tensor tractography. *Int J CARS* 9:333–339.

You X, Norr M, Murphy E, Kuschner ES, Bal E, Gaillard WD, Kenworthy L, Vaidya CJ (2013) Atypical modulation of distant functional connectivity by cognitive state in children with Autism Spectrum Disorders. *Frontiers in Human Neuroscience* 7:1–13.

Ypma RJF, Moseley RL, Holt RJ, Rughooputh N, Floris DL, Chura LR, Spencer MD, Baron-cohen S, Suckling J, Bullmore ET, Rubinov M (2016) Default Mode Hypoconnectivity Underlies a Sex-Related Autism Spectrum. *Biological Psychiatry: Cognitive Neuroscience and Neuroimaging* 1:364–371.

Yu-feng Z, Yong H, Chao-zhe Z, Qing-jiu C, Man-qiu S (2007) Altered baseline brain activity in children with ADHD revealed by resting-state functional MRI. *Brain & Development* 29:83–91.

Zalfa F, Giorgi M, Primerano B, Moro A, Di Penta A, Reis S, Oostra B, Bagni C (2003) The Fragile X Syndrome Protein FMRP Associates with BC1 RNA and Regulates the Translation of Specific mRNAs at Synapses. *Cell* 112:317–327.

Zang Y, Jiang T, Lu Y, He Y, Tian L (2004) Regional homogeneity approach to fMRI data analysis. *NeuroImage* 22:394–400.

Zerbi V, Ielacqua GD, Markicevic M, Haberl MG, Ellisman MH, A-bhaskaran A, Frick A, Rudin M, Wenderoth N (2018) Dysfunctional Autism Risk Genes Cause Circuit-Specific Connectivity Deficits With Distinct Developmental Trajectories. *Cerebral cortex* 28:2495–2506.

Zerbi V, Markicevic M, Gasparini F, Schroeter A, Rudin M, Wenderoth N (2019) Inhibiting mGluR5 activity by AFQ056/Mavoglurant rescues circuit-specific functional connectivity in Fmr1 knockout mice. *NeuroImage* 191:392–402.

Zhang D, Raichle ME (2010) Disease and the brain's dark energy. *Nature Reviews Neurology* 6:15–28.

Zhao Mg, Toyoda H, Ko SW, Ding Hk, Wu Lj, Zhuo M (2005) Deficits in Trace Fear Memory and Long-Term Potentiation in a Mouse Model for Fragile X Syndrome. *Neurobiology of Disease* 25:7385–7392.

Zhurakovskaya E, Paasonen J, Shatillo A, Lipponen A (2016) Global Functional Connectivity Differences between Sleep-Like States in Urethane Anesthetized Rats Measured by fMRI. *PLoS ONE* 11:1–12.

Zuo Xn, Kelly C, Adelstein JS, Klein DF, Castellanos FX, Milham MP (2010) Reliable intrinsic connectivity networks : Test – retest evaluation using ICA and dual regression approach. *NeuroImage* 49:2163–2177.